Measurement of protrusive forces in hyphae using lab-on-a-chip technology

---

A thesis submitted in partial fulfilment of the requirements for the Degree of Doctor of Philosophy in Cellular and Molecular Biology

at the University of Canterbury

by Ayelen B. Tayagui

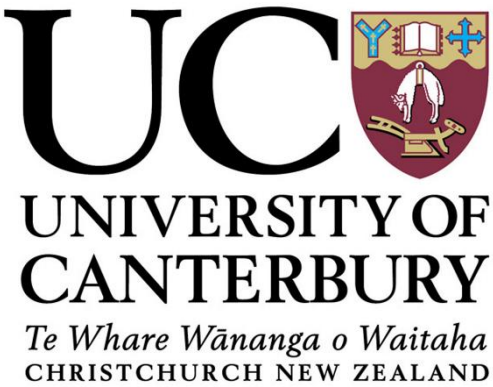

2018

Table of Contents

ABSTRACT

Fungi and oomycetes are two groups of eukaryotic microorganisms that are phylogenetically distant, yet morphologically similar. Their predominant vegetative structures are long tube-shaped cells, called hyphae, which penetrate the environment, searching for nutrients. Nutrients are broken down by the secretion of enzymes and are then absorbed by the hyphae. This process plays a vital role in nutrient recycling from dead and decaying matter in most ecosystems on the planet. Some fungal and oomycete species, however, are parasitic, and can become pathogenic, and these can have huge impacts on ecosystems with the potential loss of biodiversity. From a human perspective, pathogenic fungi and oomycetes can have significant effects on crop yields, food spoilage and, indeed, human health.

Hyphae extend by the process of tip growth, a form of polarized growth, which is characterized by extension at the extreme apex of the cell. Tip growth is driven by turgor pressure and occurs when the tip of the cells yields to that pressure. Tip yielding is likely to involve modulation to the cell wall and the cytoskeleton. This may also generate a protrusive force that, along with the secretion of enzymes, enables invasive growth through material, which is one of the key processes in pathogenicity. To understand the invasive process, one approach is to measure the protrusive force and observe the dynamics of the cytoskeleton.

The work in this thesis describes attempts to measure protrusive forces in the fungus *Neurospora crassa* and the oomycete *Achlya bisexualis*, using Lab-on-a-Chip technology. The chips were PDMS microfluidic devices that had narrow channels, which contain pillars. After inoculation on the chips, hyphae grew into the channels

and made contact with the pillars. The displacement of the pillars was optically tracked and converted into force measurements using MATLAB software. The chips enabled the measurement of protrusive forces in the micro-Newton range (< 10 μN), for both species. These could be identified as protrusive forces as, firstly, the very tip of the hypha could be observed hitting the pillar. Secondly, and less subjectively, the total force could be differentiated into its x- and y-components (F_x and F_y). F_y, which was parallel to the axis of growth, represented the protrusive force. In contrast, F_x, which was perpendicular to the axis of growth, represented a squeezing force as the side of the hypha contacted the pillar.

The relationships between cytoskeletal dynamics, invasive growth and protrusive forces, were also investigated, using the chips. Hyphae were exposed to the cytoskeletal inhibitors, latrunculin B and carbendazim, prior to hitting the pillars and the effects of these on force were measured. Unfortunately, low sample sizes, due to the sides of hyphae rather than the tips, hitting the pillars, and problems with the optical tracking, precluded any meaningful conclusions. There were indications, however, that the microfilaments may play a role in resisting turgor and thereby regulating tip yielding in *A. bisexualis*. Latrunculin B caused a transient increase in growth rate, and in the one hypha that hit a pillar with its tip, an increase in protrusive force. Earlier work has suggested that an F-actin depleted zone at the tips may regulate protrusive force in invasive hyphae (Walker et al., 2006; Suei and Garrill 2008). In contrast, in the present study microtubules were observed extending to the tips of invasive *N. crassa* hyphae. Future work is suggested using fluorescently labeled pillars to facilitate better pillar tracking and chip designs with narrower channels to make more hyphae hit the pillars with their tips rather than their sides.

Abbreviations and Definitions

ABP	Actin Binding Protein
ADP	Adenosine Diphosphate
Arp2/3	Actin-Related Proteins ARP2 and ARP3
ATP	Adenosine Triphosphate
Ca^{2+}	Calcium
cm	Centimetre
° C	Degree Celsius
DMSO	Dimethyl Sulfoxide
EGTA	Ethylene glycol-bis(β-aminoethyl ether)-N,N,N',N'-tetraacetic acid
FH1-FH2-FH3	Formin-Homology Domains
GFP	Green Fluorescent Protein
GTPases	Hydrolase Enzymes that bind and hydrolyse GTP
GTP	Guanosine Triphosphate
h	Horas
ISO	Isopropanol
LMP agar	Low-Melting-Point-Agar
LOC	Lab-on-a-Chip
MAPs	Microtubele Associated Proteins
MBC	Methyl 1H-benzimidazol-2-ylcarbamate (Carbendazim)
min	Minutes
mL	Mlillilitre
mM	Milimolar
Mpa	Megapascal
MTOC	Microtubule-Organising Centre
NA	Numerical Aperture
nm	Nanometre
nM	Nanomolar
NPFs	Nucleation Promoting Factors

σ	Visual Tracking Resolution
PBS	Phosphate buffer saline
PDMS	Polydimethylsiloxane
PIPES	Piperazine-N,N'-bis(2-ethanesulfonic acid)
PYG	Peptone Yeast Glucose
RBD	Rho-binding domain
RE	Endoplasmic Reticulum
RFP	Red Fluorescent Protein
RNA	Ribonucleic Acid
S	Seconds
SD	Standard Deviation
SDS	Sodium dodecyl sulfate
SEM	Scanning Electron Microscope
SPB	Spindle-Pole-Body
Spk	Spitzenkörper
U	Units
µN	Micro-Newton
µm	Micrometre
v/v	Volume/volume
WASP	Wiskott-Aldrich syndrome protein FAMILY
w/v	Weight/ Volume
γ-TURCs	γ-Tubulin Ring Complex

Acknowledgements

I would like to thank my supervisory team, Volker Nock, Dave Collings and Ashley Garrill and also to Paula Jameson for their help, dedication and immeasurable support throughout my research.

A big thank to all funding who trusted and invested in this project: Biomolecular Interaction Centre; Marsden Fund, and Brian Mason.

Thanks so much to Manfred Ingerfeld, Jackie Haley, Rayleen Fredericks, Craig Galilee, Matt Walter, Helen Devereux and Gary Turner for their invaluable technical support.

To my unconditional friend Steph for helping me and teaching me many confocal microscopy techniques. For those long hours experimenting together and for her beautiful friendship.

To Yiling for her patience to teach me everything about the manufacture of the chips. And above all, for giving me her warm friendship.

To my mother, Francisca, my example of life and struggle, to teach me that even in the worst adversities it is possible to get ahead and for that it is only necessary to "want to do it." And for all my family members from Argentina who have been there in one way or another.

To my friend Wafaa for her love and for those very comforting mother hugs.

To my friend Liz and Steph for being there with their warmth and affection, and for all those delicious treats contained in that amazing “Thesis Survival Kit”, that helped me in the last part of my thesis.

To all my friends from New Zealand, Uruguay and Argentina, Ceci-Ale (and Rafa and Isa), Romi-Ema (and Brianna) Frankie, Steffy-Sachin (and Samuel and Benjamin), Emily, Santiago (and Rafi) Sissi, James, Jiyhun-Nick (Rhiann and Euan), Miharu, Volker (and Felix) who have supported me unconditionally with their love, understanding and company and who are part of what I called my “chosen family”.

For my adoptive family, Hermann, Maria, Chris and Seph, for their incredible support and love that reinforced my belief that the ties of blood to be a family are not necessary.

To all my friends from Argentina, Viviana, Leandro, Ana, Jeny, Andres, Elvio, Nicolas, Maria Elena, Alejandro, Carina, Vanina, Norma, Sandra, Pedro, Marilyn y Pamela who were there encouraging me and giving me their love. Reminding me that neither time nor distance can interfere in true friendships.

Last, but not least, to my beautiful family, my Partner, James, Rosie, Moe and Lily, for their unconditional love, for their inexhaustible patience and for their unconditional support. Without them, this would not have been possible.

CHAPTER 1

INTRODUCTION

1.1 Fungi and Oomycetes

Fungi and Oomycetes can be found in almost every ecological niche on the planet (Alexopoulus, Mims, & Blackwell, 1996; S Kamoun, 2009). The two groups of organisms are morphologically very similar, generating tubular vegetative cells called hyphae and both displaying an absorptive nutrition. This has meant that there has been an historical tendency to group the oomycetes within the fungi. The advent of molecular phylogenetic techniques, however, has revealed significant molecular differences and that they belong to two very distant eukaryotic lineages (Figure 1.1). Their similarities are thus likely the result of convergent evolution, rather than phylogenetic relatedness.

Fungi belong to the Opisthokonta, a grouping that also contains animals, choanoflagellates and amoebozoans. The Opisthokonta are thought to have diverged from the other eukaryotic lineages at a very early stage in eukaryote evolution (Stechmann & Cavalier-smith, 2002). Oomycetes are stramenopiles, which are part of the SAR (stramenopiles, alveolates, and rhizaria) grouping of protists and thus they are phylogenetically related to the golden algae, brown algae and diatoms (Latijnhouwers, De Wit, & Govers, 2003; Tyler, 2001).

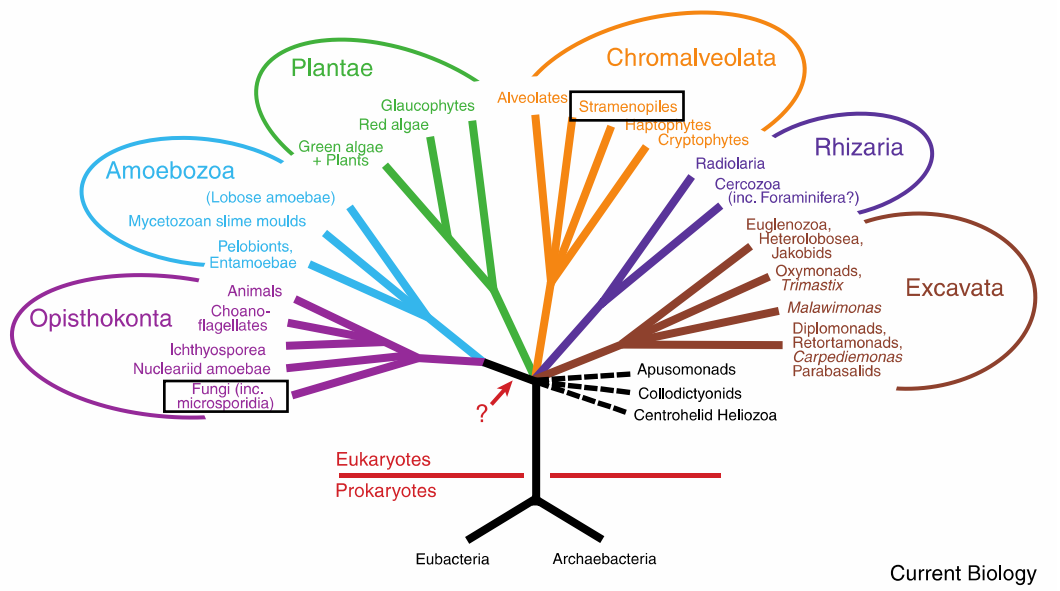

Figure 1.1: A diagrammatic representation of the major eukaryotic lineages highlighting the phylogenetic distance between the fungi and the oomycetes. These groups are boxed. The relationships among most of the major groups and the position of the root of the tree are depicted as unresolved (the arrow represents a possible placement in light of gene fusion data). Adapted and reproduced with permission from Simpson and Roger (2004).

Despite their phylogenetic distance, their morphological similarity reflects the fact that fungi and oomycetes have similar growth and nutritional strategies. Their vegetative cells extend by the process of tip growth, which is characterized by extension at the tip or apex of the cell. This leads to the formation of long tube-shaped vegetative cells that are called hyphae. Hyphae can be thought of as pressurized drill bits or “elongated mining devices”, which penetrate the environment searching for nutrients (Money, 2007). The nutrients are broken down by hydrolytic enzymes, secreted by the hyphae, and which convert complex organic material into smaller organic compounds. These are then taken up by the hyphae, structures which, are able to branch and form new additional hyphae giving a continuous network of hyphae (referred to as a mycelium). Tip growth and branching increase

the nutritive capability of the organisms, as they maximize their surface area to volume ratio and thus their ability to find, break down and absorb nutrients.

1.2 Fungi

Fungi are very important in a global context, as they are one of the main groups that degrade organic matter, which is an essential process in nutrient recycling. They fulfill this role in almost every terrestrial and aquatic habitat on the planet. This subsequently allows other organisms to assimilate essential molecules. They also form mutualistic relationships with numerous plants, algae, cyanobacteria and animals. Examples of these are the mycorrhizal species, which may have helped plants without roots to first colonise land (Brundrett, 2002) and the symbiotic endophytes, which may prevent herbivory and heavy metal stress (Voisey, 2010).

In addition to their ecological importance fungi are crucially important in industry. Pertinent examples in the pharmaceutical industry are in the production of anti-cholesterol statins, the antibiotic penicillin and the immunosuppressant cyclosporin A. For bakers and brewers, yeasts have been used for the production of bread, beers, sake and wines for many millennia. As a food source in their own right, a variety of fungal species are both produced commercially and collected in the wild. It has been estimated that worldwide almost 8 million tonnes of fungi were consumed in 2011. They have also been invaluable as model eukaryotic research organisms – work on the cell cycle in yeasts, for example, have provided key insights into cancer (Alexopoulus et al., 1996; Carlile, 1995; Griffin, 1994).

We currently know of around 100,000 species of fungi, yet there are estimated to be as many as 1.5 million species, which is second to only the insects among the eukaryotes. These species are distributed across nine phyla: Microsporidia,

Rozellomycota, Chytridiomycota, Blastocladiomycota, Zoopagomycota, Mucormycota, Glomeromycota, Basidiomycota and Ascomycota (Fisher, Gow, & Gurr, 2016). Fungi reproduce via spores either sexually or asexually (or indeed both), depending on the species and form a multitude of reproductive structures.

1.3 Oomycetes

The oomycetes are a much smaller group than the fungi, yet they still contain more than 500 known species and, as detailed below, their impact on human affairs can be significant. Their phylogenetic closeness to photosynthetic protists means they are thought to have descended from an ancient plastid-bearing ancestor. The loss of plastids has meant a reliance on absorptive nutrition and thus, like the fungi, they play key roles in nutrient recycling. There is fossil evidence to suggest some early endophytic associations with land plants around 350 million years ago (Krings, Taylor, & Dotzler, 2011). Like the fungi these modes of nutrition have necessitated the evolution of filamentous structures with a high surface area to volume ratio, hence the convergent evolution of the hyphal growth form, and tip growth.

1.4 Fungal and Oomycete pathogens

While fungi and oomycetes are essential in an ecological context and are useful in many industrial processes, they can also have less desirable effect (Alexopoulus et al., 1996; Griffin, 1994). Around 30% of the 100,000 known fungal species live as parasites (i.e. absorbing nutrients from the host, providing no benefits in return and potentially causing harm to the host) and these can become pathogenic (i.e. causing disease). The damage caused by fungi to animal and plant tissues leads to huge economic losses worldwide. For example, it is estimated that between 10-50% of the world's fruit harvest is lost annually due to fungi (Borkovich et al., 2004). Perhaps

more concerning is the potential loss of biodiversity - fungi and oomycetes are responsible for a considerable number of diseases that have caused severe die-offs and also extinctions of animals and plants (Fisher et al., 2012). Also, this will likely increase with climate change with the reported movement of pathogenic fungi and oomycetes towards the Poles at a rate of 2.8 km yr^{-1} (Bebber, Ramotowski, & Gurr, 2013).

Well known examples of fungal diseases of plants include Dutch elm disease caused by the ascomycetes *Ophistioma ulmi*, *Ophiostoma novo-ulmi* and *Ophiostoma himal-ulmi* and Chestnut blight caused by *Cryphonectria parasitica*. Rice plants are susceptible to *Magnoporthe oryzae*, which is present in 85 countries and can be responsible for the loss of up to 35% of rice harvests (Greer & Webster, 2001). Many cereal and grass species are susceptible to *Puccinia graminis,* which most importantly causes stem rust disease in wheat (Berlin, Samils, & Andersson, 2017). An emerging fungal disease in New Zealand is myrtle rust (*Austropuccinia psidii*), which has been found in Northland, Waikato, Te Puke, Taranaki, Lower Hutt and Auckland. This has attracted wide coverage in the mainstream media. The fungus attacks plants belonging to the myrtle family, which include the iconic pōhutukawa, mānuka and rātā. It is believed to have reached New Zealand through spores blown from Australia's eastern seaboard (http://www.doc.govt.nz/myrtle-rust).

In animals, pertinent examples of fungi causing disease include *Batrachochytrium dendrobatidis,* a generalist pathogen that infects amphibians, species of the genus *Nosema* which cause colony collapse disorder in bees, *Aspergillus sydowii* which infects coral, *Geomyces destructans* affecting bats (Fisher et al., 2012) and *Ophidiomyces ophiodiicola* which is severely affecting snake populations, causing snake fungal disease (Lorch et al., 2015). According to the Center for Disease

Control, there are currently around 300 known fungal diseases of humans (http://www.cdc.gov). *Aspergillus* can cause many diverse types of aspergillosis, primarily in the lungs and sinuses. People at most risk are those with a compromised immune system or other lung conditions (Saral, 1991). *Candida albicans* is a normal human commensal, but it can cause infections of the mouth, throat, oesophagus and the genitourinary tract. More serious is invasive candidiasis, where the fungus enters the bloodstream and can cause systemic infections (Saral, 1991). Blastomycosis, which can occur when spores of *Blastomyces* are inhaled can cause flu-like symptoms and in the immunocompromised can become severe. This is also the case with *Cryptococcus neoformans* infections, which are rare, but in the severely immunocompromised can cause meningitis, and with *Pneumocystis jirovecii*, which can cause pneumonia. Other less serious fungal infections that can nonetheless still affect quality of life include ringworm or athletes foot, caused by several species including *Trichophyton mentagrophytes.*

While there are fewer known species, the oomycetes can be just as problematic as the fungi, if not more so. There is evidence to suggest that parasitic oomycetes were present 320 million years ago and that parasitism has evolved in 3 distinct lineages. The most well-known pathogenic species (*Phytophthora*, *Pythium* and the downy mildews) are thought to have evolved from a single common plant parasitic ancestor (Thines and Kamoun, 2010). A recent review in the journal *Molecular Plant Pathology* surveyed 62 scientists across 15 countries to produce a ranked list of the ten most problematic oomycete pathogens, based on their scientific and economic importance. The species and their ranking were 1) *Phytophthora infestans*, 2 =) *Phytophthora ramorum* and *Hyaloperonospora arabidopsis*, 4) *Phytopthora sojae*, 5) *Phytophthora capsica*, 6) *Plasmopara viticola*, 7) *Phytophthora cinnamomi*, 8 =)

Phytophthora parasitica and *Pythium ultimum* and 10) *Albugo candida* (Kamoun et al., 2015). Some of these are considered in more detail below.

There are around 100 species of *Phytophthora,* which include some of the most devastating plant pathogens known. Most of these infect eudicotyledons and are host specific, but some species can infect a multitude of hosts. *Phytophthora* species have had a profound influence on humanity's wellbeing and society, probably the best example of this is *Phytophthora infestans* the causative agent of the Irish potato blight (Alexopoulus et al., 1996; Kamoun, 2009). The loss of around three quarters of the potato crop in the 1840s is estimated to have caused the death of one million people and the emigration of a million more, effectively reducing the population of Ireland by a quarter. In addition to its impact on human demographics, the famine and its effects also permanently changed the island's political and cultural landscape. Less well known was an outbreak in Germany in the 1940s, which caused an estimated 700,000 deaths. This was in part due to a shortage of copper sulphate, which was normally used to spray and protect the potatoes, but which had instead been used for shell casings and electric wire in the war effort (Carefoot & Sprott, 1967).

Other prominent *Phytophthora* species include *P. ramorum* which causes sudden oak death syndrome and *P. cinnamomi* which causes cinnamon root rot. Both species can infect many other hosts; indeed, it is estimated that *P. cinnamomi* can infect upwards of 5,000 different plant species (Hardham & Blackman, 2017). Another species that has had profound economic effects is *Phytophthora megakarya* which has decimated cocoa crops in Western Africa. In severe cases, this can lead to the loss of 80% of cocoa pods and up to 10% of cocoa trees annually. In New Zealand, *Phytophthora agathidicida* has received widespread coverage in the

mainstream media as the causative agent of Kauri dieback. This is a relative new, introduced species and has the potential to extinguish our perhaps most iconic tree. Once a Kauri has been infected, there is no cure or treatment to combat the dieback (Beever et al., 2007; Bellgard et al., 2016; Weir et al., 2015).

Closely related to *Phytophthora*, the Peronosporaceae are a family that contains 700 species that cause downy mildew on the foliage of many important crops species. These species are mostly host specific. *Hyaloperonospora arabidopsis* has received interest as it is an obligate parasite of the model plant *Arabidopsis thaliana* and, as such, has been used to reveal important insights into host-parasite interactions. Other downy mildews that can have important economic consequences include *Plasmopara viticola* which infects grape vines. With the right conditions (climatic and lack of treatment), *P. viticola* is capable of reducing grape production by 75% in a single season (Madden et al., 2000; Rossi & Caffi, 2012).

In the same lineage as *Phytophthora* and downy mildews are *Pythium* species that can cause root rot in many plants. The most prominent of these is *P. ultimum* which is suspected to be able to infect more than 300 species, including corn and soybean. Furthermore, *Pythium* species also cause disease in animals and humans; *Pythium insidiosum* is the causative agent of pythiosis, a rare yet fatal tropical disease characterised by ulcerative skin lesions. Numerous animal species can be susceptible to the disease which is contracted after exposure of fresh wounds to the fungus in stagnant bodies of fresh water (Krajaejun et al., 2014).

Additional animal pathogenic oomycetes belong to the order Saprolegniales which contain three main genera, *Saprolegnia*, *Achlya* and *Aphanomyces. Saprolegnia parasitica* is a parasitic species that can affect the health of fish and can have

significant impacts on the aquaculture industry. Saprolegniasis is estimated to lead to the loss of 10% of all hatched salmon, causing major financial loss in the salmon industry, which accounts for almost a third of global fish production for consumption (Earle & Hintz, 2014).

1.5 Fungal and Oomycete infective strategies

As fungal and oomycete species infect plants, they intimately associate with the plant tissue and become partially or wholly biotrophic, obtaining nutrients from the cells of their hosts. These interactions may involve the development of specialized infection and parasitic structures within the plant (Figure 1.2). In addition to the regular hyphae which explore the extracellular space (apoplast), there are also appresoria, invasive hyphae and haustoria which penetrate host cell cavities and invaginate the host's plasma membrane. These latter structures have historically been described as feeding structures that facilitate the nutrition of the fungus or oomycete, but they are also responsible for the secretion and translocation into host cells of effector proteins. These virulence proteins manipulate processes in the plant and promote host infection and colonization, yet in resistant plants they may also activate plant immune receptors (Petre & Kamoun, 2014).

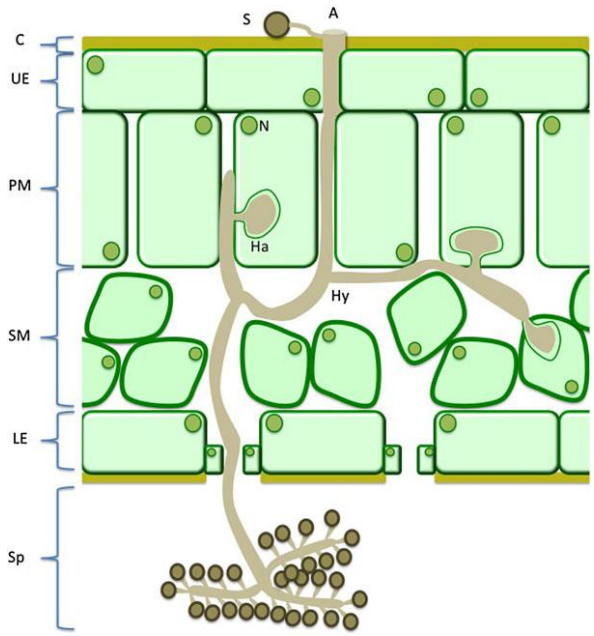

Figure 1.2: A diagrammatic representation of the infection of a leaf of *Arabidopsis thaliana* by the oomycete *Hyaloperonospora arabidopsis*. A sporangiospore (S) lands on the leaf surface and puts out a germ tube, which then forms an appressorium (A). From the appressorium the oomycete infects the leaf using invasive hyphae (Hy) and haustoria (Ha). Eventually additional mature sporangiophores (Sp) are formed on the lower surface of the leaf. Additional structures shown are the cuticle (C), upper and lower epidermis (UE and LE), nucleus (N), palisade layer (PM) and spongy mesophyll (SM). Note that the sporangiospores are not drawn to scale. Reproduced with permission from Kamoun et al (2015).

1.6 Fungal and oomycete growth

In both fungi and oomycetes hyphae extend primarily by the process of tip growth. This is a complex process which, in fungi, can probably be best described through three models – the “vesicle supply centre’ model, “steady-state” model and the “unitary” model, which are described further below. As detailed above, tip growth generates a cylindrical cell with a tapered end (like a drill bit) that enables penetration of the medium and the maintenance of a high surface-to-volume ratio. It is a mode of growth also displayed by pollen tubes and root hairs in plants, rhizoids

in algae and protonemata in mosses. In plants, pollen tubes extend from the pollen grain through the stigma of angiosperms to deliver the male gametes to the ovule, a process that requires penetrative growth. Similarly, root hairs penetrate soil, but also, analogous to hyphae, their high surface area to volume ratio enables the uptake of nutrients from the soil. In the algae, rhizoids play a similar role to the root hairs of vascular plants. It is thus likely that the process of tip growth has evolved in several different systems to fulfil similar needs, i.e. penetration and high surface area to volume ratios.

While tip growth is the primary mode of hyphal extension and is the focus of this thesis, it should be noted that certain hyphae and structures in the fungi grow diffusively along the length of their hyphae by intercalary growth. Examples of intercalary growth include the fruiting bodies of Basidiomycete mushrooms and the rhizomorphs of *Armillaria gallica* (Voisey, 2010). Intercalary hyphal growth is also prominent in *Epichloë*, a biotrophic endophyte of grasses, which grows synchronously as the aerial portions of the host develop (Voisey 2010). This growth differs from that in the fruiting bodies in that the hyphal compartments undergo mitosis and septation during growth, and compartment volumes do not increase significantly (Christensen et al., 2008). It has been suggested that this unique mechanism evolved as a result of hyphal attachment to the growing host cells, which would otherwise have compromised hyphal integrity (Voisey 2010).

Tip growth is a complex process that is characterized by the synthesis and deposition of new cell wall material, membrane and proteins at the tip of the hyphae (Bartnicki-Garcia & Lippman, 1969) (Figure 1.3). The deposition occurs due to exocytosis of secretory vesicles containing different components including cell wall synthases, which accumulate at the tip (Bartnicki-Garcia & Lippman, 1969;

Riquelme, 2013). The importance of vesicle delivery was first suggested by Brunswick (1924), who used a phase contrast microscope to observe an accumulation of vesicles at the tips of hyphae. Brunswik called this cloud of vesicles a "Spitzenkörper" (Spk) or apical body and the work of Brunswik was followed by the pioneering studies of Girbardt (1956). The Spk is believed to function as a “vesicle supply center”, receiving Golgi-derived vesicles and then transporting these to the membrane at the tip. It is now known to consist of an accumulation of both microvesicles (30 to 40 nm), which contain chitin synthase, and macrovesicles (70 to 120 nm), which contain glucan synthase; these surround a central area containing microfilaments. Also present are ribosomes and uncharacterised amorphous material. The vesicles contain the new wall synthesizing machinery, membrane and protein material necessary for cell-surface expansion. According to the “vesicle supply centre” model of tip growth, the position of the Spk determines the direction and speed of growth and crucially the Spk itself moves forward; its position creating an exocytotic gradient although it is not fully understood how the Spk moves with the tip (Bartnicki-Garcia, Hergert, & Gierz, 1989; Berepiki, Lichius, & Read, 2011; Fischer, 2007; Riquelme et al.,1998; Virag & Harris, 2006). The trafficking of vesicles to and from the Spk is thought to occur along cytoskeletal proteins and is likely coordinated by the combined action of coats, tethers, Rab GTPases, motor proteins, and t- and v- SNARE proteins. Also important is the exocyst, a tethering collective comprised of eight proteins, which are found in the Spk and which are present at sites where secretory vesicles fuse with the plasma membrane (Riquelme & Sánchez-León, 2014) (Figure 1.4).

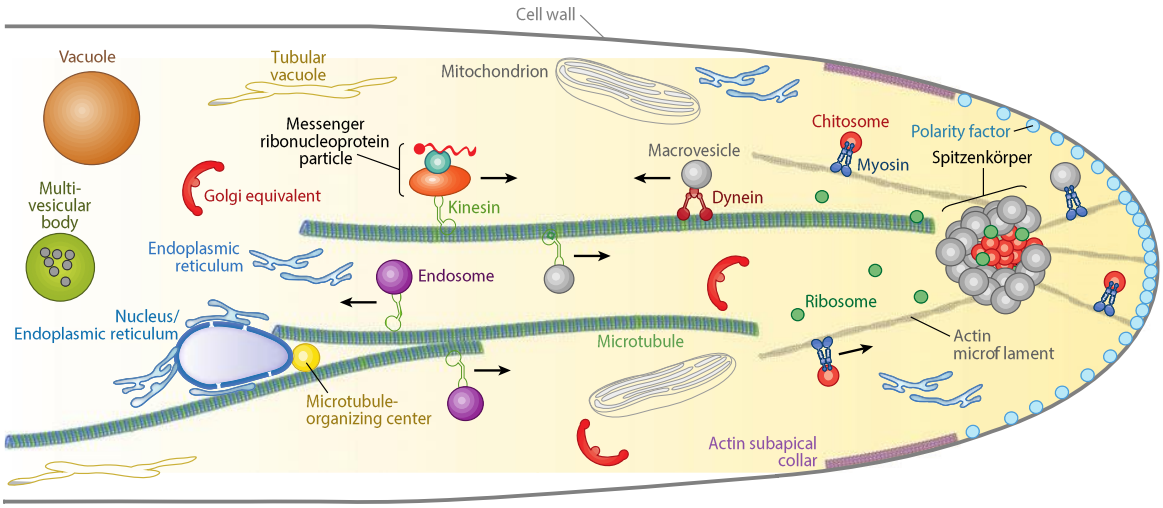

Figure 1.3: Diagram of the tip of a fungal hypha showing some of the main components involved in tip growth. Microtubules deliver landmark proteins that set up polarity in the hypha leading to microfilament nucleation and polymerization. Vesicles from the Spk deliver cell wall synthases to the tip where wall deposition enables growth. The hypha has a characteristic distribution of organelles, these move forward retaining their respective positions as growth occurs. The process of growth is driven by turgor pressure and the tip yields to this pressure. Figure produced by E. Sanchez-Leon and reproduced with permission from Riquelme (2013).

1.6.1 Fungi

In fungi, the wall is made up of various components such as chitin, glucans and glycoproteins. These are synthesized by cell wall synthases, proteins which have been referred to as nanofactories. Different synthases are carried in different vesicles with, for example, those carrying chitin synthases referred to as chitosomes. Once in the plasma membrane chitin synthases utilize N-acetyl glucosamine subunits (GlcNac) and glucan synthases utilize glucose subunits, from the cytoplasmic side of the membrane and incorporate them into growing chains of chitin microfibrils and β-1, 3-glucan, respectively (Bartnicki-Garcia et al., 1989). The

demonstration of the cell wall synthases in the Spk was a key piece of evidence linking the Spk and the vesicle supply center (Riquelme et al., 2007).

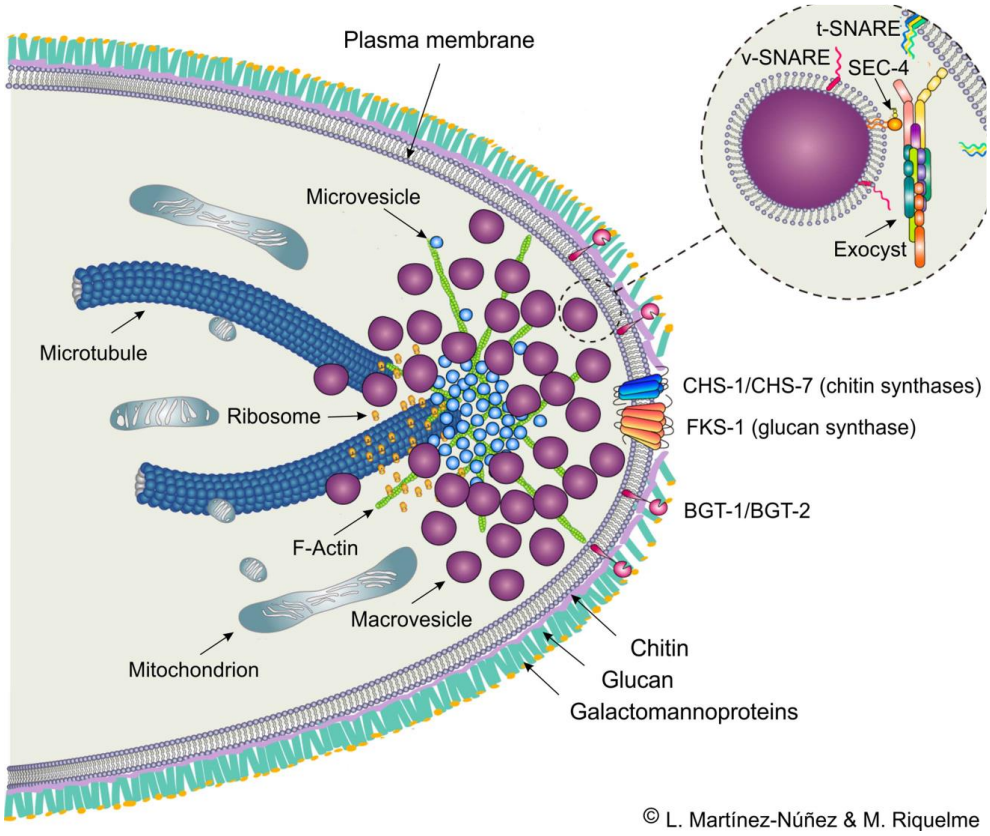

Figure 1.4: A diagram depicting vesicles from the Spk delivering cell wall synthases to the tips of hyphae. Vesicle fusion occurs due to the exocyst, which is a characteristic eukaryotic tethering complex. Reproduced with permission from Riquelme et al. (2016).

In addition to the exocytosis of vesicles at the tip, endocytic uptake of soluble and membrane-bound material into the cell occurs distal to the tip (Steinberg, Peñalva, Riquelme, Wösten, & Harris, 2017) (Figure 1.5). In addition to a role in recycling of material, the early endosomes that are formed as the first intracellular compartment in the endocytic pathway appear to perform essential additional functions as spatial organizers and mediators of signaling in the hypha (Steinberg et al., 2017). This is

likely to also be an important factor in the determination of polarity, essentially removing determinants of the tip of the cell from the sub apical regions.

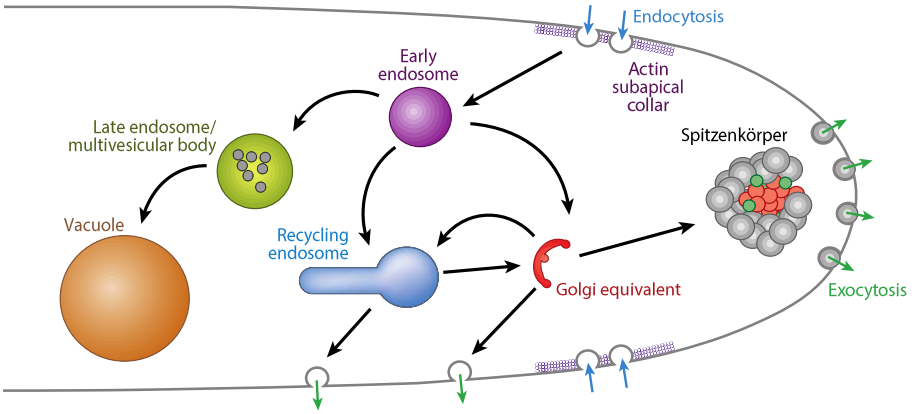

Figure 1.5: A diagram showing exocytosis and endocytosis and their respective importance to tip growth. Exocytosis enables growth through the delivery of cell wall synthases and new plasma membrane while endocytosis enables recovery of membrane and the removal of tip polarity markers from sub-apical regions. Reproduced with permission from Riquelme (2013).

While the “vesicle-supply centre” model can be used to explain the delivery of wall material to the site of growth, the “steady-state” and/or “unitary” models of tip growth can be used to explain the different characteristics of the cell wall along a hypha. The fungal cell wall comprises an internal (insoluble) layer that has fibrils of chitin (β-1,4- GlcNAc) and β (1,3)- and β (1,7)-glucans inserted in a soluble gel-like layer composed of galactomannoproteins (glycoproteins) and polysaccharides [α (1,3)-glucans] (Hunsley & Burnett, 1970). According to the “steady-state model”, as the wall components are synthesized, they are not yet cross-linked and, thus at the tip, the wall is still flexible or plastic (Wessels, Soll, & Knecht, 1988). As the tip expands, the chitin crystallizes in the subapical regions and becomes covalently bound to β-

1,3-glucans. This creates a more solidified (elastic) wall behind the tip. An alternate to the “steady-state model” is the “unitary model” (Bartnicki-Garcia, 1973; Gooday, 1978) which invokes the simultaneous action of cell wall–loosening enzymes and cell wall–synthesizing enzymes. Irrespective of which model is correct, in both, growth is thought to occur as a turgid protoplast pushes against the plastic wall at the tip causing hyphal expansion (and hence the tip yields to turgor pressure) and thus creating the characteristic hyphal cell shape. The elastic wall further back from the tip does not yield to the pressure. Yielding of the tip to turgor pressure is one of the main focii of this thesis and is considered in more detail below.

As tip growth is a form of polarized cell growth it is not surprising that hyphae are themselves polar and have a characteristic asymmetric distribution of cell components (Figure 1.3). The first 5 μm of the hypha contains the Spk, the polarisome, exocysts, a few mitochondria, and occasionally smooth endoplasmic reticulum (ER) and Woronin bodies (WBs). In the next 10 – 20 μm, the cytoplasm contains mitochondria and ER cisternae. From 20 μm back to the first septum, the cytoplasm contains the complete collection of organelles, including nuclei. Back from the first septum the compartments contain all the organelles, but the distribution of these may differ from those in the tip most compartment. Individual compartments within a septated hypha are able to communicate with each other via septal pores. These pores can allow the passage of cytoplasm or organelles and facilitate differentiation within the mycelium.

The polar nature of hyphae raises the question of what factors generate and maintain this polarity. Important insights have come from studies on budding and fission yeasts although in both cases these are perhaps not ideal models for tip growth in filamentous species (Riquelme, 2013). Both yeasts are unicellular and

divide asexually by either budding of fission. To bud, the yeast will establish a site of polarity and then grow apically at this site for a short period before the daughter cell grows isotropically to generate the typical yeast shape, prior to cytokinesis. In the fission yeast, a lozenge shaped cell will expand at both ends. Polarity in both of these is controlled during the cell cycle and established by landmark proteins that set up spatial cues (Nelson, 2003) .The identification of these proteins in yeast has enabled the search for their homologues in filamentous species.

In the budding yeast, new buds form adjacent to previous sites of division. These sites are established by the landmark proteins Bud3, Bud4 and Bud10 (Chang & Peter, 2003). In *N. crassa* Bud3 and Bud4 play roles in septa formation and not in tip growth *per se* (Si, Justa-Schuch, Seiler, & Harris, 2010). More pertinent for filamentous species are the Tea proteins of the fission yeast, in which growth occurs initially at previous areas of cell growth, and then at sites where cell division has previously occurred. A key part of this process is the delivery of the landmark protein Tea1, via microtubules (Feierbach, Verde, & Chang, 2004). Tea proteins appear to move either through the operation of motor proteins such as kinesin-7 or through microtubule elongation itself at the plus end. In the filamentous fungus *Aspergillus nidulans* the Tea1 orthologue and cell end marker, TeaA, is localized to the site of polarized growth via microtubules and anchored to the apex through a membrane-associated protein TeaR (Figure 6). The importance of microtubules in this process has been demonstrated using benomyl, a microtubule destabilizer (Fischer, Zekert, & Takeshita, 2008; Takeshita et al., 2008). That TeaA is important in both the generation and maintenance of polarity is supported by the observation that it may also be responsible for marking sites of branch formation (Takeshita & Fischer, 2011).

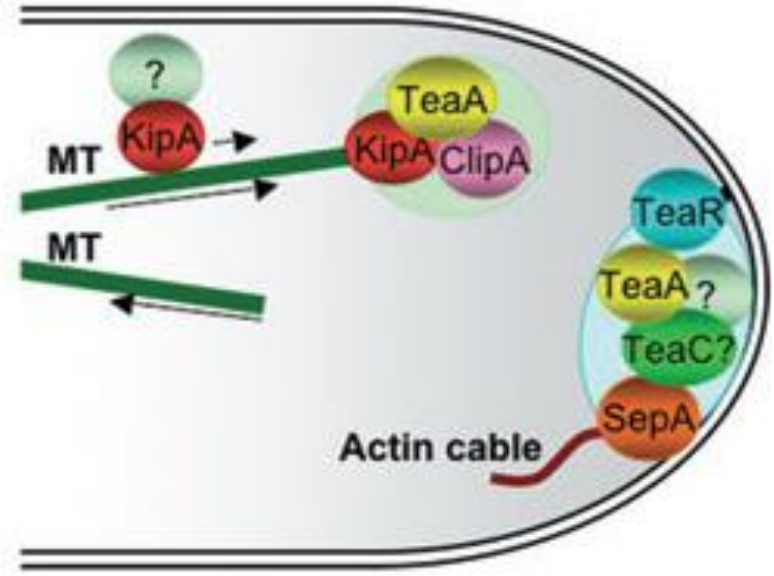

Figure 1.6: A diagram showing the delivery of the cell end marker protein TeaA and associated proteins to the tip of a hypha of the fungus *Aspergillus nidulans*. TeaA is present at the plus end of a growing microtubule. Upon delivery at the tip the actin nucleating protein SepA, which is a formin, nucleates the formation of F-actin cables. Reproduced with permission from Fischer et al. (2008).

Upon the delivery of these landmark proteins, several small GTPases including Cdc42 (important in polarity establishment) and Rac (important in polarity maintenance) are activated; these act to transduce the positional information to effectors that localize the polarisome. The polarisome is a multiprotein complex that maintains cell polarity by directing the localized assembly of microfilaments. One of the key proteins within the polarisome is formin. The formins are a family of actin nucleating proteins described in more detail below. In several species, formin homologues have been found at the tips of hyphae, either as a moon-shaped crescent along the cell surface or with a more punctate appearance in the SPK (Crampin et al., 2005; Schmitz et al.; Sharpless & Harris, 2002)

The importance of microfilament nucleation and assembly, and indeed the cytoskeleton as a whole, in hyphal morphogenesis has long been recognized (Bartnicki-Garcia, 2002). Microtubules are thought to be primarily responsible for the long-distance transport of vesicles to the Spk, while actin microfilaments control facets of vesicle organization within the Spk and their subsequent transport to the membrane at the hyphal apex. Indeed, some have described the Spk as a switching station from microtubule-based to microfilament-based vesicle transport (Harris et al., 2005). There were early indications that the Spk may also function as a microtubule organising centre (MTOC) although in the majority of species γ-tubulin does not appear to be present in the Spk (Harris et al., 2005). A key facet of tip growth, in addition to localised extension at the apex, is the net migration forward of organelles at the same rate as the tip grows. In addition, these organelles maintain their respective positions relative to the tip. This is likely to come about through motor proteins moving along cytoskeletal tracks, although there may be some role for mass flow in this process (Lew, 2011; Muralidhar et al., 2016).

1.6.2 Oomycetes

Less is known about the mechanism of tip growth in the oomycetes, although there does seem to be much commonality with the fungi. Oomycete hyphae are polar structures with a characteristic distribution of organelles moving back from the tip that is similar to that in fungi. Vesicles accumulate at the tips, although there is no distinct Spk. These vesicles deliver wall synthases to the tip and again there is a gradient of wall plasticity. Small amounts (~0.05%) of chitin have been reported in the wall of some oomycetes and there have been reports of chitin synthase genes,

but the main component of the wall is cellulose. Further back from the tip are increasing numbers of mitochondria, golgi, ER, nuclei and vacuoles. Classic ultrastructural studies by Grove et al. (1970) led to the suggestion that vesicles moved from the ER through the Golgi, where they are processed prior to moving to and fusing with the plasma membrane at the tip. While septa are largely absent from the hyphae, there are some species such as *Peronospora tabacina* that have the ability to form septa that compartmentalize hyphae (Kortekamp, 2005). Again, the movement of vesicles has been proposed to occur via motor proteins, microtubules and microfilaments (Heath, 1980). Staining with phalloidin has revealed a high concentration of microfilaments at the hyphal tip, in a structure referred to as the apical F-actin cap (Yu, Jackson, & Garrill, 2004). Further back from the tip actin forms discrete plaques and filaments (Walker et al., 2006).

1.7 Tip growth in pollen tubes

As detailed above, tip growth occurs in other systems such as pollen tubes and root hairs of plants, algal rhizoids, moss protonemata and the growth cones of neurons in animals. As the basic principles are the same for the different tip growing systems, only pollen tube growth will be described here. Pollen tubes are most pertinent to the work described in this thesis as there have been a number of studies detailing protrusive force measurement in these cells (Nezhad & Geitmann, 2013).

Like a hypha, a pollen tube is a polarised structure. Pollen tubes extend out from a pollen grain by tip growth once the grain lands on the stigma. While there are differences between species, a typical pollen tube will have an apical clear zone containing vesicles which form an inverted cone structure, further back are

organellar regions (containing mitochondria, ER and Golgi), then a nuclear region (containing the male genetic material) and finally in more mature pollen tubes, a vacuolar region. Tip growth is thought to arise due to deposition of wall material via exocytosis at the tip and/or just behind the tip, and localised wall yielding in response to turgor pressure.

The pollen tube cell wall typically consists of a primary layer of pectin and cellulose and a secondary layer of callose. This callose layer appears to be absent from the tip and so pectin appears to be a key component in the areas where the tip yields to pressure (Holdaway-Clarke & Hepler, 2003). There is a gradient of esterification of the pectin which is secreted at the tip in the esterified form. Further back, as the wall matures, these pectins are de-esterified by the enzyme pectin methylesterase (Geitmann, 1999). This process of de-esterification permits Ca^{2+} to cross-link the acidic pectins which affects the mechanical properties of the wall. Esterified pectins at the tip will allow the tip to yield to turgor pressure, whereas the non-esterified cross-linked pectins further back will resist the turgor pressure. Thus, like hyphae there is a yielding plastic area at the tip and an elastic area back from the tip.

The small GTPase ROP1 plays a role in the generation and maintenance of polarity. Polarity is also aided by the cytoskeleton (as of course microfilaments and microtubules are themselves polar structures). Microfilaments form an apical fringe or collar and these, along with myosin, are thought to enable the transport of vesicles to the site of exocytosis (Rounds, Hepler, & Winship, 2014). Microtubules, with associated kinesin motor proteins are also thought to also enable the movement of organelles. It is thought that tip-high gradients of Ca^{2+} may direct the movement and delivery of secretory vesicles to the clear zone and the tip (Roy et al., 1999).

1.8 The fungal and oomycete cytoskeleton

As detailed above, and further below, the cytoskeleton of fungi and oomycetes plays a key role in growth. It is highly dynamic and can be assembled and disassembled according to cellular needs. These dynamics, and the functioning of the cytoskeleton, arise due to the activity of a large number of associated proteins named ABPs (actin binding proteins) and MAPs (microtubule associated proteins) (Levina, Lew, & Heath, 1994). In addition, motor proteins move along the microfilaments and microtubules transporting proteins, RNA, vesicles and other organelles within the cell. While they play distinct roles in fungi and oomycetes, there is likely to be close interplay between microfilaments and microtubules. This could involve physical contact through proteins that link both cytoskeleton polymers, or by partial functional interdependency without actual physical contact (Berepiki et al., 2011; Lichius, Berepiki, & Read, 2011; Yarm, Sagot, & Pellman, 2001).

1.8.1 Microfilaments

Microfilaments (filamentous or F-actin) are made up from globular actin monomers (G-actin). G-actin has polarity (with a plus and a minus end) and has a bound but exchangeable nucleotide (ATP or ADP), which is present in a cleft at the minus end of the monomer. The monomers can associate end-to-end to form a polarized polymer, again with a plus (also referred to as a barbed end) and a minus (also referred to as a pointed end) end. Two of these polymers associate to form a double-helical chain – this is an individual microfilament (Figure 1.7). Because of their polarity and the action of ABPs, microfilaments show distinctive and different rates of assembly and disassembly at their two ends. Typically, assembly and hence growth

will occur faster at the plus end and disassembly will occur faster at the minus end. Thus, there is a dynamic equilibrium in cells between the monomeric and filamentous forms. In fungi, some of the functions of microfilaments, such as short distance transport of secretory vesicles to the Spk, appears to be directly related to the dynamic balance between the amount of G-actin and F-actin (Berepiki, Lichius, Shoji, Tilsner, & Read, 2010b; Lichius et al., 2011).

In hyphae, there are three main arrangements of microfilament: F-actin cables are composed of linear filaments found at sites of active growth and these form the tracks for myosin motor proteins and their cargos; F-actin patches (filasomes) which are associated with the plasma membrane, form clusters around endocytic vesicles, and; F-actin rings**,** composed of actomyosin contractile rings, which are very important in the process of cytokinesis in budding yeasts and septation in filamentous fungi (Berepiki et al., 2010b; Geitmann & Emons, 2000; Lichius et al., 2011) (Figure 7b). These arrangements arise due to the nucleating action of the proteins formin and Arp2/3, which initiate the formation of microfilaments from G-actin (Faix & Grosse, 2006; Gladfelter, 2006; Lew, 2002; Pollard, 2007; Pring, Evangelista, Boone, Yang, & Zigmond, 2003; Sagot, Rodal, Moseley, Goode, & Pellman, 2002). In the context of this thesis which pertains to tip growth and protrusive force, the patches and cables are the most relevant arrangements and so these will be considered further.

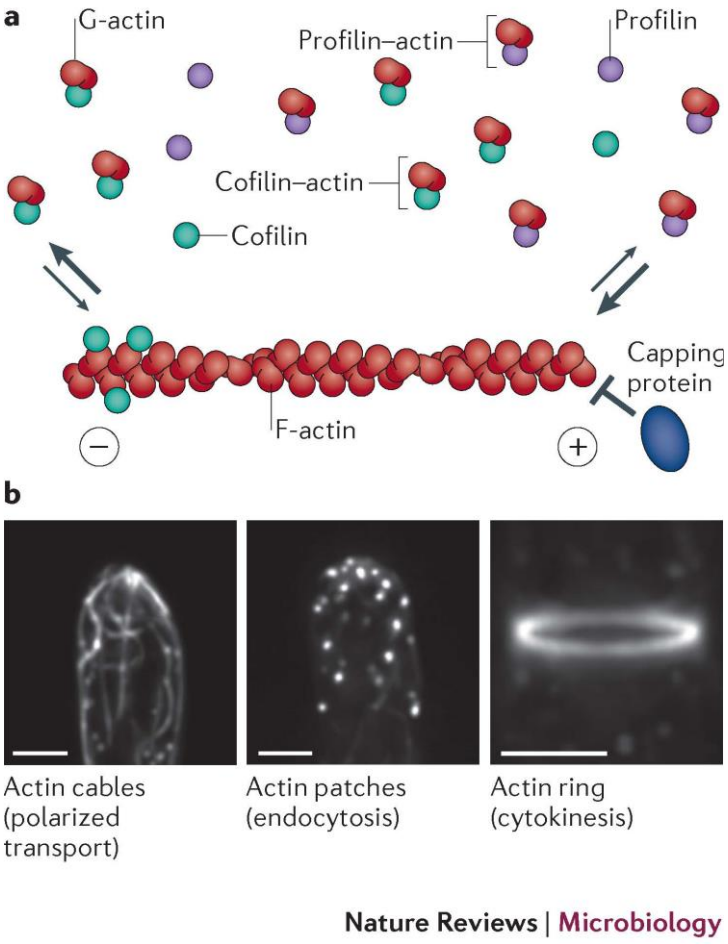

Figure 1.7**:** Microfilament formation and arrangements in fungi and oomycetes. Microfilaments (F-actin) are formed when G-actin monomers associate end-to-end. This association is enhanced in the presence of the ABP profilin. The inherent polarity of monomers leads to polarity in the filaments with a plus end (also known as the barbed end) and a minus end (also known as the pointed end). Two filaments form a helical microfilament. The plus end is the fast-growing end with net addition of subunits, whereas the minus end is a slower-growing end and also the end where disassembly can occur at a faster rate. Also shown are profilin, which promotes F-actin growth, cofilin, which disassembles F-actin and capping protein, which caps the plus end of filaments, inhibiting their disassembly (some capping proteins bind the minus end). b) In fungi F-actin forms three higher-order structures, which fulfill different roles. Actin cables (extended lines) are important in polarized transport (e.g. vesicles moving from the Spk to the tip), actin patches (dots) mediate endocytosis and actin rings are contractile structures that guide septa formation during cytokinesis. Similar structures are also seen in the oomycetes. Scale bars represent 2 μm. Figure reproduced with permission from Berepiki et al. (2011).

The Arp2/3 complex is a group of conserved proteins that are widely distributed among eukaryotes (Welch, 1997). It nucleates the branched network of microfilaments that are seen as actin patches and are thought to be the sites of endocytosis. These patches are composed of more than 60 different proteins. The Arp2/3 complex is composed of seven subunits, of which Arp2 and Arp3 are the key components due to their structural similarity with G-actin. The other five units are species specific; however, it has been demonstrated that metazoans, fungi, amoebae and plants express essentially the same subunits, usually named according to their size: ARPC1 (for the 40-kDa subunit), ARPC2 (35-kDa subunit), ARPC3 (21-kDa subunit), ARPC4 (20-kDa subunit) and ARPC5 (16-kDa subunit) (Pollard & Beltzner, 2002; Pollard, 2007; Volkmann et al., 2001; Weaver et al., 2003).

The mechanism of activation of the Arp2/3 complex is highly regulated and is initiated by the participation of the NPFs (nucleation-promoting factors), which are regulatory proteins that stimulate the inactive Arp2/3 complex to form a new microfilament on the side of a preexisting one at an angle of 70°. The main activators of this complex are the Wiskott-Aldrich syndrome protein (WASP) family and the cortactin family, both family members have an acidic (A) domain that binds the Arp2/3 complex which promotes a conformational change (Mullins & Pollard, 1999; Pollard & Beltzner, 2002; Pollard, 2007; Welch & Mullins, 2002) (Figure 8).

Much of what we know of the process of patch formation comes from research on the budding yeast. The Arp2/3 complex is recruited to sites of endocytosis by an accumulation of clathrin and endocytic adaptor proteins at the plasma membrane (Kaksonen, Sun, & Drubin, 2003; Kaksonen, Toret, & Drubin, 2005). Arp2/3 is activated by Las17 (Bee1), which is a Wiskott–Aldrich syndrome protein (WASP)

family member (Madania et al., 1999), and myosin I (Sun et al., 2006). The branched actin network that is generated is stabilized by the cross-linking protein fimbrin (Kaksonen et al., 2005) and, along with myosin I, provides the force necessary for the invagination of the plasma membrane invagination and scission of endocytic vesicles – processes which have to overcome the opposing turgor pressure (Robertson et al., 2009). Patch formation and endocytosis are likely to occur by similar processes in hyphae, based on the high degree of ABP conservation between the budding yeast and the filamentous species *N. crassa* and *A. nidulans* (Berepiki et al., 2011).

The formins are a family of actin nucleating proteins that nucleate G-actin into linear cables, which as described above, are used as a track to transport vesicles from the Spk to sites of exocytosis (Figure 1.8). In *A. nidulans* and *N. crassa*, the formin gene (*sepA* and *bni-1*, respectively) is essential for normal growth and mutant strains lacking these exhibit aberrant growth patterns and morphology. The product of the formin gene SepA in *A. nidulans* is concentrated in the polarisome at the tips and of hyphae and moves as the direction of growth changes (Berepiki et al., 2011). These movements are likely dictated by the action of the small GTPases Cdc42 and Rac1, both crucial for proper hyphal morphogenesis in that they modulate polarisome localization and activity.

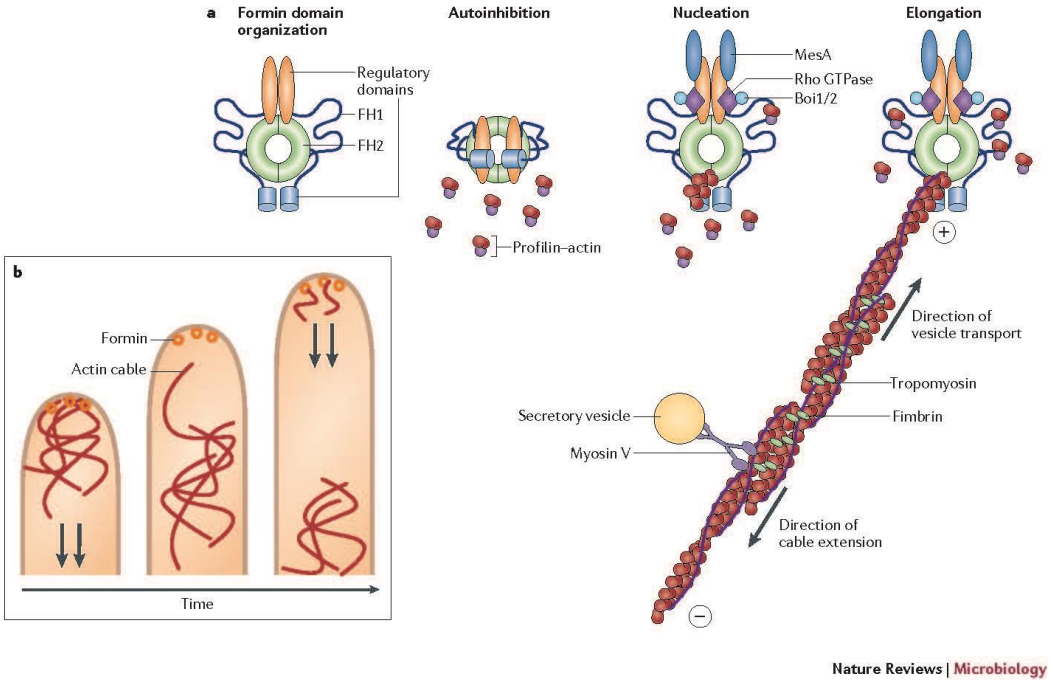

Figure 1.8: A diagrammatic representation of the nucleation and growth of F-actin cables at the tip of a hypha. a) Key domains of the nucleating protein formin are the formin homology 1 (FH1) and FH2 domains and regulatory domains. Formin is activated when it binds an activated Rho GTPase, this allows profilin–actin complexes to access the FH1 and FH2 domains. Additional regulatory proteins, such as MesA and Boi1/2, contribute to activation and localization in fungi. Profilin–actin complexes bind to the FH1 domain and are delivered to the FH2 domain, which catalyses filament nucleation in a processive manner. Assembled microfilaments are bundled into cables by fimbrin and tropomyosin and serve as tracks along which the motor protein myosin V moves secretory vesicles to sites of growth. b) In *Neurospora crassa*, dense arrays of actin cables undergo retrograde movement from the tip of germ tubes during growth. Formin-mediated cable formation has been proposed to drive retrograde movement of actin cable arrays. Reproduced with permission from Berepiki et al. (2011).

Key domains in the formins are the Rho-binding domain (RBD) and three formin-homology domains (FH1 and FH2). FH1 is rich in proline and binds profilin. Profilin is an ABP that binds to the plus end of G-actin. This facilitates the interchange of ADP for ATP in the nucleotide-binding domain of G-actin and leaves the minus end free. Both factors enhance the growth of a microfilament as they promote binding of the

monomers to the plus end of a microfilament. Thus, the FH1 domain and profilin act as a delivery system, providing monomers for the growth of a microfilament. The FH2 domain is responsible for filament nucleation binding to the plus end of two monomers initially. Additional monomers are then added (via the FH1 domain and profilin) to the plus end of these initial monomers. The FH2 domain, which binds to the plus end in a processive manner, has to change conformation to allow the addition of these new monomers. This is thought to involve a stepping-up like motion (Berepiki et al., 2011; Evangelista, Pruyne, Amberg, Boone, & Bretscher, 2002; Pollard, 2007; Pruyne et al., 2002; Sagot et al., 2002; Wallar & Alberts, 2003).

1.8.2 Microtubules

The other major cytoskeleton component that plays an essential role in fungal growth is the microtubule. In *N. crassa*, research using total internal reflection (TIRF) microscopy, has demonstrated that growth at the tips of mature hyphae is controlled by the fast dynamics of cortical microtubules which, in turn, are regulated by motor proteins (Uchida, Mouriño-Pérez, & Roberson, 2010). As detailed above, these structures are responsible for the long-distance transport of vesicles and the delivery of landmark proteins/cell end markers to the sites of growth.

Microtubules are slightly rigid, long cylinders, approximately 25 nm wide, that are formed from around 13 protofilaments. The protofilaments are formed by tubulin heterodimers, which are composed of α- and β- tubulin subunits. Both isoforms have a bound nucleotide, GTP in the case of α- tubulin (which is permanently bound) and either GTP or GDP for β- tubulin, which is bound but exchangeable. The heterodimers are polar, having a plus and a minus end, and when they assemble

into protofilaments this polarity is carried over to the polymer. Thus, microtubules like microfilaments have a polarity (Alberts et al., 2008; Berepiki et al., 2011; Lichius et al., 2011; Valiron, Caudron, & Job, 2001).

Microtubule nucleation is carried out by a multiprotein structure, the γ-tubulin ring complex (γ-TURC). Numerous γ-TURCs are part of the microtubule-organising centre (MTOC) or the nuclear envelope-associated spindle pole body (SPB) in fungi. Various proteins hold γ-tubulin in a ring structure and the structural similarity between it and the other two tubulin isoforms means that tubulin heterodimers will associate with the plus end of the γ-tubulin. Additional heterodimers will associate with the plus end of each protofilaments and so with the ring structure a microtubule will form and grow. Thus, the plus ends grow out from the SPB towards the periphery of the cell and grow parallel to the axis of growth (Figure 1.9). How cell end markers are delivered to the tips is not well understood, but TeaA is believed to play some role along with other proteins such as the microtubule polymerase, AlpA, which is an XMAP215 orthologue (Takeshita et al., 2014).

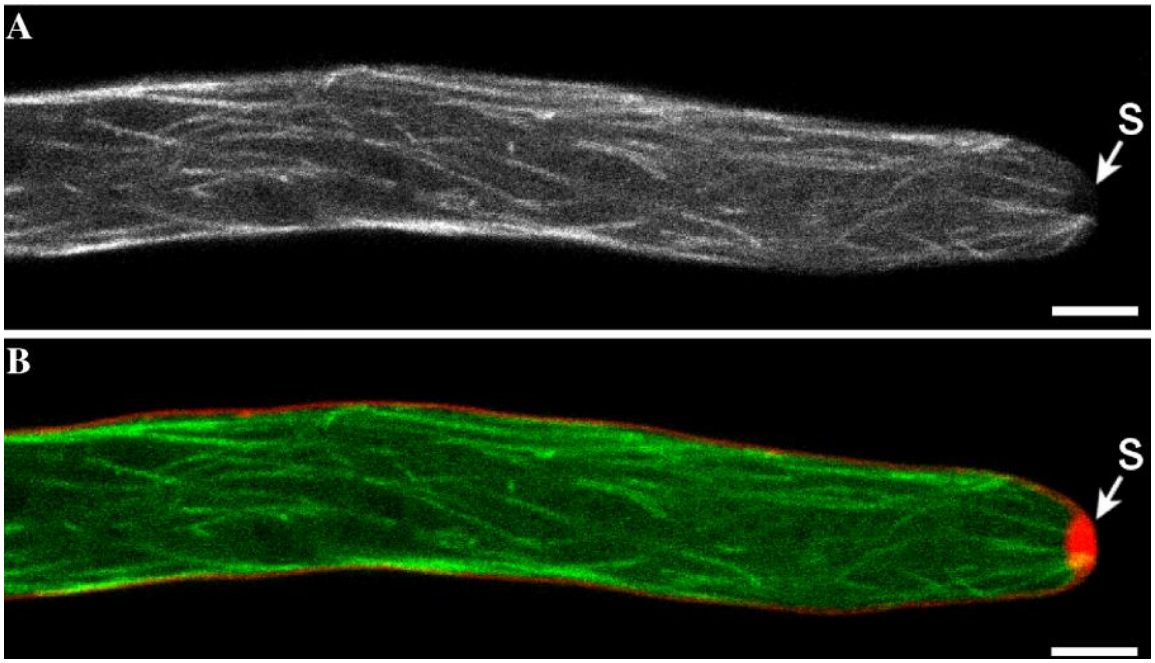

Figure 1.9: A hypha of the fungus *N. crassa* expressing β-tubulin-GFP. Microtubules extend parallel to the axis of growth (A) and toward the Spk (S) which in (B) is labeled with the membrane-selective dye FM4-64 (red). While there is no obvious Spk in oomycetes, a similar distribution of microtubules is observed. Scale bar = 5 μm. Reproduced with permission from Freitag et al. (2004).

Microtubules are prone to a phenomenon known as "dynamic instability", which occurs at the plus ends and is characterized by periods of elongation and then rapid shortening (a so-called catastrophe) (Desai & Mitchison, 1997; Levina et al., 1994; Gero Steinberg, 2007). *In vitro* assays have shown that in *Aspergillus nidulans,* the cell end marker TeaA increases the catastrophe frequency when AlpA is present, and that TeaA reduces the activity of AlpA (Takeshita et al., 2013). From this it has been postulated that plus end growth of the microtubules are promoted by AlpA, until they reach the hyphal tip. At this point, TeaA inhibits AlpA activity and induces a catastrophe event (Takeshita et al., 2013).

1.9 Invasive and non-invasive growth

1.9.1 Turgor pressure

Tip growth is often described as being driven by turgor pressure, in that a pressurized protoplast pushes against a plastic deformable wall, which will yield to that pressure. Furthermore, if a hypha is to be invasive then it needs to push against its surroundings – essentially it needs to generate a protrusive force. This will be determined by two factors – firstly the magnitude of the turgor pressure inside the cells and secondly the degree to which the tip yields to that pressure. Clearly, turgor is of vital importance to fungi and oomycetes.

Turgor is an internal hydrostatic pressure which cells generate by regulating the internal concentration of osmotically-active solutes (osmolytes), such that they are at a higher concentration than those in the surrounding media. This creates an osmotic gradient across the plasma membrane down which water will flow. The influx of water will increase the volume of the protoplast until that increase is resisted by the cell wall. Thus, a cell is said to be turgid when the plasma membrane is pressing against the cell wall. If the wall yields to this pressure, then the cell volume increases and it will grow.

Pressure, cell volume and solute concentration are intimately related as indicated by the Ideal Gas Law

$$PV = nRT$$

where P is pressure, V is cell volume, n is the number of moles of osmotically active solutes, R is the gas constant and T is temperature which can be assumed to remain constant.

Because of this, if the volume increases when the cell grows, then both the solute concentration and the pressure will decrease. Therefore, to keep growing, there needs to be an influx, or synthesis, of osmolytes and resultant uptake of water to keep the pressure constant. It should be noted, however, that the relationship between turgor and growth is complex. Kaminskyj (1992) reported that turgor was needed for growth, but that it alone was not sufficient to explain tip growth rates in the oomycete *Saprolegnia ferax*. Furthermore, certain oomycetes have also been shown to grow at very low levels of turgor (at least below our ability to measure them) (Money & Harold, 1993). This has led to the suggestion that under certain conditions the cytoskeleton itself may drive growth, with microfilament elongation at the tips of hyphae providing a pushing force similar to the lamellipodia and filapodia of migrating animal cells (Heath & Steinberg, 1999). This is an intriguing possibility especially given the fact that a wall-less (and hence turgor-less) mutant of *N. crassa* can put out extended protrusions that are similar to filapodia (Steinberg & Schliwa, 1993). However, a more likely scenario, especially in the case of the oomycetes, is extreme softening of the cell wall due to the secretion of endoglucanases (Money & Hill, 1997), which also highlights the importance of tip yielding in growth.

Turgor can be measured by a variety of indirect means (Money, 1994), but can perhaps be best measured directly using a single cell pressure probe. This relies on the insertion into a hypha of a silicon-oil filled micropipette, which is attached to a pressure transducer and which contains a motorized, thin steel rod. As the pipette enters the hypha, the protoplast will move up into the pipette due to turgor pressure, and a meniscus forms, marking the boundary between the protoplast and the silicon oil. The steel rod is then used to counter the turgor and to push the meniscus back to the mouth of the pipette. At this point, the pressure applied by the rod and measured

by the transducer is said to equal the turgor pressure of the cell. Using this technique, Lew et al. 2004 have reported values of turgor in the oomycete *Achlya bisexualis* of between 0.46 and 0.65 MPa, depending on the media in which it is growing, and Money and Harold (1993) report a turgor value of 0.4 MPa in *S. ferax*. Indirect measurements by vapor pressure deficit osmometry and incipient plasmolysis give values of between 0.3 and 2.5 MPa depending on the species (Hoch & Mitchell, 1973; Kaminskyj et al., 1992; Luard, 1982; MacDonald, 2002; Woods & Duniway, 1986). For fungal species, pressure probe measurements have given values of 0.2 MPa (Money 1994) and 0.48 MPa for *N. crassa* (Lew et al., 2004) and 1.0 MPa for *Morchella esculenta* (Amir et al., 1995). Indirect measurements on a variety of different species have given values between 0.2 and 2.5 MPa (Kelly & Budd, 1990; Robertson & Rizvi, 1968). However, specialized infection structures generate much higher values as indicated below.

The ability to keep turgor at a constant value is referred to as turgor regulation (Garrill, Clipson & Jennings 1992). This ability is important, as hyphae are likely to encounter different external solute concentrations as they move through their environment. Without turgor regulation turgor would fluctuate, which could affect the ability to grow. Lew et al. (2004) reported differences between fungi and oomycetes in their ability to turgor regulate after a hyperosmotic challenge. Their study exposed *N. crassa* and *A. bisexualis* to a shock of approximately 0.6 MPa and found that *N. crassa* was able to recover turgor, and that this was concurrent with changes in ion transport, specifically a hyperpolarization of the plasma membrane potential and a decline in transmembrane ion conductance. In contrast, *A. bisexualis*, did not recover turgor after hyperosmotic treatment, although small transient increases in turgor were occasionally observed. It was also proposed that these differences

reflected the environmental niches these two organisms are found in: *N. crassa* is a terrestrial species and thus is more likely to be exposed to environments of different osmotic potentials whereas *A. bisexualis* is aquatic where the osmotic potential is likely to be more uniform (Lew et al., 2004). Furthermore, Lew et al. (2004) concluded that, as both organisms grew at similar rates, had similar morphologies and basal levels of turgor (0.4–0.7 MPa), their different responses to hyperosmotic stress did not support a universal mechanism of tip growth that was driven by turgor.

This latter conclusion has been challenged by (Muralidhar et al., 2013), who carried out pressure probe measurements on species of the yellow-golden alga *Vaucheria*. These are Stramenopiles and, as such, are closely related to the oomycetes. Muralidhar et al. (2013) made comparisons of the turgor-regulating capacity of freshwater and estuarine species. Both were found to be able to turgor-regulate, but there was a threshold value of approximately 0.5 MPa; at values below this all species were able to turgor-regulate, but above this only estuarine species (which are exposed to constant changes in external osmotic potential due to the tidal cycle) were able to turgor regulate. Thus, Muralidhar et al. (2013, 2016) postulated that the osmotic challenge in the study of Lew et al. (2004) may have been too great for *A. bisexualis* to recover from, and that further studies were warranted with oomycetes exposed to a less severe osmotic challenge.

In pollen, reported turgor values of 0.2 MPa have been obtained with a pressure probe and 0.79 MPa via indirect methods (Benkert, Obermeyer, & Bentrup, 1997). In addition, it was found that turgor pressure was not significantly correlated with tube growth rate or with tube length. While the tubes were not challenged in the same way as in the experiments of Lew et al. (2004) and Muralidhar et al. (2016) described above, Benkert et al. (1997) found that an increase in the external osmotic pressure

from 0.36 to 1.08 MPa, decreased mean turgor pressure only slightly from 0.27 to 0.18 MPa. Thus, it was concluded that lily pollen regulates its turgor pressure well, despite substantial variations in tube growth rate, tube length, and osmotic pressure of the media.

In addition to its importance in hyphae, turgor plays other crucial roles in fungal and oomycete biology. Perhaps the most striking example occurs in appressoria, structures that have evolved in many plant pathogenic species that enable penetration of the intact cuticles of their host plants (Figure 1.2). Appressoria can form as simple terminal swellings of the tips of germ tubes emerging from spores that land on the surface of the leaf. In some species, these can become melanin-pigmented, septate structures that subsequently differentiate into dome-shaped complex infection structures (Ryder & Talbot, 2015). Irrespective of their individual structures, appressoria can generate some of the greatest turgor pressure in biology, upwards of 8 MPa (Howard et al., 1991). As the appressorium develops in the rice blast fungus, *M. oryzae*, glycerol and other polyols are synthesized rapidly. The accompanying formation of a thick, differentiated melanin layer on the inner side of the appressorium cell wall provides structural rigidity that enables such high pressures. In other species, high turgor generation and/or penetration of intact leaves is still possible even in the absence of melanin (Ludwig et al., 2014).

1.9.2 Invasive hyphal growth

As detailed in earlier sections, invasive hyphal growth is an important process in parasitic/pathogenic species as it enables hyphae to grow within host tissue. As for normal tip growth, the driving force for this invasive growth comes from turgor. Its

importance has been recognized by Money (2007) who highlighted a number of key principles:

i) turgor pressure powers the penetration of solid materials;

(ii) without turgor, hyphae are non-invasive;

(iii) the pressure exerted by the tips of hyphae appears to be controlled by loosening of the apical wall, so that a hypha with a looser apical wall applies more of its internal pressure against its surroundings;

(iv) invasive growth involves a combination of enzyme- catalysed digestion of the substrate and pressure-driven penetration of residual mechanical obstacles, and,

(v) the relative significance of enzymes and turgor in invasive growth differs from species-to-species and between substrates of varying resistance.

As Money's principles illustrate, while turgor provides a driving force, the tip of the cell has to yield to the turgor for growth to occur. The degree to which the tip yields will determine the magnitude of any protrusive force that is exerted on the surroundings. Thus, a high-yielding, more compliant tip will enable more of the turgor to be directed towards protrusion, whereas a wall that yields less and is less compliant will generate less protrusive force. The compliance of the wall will be determined by the degree of crosslinking of the wall polymers, which is influenced by the rate of crosslinking itself, once polymers are synthesized at the tip, or by the release of enzymes such as endoglucanases (Money & Hill, 1997).

It is also possible that the actin cytoskeleton plays a role in tip yielding (Walker & Garrill 2006). There is evidence to suggest that microfilaments strengthen the tip of oomycete hyphae as disruption of the F-actin cap with a UV micro-beam has been shown to cause hyphae to rupture and burst (Jackson & Heath, 1990). This has

been supported by experiments using drugs that disrupt F-actin which caused an initial increase in growth rate, as would be predicted if the actin were resisting/restraining turgor pressure at the tip (Gupta & Heath, 1997; Jackson & Heath, 1990). Presumably, if actin were strengthening the tip and effectively resisting turgor, then this would necessitate the existence of some sort of linkage to the wall back from the tip. Such wall – membrane attachment points have been observed in plasmolysed hyphae and these attachments are rich in F-actin (Chitcholtan & Garrill, 2005; Kaminskyj & Heath, 1995). Furthermore, Harold et al.(1996) exposed oomycete hyphae to low turgor conditions through the addition of sucrose to the media and reported a reduction of F-actin at the tips of hyphae. The reduction in turgor decreased the driving force for growth in these hyphae and the reduction in actin at the tip was proposed to increase compliance at the tip to enable the hyphae to grow. With respect to actual invasive growth, evidence for a possible role of F-actin in controlling tip yielding comes from the work of Walker et al. (2006) and Suei and Garrill (2008), who report higher proportions of an F-actin depleted zone in the tips of invasively growing hyphae of the oomycetes *A. bisexualis* and *P. cinnamomi* and the fungus *N. crassa,* relative to non-invasively growing hyphae (Figure 1.10). In the case of the latter species the size of the F-actin depleted zone increased as the agar concentration of the media was increased; it was proposed that with more agar, a greater penetrative force was required for growth through the agar and that the F-actin depleted zone was a means of accomplishing this. There was a corresponding increase in cofilin, an F-actin depolymerizing protein, at the tips of invasive hyphae compared to non-invasive hyphae (Suei & Garrill, 2008) and, conversely, a decrease in the actin-nucleating protein formin (Suei and Garrill; unpublished results).

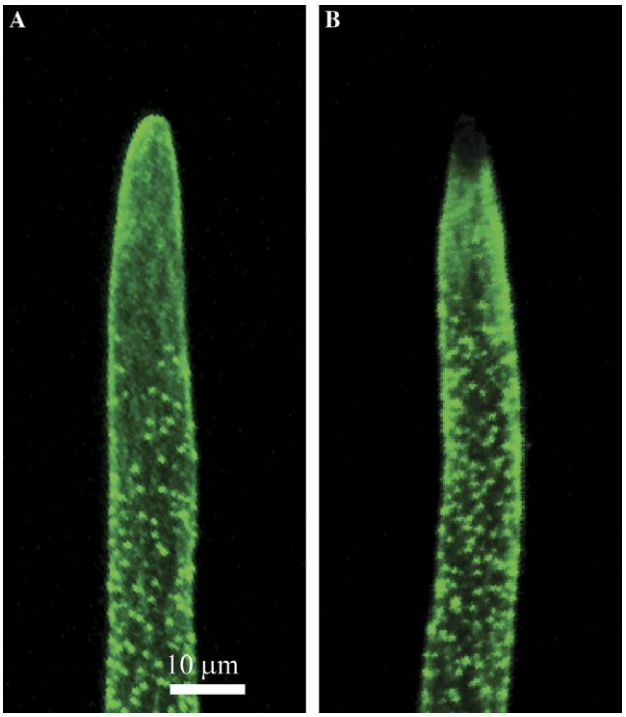

Figure 1.10: Confocal images showing microfilaments in non-invasive (A) and invasive (B) hyphae of the oomycete *A. bisexualis*. The invasive hypha has a distinct F-actin depleted zone at the tip of the hypha whereas the non-invasive hypha has an F-actin cap. The depleted zone was proposed to increase the protrusive force that was required for protrusive growth. Hyphae were fixed and stained with Alexa 488 Phalloidin. Similar arrangements of microfilaments have been observed in non-invasive and invasive hyphae of the fungus *N. crassa*. Figure reproduced with permission from Walker et al. (2006).

1.9.3 Protrusive force

Measurements of protrusive forces have been made using a variety of techniques. These include substrates with calibrated stiffness (e.g. agarose), waveguide sensors, optical traps and micro-strain gauge placed in front of an advancing cell (Nezhad & Geitmann, 2013) (Figure 1.11). Of these, micro-strain gauge cantilevers have proven to be most suitable in measuring the force magnitude. Money et al., (2004) combined micro-strain gauge measurements with pressure probe measurements and reported that for *A. bisexualis*, pressures of 0.11 MPa were

exerted on the gauge by hyphae that had turgor of 0.69 MPa. This indicates that only 16 percent of turgor was generating protrusive force at the tip and is consistent with low compliance of the wall/cytoskeleton at the tip. That is, the tip does not yield much to the turgor pressure. For other oomycete species, Money et al. (2004) reported values ranging from 2% to 54% of turgor generating protrusive force, with the higher value only observed under certain conditions. For fungal species, these values ranged from 9% to 32%, again suggestive of a non-compliant tip (Money et al., 2004). However, the strain gauge technique risks underestimating the effective invasive force in hyphae because of a cellular shape change upon orthogonal contact of the tip-growing cell with the flat surface of the sensor. Furthermore, Walker et al. (2006) have argued that the strain gauge does not permit the measurement of forces in invasive hyphae as they grew out of agar media prior to hitting the gauge and thus could be considered non-invasive hyphae.

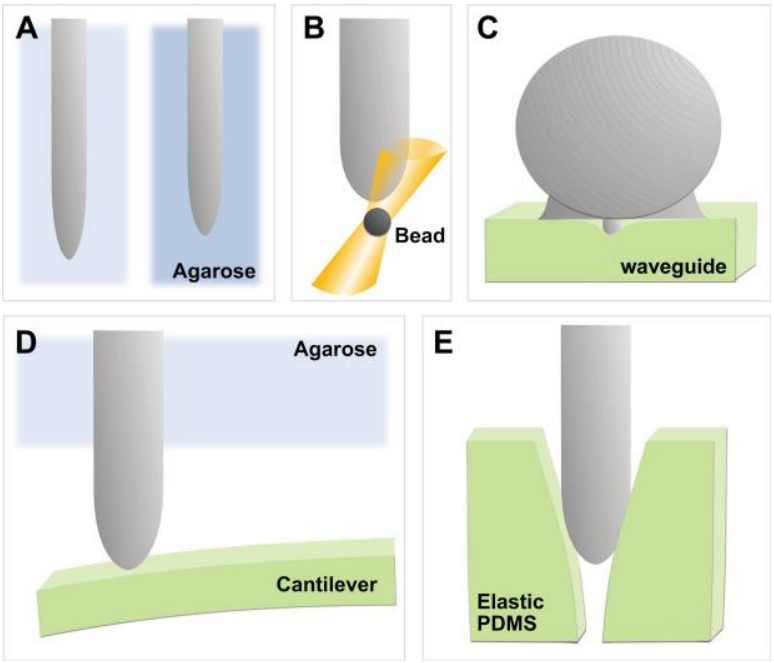

Figure 1.11: Various strategies have been used to measure protrusive force in tip growing systems. These include substrates with calibrated stiffness (A), optical trapping of beads in the growth path of a cell (B), attachment to a waveguide (C), displaceable cantilevers, in the micro-strain gauge, that are placed perpendicular to the growth path (D) and wedge-shaped openings in PDMS microfluidic devices that have calibrated plasticity. Reproduced with permission from Nezhad and Geitmann (2013).

The problems with the micro-strain gauge have been somewhat overcome by researchers who have grown pollen tubes into narrow openings in channels that were made using microfluidic Lab-on-a-Chip (LOC) technology from materials with calibrated elasticity such as polydimethylsiloxane (PDMS). These narrow openings were presented as obstacles to the pollen tubes growing on the chip. Finite element modeling, and measurement of the dilating force exerted normal to the gap wall, were then used to deduce the penetration pressure as the pollen tubes grew into the openings (Nezhad et al., 2013). These techniques have led to the measurement of a maximum protrusive pressure of 0.15 MPa. As detailed earlier, reported values of turgor in pollen are around 0.2 MPa. These values are suggestive of a much more

compliant tip in pollen compared to oomycete and fungal hyphae. This means that a much higher proportion of turgor (around 75%) is generating protrusive force rather than overcoming wall/cytoskeletal resistance. However, there is still the question of the accuracy of the micro-strain gauge and how this may have impacted the protrusive pressure values for the oomycete and fungal hyphae.

Advances in micro-fabrication and live-cell imaging have meant that microfluidic devices are increasingly being used to study the forces that guide cellular processes, and such devices have been used extensively to measure mechanical forces in animal cells (Harris et al., 2011; Iskratsch et al., 2013). However, as evidenced by the pollen work above, LOC technology has begun to be adapted for use with tip-growing organisms. Other studies include the measurement of mechanical forces in fission yeast cells (Minc et al., 2009), the study of maze solving and dynamic behavior of basidiomycete fungi (Hanson et al., 2006) and the study of contact-induced apical asymmetry in the thigmotropic responses of *Candida albicans* (Thomson et al., 2015; Thomson et al., 2016). More advanced devices have been employed to quantify the Young's modulus of primary plant cell walls (Nezhad et al., 2013) characterize the 3D morphology and mechanics of developing plant cells (Felekis et al., 2015; Hu et al., 2017; Shamsudhin et al., 2016) and perform high-throughput analysis of single cell polarized growth and dynamics (Agudelo et al., 2013; Geng et al., 2015).

A technically simpler approach to measure forces exerted by cells and organisms as they grow, and move is to use elastomeric micropillar arrays which were initially developed to study traction forces in cells. Such pillar arrays have been adopted for use with smaller single organisms such as nematodes (Johari et al, 2013). This approach typically combines optical tracking of a pillar top with a simple mechanical

model. These are then used to measure forces as the organism/cell grows or pushes against the pillar(s). Given the correct modifications, these arrays are applicable to oomycetes and fungi and could provide the capability to also determine the directionality of forces. Additionally, the appropriate design of the devices and use of appropriately transformed/stained hyphae should enable the observation of cellular dynamics/changes that might underlie force generation.

1.10 Summary and Hypotheses

From the above discussion, it is clear that fungi and oomycetes are very important groups of organisms playing key roles in the ecosystems where they are found. At the same time, they can have severe detrimental effects causing disease in both plants and animals. The key vegetative structure of both of these groups of organisms is the hypha, which has evolved to enable both penetrative growth and provide a high surface area to volume ratio. This is ideally suited to both the search for and the uptake of nutrients.

Hyphae extend by the process of tip growth, a very complex process characterized by localized extension at the very tip of the cell. This occurs by the localized delivery of wall synthesizing machinery and tip yielding in response to turgor pressure at the sites of growth. The degree of compliance of the tip will determine the protrusive force that a hypha will be able to impart on its substrata. This force, coupled with the secretion of enzymes that will break down the substrate enable the hyphae to grow invasively which is a key to fungal and oomycete pathogenicity.

The cytoskeleton is thought to play a key role in tip growth. Microfilaments and microtubules provide the tracks along which motor proteins move, delivering cell wall

synthase containing vesicles to the tips but also moving organelles such that they retain characteristic distributions as the tip moves forward. Microtubules also deliver cell end marker proteins, which are crucial for polarity development and maintenance. Microfilaments and associated motor proteins generate force for endocytosis, but they also may provide restraint at the tip and thus play a key role in regulation of tip compliance. The presence of an F-actin depleted zone may be indicative of areas where tip yielding occurs.

Our understanding of the link between the cytoskeleton and the generation of protrusive force is limited, in part because direct measurement of that force is difficult in invasive hyphae and also because there have been no simultaneous measurements of force and imaging of the cytoskeleton. Protrusive force measurements have recently been made on tip growing pollen tubes using microfluidic LOC devices. These devices have great potential for force measurements on individual hyphae and could enable concurrent force measurement and cytoskeletal imaging.

In view of these questions, this thesis describes the development of species-specific LOC devices that incorporate micropillar arrays that enable simultaneous force measurement and cytoskeletal imaging in individual hyphae.

The hypotheses tested are:

1. Protrusive force in hyphae of fungi and oomycetes can be measured using micropillar arrays in LOC devices.
2. LOC devices will enable the measurement of protrusive force in invasive hyphae.

3. The LOC devices will enable concurrent measurement of protrusive force and cytoskeletal imaging.
4. Microfilaments restrain the tips in hyphae and an F-actin depleted zone at the tip is responsible for the provision of protrusive force.
5. Microtubules extend to the tips of invasive hyphae.

Two species have been investigated, the fungus *N. crassa* and the oomycete *A. bisexualis*. These were chosen for the reasons detailed below.

1.10.1 *Neurospora crassa*

N. crassa is an ascomycete and is a red bread mold which typically lives in tropical and sub-tropical regions, growing on dead plant matter, particularly after fires. It has been a mainstay in scientific research and has been central to our understanding of the molecular events that underlie many aspects of eukaryotic cell biology, genetics and biochemistry including circadian rhythms, epigenetics and gene silencing, cell polarity, cell fusion and development. It was central to Beadle and Tatum's work on the relationship between genes and proteins which led to the 'one-gene-one-enzyme' hypothesis (Tatum & Beadle, 1945). Its widespread use in research comes about partly because of its ease of culture, relatively rapid growth rate and its haploid life cycle. Transformed strains of the fungus are widely available from resources such as the Fungal Genetics Stock Centre.

The *N. crassa* genome was sequenced in 2003, which revealed a 40-Mbase genome that contains approximately 10,000 protein-coding genes (Galagan et al., 2003). With respect to our understanding of fungal cell biology and fungal growth, *N. crassa* has perhaps been just as useful (if not more useful) than the other model fungal

organism, the yeast *Saccharomyces cerevisiae*, given that its hyphal growth form is more representative of the majority of fungi than the yeast growth form. Thus, *N. crassa* has been described as the workhorse of fungal research and a key tool in research to further our understanding of the establishment and maintenance of polarity, hyphal tip growth, septation, branching and differentiation (Riquelme et al., 2011)

With respect to the proposed research in this thesis, concurrent measurement of protrusive force and cytoskeletal imaging are of great interest given the observation of an F-actin depleted zone in invasive hyphae of *N. crassa* (Suei & Garrill 2008). Also, it has been shown to grow successfully in LOC devices (Geng et al., 2015). Transformed strains of *N. crassa* have been developed that express fluorescent LifeAct (Roca et al., 2010) and the use of these strains provides the possibility to image the dynamics of microfilaments concurrently with making force measurements. Furthermore, strains expressing fluorescent tubulin should enable similar experiments looking at the role of microtubules in invasive growth and force generation.

1.10.2 *Achlya bisexualis*

While there are several species of fungi that can be regarded as “model organisms” such as *Saccharomyces cerevisiae, Schizosaccaromyces pombe, N. crassa, Aspergillus nidulans* and *Ashbya gossypii*, there are no classic model oomycetes. The publication of the genomes of several oomycetes (Tripathy et al, 2006) means that the oomycetes are now more amenable to molecular investigations, and transformed species of *Phytophthora* are available (Kortekamp et al., 2017).

However, the strict rules regarding the import of these strains into New Zealand mean that such lines are not be available for research carried out in laboratories in this country. An application to import transformed *P. infestans* from the Netherlands for the research in this thesis was declined by the Environmental Protection Agency.

Investigations using *Saprolegnia ferax,* which belongs to the order *Saprolegniales*, a grouping that includes fish pathogens, has revealed much about tip growth in the oomycetes. This species is ideal for such work because of its relatively ease of culture and growth, its large hyphal size and its ease with respect to imaging of the cytoskeleton. *Achlya bisexualis* offers all of these qualities, but this species has also been used in many studies of turgor and tip growth (Money & Harold, 1993; Walker et al., 2006). Furthermore, there are reports of protrusive force measurement using cantilevers (Money et al., 2004). For these reasons, *A. bisexualis*, which was isolated from a New Zealand source, was chosen as the representative oomycete in this thesis.

CHAPTER 2

Materials and Methods

2.1 Materials

2.1.1 Liquid and Solid Reagents

Liquid reagents that were used in the research were obtained from the following sources (Table 2.1) while solid reagents were obtained from other sources (Table 2.2).

Table 2.1 Liquid reagents

Component	Source/Origin
AF1	Citifluor, Hatfield, PA, USA
Glycerol	BDH, Poole, England
Methanol	Thermo Fisher Scientific, Auckland, NZ
DMSO	BDH
Triton X-100	BioRad, Hercules, CA, USA
Tween-20	BioRad
Ethanol	BDH
Formaldehyde	Thermo Fisher Scientific
Methylglyoxal (Acetylformaldehyde)	Sigma Aldrich, Switzerland
Isopropanol	Thermo Fisher Scientific
Acetone	Thermo Fisher Scientific
Positive Photoresist AZ12XT	M.M.R.C. Malvern, Vic, Australia
Positive Photoresist AZ40XT	M.M.R.C.
Polydimethylsiloxane-PDMS-Sylgard 184	Dow Corning, Auburn, MI, USA
Propylene Glycol Monomethyl Ether Acetate	Sigma Aldrich, St Louis MO, USA
Trichloro(1H,1H,2H,2H-perfluorooctyl) Silane	Sigma Aldrich
Developer AZ326MIF	M.M.R.C
Chloroform	Thermo Fisher Scientific

Table 2.2 Solid reagents

Component	Source/Origin
Agar Bacteriological (Agar Nº 1)	OXOID, Hampshire, England
Bacteriological Peptone (IVD)	OXOID
Yeast Extract (IVD)	OXOID
D- (+)-Glucose	VETEC, Sigma Aldrich, Auckland, NZ
UltraPure L.M.P.(Low-Melting-Point) Agar	Invitrogen, ThermoFisher, Auckland, NZ
Sucrose	OmniPur, Calbiochem, Atlanta, GA, USA
PIPES [piperazine-N,N'-bis(2-ethanesulfonic acid)]	Sigma Aldrich, St Louis MO, USA
EGTA	Sigma Aldrich
Carbendazim (MBC)	Sigma Aldrich
Latrunculin B	Sigma Aldrich, Seelze, Germany
Oryzalin	Sigma Aldrich
Biotin	Sigma Aldrich
Bovine Serum Albumin (BSA)	Sigma-Aldrich, Auckland, NZ
Alexa Fluor 488 phalloidin	Invitrogen, ThermoFisher, Auckland, NZ
Driselase, from Basidiomycetes	Sigma Aldrich
Beta-D-Glucanase G	InterSpex, San Mateo, CA, USA
o-Phenylenediamine Dihydrochloride Tablet Sets	Sigma Aldrich
Ammonium Nitrate (NH_4NO_3)	Sigma Aldrich
Sodium Citrate ($Na_3C_6H_5O_7\ 2H_2O$)	BDH, Poole, England
Boric Acid, anhydrous (H_3BO_3)	Sigma Aldrich
Calcium Chloride Dihydrate ($CaCl_2.2H_2O$)	BDH
Citric Acid ($C_6H_8O_7 1\ H_2O$)	J. T. Baker, Center Valley, PA, USA
Copper Sulfate Pentahydrate ($CuSO_4.5H_2O$)	Sigma-Aldrich, United Kingdom
Disodium Hydrogen phosphate (Na_2HPO_4)	Sigma-Aldrich, NZ

Ferrous Ammonium Sulfate Hexahydrate ($Fe(NH_4)_2(SO_4)2.6H_2O$)	BDH
Sodium Molybdate dihydrate ($Na_2MoO_4.2H_2O$)	BDH
Magnesium Chloride ($MgCl_2$)	BDH
Magnesium Sulfate Heptahydrate ($MgSO_4.7H_2O$)	BDH
Manganese Sulfate Monohydrate ($MnSO_4.1H_2O$)	BDH
Monopotassium phosphate, anhydrous (KH_2PO_4)	Sigma-Aldrich, NZ
Negative Photoresist ADEX	Microlaminates, USA
Potassium Chloride (KCl)	Thermo Fisher Scientific,Auckland, NZ
Potassium Hydroxide (KOH)	Thermo Fisher Scientific
Skimmed Milk Powder	Anchor, Auckland, NZ
Sodium Chloride (NaCl)	Thermo Fisher Scientific
Trichloro(1H,1H,2H,2H-perfluorooctyl) silane ($CF_3(CF_2)_5CH_2CH_2SiCl_3$)	Sigma-Aldrich
Tris-Hydrochloride (Tris-HCL)	Sigma-Aldrich
Tris	Invitrogen, ThermoFisher, Auckland, NZ
Sodium Azide (NaN_3)	Thermo Fisher Scientific
Zinc Sulfate Heptahydrate ($ZnSO_4.7H_2O$)	BDH

2.2 Methods

2.2.1 Stock Cultures

2.2.1.1 *Achlya bisexualis*

A female strain of the oomycete *A. bisexualis* (Coker, 1927), which was originally isolated in New Zealand from *Xenopus laevis* dung, was obtained from the culture collection of the University of Canterbury. The stock culture was maintained at room temperature on PYG agar media. The PYG media was made up with distilled water and contained bacteriological peptone (1.25 $g.L^{-1}$), yeast extract (1.25 $g.L^{-1}$), glucose (3 $g.L^{-1}$) and bacteriological agar (20 $g.L^{-1}$). The strain was subcultured weekly using a 6 mm cork-borer to cut a mycelial agar plug from the growing edge of a colony grown on a Petri dish and then transferred to a new dish containing PYG media.

2.2.1.2 *Neurospora crassa*

Several different strains of the fungus *N. crassa* (Shear & Dodge, 1927) were used including wildtype strains, along with strains that had been transformed to express fluorescent β-tubulin and fluorescent LifeAct, which were used to image microtubules and microfilaments respectively (Berepiki et al., 2010; Uchida et al., 2010). *Neurospora crassa,* mating type A (C213) and mating type a (C212) wild type strains were obtained from the University of Canterbury culture collection. *N. crassa* strains FGSC# 9519 mating type **a** (rid(RIP4) mat a his-3+::Pccg-1-Bml+-sgfp+) and FGSC# 9520 mating type **A** (rid(RIP1) mat A his-3+::Pccg-1-Bml+-sgfp+), used to image microtubules, were imported from the Fungal Genetic Stock Centre (University of Missouri, Kansas City, USA). *N.* crassa strains FGSC#10598 mating type **a** (pAL12-

Lifeact [Ptef-1::Lifeact-TagRFP-T::nat1]) and FGSC#10599 mating type **A** (pAL12-Lifeact [Ptef-1::Lifeact-TagRFP-T::nat1]), which express LifeAct-RFP, were imported from the Fungal Genetic Stock Centre (University of Missouri, Kansas City, USA).

These were maintained at room temperature on Vogel's Medium N (Minimal) (Vogel, 1956) which was made up in a multi-step procedure (Table 2.3).

Table 2.3. Vogel's minimal media

Basic media

contents	*amount per litre*
Sucrose	15 g
Agar	15 g
Vogel's 50X salts	20 mL

Vogel's 50X salts

contents	*amount per litre*
$Na_3C_6H_5O_7\ 2H_2O$	125 g
KH_2PO_4	250 g
NH_4NO_3	100 g
$MgSO_4.7H_2O$	10 g
$CaCl_2.2H_2O$	5 g
Vogel's trace element solution	2.5 mL
Biotin solution (0.1 $g.L^{-1}$)	2.5 mL
chloroform (as a preservative)	2.7 mL

Vogel's trace element solution

contents	*amount per litre*
$C_6H_8O_7.1\ H_2O$	5 g
$ZnSO_4.7H_2O$	5 g
$Fe(NH_4)_2(SO_4)_2.6H_2O$	1 g
$CuSO_4.5H_2O$	0.25 g
$MnSO_4.1H_2O$	0.05 g
$Na_2MoO_4.2H_2O$	0.05 g
chloroform (as a preservative)	10 mL

The strains were subcultured weekly by using a 6 mm diameter cork-borer to obtain mycelial agar plugs from the growing edge of a colony grown on Petri dishes. These were transferred to a new Petri dish containing Vogel's minimal media.

2.2.1.3 Experimental Cultures

For experimental purposes, cultures were initially grown on cellophane overlaying the respective growth media described above. This ensured that hyphae grew in a more linear fashion and that individual hyphae were easier to resolve. Thus, either Vogel's (*N. crassa*) or PYG (*A. bisexualis*) media in a Petri dish was overlaid with an 85 mm wide sterile circular piece of colorless cellophane (Hallmark Brand). Prior to sterilization the cellophane pieces were washed in boiling water for 30 min, with a change of water every 10 min, to ensure that any chemical residues from manufacturing were eliminated. Cellophane membranes were sterilised using an autoclave prior to use.

Petri dishes were inoculated with 6 mm wide mycelial agar plugs, taken from the growing edge of a stock culture using a 6 mm diameter cork-borer. The experimental cultures were grown at 26°C for 2-5 days (*A. bisexualis*) or 24 h (*N. crassa*) prior to use. In some instances, the cellophane impacted on the ability to image the hyphae, or in the case of the PDMS chips, affected the growth of the hyphae into the channels. In these instances, experimental cultures were set up without the cellophane overlay on the Petri dish.

In order to stimulate invasive growth in *N. crassa* cultures (i.e. growth through the agar rather than on top of it), experimental cellophane plates containing Vogel's media were inoculated and incubated at 26°C for 20 h. After the incubation, the

cultures were overlaid with 1%, 2%, 3% or 4% (w/v) low melting point (LMP) agar, to form a thin layer of agar on top of the colony. The cultures were left for 2 h to resume their growth, then hyphae were cut 1.5 cm behind the growing edge of the colony inverted and placed on a 35 mm Fluorodish cell culture dish (World Precision Instruments, Sarasota, FL USA). These dishes were necessary when experiments were observed using the inverted confocal microscope.

2.2.2 PDMS Chips

The chips used to perform experiments to measure protrusive forces were made with polydimethylsiloxane (PDMS). The basic principle behind the chips was that growing hyphae would grow into small PDMS pillars and deflect them, and that the degree of displacement of the pillar would enable the estimation of a protrusive force exerted by the tips of the hyphae. Further details of the principles underlying the chips and protrusive force measurement are covered in Chapter 3.

2.2.2.1 PDMS Chips - *A. bisexualis*

Several PDMS chips were designed for use with *A. bisexualis*. These consisted of a seeding area in which agar mycelial plugs could be inoculated, multiple channels that were intended to direct the growth of the hyphae toward sensor pillars inside the channels, and an inlet area for the application of liquid media. The individual designs differed in overall layout of the various compartments, channel number, channel dimensions, pillar arrangement and pillar dimensions. The design layouts are described in more detail in Chapter 3.

The PDMS chips were fabricated using replica-molding of a two-layer resist master, which was a combination of negative and positive photoresists. Briefly, two 10.2 cm diameter chrome-on-glass photomasks (Nanofilm, Westlake Village, CA, USA) were prepared using a laser mask writer (uPG101, Heidelberg Instruments, [Heidelberg, Germany). The first layer mask contained the channel outlines and ports (Figure 2.1a), while the second mask contained the same features, plus the measurement pillars (Figure 2.1b).

Initially a 5 µm-thick negative-tone resist (ADEX5, DJDevcorp, Sudbury, MA, USA) was laminated in parallel onto a clean 10.2 cm diameter silicon wafer using a hot-roll laminator (SKY335R6, Sky-Dsb, Seoul, Korea). Lamination was performed at 65°C and at the speed 1 setting. Then, the first layer mask was exposed to the ADEX5 layer using a mask aligner (MA-6, Suss MicroTec, Garching, Germany) set in the vacuum contact mode with a filter (PL-360), using a dose of 170 mJ/cm^2. This was followed by a ramped post-exposure bake for 5 min at 65°C and 10 min at 95°C on a contact hotplate (HP30, Torrey Pines Scientific, Carlsbad, CA, USA). The wafer was developed in propylene glycol monomethyl ether acetate, rinsed with isopropanol and dried using nitrogen gas.

A second layer of positive-tone photoresist AZ40XT (M.M.R.C, Malvern, Vic, Australia) was spin-coated at 2000 rpm for 30 s onto the first layer to a thickness of 25 µm using a spin-coater (WS-650, Laurell, North Wales, PA, USA). A thick positive resist, rather than a negative resist, was used for this layer defining the measurement pillars in order to overcome the optical problem of shadow-masking a high-aspect cavity inside a narrow channel into a lithographically simpler layer. After edgebead removal, the resist was soft-baked for 3 min at 126°C on a hotplate and exposed using the second layer mask. This was followed by a post-exposure bake

for 80 s at 105°C on a contact hotplate. Transferred patterns were developed by immersion into developer (AZ326MIF, M.M.R.C) for 3 min, rinsed with distilled water and dried using nitrogen (Figure 2.1c).

Before PDMS casting, the mold was treated for 2 h with trichloro(1H,1H,2H,2H-perfluorooctyl) silane in a vacuum to facilitate mold release. The PDMS base was mixed with a curing agent at a 10:1 (w/w) ratio, degassed and then poured onto the mold. After baking for 2 h at 80°C on a hotplate, the cured PDMS was peeled off from the mold and baked for an additional 4 h at 80°C to ensure the desired hardening (Figure 2.1c).

To prevent hyphae growing above the channels and the pillars, glass covers were placed onto the chips. These were prepared by drilling holes into standard 75 x 25 mm glass microscope slides (VWR, Auckland, NZ) using a 3 mm diameter diamond-coated hole drill (28.5030, Esslinger, Saint Paul, MN, USA). The covers were manually aligned to the seeding and the inlet areas on the chips, and bonded using a 30 s exposure to 100 W oxygen plasma in a barrel asher (Emitech K1050X, Quarum Technologies, Laughton, East Sussex, UK). Then the chips that were bonded to the glass covers were baked for 2 h at 80°C on a hotplate to strengthen the bonding. Once ready, the PDMS chips were placed in a vacuum chamber and degassed for 2 h to prepare for vacuum-assisted filling. Degassed chips were sealed into food-grade vacuum bags using a vacuum sealer (Sun-beam Food Saver) and stored until use.

When the chips were prepared for observation through the confocal microscope, they were bonded upside down to the bottom of a Fluorodish. Prior to attachment, the chips were punched with a 3 mm biopsy punch to get access to the seeding area

and the media supply area. After bonding, the process was the same as described above for the chips that were attached to the glass microscope slides.

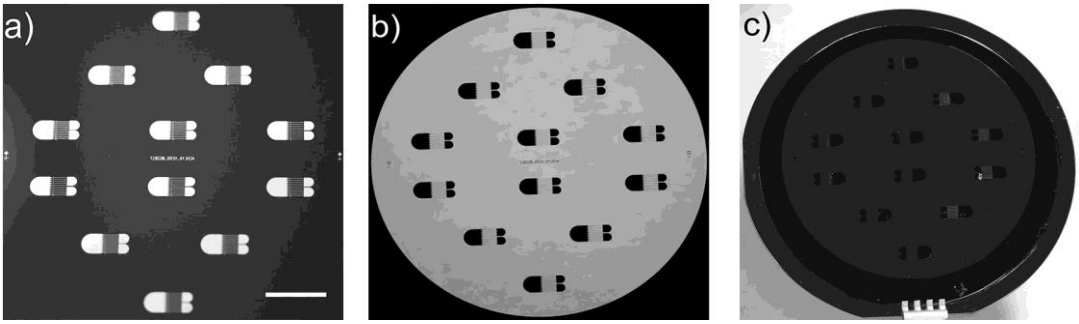

Figure 2.1: Images of the two 10.2 cm diameter chrome-on-glass photomasks. The first negative layer contained the channel outlines and ports (a). The second positive layer containing the channel outlines, seeding areas, media supply areas and measurement pillars (b). The silicon wafer with the transferred pattern of the chips (c). Scale bar = 2 cm.

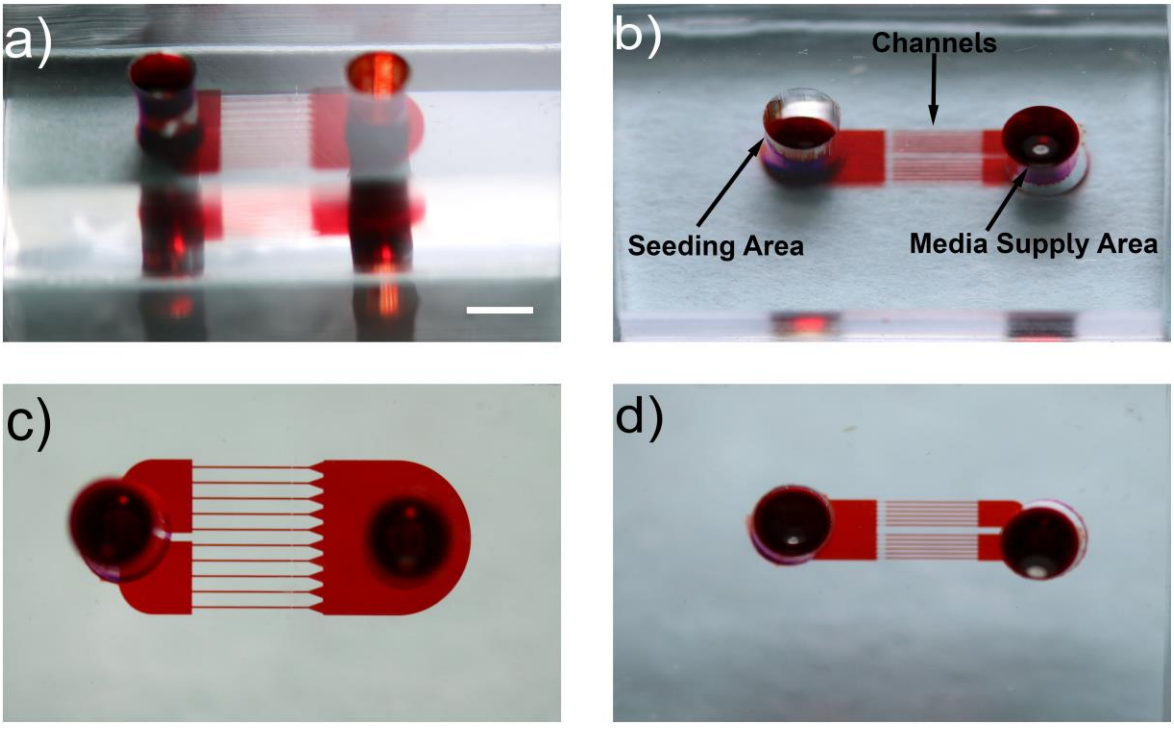

Figure 2.2: PDMS chips for *A. bisexualis* (a and c) and *N. crassa* (b and d). The chips have been filled with red food coloring to enhance imaging of the seeding area, the channels and the media supply area. Scale bar = 0.3 cm.

2.2.2.2 PDMS chips – *N. crassa*

The basic design of the chips that were used for *N. crassa* were the same as for *A. bisexualis,* although the smaller size of the *N. crassa* hyphae meant that the dimensions of the channels and pillars had to be changed. Again, two 10.2 cm diameter chrome-on-glass photomasks (Nanofilm) were prepared using a laser mask writer (uPG101, Heidelberg Instruments), with the first layer mask containing the channel outlines and ports, and the second mask the same features plus the measurement pillars. The negative resist AZ15nXT (M.M.R.C.) was spin coated at 5000 rpm for 30 s onto a silicon wafer. Then, the first layer mask was exposed to the AZ15nXT layer using a mask aligner (MA-6, Suss MicroTec) in vacuum contact mode at 90 mJ/cm^2. This was followed by a post-exposure bake of 1 min at 120°C on a contact hotplate (HP30, Torrey Pines Scientific). The wafer was developed in AZ326MIF (M.M.R.C) for 50 s, rinsed with water and dried using nitrogen. A second layer of positive-tone photoresist AZ12XT (M.M.R.C) was spin-coated at 1500 rpm onto the first layer to a thickness of 12 µm using a spin-coater (WS-650, Laurell). After edgebead removal, the resist was soft-baked for 3 min at 110°C on a hotplate and exposed using the second layer mask. This was followed by a post-exposure bake of 1 min at 90°C on a contact hotplate. Transferred patterns were developed by immersion into developer AZ326MIF (M.M.R.C) for 2 min, rinsed with distilled water and dried using nitrogen.

A PDMS copy of the mold was produced using the same protocol as described above for the *A. bisexualis* chips.

2.2.2.3 Inoculation of PDMS Chips

Prior to inoculation onto PDMS chips, experimental cultures of *A. bisexualis* and *N. crassa* were grown as described above. Initially, these were grown on the cellophane overlay, but this was found to affect the growth of the hyphae in the channels and so the cellophane was subsequently omitted. Three millimeters diameter agar plugs were obtained from the growing edge of a colony using a biopsy punch.

The PDMS chips were bonded to glass microscope slides, which had holes drilled in them to provide access to the seeding area and the media supply area. Prior to inoculation, the chips were filled with PYG (*A. bisexualis*) or Vogel's (*N. crassa*) broth (Figure 2.3a) and checked using a Nikon Eclipse 80i microscope to ensure that all the channels were filled with media. PYG broth was prepared with distilled water and contained bacteriological peptone (1.25 $g.L^{-1}$), yeast extract (1.25 $g.L^{-1}$) and glucose (3 $g.L^{-1}$). Vogel's broth was made with distilled water containing sucrose 15 ($g.L^{-1}$) and 20 $mL.L^{-1}$ of Vogel's 50X salts (Table 2.3).

Chips were inoculated using a scalpel to transfer an inverted agar plug (with the hyphae on the bottom of the plug) into the seeding area of a chip (Figure 2.3b). The inoculum was positioned such that the hyphal tips were facing towards the entrance of the channel. The chips were kept at room temperature in the dark for the duration of an experiment, typically between 8 to 12 h, depending on the growth rate of the hyphae on the chips. The chips were monitored every 30 min to check the growth of the hyphae and, if necessary, to top up the PYG or Vogel's broth, thereby avoiding dehydration of the hyphae. The hyphae were checked more frequently, using the 5X (NA 0.15) and 10X (NA 0.30) objectives of a Nikon Eclipse 80i upright microscope fitted with a digital camera (ORCA-Flash 4.0 V2, Hamamatsu, Hamamatsu City,

Japan), once they were close to the entrance of the channels. When the tip of the hyphae was about 100 µm from the sensor pillars the 20X (NA 0.50) or 50X (NA 0.80) objectives were used to record the deflection of the top of the pillars.

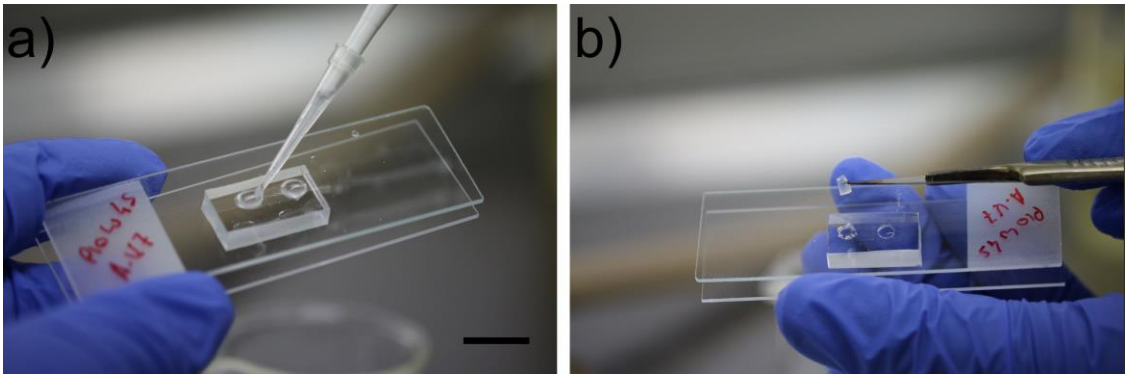

Figure 2.3: Inoculation of a PDMS chip with *A. bisexualis*. The media supply area was filled with PYG broth (a). An agar plug on which hyphae are growing is placed in the seeding area to inoculate the chip. The plug was inverted to ensure that the hyphae were on the bottom of the plug (b). Scale bar = 2 cm.

For experiments involving the imaging of chips using a confocal microscope, cultures were grown and maintained as per the protocol described above. However, to obtain the inocula, a slightly smaller 2.5 mm biopsy punch was used to cut the agar plug and was used to inoculate PDMS chips that had been bonded to Fluorodishes. Again, the inoculum was positioned such that the hyphal tips were facing the entrance of the channels. The chips were kept at room temperature in the dark for the duration of an experiment, typically between 8 to 12 h depending on the growth rate of the hyphae. The chips were monitored every 30 min to check the growth of the hyphae and, if necessary, to top up the PYG or Vogel's broth. The hyphae were checked more frequently once they were at the entrance of the channels, using the 20X (NA 0.7) objective of a Leica SP5 confocal microscope system with a DMI6000 inverted microscope (Leica, Wetzlar, Germany). When the tip of a hypha was at about 100 µm from the sensor pillars the 63X (NA 1.3) glycerol immersion objective was used to record the deflection of the top of the pillars. For the *N. crassa* strains expressing β-tubulin-GFP, the argon laser at 488 nm and 30% intensity was used for

excitation. The emission bandwidth used was 496-592 nm. The fluorescence was detected concurrently with transmitted light images collected with bright field optics.

For experiments with invasive *N. crassa* hyphae, chips which had been bonded to fluorodishes, were placed in a 50°C oven 2 h prior to inoculation. As these experiments required the channels to be filled with low melting point agar this pre-heating was necessary to prevent the solidification of the media while it was flowing through and filling the channels. Vogel's broth containing either 1 or 2 % (w/v) LMP agar was heated in a microwave prior to pouring into the chips. This contained sucrose (15 $g.L^{-1}$), LMP agar (10 or 20 $g.L^{-1}$ for 1% or 2% (w/v) agar) and 20 $mL.L^{-1}$ of Vogel's 50X salts (Table 2.3).

Once the chip was full and the agar had solidified, a 2.5 mm biopsy punch was used to remove a block of agar from the seeding area. This block was then replaced with an agar inoculation plug that had been taken from the growing edge of an experimental culture, as described above (with the cellophane omitted). This agar plug was inverted such that the hyphae were on the bottom of the plug once it was placed in the seeding area of the chips. The plug was oriented such that the hyphal tips were facing the channel entrance. The hyphae were then observed using the confocal microscope as described earlier.

2.2.3 Force Measurement

The deflection of the pillars, as hyphae grew into them, was observed with a 20X (NA 0.50) and a 50X (NA 0.80) objective on a Nikon Eclipse 80i microscope and was recorded using a digital camera (ORCA-Flash 4.0 V2, Hamamatsu). The microscope

was, for the most part, focused on the top of the pillar, rather than the tip of the hypha. The camera was connected to a computer and images were collected as TIFF files using HCImageLive (Hamamatsu) software. Initially, the TIFF image was used to create an AVI file to determine whether pillar deflection had occurred. The TIFF images were then imported into ImageJ (V1.51 h, FIJI installation) as a sequence, converted into an 8-bit-gray-scale format and the deflections of the pillars were tracked using the TrackMate plugin (V3.4.2). Tracking files were imported into MATLAB (2016a, Mathworks) as a BMP file and a custom script was used, in conjunction with pre-calibrated mechanical pillar properties, to convert the measured deflections into force magnitudes and directions. The height of the contact point on the pillar was determined on the microscope by focusing on the top of the pillar, then re-focusing on the hyphal tip and recording the distance as indicated by the microscope focus knob that the stage had moved. In addition to ImageJ, the TIF files were also imported into Adobe Photoshop CS6 and used to determine hyphal growth rates and diameters.

Some experiments were carried out using the confocal microscope on which images were obtained by using a 63X glycerol immersion objective lens. For these experiments, the height of the contact point on the hyphae with the pillars was confirmed by performing a Z-Stack series which were imported and analysed with ImageJ. The images sequences obtained were processed using LAS AF Lite 2.6.0 (Germany) and then imported to ImageJ and converted to 8-bit-gray-scale format. The deflections of the pillars were tracked using the TrackMate plugin and the tracking files were imported into MATLAB and processed as described above.

For *A. bisexualis* the contact point on the pillars was further determined using fluorescence imaging with the confocal microscope. For these experiments hyphae

were inoculated and grown on PDMS chips as described earlier (Section 2.2.2.3). Just prior to the hyphae growing into the pillars the PYG broth on the chip was replaced with PYG containing tartrazine (trisodium 1-(4-sulfonatophenyl)-4-(4-sulfonatophenylazo)-5-pyrazolone-3-carboxylate)), which is a synthetic lemon-yellow dye that is commonly used as a food colouring (E102). The tartrazine was bought as Hansells Yellow Colouring (Hansells Food Group, Auckland, NZ) and obtained from a local supermarket (Pak n Save, Papanui, Christchurch). Solutions on the Chip were changed using a perfusion method that is described in more detail below (Section 2.2.4.4). Hyphae and pillars were then imaged with the confocal microscope using the 63X (NA 1.3) glycerol objective lens. Tartrazine was excited using the argon laser at 488 nm with 30% intensity with an emission bandwidth of 502-605 nm. The fluorescence was detected concurrently with transmitted light images collected with bright field optics.

2.2.4 Cytoskeletal imaging

Microfilaments and microtubules were imaged in both invasive and non-invasive hyphae of *N. crassa* using transformed strains expressing β-tubulin-GFP and LifeAct-RFP respectively. LifeAct is an actin-binding protein and in the transformed strains this was fused with RFP. To complement these experiments, immunolabelling was also used. For *A. bisexualis*, no transformed strains were available and so immunolabelling and Alexa Fluor 488-phalloidin labelling were used.

2.2.4.1 Live Imaging of transformed β-tubulin-GFP *N. crassa*

Invasive cultures of *N. crassa* strains expressing β-tubulin-GFP were set up using four different agar concentrations (1%, 2%, 3% and 4% (w/v)) and a non-invasive culture was set up with Vogel's broth. After the cultures were placed onto Fluorodishes they were then examined with the confocal microscope using the 63X (NA 1.3) glycerol objective lens. The GFP tag was excited using the argon laser at 488 nm with 30% intensity with an emission bandwidth of 500-550 nm. The fluorescence was detected concurrently with transmitted light images collected with bright field optics.

2.2.4.2 Live Imaging of transformed LifeAct-RFP *N. crassa*

N. crassa strains expressing the LifeAct-RFP protein fusion were cultured in PYG agar 2% (w/v) and grown at 26°C for 2 days. Hyphae were cut 1.5 cm behind the growing edge of the colony inverted and placed on a 35 mm Fluorodish cell culture dish. Once the cultures were ready, they were examined with the confocal microscope using the 63X (NA 1.3) glycerol objective lens. The RFP tag was excited using the DPSS 561 nm laser with 20% intensity with an emission bandwidth of 570-672 nm. The fluorescence was detected concurrently with transmitted light images collected with bright field optics.

2.2.4.3 Alexa-phalloidin staining of microfilaments in *A. bisexualis*

Hyphae that were to be stained with Alexa Fluor 488-phalloidin were obtained by cutting mycelial sections of agar about 1.5 cm from the growing edge of an experimental colony and these were placed in a Fluorodish and left in the dark for an hour to recover growth. After that, they were fixed for 45 min with fixative solution (as described in the immunological staining section above) and then rinsed twice with saline solution, for 15 min each time. The hyphae were then stained with Alexa Fluor 488 phalloidin at a concentration of 200 U/mL (300 U diluted in 1.5 mL methanol), for 30 min. During staining the cultures were kept in the dark to prevent photo-bleaching. After staining, the hyphae were washed two times with saline solution for 15 min each. After the second wash, 0.1% (w/v) p-phenylenediamine was added as an antifading agent, then the samples were covered with tin foil and left in the fridge until they were observed. Stained hyphae were observed using the 63X (NA 1.3) glycerol immersion objective lens. Alexa Fluor phalloidin 488 was excited by the argon laser at 488 nm and at 30% intensity. The emission bandwidth used was 500-681 nm. The fluorescence was detected concurrently with transmitted light images collected with bright field optics. Confocal images were processed using LAS AF Lite 2.6.0 (Germany) and Adobe Photoshop CS6 (64 Bit, Ireland). The pictures collected were imported into ImageJ and then analysed with Adobe Photoshop CS6.

For observation of microfilaments in hyphae growing in channels on the PDMS chips, *A. bisexualis* was grown and maintained as per the protocol described above. Once the hyphae were around 50-100 µm from the pillars, the PYG broth in the chips was replaced with fixative solution. This was done by first removing some of the PYG

broth from the seeding area on the chip using a pipette and then, before the channels dried out, adding the fixative solution to the media supply port. As they were close to the pillars, the hyphal tips were closer to the media supply port than the seeding area. Also, the added solution was expelled with force from the tip of the pipette such that the solution reached the growing tip of a hypha mostly by convectional flow, rather than just by simple diffusion. All subsequent solution changes were performed using this perfusion technique. The hyphae were fixed for 45 min with additional fixative solution added to the supply port as required to prevent the channels drying out. After fixation they were rinsed twice with saline solution, for 15 min each time. The hyphae were then stained with Alexa Fluor 488-phalloidin for 30 min. During staining the cultures were kept in the dark to prevent photo-bleaching. After staining the hyphae were washed twice each time for 15 min. After the second wash 0.1% (w/v) p-phenylenediamine was added as an anti-fading agent and the samples were covered with tin foil and left in the fridge until they were observed using the confocal microscope under the settings described above.

2.2.5 Actin Inhibitor Experiments

2.2.5.1 The effect of microfilament inhibition on growth on Petri dishes

To test the effect of microfilament inhibition on hyphal growth of *A. bisexualis* and *N. crassa* on Petri dishes, aliquots of latrunculin B (from a 2 mM stock solution made up in DMSO) were added to PYG or Vogel's media prior to pouring into the dishes to give final concentrations of 1, 0.5, 0.1 and 0.05 µM respectively. After swirling to ensure mixing, the agar was poured and allowed to set. A mycelial plug taken from

the edge of an experimental culture was used to inoculate the dishes. For control experiments, DMSO at a concentration of 0.05% (v/v) (i.e. the highest concentration that the hyphae were exposed to on the experimental dishes) was used. Six replicate plates at each concentration were made, and the cultures were kept at 26°C for 51 h (*A. bisexualis*) or 16 hours (*N. crassa*). Radial growth was measured over this period by drawing six lines that were separated by an angle of 60^{o} from the edge of the inoculation plug and then measuring how far the edge of the colony had grown along these lines and taking an average value.

2.2.5.2 The effect of microfilament inhibition on growth on PDMS chips

In order to investigate the effects of microfilament inhibition on hyphal growth and protrusive force, hyphae from an experimental culture were inoculated onto PDMS chips, as described earlier. After checking that the hyphae were growing normally in the channels, 0.05 μM (*A. bisexualis*) or 1 μM latrunculin B (*N. crassa*) was added when they were approximately 50 μm from a pillar. The different concentrations reflected the differing sensitivities to the inhibitors of the two species, as determined from the Petri dish experiments.

Latrunculin B (from the 2 mM stock solution) was added using the perfusion system (section 2.2.4.3), via the media supply inlet to give a final concentration of 0.05 mM. The volume of liquid in a chip was calculated to be approximately 20 μL (in both *A. bisexualis* and *N. crassa* chips). Again, the latrunculin was added with a pipette and was expelled with force from the tip, such that the inhibitor reached the hyphae mostly by convectional flow rather than simple diffusion. The latrunculin B was

dissolved in DMSO and the highest concentration of DMSO that hyphae were exposed to (0.025% v/v) was used as a control experiment. Once the latrunculin B was added, growth and pillar deflection were observed and recorded, and protrusive force was calculated as described previously.

Experiments were carried out to image the microfilaments in latrunculin B-treated *A. bisexualis* hyphae on PDMS chips. PDMS chips were inoculated with *A. bisexualis* as described previously. When the hyphae were around 50 μm from the pillars the PYG broth was replaced with 0.05 μM latrunculin B using the perfusion system. After either 15 or 30 s the latrunculin B was replaced with the fixation solution. The hyphae were fixed for 45 min with additional fixative solution added to the supply port as required to prevent the channels drying out. All solution changes were made using the perfusion system (section 2.2.4.3). After fixation they were rinsed twice with saline solution, for 15 min each time. The hyphae were then stained with Alexa Fluor 488 phalloidin for 30 min. During staining the cultures were kept in the dark to prevent photo-bleaching. After staining the hyphae were washed twice each time for 15 min. After the second wash, 0.1% (w/v) p-phenylenediamine was added as an antifading agent, then the samples were covered with tin foil and left in the fridge until they were observed using the confocal microscope as described above.

2.2.6 Microtubule Inhibitor Experiments

2.2.6.1 The effect of microtubule inhibition on growth on Petri dishes

To test the effect of microtubule inhibition on hyphal growth of *A. bisexualis* and *N. crassa* on Petri dishes, aliquots of oryzalin (from a 20 mM stock solution made up in DMSO) was added to PYG or Vogel's media prior to pouring into the dishes to give final concentrations of 1, 0.5, 0.1 and 0.05 µM for *A. bisexualis* and 1, 0.5 and 0.1 µM for *N. crassa*. After swirling to ensure mixing, the agar was poured and allowed to set. A mycelial plug taken from the edge of an experimental culture was used to inoculate the dishes. For control experiments DMSO at a concentration of 0.05% (v/v) (i.e. the highest concentration that the hyphae were exposed to on the experimental dishes) was used. Six replicate plates at each concentration were made, and the cultures were kept at 26°C for 51 h (*A. bisexualis*) or 16 h (*N. crassa*). Radial growth was measured over this period by drawing six lines that were separated by an angle of 60^{o} from the edge of the inoculation plug and then measuring how far the edge of the colony had grown along these lines, and an average was taken.

Additional microtubule inhibitor experiments were carried out on *N. crassa* with carbendazim (MBC). Basically, the same methodology was used as for the oryzalin experiments. MBC, rather than oryzalin, was added at final concentrations of 0.005 µg.mL^{-1}, 0.01 µg.mL^{-1}, 0,025 µg.mL^{-1}, 0.05 µg.mL^{-1}, and 0.07 µg.mL^{-1} via serial dilutions of a 10 mg.mL^{-1} MBC stock solution in DMSO. DMSO at a concentration of 0.07% (v/v) was used as a control, as well as plain Vogel's medium plates. The cultures were incubated at 26°C for 24 h and growth was determined as previously described.

2.2.6.2 The effect of microtubule inhibition on growth on PDMS chips

In order to investigate the effects of microtubule inhibition on hyphal growth and protrusive force in *N. crassa*, hyphae from an experimental culture were inoculated onto PDMS chips as described earlier. MBC was introduced using the perfusion technique to give a final concentration of 0.05 μg .mL^{-1} as hyphae were approximately 50 μm from the pillars. Five repetitions of the same concentration were performed. Once the MBC was added, growth and pillar deflection were observed and recorded, and protrusive force was calculated as described previously.

2.2.7 Statistical Analysis

Statistical analyses were perform using OriginPro 8 (OriginLab, UK). One-Way ANOVA was used to test for statistical significance. The following denotations; $p \leq 0.05$ - *, $p \leq 0.01$ - **, $p \leq 0.001$- ***, $p \leq 0.0001$ - ****, were used to show statistical significance.

CHAPTER 3

THE DESIGN AND FABRICATION OF AN ELASTOMERIC MICROPILLAR PLATFORM FOR THE STUDY OF PROTRUSIVE FORCES IN HYPHAE

Portions of the work in this chapter have been published in the following journal and conference proceedings:

- **Tayagui A**., Sun Y., Collings DA., Garrill A. and Nock VM. (2017) An elastomeric micropillar platform for the study of protrusive forces in hyphal invasion*. Lab on a Chip* 17(21): 3643-3653.
- **Tayagui, A**. Garrill, A., Collings, DA., and Nock, V. (2016) On-chip measurement of protrusive force exerted by individual hyphal tips during hyphal growth. *Proceedings of the 20th MicroTas Conference*, Dublin Ireland, pp 150-151.
- Nock, V., **Tayagui, A.** and Garrill, A. (2015) Elastomeric Micropillar Arrays for the Study of Protrusive Forces in Hyphal Invasion. *Proceeding of the 19th International Conference on Miniaturized Systems for Chemistry and Life Sciences*, Gyeongju, South Korea, pp 692-694.

3.1 Introduction

As discussed in Chapter 1, invasive growth is important in both pathogenic and non-pathogenic fungi and oomycetes. Invasive growth is possible through the generation of a protrusive force and the secretion of enzymes that break down host tissue and their substrata (Money, 2004). Protrusive force is a product of turgor pressure and tip yielding or compliance. The more compliant the tip, the greater the protrusive force that turgor is able to generate. To fully understand the process of invasive growth we need to be able to measure protrusive force and to concurrently image/perturb the components that underlie its generation. This is not an easy proposition, given the small size of cells and that the forces are likely in the micro-Newton range.

A variety of methods have been used to measure the forces generated by individual cells. These include inducing cells to grow and/or move into piezo-resistive cantilevers or into substrates with a calibrated stiffness (Nezhad & Geitmann, 2013), the use of optical/magnetic tweezers (Conia et al., 1997; Zhang et al, 2010), atomic force microscopy (Charras et al, 2001) and magnetic beads (Fass & Odde, 2003). Another approach has been the development of microfluidic LOC devices.

These had their origin more than thirty years ago when cross-linked silicon fluids were used to characterize mechanical interactions between cells and their environment (Harris et al., 1980). Thin, flexible siliconised structures have since been used to measure traction forces generated by smooth muscle and epithelial cells (Du Roure et al., 2005; Tan & Desai, 2003), and cardiac myocytes (Zhao & Zhang, 2006). Microfluidic devices have been used to investigate various aspects of the biology of fungal cells, such as fission yeast cell division (Minc et al., 2009), thigmotropic responses in *Candida albicans* (Thomson et al, 2015) and growth of

Neurospora crassa (Geng et al, 2015), but to the best of my knowledge none have been designed and used specifically for the measurement of protrusive force. In addition, there appear to be no reports of the growth of oomycetes on LOC devices.

With respect to other tip growing cells, LOC devices have been used to measure penetrative pressures in pollen tubes (Nezhad et al, 2013). Narrow openings in PDMS channels on LOC devices, that had a calibrated elasticity, were used to present an obstacle to pollen tube growth. As the tubes grew down the channels, they penetrated the openings. Then finite element modeling and measurement of the dilating force exerted normal to the gap wall were used to deduce a penetration pressure of 0.15 MPa (Nezhad et al., 2013). This pressure was close to previously reported values of turgor pressure in pollen tubes (0.2 MPa up to 0.35 MPa), suggesting that the wall was relatively compliant, i.e. a high proportion of turgor was generating protrusive force rather than overcoming wall/cytoskeletal resistance.

Another means of measuring force on LOC microfluidic devices involves PDMS based micropillar arrays, which have been used in a variety of cell types including the nematode worm *Caenorhabditis elegans* (Ghanbari et al., 2012; Johari et al., 2013). This technique is reliant upon the cells making contact with the pillars, with a vision-based algorithm then used to resolve both the magnitude and the direction of the force from the deflection of the cantilever-like pillar. A key to the success of such an array lies in its design. Johari et al (2013) used two different LOC devices, termed the lattice and honeycomb designs, for the micropillar arrays and found that the design and layout of the pillars significantly affected the contraction force, the locomotion speed and the undulation frequency of *C. elegans*. Maximal forces of between 19 μN (lattice) and 33 μN (honeycomb) were measured.

While the size of a typical nematode (~20 µm wide and ~1 mm) is much larger than that of oomycete or fungal hyphae (5 - 20 µm diameter), given the correct modifications using photolithographic miniaturization approaches, it is likely that these arrays are applicable to micro-Newton force measurement in hyphae. Furthermore, they would provide the ability to measure force directionality. LOC devices are also likely to enable the concurrent measurement of force and imaging of cellular components.

In view of the above, an initial study was carried out to design and fabricate LOC devices containing micropillar arrays that enable the measurement of protrusive force in oomycete and fungal hypha. Key considerations and questions in the design were:

(1) Will hyphae grow on the devices at similar rates to what they would grow on Petri dishes?
(2) Will hyphae on the devices have a similar morphology to those grown on Petri dishes?
(3) How reliably will hyphae grow into the micropillar arrays?
(4) How reliably will hyphae deflect micropillars?
(5) How easily can hyphae be inoculated onto the devices?
(6) How rapidly can solution changes be made on the devices?
(7) Will the devices enable high resolution imaging of the pillar tops?
(8) Will the devices enable imaging of transformed or stained hyphae on a confocal microscope?

The results of this investigation are described in this chapter. A more detailed consideration of the capability of the devices to measure force and hyphal characteristics is covered in the following chapter (Chapter 4).

3.2 Materials and Methods

The materials and methods were as described in Chapter 2

3.3 Results

In total, seven different types of chips were designed and fabricated. Five of these (referred to as *A. bisexualis* Version 1, 2, 3, 4 and 5 chips) were for use with *A. bisexualis* and two (termed *N. crassa* Version 1 and 2) were for use with *N. crassa*. The chips differed in pillar and channel characteristics and these are summarized in Table 3.1.

Chip Version	Pillar arrangement	Tapered/Straight channels	Channel width*/depth (μm)	Pillar height (μm)	Pillar widths (μm)
Achlya bisexualis					
Version 1	Lattice	-	-	30	15
Version 2	Array	Tapered	30/35	30	10
Version 3	Single	Tapered	30/35	30	10
Version 4	Single	Tapered	35/30	25	5, 7, 10
Version 5	Single	Straight	35/30	25	5, 7, 10
Neurospora crassa					
Version 1	Single	Tapered	10, 17/16	13	5, 7
Version 2	Single	Tapered	10, 17/14	11.4	5, 7

Table 3.1 Key characteristics of the different chips. Further details of the chips are given in the relevant sections of the results. Version 1 *A. bisexualis* chips did not contain any channels. * represents the width of the channel at the narrowest point. The different channel and pillar widths were all on different chips, not on the same chip.

3.3.1 *Achlya bisexualis* Version 1 chips

The first chips (Version 1) were, essentially, proof-of-concept devices that were intended to address the questions posed in the introduction of this chapter, namely, would hyphae grow on the devices at similar rates and have a similar morphology to those on Petri dishes? Would they reliably grow into and deflect the micropillars? The design also took account of the need for devices that could be inoculated easily.

These chips were based on those previously used to measure the forces exerted by nematode worms (Ghanbari et al., 2012; Johari et al., 2013) and comprised a lattice arrangement of pillars and an adjacent pillar-free seeding area (Figure 3.1). Individual pillars were 15 μm in diameter and 30 μm high and there was a 5 μm spacer-layer to enable free movement of the pillar tops.

A. bisexualis hyphae grew on these chips at an average rate of 5.1 ± 0.3 μm/min (mean ± SD; range = 4.7 – 5.9 μm/min (n = 20 hyphae)) (Figure 3.2). This was slightly, but significantly (student's t-test ($P < 0.05$)), slower than the average rate of 6.1 ± 0.5 μm/min (mean ± SD; range = 5.7 – 6.9 μm/min (n = 5 Petri dishes)) for hyphae growing on Petri dishes (as measured by the colony diameter).

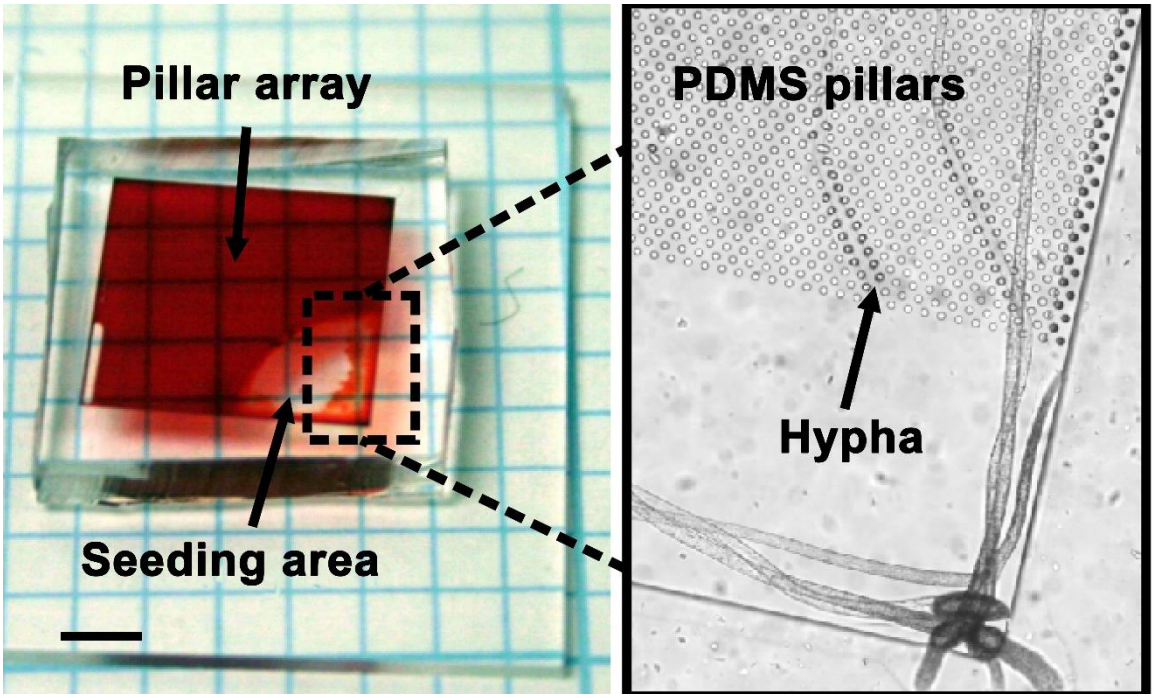

Figure 3.1: *A. bisexualis* chip design Version 1. A whole chip is shown on the left and is filled with red food coloring to show the seeding area and the pillar arrays and in the enlargement (right) inoculated hyphae can be observed growing on the chip and extending out into the pillar arrays. Scale bar (left = 5 mm, right = 20 μm)

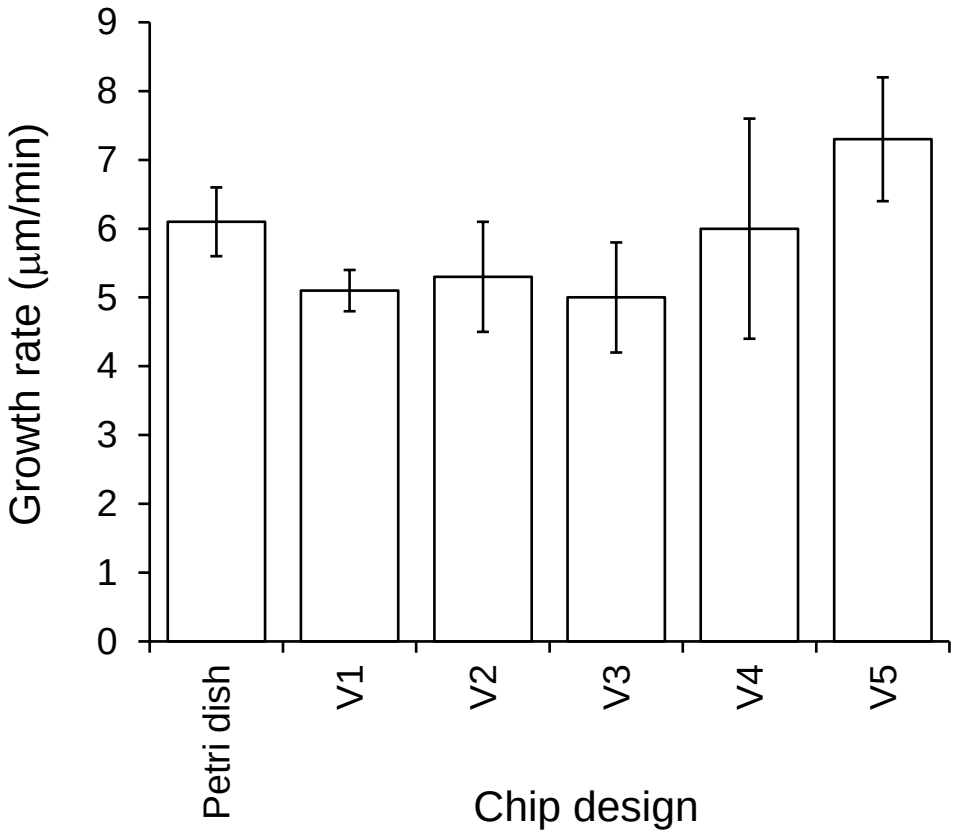

Figure 3.2: Growth rate of *A. bisexualis* hyphae on the various chip designs. V1- V5 refers to Version 1 – Version 5 chips. Data are the mean growth rates ± SD (n = 20 hyphae for the chips and n = 5 Petri dishes).

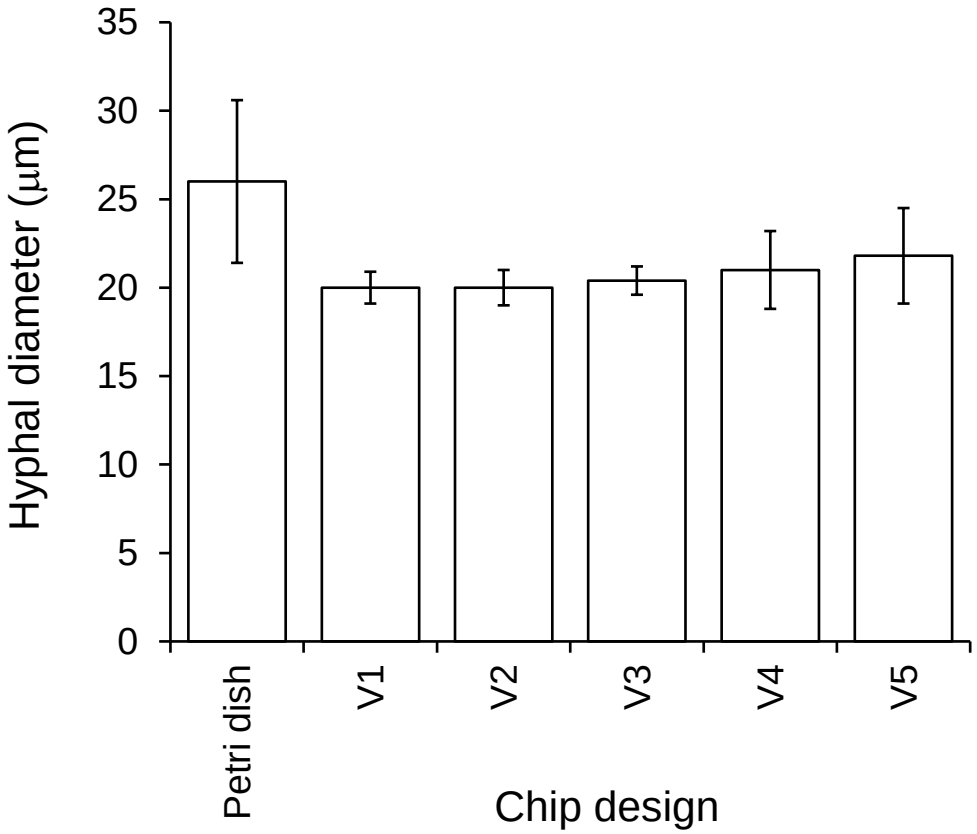

Figure 3.3: The diameter of *A. bisexualis* hyphae (mean ± SD, n= 20 hyphae) as measured 100 μm behind the tips. V1 - V5 refers to Version 1 – Version 5 chips.

The tips of hyphae on the Version 1 chips had the long-defined taper that is typical of *A. bisexualis* and the mean diameter taken 100 μm behind the tip was 20 ± 0.9 μm (mean ± SD; range = 18.5 - 22.4 μm (n = 20 hyphae)) (Figure 3.3). This was significantly narrower than the average diameter of 26 ± 4.6 μm (mean ± SD; range = 19.6 – 39.2 μm (n = 20 hyphae)) of hyphae that were grown on Petri dishes.

Hyphae tended to grow between the pillars (Figure 3.4) and so it was not possible to reliably measure protrusive forces at the tips of hyphae. Despite this the pillars were capable of measuring a squeezing force as the flanks of the hyphae pushed against and displaced the pillars once the tip had grown beyond the pillar (Figure 3.4).

While the Version 1 chips were easily inoculated, supported growth of hyphae that had a normal morphology and enabled the measurement of squeezing force, their use was discontinued as they were unsuitable for reliable measurement of protrusive force at the tips of hyphae

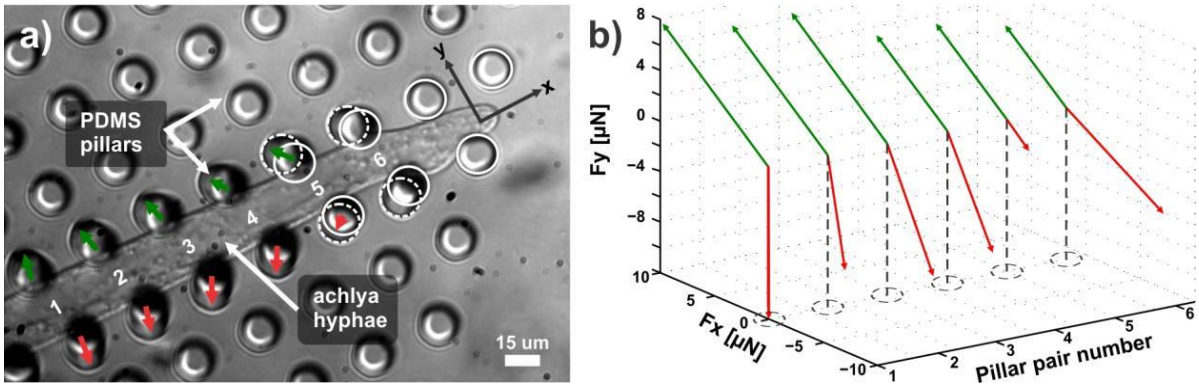

Figure 3.4: The measurement of squeezing forces using the Version 1 chips. While the tips avoided contact with the pillars the subapical flanks of the hyphae tended to push against the pillars causing pillar displacement (a). The solid white circles indicate the original pillar position for pillar pairs 5 and 6 and the dashed lines indicate displacement of the pillars (a). This enabled the measurement of force in both the x- and y- direction (b).

3.3.2 *Achlya bisexualis* Version 2 and 3 chips

From the images showing the growth of hyphae on Version 1 chips in Figure 3.4, it was evident that the arrangement of the pillars precluded measurement of protrusive force, as the gaps between the pillars were sufficiently large that the hyphae were able to grow between the pillars, with the hyphal tips able to avoid collision with the pillars. In view of this, a further four chips were then designed with the pillars in narrow and/or tapered channels that emanated out either radially (effectively star shaped) (Version 2 and 3) or linearly (Version 4 and 5) from a seeding (inoculation) area (Figures 3.5 – 3.8). The idea behind these designs was that the hyphal tips would be more likely to hit the pillars because of the tapering and the narrowness of channels. This design provided challenges with fabrication, as the narrowness of the channels meant that it was at times difficult to produce the pillars without some damage or fabrication residue (see for example Figure 3.5c, Figure 3.6b). Some of these chips had to be discarded because of these problems, although those that had their pillars largely intact still enabled the measurement of protrusive force.

In Version 2 chips, sixteen channels radiated out from a central seeding area (Figure 3.5a, b). This enabled the measurement of protrusive forces from multiple hyphae on the same device (considered in more detail in Chapter 4). The radial design was conceived because it meant that, as hyphae grew out from the edges of the circular inoculation plug, there would be channels surrounding the plug. This meant that more of the hyphae had the potential to grow down the channels and into the pillars. The pillars, which were 35 µm high, were arranged in a tapered array that was located 400 µm from the entrance of a tapered channel (as shown by the area in the white box in Figure 3.5b and Figure 3.5c). The channels were 35 µm deep ensuring a gap of 5 µm between the top of the pillar and the channel lid. The tapering of the

channels and pillars was intended to guide the hyphal tips into one of the pillars. Beyond the pillar array, the width of the channels remained constant to the individual media supply areas, which were designed to facilitate solution changes.

Hyphae grew down the channels at an average rate of 5.3 ± 0.8 µm/min (mean ± SD; range = 4 – 6.5 µm/min (n = 20 hyphae)) (Figure 3.2). The mean hyphal diameter taken 100 µm behind the tip was 20 ± 1.0 µm (mean ± SD; range = 18.5 – 21.8 µm (n = 20 hyphae)) (Figure 3.3). Hyphae grew down the tapered channels and the tips impacted with the pillars enabling the measurement of protrusive forces, which are considered further in Chapter 4.

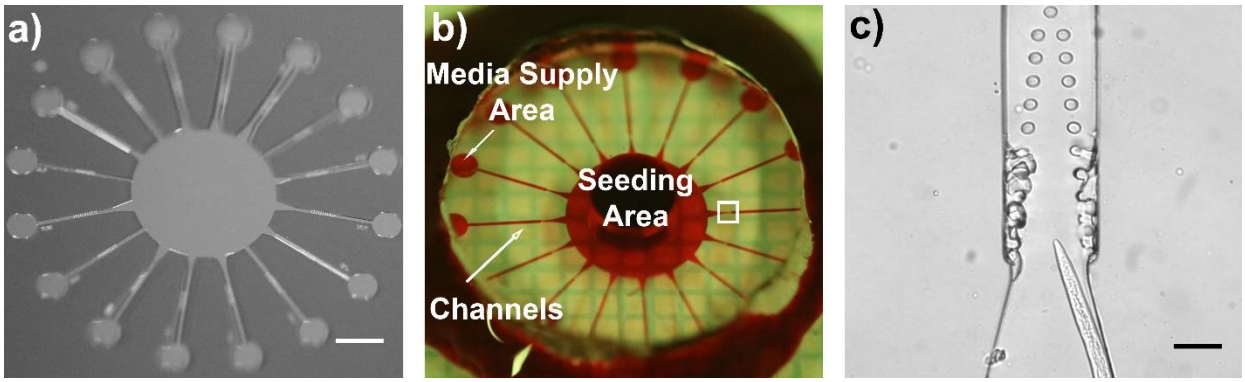

Figure 3.5: *A. bisexualis* chip design Version 2. Sixteen channels emanated out radially from a central seeding area, where mycelial plugs were placed to inoculate the devices (a, b). In (b) the device has been filled with red food dye to highlight the various areas. The white box indicates the area in one of the channels where it narrowed into a tapering array of pillars (b). Beyond the pillar arrays channels were straight and ended in media supply areas that enabled solution changes. Hyphae grew down the channels with the tapers of both the channel and the pillar arrays directing growth towards the pillars (c). Some chips contained fabrication residue which can be clearly seen in (c). Scale bars: a, b = 7 mm, c = 105 µm.

Version 3 chips had a similar design to the Version 2 chips with sixteen narrow channels emanating from a central seeding area and ending in media supply areas. The channels had a narrow taper and contained a single 30 µm high pillar rather than a tapered array of pillars (Figure 3.6). The width of the channel was 35 µm at the narrowest point and the pillar width tested was 10 µm. The gap between the edge of the pillar and the side of the channel was 12.5 µm. The channels were 35 µm deep. Hyphae grew down the channels at an average rate of 5.0 $\pm$ 0.8 µm/min (mean ± SD; range = 3.8 – 6.4 µm/min (n = 20 hyphae)) (Figure 3.2). The mean diameter taken 100 µm behind the tip was 20.4 ± 0.8 µm (mean $\pm$ SD; range = 18.9 – 21.6 µm (n = 20 hyphae)) (Figure 3.3). For those hyphae that grew into the pillars, the pillars were deflected better, and a force was measured. Again, this is considered in more detail in Chapter 4.

For both the Version 2 and 3 chips, the growth rates were slightly (but significantly (student's t-test ($P<0.05$)) slower than the average rate of 6.1 ± 0.5 µm/min (mean ± SD; range = 5.7 – 6.9 µm/min (n = 5 Petri dishes)) for hyphae growing on Petri dishes (Figure 3.2). There was no significant difference between the growth rates of hyphae on the Version 1, 2 or 3 chips (student's t-test ($P>0.05$)). The hyphal diameter was significantly narrower (student's t-test ($P<0.05$)) on Version 2 and 3 chips, compared to hyphae growing on Petri dishes (26 ± 4.6 µm (mean ± SD; range = 19.6 – 39.2 µm (n = 20 hyphae))) (Figure 3.3). However, despite this difference they still displayed the typical hyphal shape of healthy growing hyphae with their characteristic taper at the apex. There was no significant difference in the diameters of the hyphae on the Version 1, 2 or 3 chips (student's t-test ($P>0.05$)).

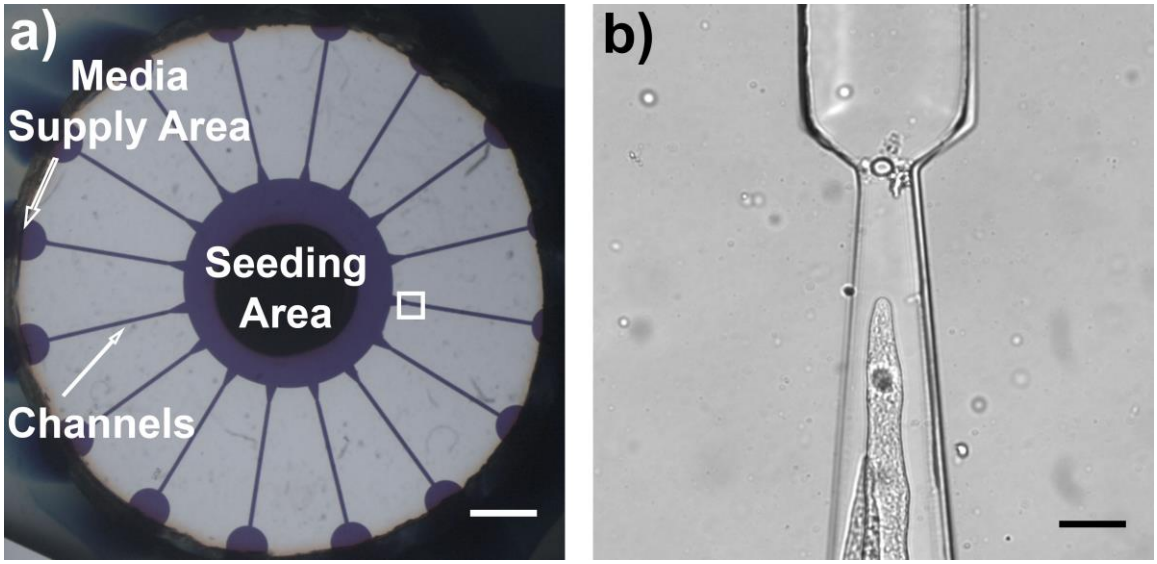

Figure 3.6: *A. bisexualis* chip design Version 3. Similar to Version 2 devices, sixteen channels emanated out radially from a central seeding area, where mycelial plugs were placed to inoculate the devices (a). The device has been filled with purple food dye to highlight the various areas. The white box indicates the area in one of the narrow channels where it tapers towards a single pillar (b). Beyond the pillar, channels were straight and ended in media supply areas that enabled solution changes. Hyphae grew down the tapered channels and collided with the pillars (b). Scale bars: a = 7.2 mm, b = 110 μm.

3.3.3 *Achlya bisexualis* Version 4 and 5 chips

The radial arrays of channels enabled the measurement of protrusive forces. However, the arrangement of the channels was such that concurrent imaging of multiple channels was difficult. This meant that, on occasions where hyphae in different channels were reaching the pillars at around the same time, it was only possible to record one of these events, and thus data collection was not optimal. To overcome this problem, Version 4 and 5 chip designs were made in which ten channels emanated linearly from the seeding area and ended in a single media supply center (Figure 3.7 and Figure 3.8). This enabled the concurrent imaging of several channels.

In Version 4 and 5 chips, single 25 μm high pillars were used. In Version 4 chips, these were positioned at the ends of double tapered channels, 400 μm from the start of the second taper. The width of each channel was 35 μm at the narrowest point, and they had a depth of 30 μm. Pillar widths of 5, 7 and 10 μm was tested. The gaps between the edges of the pillars and the sides of the channel were 15, 14 and 12.5 μm respectively.

In the Version 4 devices, hyphae grew down the channels at an average rate of 6.0 ± 1.6 μm/min (mean ± SD; range = 4.3 – 9.5 μm/min (n = 20 hyphae)) (Figure 3.2). The mean diameter taken 100 μm behind the tip was 21 ± 2.2 μm (mean ± SD; range = 18.5 - 22.4 μm (n = 20 hyphae)) (Figure 3.3). Hyphal tips grew into the pillars and enabled the measurement of protrusive force. This is considered in more detail in Chapter 4.

In the Version 5 devices, the tapers led into straight channels that were 35 μm wide and 30 μm deep. Pillars were located 400 μm from the start of these straight channels. As for the V4 chips, three pillar widths were trialed, 5, 7 and 10 μm. The gaps between the sides of these pillars and the side of the channel were 15, 14 and 12.5 μm respectively. Hyphae grew down the channels at an average rate of 7.3 ± 0.9 μm/min (mean ± SD; range = 5.3 – 8.7 μm/min (n = 20 hyphae)) (Figure 3.2). The mean diameter taken 100 μm behind the tip was 21.8 ± 2.7 μm (mean ± SD; range = 15.9 – 26.9 μm (n = 20 hyphae)) (Figure 3.3). Again, hyphae grew into the pillars and enabled the measurement of protrusive force, which is considered further in Chapter 4.

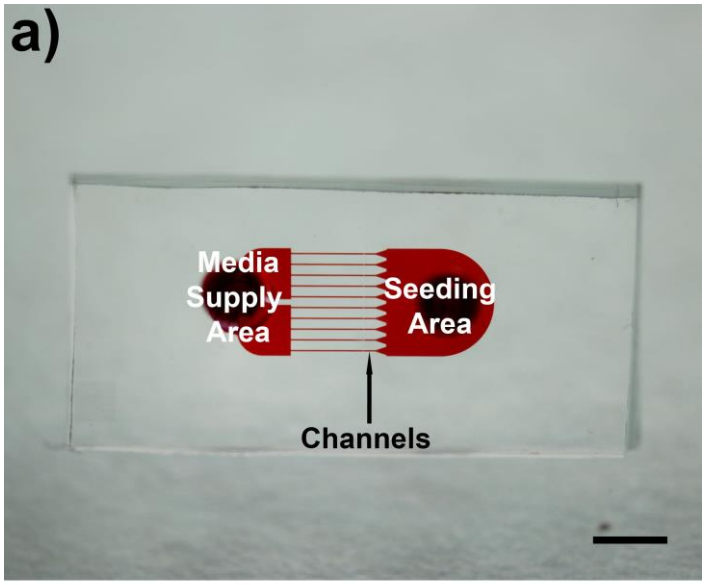

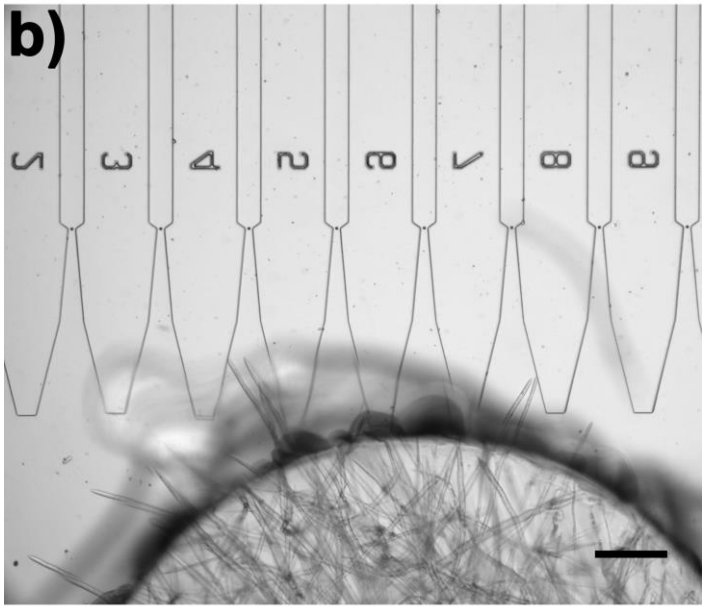

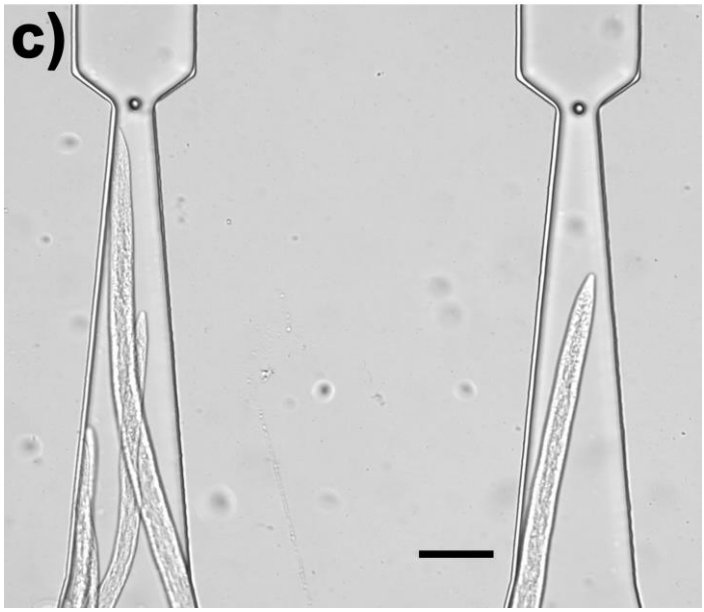

Figure 3.7: *A. bisexualis* chip design Version 4. Ten channels emanated out linearly from a seeding area, where mycelial plugs were placed to inoculate the devices (a, b). In (a) the device has been filled with red food dye to highlight the various areas. The channels taper and lead to a single pillar (b). Beyond the pillar, the channels were straight and they all entered a single media supply area that enabled solution changes. Hyphae grew out from the seeding area (b) and down the channels with the taper of the channel and the narrow gap between the pillar and the channel wall enhancing growth into the pillar (c). The close spacing and linear arrangement of the channels enabled concurrent imaging of multiple channels (c). Scale bars: a = 13 mm, b = 250 μm, c = 115 μm

For the Version 4 and 5 chips, the measured growth rates were slightly but significantly (student's t-test ($P<0.05$) faster than the average rates of 6.1 ± 0.5 μm/min (mean ± SD; range = 5.7 – 6.9 μm/min (n = 5 Petri dishes)) for hyphae growing on Petri dishes. The rates were also slightly but significantly (student's t-test ($P<0.05$) faster than the average growth rates of hyphae on the Version 1, 2 and 3 chips. The hyphal diameter was significantly narrower (student's t-test ($P<0.05$)) on Version 4 and 5 chips, compared to hyphae growing on Petri dishes (26 ± 4.6μm (mean ± SD; range = 19.6 – 39.2 μm (n = 20 hyphae))). In addition, the hyphae on the Version 5 chips had a significantly wider diameter than those on the Version 1, 2, 3 or 4 chips (student's t-test ($P<0.05$)). However, as for all the other chips, despite this difference they still displayed the typical hyphal shape of healthy growing *A. bisexualis* hyphae with a characteristic taper to the apex.

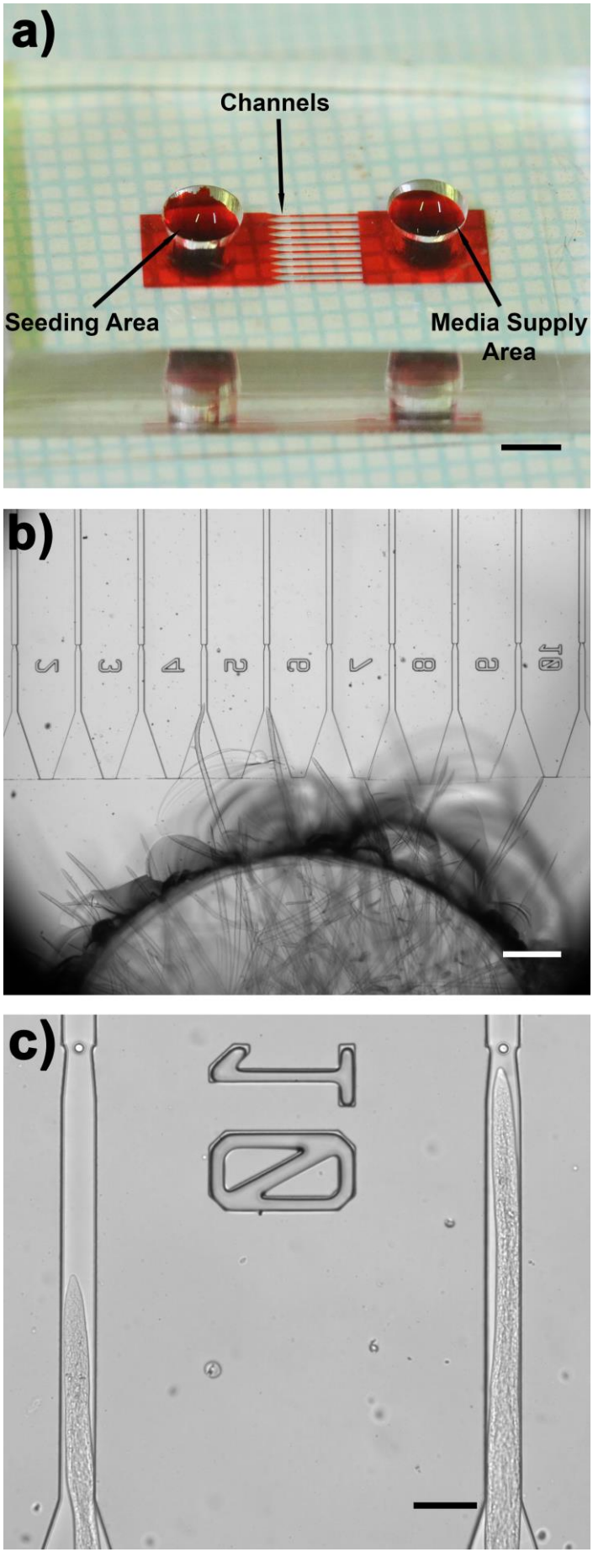

Figure 3.8: *A. bisexualis* chip design Version 5. As for chip Version 4, ten channels emanated out linearly from a seeding area, where mycelial plugs were placed to inoculate the devices (a, b). In (a) the device has been filled with red food dye to highlight the various areas. The channels taper and then lead to a narrower channel suitable for the growth of a single hypha. A single pillar was located 400 μm from the start of this narrow part of the channel (b). Beyond the pillar the channels were straight and entered a single media supply area that enabled solution changes. Hyphae grew out from the seeding area (b) and down the channels. The taper of the channel and the narrow gap between the pillar and the channel wall enhanced growth of a single hypha into the pillar (c). The close spacing and linear arrangement of the channels enabled concurrent imaging of multiple channels (c). Scale bar a = 12.2 mm, b = 224 μm, c = 112 μm.

3.4 *N. crassa* Version 1 and 2 chips

On the basis of the results of the chips for use with *A. bisexualis* hyphae, chips were then designed and fabricated for use with *N. crassa* hyphae. The smaller size of the *N. crassa* hyphae was a consideration in the design of these chips. Version 1 chips had 24 channels that emanated from a seeding area in a linear arrangement (Figure 3.9a). Upon inoculation of the chips hyphae grew from this seeding area towards the channels (Figure 3.9b). The channels comprised an initial tapered portion, which directed the hyphae towards a narrow part of the channel and at the end of this channel (350 μm from the beginning) there was a single pillar. The pillars were 13 μm high and had a diameter of either 5 or 7 μm. Channels were 16 μm deep and either 10 or 17 μm wide. After the pillar the channel widened and led to a media supply area that allowed a change of solution. N. *crassa* Version 2 chips differed in that there were only 12 channels, but these had the same width as Version 1 channels and the depth was 14 μm. The distance from the entrance of the channels to the pillars was 130 μm (Figure 3.10a) and the pillars were 11.4 μm high. Hyphae were observed to grow down the channels on both chips (Figure 3.9 c, d; Figure 3.10d, e) and displaced the pillars as they grew into them, potentially enabling the measurement of protrusive force (described further in Chapter 4).

Hyphae grew down the channels on the Version 1 chips at an average rate of 2.8 ± 0.7 μm/min (mean ± SD; range = 1.2 – 4.8 μm/min (n = 20 hyphae)) and on the Version 2 chips at an average rate of 2.9 ± 1.2 μm/min (mean ± SD; range = 1.3 – 5.7 μm/min (n = 20 hyphae)) (Figure 3.11). The growth rates on the two versions of the chip were not significantly different from one another (Student's t-test ($P>0.05$)), but were significantly different from the measured rates of 29.2 ± 0.4 μm/min (mean

± SD; range = 1.3 – 5.7 μm/min (n = 3 Petri dishes)). Hyphal diameters were 6.0 ± 0.3 μm (mean ± SD; range = 5.5 – 6.6 μm (n = 20 hyphae)) on Version 1 chips, 6.8 ± 1.3 μm (mean ± SD; range = 4.8 – 9.4 μm (n = 20 hyphae)) for Version 2 chips and 5.8 ± 0.9 μm (mean ± SD; range = 4.8 – 7.9 μm (n = 20 hyphae)) for the Petri dishes. The diameters of hyphae on the Version 2 chips were significantly wider than those on the Version 1 chips or the Petri dishes (Student's t-test ($P<0.05$)). Irrespective of the diameter, hyphae had the characteristic shape of *N. crassa* with a semi-circular tip that was much less tapered than that of *A. bisexualis*.

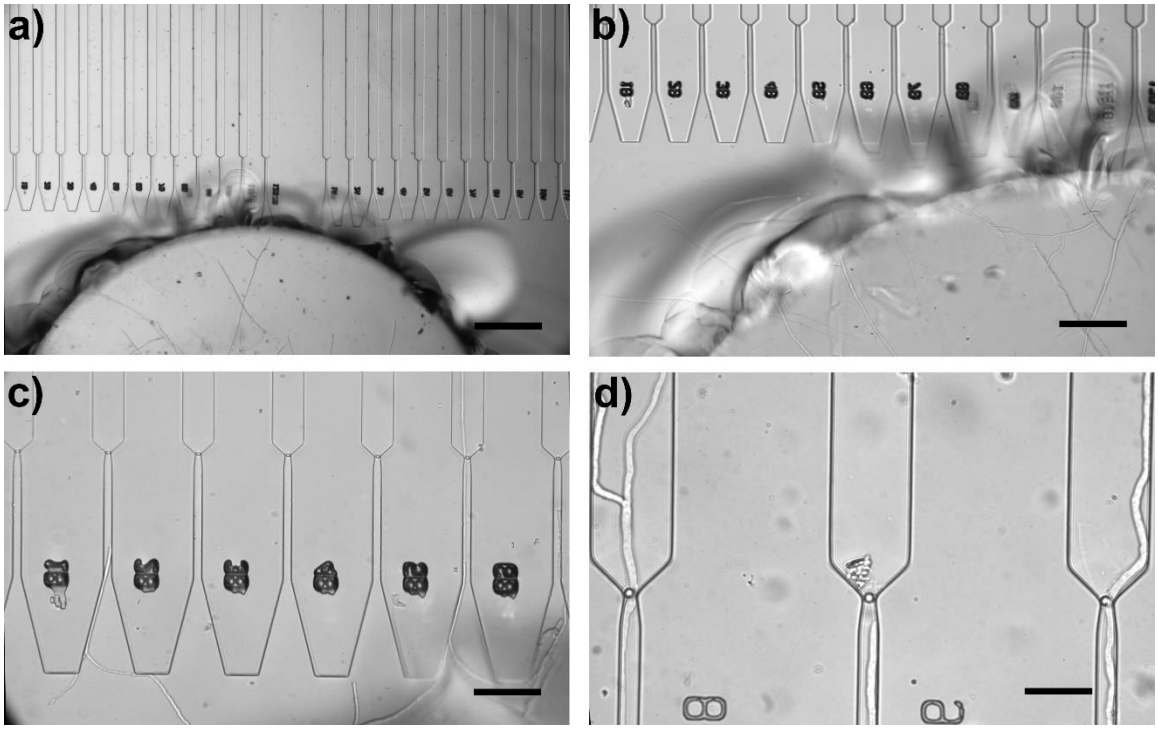

Figure 3.9: *N. crassa* chip design Version 1. Twenty-four channels emanated out linearly from a seeding area, where mycelial plugs were placed to inoculate the devices (a, b). The channels tapered and then led to a narrower channel suitable for the growth of a single hypha (c, d). A single pillar was located 200 μm from the start of this narrow part of the channel (d). Beyond the pillar the channels widened, were straight and entered a single media supply area that enabled solution changes. Hyphae grew out from the seeding area (b, c, d) and down the channels. The taper of the channel and the narrow gap between the pillar and the channel wall enhanced growth of a single hypha into the pillar (d). The close spacing and linear arrangement of the channels enabled concurrent imaging of multiple channels (c, d). Scale bars: a = 427 μm, b = 214 μm, c = 109 μm, d = 44 μm.

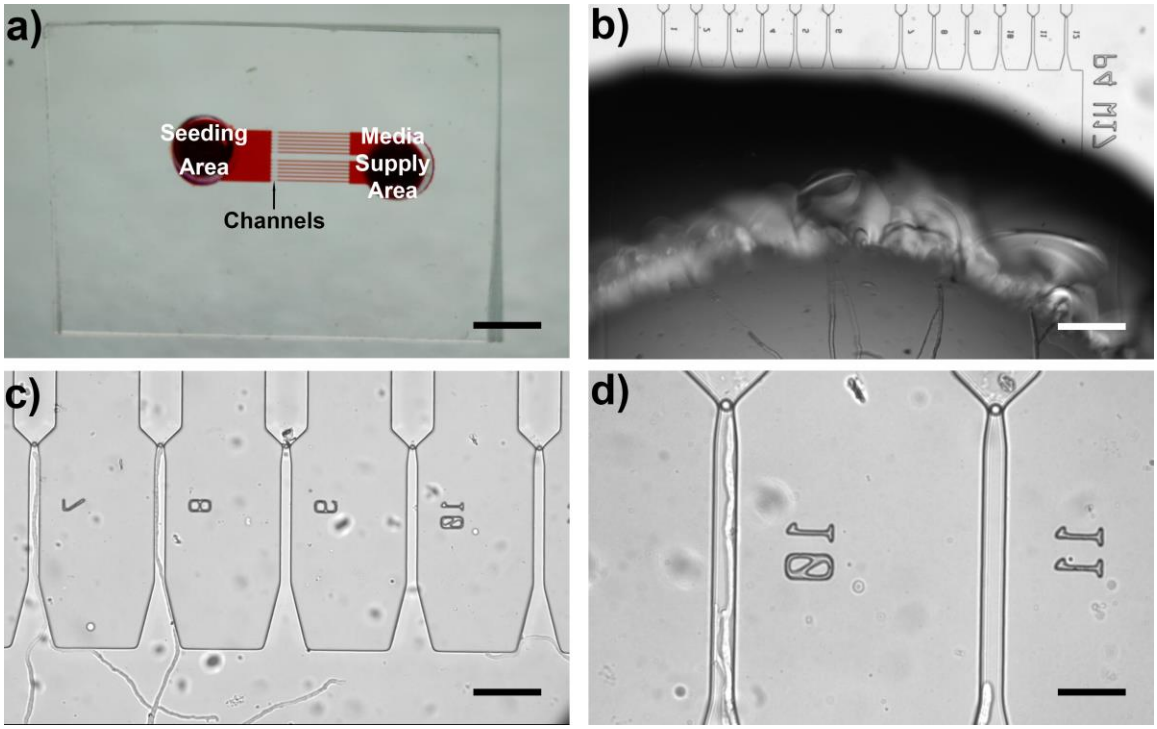

Figure 3.10: *N. crassa* chip design Version 2. In the Version 2 chips twelve channels emanated out linearly from a seeding area, where mycelial plugs were placed to inoculate the devices (a, b). In (a) the chip was filled with red food colour to highlight the different areas. The channels tapered and then led to a narrower channel suitable for the growth of a single hypha (d). A single pillar was located 85 μm from the start of this narrow part of the channel (d). Beyond the pillar the channels widened and straightened and entered a single media supply area that enabled solution changes. Hyphae grew out from the seeding area (b, d) and down the channels. The taper of the channel and the narrow gap between the pillar and the channel wall enhanced growth of a single hypha into the pillar (d). The close spacing and linear arrangement of the channels enabled concurrent imaging of multiple channels (d, e). Scale bar a = 12.4 mm, b = 579 μm, c = 223 μm, d = 114 μm.

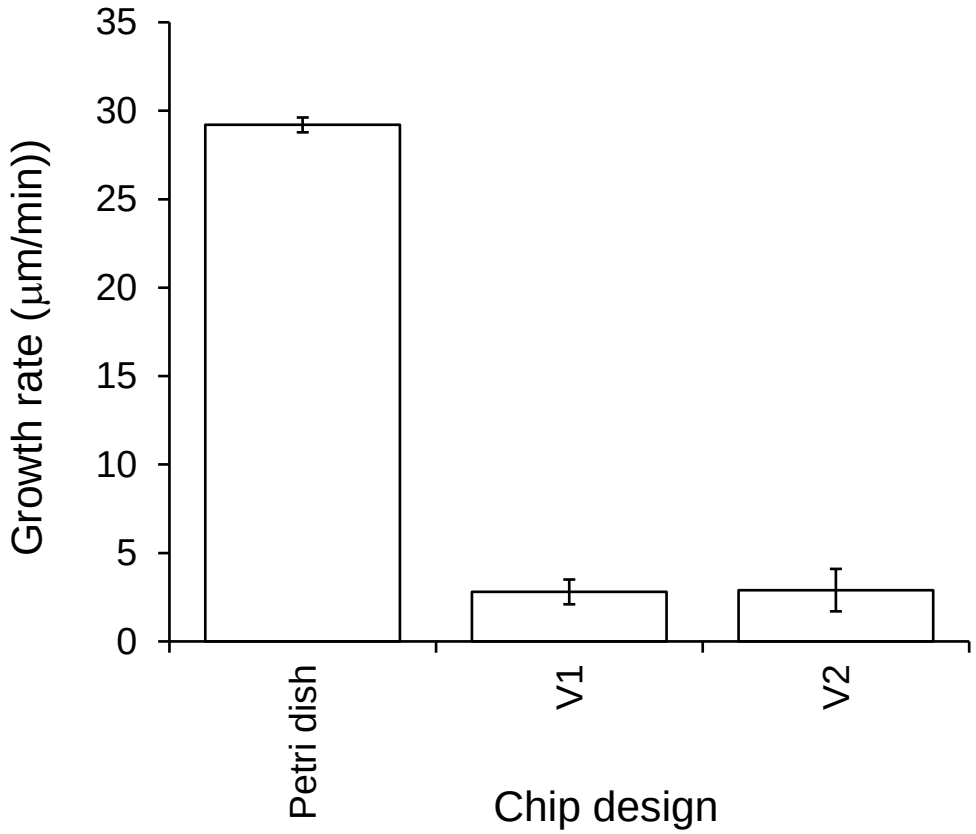

Figure 3.11: Growth rate of *N. crassa* hyphae on the two chip designs. V1 and V2 refer to Version 1 and Version 2 chips. Data are the mean growth rates ± SD (n = 20 hyphae and n = 3 Petri dishes).

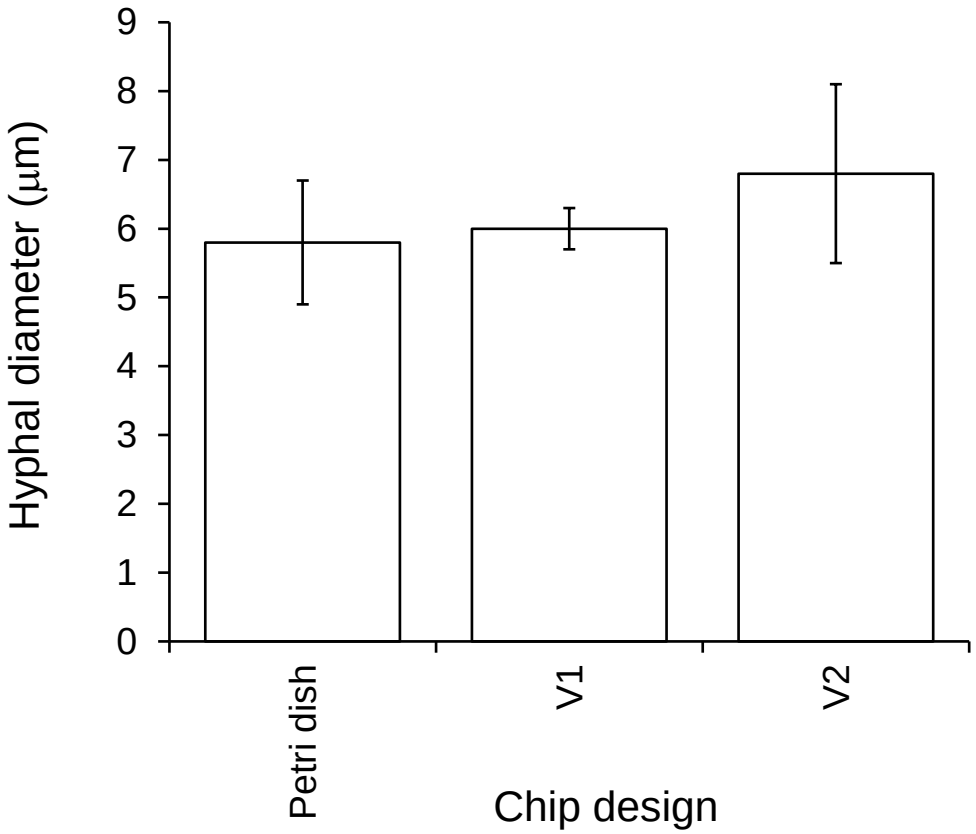

Figure 3.12: The diameter of *N. crassa* hyphae on Version 1 (V1) and Version 2 (V2) chips. Data are shown as the mean ± SD (n= 20 hyphae) as measured 100 μm behind the tips.

3.5 Discussion

Fungal and oomycete hyphae grow by the process of tip growth. These organisms play important roles in ecosystems throughout the world breaking down and recyling complex organic molecules from dead and decaying matter. Certain species can be parasitic and become pathogenic. A key aspect of this is the ability to grow invasively. This requires the breakdown of the material that they are growing through and the generation of a protrusive force. This is likely to involve a complex interplay between turgor pressure and the yielding of the tips of the hyphae. The more that a tip yields, the greater the protrusive force that is generated. To fully understand the process of invasive growth and its underlying mechanisms it is necessary to measure the magnitude of the protrusive force. The small size of individual hyphae, and forces that are likely to be in the micro-Newton range, mean that measurements of force are technically difficult.

LOC devices are being increasingly used to address biological questions and problems, including the study of complex cellular processes such as force generation (Lee, 2009). In addition to the pollen tube work described above, flexible siliconised structures have enabled force measurement in various mammalian cells, including cardiac myocytes (Zhao and Zhang, 2006), smooth muscle and epithelial cells (Tan et al., 2003; Du Roure et al., 2005). Some LOC devices have utilised micropillar arrays to measure force. The thinking behind these cantilever-like pillars is that as a cell grows or moves into a pillar, the pillar is deflected. A vision-based algorithm can then be used to resolve both the magnitude and the direction of the force from the deflection. Johari et al (2013) have used such devices to measure the contraction force, the locomotion speed and the undulation frequency of the nematode worm *C. elegans* as it moves. In the current study, these devices were used as a blueprint for

the design of chips that would enable force measurements on individual hyphae of *A. bisexualis* and *N. crassa*. The initial designs (Version 1 chips) were essentially proof of concept devices that were made to investigate if hyphae would grow on them, to see if their morphology was affected and if they could grow into and deflect the pillars. Experiments were first carried out with *A. bisexualis* due to the larger size of its hyphae, which meant that the chips would be easier to fabricate.

During the fabrication of the chips, the PDMS presents a hydrophobic surface as it solidifies after polymerization and cross-linking (Mcdonald et al., 2000). This presents a significant problem for the growth of hyphae. It has been shown that cell adherence and hyphal reorientation of the polymorphic yeast *Candida albicans* are affected when it is grown on untreated and oxygen plasma treated PDMS, compared to when it is grown on surface-modified PDMS (Thomson et al., 2015). In the devices described in this chapter, PDMS constitutes the bottom surface and walls of the channels, as well as the complete external surface of the measurement pillars. Therefore, all chips were plasma-treated prior to use in an attempt to increase the hydrophilicity (Section 2.2.2.1). Any chips that could not be completely filled with PYG broth (presumably due to hydrophobic areas) were discarded (around 10% of total chips).

To better understand what influence the PDMS and indeed the channels may have on hyphal growth, the growth rates of *A. bisexualis* hyphae in the channels were compared to radial extension rates of mycelia on PYG agar plates. While there were some statistically significant differences, growth rates were comparable. For example, the range of average growth rates on the chips was 5 – 7.3 μm/min, respectively, compared to an average rate of 6.1 μm/min on the Petri dishes. This suggests that the confines of the chip or the chip microenvironment had only a

minimal effect on the growth rate of *A. bisexualis* hyphae. This is consistent with reports of tip growing pollen tubes, which on chip also grow at rates comparable to those in *in vivo* conditions (Hu et al., 2017). Growth rates of oomycetes can be variable, typically ranging from 1–10 μm/min (McKerracher & Heath, 1987). For the isolate of *A. bisexualis* used in the current study, rates around 5–8 μm/min have been previously reported (Muralidhar et al., 2016), which is consistent with those observed on both the chips and Petri dishes.

In contrast, the growth rates of *N. crassa* hyphae were very much slower on the chips than on Petri dishes. In other studies where *N. crassa* was grown on PDMS chips, variable growth rates have also been reported when hyphae were growing in very long channels and (the channel length appeared to be the most crucial parameter affecting growth rate (Geng et al., 2015). It would be interesting to see if *N. crassa* growth rates increased with shorter channels on our chips, but unfortunately, we are limited in terms of the shortest possible channel length due to the cored inlets and the need to be able to do microscopy. Other works have described a slower rate of growth for *N. crassa* in spiral channels compared to wider channels (Lee et al, 2016). The data presented suggest that there are differences in the effect of the chip environment on growth rates and this needs to be kept in mind with respect to the force measurements that are considered in later chapters of this thesis.

Irrespective of the effects on growth rate, both oomycete and fungal hyphae appeared healthy on the chips and displayed the usual characteristics of tip growth typically discernible with a light microscope such as the forward movement of the bulk cytoplasm with the extending tip, and retrograde and anterograde movement of small refractile vesicles. The diameter of *A. bisexualis*, measured 100 μm behind the

tips, was slightly narrower in the channels, compared to PYG agar plates, ranging from 20 – 21.8 μm on the various chips and 26 μm on Petri dishes. For the much thinner *N. crassa* hyphae, the diameters on the chips were 6.0 and 6.8 μm on the chips and 5.8 μm on the Petri dishes. These values for the fungus are broadly comparable, which is in stark contrast to the growth rates. The diameter of pollen tubes can be influenced by channel parameters with pollen tubes becoming thinner as they grow through constrictions (Nezhad et al., 2013). The fungal and oomycete hyphae on the various chips were not growing through any constrictions, per se, but it is likely that they were able to sense that they were growing in a channel and indeed sense the geometry of the channel. Hyphal cells of the polymorphic yeast *Candida albicans* have also been shown to alter their growth depending on the design of the channels on PDMS chips (Thomson et al., 2015). That hyphae can sense the geometry of the chips is also evident with the Version 1 *A. bisexualis* chips, where the tips of hyphae did not hit pillars, instead they grew in the spaces between the pillars. Furthermore, if there were sufficient space between the pillar and the channel wall in the other chip designs (Versions 2 – 5 for *A. bisexualis* and Versions 1 and 2 for *N. crassa*) the hypha would often grow through this space rather than hitting the pillar directly. This often led to deflection of the pillars from the side and is discussed in more detail in Chapter 4 as it impacts on the measurement of protrusive force.

In conclusion, despite some differences in growth rates and hyphal diameters the results presented in this Chapter demonstrate that hyphae grew on each of the chips. The initial Version 1 proof of concept devices that were used with *A. bisexualis* had pillars that were not deflected by hyphal tips and so these were unsuitable for measurement of protrusive forces. The fact that the pillars deflected as the sides of

hyphae hit them did however demonstrate that forces could actually be measured on the chips. The subsequent designs incorporated channels, tapers and various arrangements of pillars to induce the growth of the hyphal tips into the pillar. These were successful and enabled the measurement of forces, which form the basis of Chapters 4 and 5.

CHAPTER 4

THE USE OF MICROPILLAR ARRAYS TO MEASURE PROTRUSIVE FORCES IN HYPHAE

Portions of the work in this chapter have been published in the following paper and refereed conference proceedings:

- **Tayagui A**., Sun Y., Collings DA., Garrill A. and Nock VM. (2017) An elastomeric micropillar platform for the study of protrusive forces in hyphal invasion*. Lab on a Chip* 17(21): 3643-3653.
- **Tayagui A**., Garrill A., Collings DA. and Nock VM. (2016) On-chip measurement of protrusive force exerted by individual hyphal tips during hyphal growth. *Proceedings of the 20th MicroTas Conference*, Dublin Ireland, pp 150-151.
- Sun Y., **Tayagui A**., Shearer H., Garrill A. and Nock VM. (2018) A microfluidic platform with integrated sensing pillars for protrusive force measurements on *Neurospora crassa. Proceedings of the 31st IEEE Conference on Microelectronic and Mechanical Engineering, Belfast, Northern Ireland* (in print).

4.1 Introduction

In Chapter 3, previous studies by others on protrusive forces in hyphae and germ tubes of fungi and oomycetes were discussed. In these studies, force measurements were made using a variety of techniques, including elastic optical wave guides (Bechinger et al., 1999), micro-strain gauges (Money et al., 2004) and optical tweezers (Wright et al., 2007). Such measurements are important if we are to fully understand the mechanisms of invasive growth and fungal pathogenicity. Optical waveguides have been used to visualize and measure the forces that were exerted by single appressoria of *Colletotrichum graminicola.* The forces averaged 17 μN which, given the size of the penetration hyphae of *C. graminicola* (approximately 2 μm diameter) would mean that the pressure within the appressorium would be 5.4 MPa (Bechinger et al., 1999). These values are comparable with earlier reports of pressures of 8.0 MPa in appressoria of *Magnoporthe grisea,* which were then calculated to correspond to a force of 8 μN, assuming that the surface of the penetration peg in this fungus is 1 μm^2 (Howard et al., 1991). Thus, the measured forces using the waveguides are likely to be accurate, given that they were comparable to the calculated forces. These forces are likely to be sufficient to break through the cuticle and epidermal cell wall of plants (Bechinger et al., 1999).

Money and colleagues (Money et al., 2004; MacDonald et al., 2002) have used the displacement of a miniature silicon bridge strain gauge to measure forces exerted by the tip of a variety of fungi and oomycetes. To account for differences in the sizes of individual hyphae, the forces were converted into pressures by taking into account the area of contact between the hyphae and the gauges. Both groups of organisms generated pressures of around 0.2 MPa at their tips and this was used to argue for

the convergent evolution of the biophysical parameters of the invasive lifestyle (Money et al., 2004).

The first attempts to use optical tweezers to measure forces at the tips of hyphae were made by Wright et al. (2007). Beads that were trapped with known forces were placed in the way of leading edge hyphae of *N. crassa*. These experiments showed that the growth forces of the hyphae exceeded the pico-Newton forces, which optical tweezers can be used to readily measure, and supported the μN forces reported using both the optical wave guides (Bechinger et al., 1999) and the micro-strain gauges (Money et al., 2004).

Of these techniques, micro-strain gauge cantilevers have proven to be most suitable given the magnitude of the forces to be measured. However, because of shape changes in cells following the orthogonal contact between the extending cell tip with the flat surface of the sensor. There have also been questions raised as to its applicability for measuring the forces exerted by invasively growing hyphae, as the solidified media required for invasive growth would affect the operation of the gauge (Walker et al., 2006).

Advances in microfabrication capabilities and live-cell imaging have meant that microfluidic LOC devices are increasingly being used to study the forces that guide cellular processes. Traditionally, such devices have been used to measure mechanical forces related to mammalian cells (Eisenstein, 2017; Harris,et al., 2011; Iskratschet al., 2014). More recently, LOC technology has been adapted for use with plants and fungi (Stanley & Der, 2017). In the fungi, these include the study of growth patterns of basidiomycetes (Hanson et al., 2006) and the thigmotropic responses of *Candida albicans* (Thomson et al., 2015, 2016). More advanced

devices have attempted to quantify the Young's modulus (also known as the elastic modulus, which is a measure of the stiffness of a solid material) of primary plant cell walls (Nezhad et al., 2013) and to characterize the three-dimensional morphology and mechanics of developing plant cells (Felekis et al., 2015; Shamsudhin et al., 2016; Hu et al., 2017). They have also been used to perform high-throughput analysis of single cell polarized growth and dynamics (Agudelo et al, 2013; Geng et al, 2015).

The first LOC devices that were used to measure forces in fungi contained cylindrical PDMS microchambers that had various elasticities, and which were loaded with single cells of the fission yeast *Schizosaccharomyces pombe*. By measuring the buckling of the individual cells in these femtolitre-sized chambers, a value for the elastic modulus of the cell wall of 20.2 N/m was obtained (Minc et al., 2009). Furthermore, as the cells grew and pushed against the walls of the chamber, force-velocity relationships and values for turgor pressure of 0.85 MPa were derived. On the basis of these observations, and through the use of strains with mutations in the glycerol synthase gene, Minc et al. (2009) concluded that force generation was dependent on turgor pressure and that this was generated through the synthesis of glycerol. While the chambers represented a significant step forward in the use of LOC devices to study the biology of fungi, further development is required for the use of these devices to measure forces at the tips of hyphae.

In other tip growing cells, LOC devices have been used to measure penetrative pressures in pollen tubes. The devices were designed such that they presented obstacles to the growing pollen tubes (Nezhad et al., 2013). Finite element modeling and measurement of the dilating force exerted normal to the gap wall were then used to deduce penetration pressures of the order of 0.15 MPa. The data revealed that

increasing mechanical impedance was countered by changes in cell wall compliance and, thus, a change in the force acting on the obstacle (Nezhad et al., 2013).

A technically simpler approach to measure forces exerted by cells as they grow and move is through the use of elastomeric micropillar arrays on LOC devices (Gupta et al., 2015). Initially developed to study cellular traction forces, these pillar arrays have been adopted for use with microorganisms such as nematodes (Ghanbari et al., 2010, 2012; Johari et al., 2013). The pillar-based approach typically combines optical tracking of a pillar top with a simple mechanical model to measure forces. Given the correct modifications these arrays are applicable to fungal and oomycete hyphae and provide the capability to also determine the directionality of forces generated (Johari et al., 2013). Using photolithographic miniaturization approaches, it is possible to tailor the pillar system to the size appropriate for the hyphae.

In Chapter 3, data was presented that showed that both fungal and oomycete hyphae will grow on LOC devices and, with the correct chip design the tips of hyphae will grow into and displace pillars. The open arrays of pillars in the *A. bisexualis* Version 1 chips were clearly unsuitable for protrusive force experiments, as only squeezing forces could be recorded. This was because the hyphae grew into inter-pillar spaces and not against the pillars. This led to the development of Version 2, 3, 4 and 5 *A. bisexualis* chips and Version 1 and 2 *N. crassa* chips, which had tapered channels, tapered arrays of pillars and single pillars in narrow channels as a means of inducing hyphal tips to grow into the pillars.

In the present chapter, the measurement of force in the Version 2, 3, 4 and 5 *A. bisexualis* chips and the Version 2 *N. crassa* chips is described. Unfortunately, due to the confines of time, replicate data was not able to be obtained for force

measurements with the Version 1 *N. crassa* chips and so these are excluded from this analysis. The data presented in this chapter demonstrate the ability of these devices to measure μN forces at the tips of individual hyphae, in both the x- and y-directions. The use of parallel channels on the chips means that data from multiple hyphae can be obtained simultaneously and with appropriate modification should work for different fungal and oomycete species.

4.2 Materials and Methods

Materials and methods were as described in Chapter 2.

4.3 Results

On the basis of the results presented in Chapter 3, Version 2, 3, 4 and 5 *A. bisexualis* chips and Version 2 *N. crassa* chips were further investigated for their respective abilities to measure protrusive force at the tips of hyphae. These were chosen, firstly because hyphae grew in the channels and secondly, because hyphae grew into pillars and displaced the pillars enabling force measurement. The tapers and narrow channels had the effect of directing the hyphae towards the pillars. The characteristics of each of these chips were summarized in Table 3.1.

In the results that are presented below, the Version 3 *A. bisexualis* chips are used to describe the development of the force sensing principle. This principle had previously been used in studies on *C. elegans* (Ghanbari et al., 2012), but was modified to make it suitable for measurement of hyphal forces. The Version 2 *A. bisexualis* chips are used to describe how the chips enable the study of hyphal morphology and growth rate, as well as force. Version 4 and 5 *A. bisexualis* chips and Version 1 and 2 *N. crassa* chips, followed the same principles, but each of these had a linear arrangement of channels, which enabled force measurements in multiple hyphae in the same field of view of the microscope.

4.4 The force sensing principle

The principle of force sensing as described below is explained using Version 3 chips as an example. Data obtained using all the chips (Version 2 – 5 for *A. bisexualis* and Versions 1 and 2 for *N. crassa*) are presented in Table 4.1. The protrusive force exerted by hyphae was measured via the deflection this force caused in the cylindrical pillars that were made of elastic PDMS. This hypha-pillar contact force

was collectively and equally loaded on the pillar, causing it to deflect as an elastic entity, similar to the pillars that had previously been used to measure forces exerted by nematodes (Ghanbari et al., 2012). While the hypha can be regarded as a soft entity, the force that it exerts can be treated as a concentrated load at the center point of the contact area. Applying this force–deflection model, the total force *f* applied by the hypha corresponds to the total deflection of the pillar. Fluidic drag applied by the environment can be safely ignored (Ghanbari et al., 2012) and no measurable adhesion force between the hyphal tip and pillar could be observed, when tips disestablished contact. The deflection *Δ* of the free end of the pillar was recorded using a camera mounted on a microscope and measured using an open-source feature-tracking algorithm (Tinevez et al., 2017). A linear-spring force deflection model combining pure bending and shear (Ghanbari et al., 2012), where *L* is the contact height, *I* the moment of inertia, *E* and *γ* the Young's modulus and the Poisson's ratio for PDMS, respectively, and *h* the pillar height, was used to convert pillar deflection to force (equation 4.1).

Equation 4.1:
$$f = \frac{\Delta}{\left(\frac{L^3}{3EI} + \frac{d^2(1+\gamma)L}{4EI}\right) + \frac{L^2}{2EI}(h-L)}$$

A Poisson's ratio *γ* of 0.5 was used for PDMS (Mark, 2009). The moment of inertia *I* in equation 4.1 was calculated using equation 4.2, where *d* is the diameter of the measurement pillar.

Equation 4.2:
$$I = \frac{\pi d^4}{64}$$

A. bisexualis Version 3 chips were prepared with 30 μm high pillars that had a diameter of 10 μm, giving a pillar aspect ratio of 2.5. With a hyphal diameter of approximately 20.4 μm (Chapter 3), this would mean a pillar stiffness of 0.41 μN/μm (see Table 4.1 in which a summary of the pillar stiffness for all the chips is presented). SEM imaging confirmed that pillar diameters were uniform along the height. A piezoresistive force sensor setup was used to measure the Young's modulus *E*, as described previously (Johari et al., 2015) and was determined to be 1.47 MPa, using a set of calibration samples processed under the same thermal conditions as the chips. This value was confirmed using an electromechanical universal test system (MTS Criterion - model 43) using a 100 N load cell, MTS Testworks 4 software and MTS Videotraction to measure the strain. As *A. bisexualis* hyphae have a cylindrical body shape (Coker, 1927), it was assumed that a hypha applies force to the pillar with the tip, which is at half its body height. This was confirmed by growing hyphae on chips in PYG broth containing the yellow food dye, Tetrazine. The dye was taken up by the hyphae and it also stained the pillar, as shown in Figure 4.1. If a line was drawn along the y-coordinate from the tip of the hypha to the pillar, it could be seen that the height of the point of contact (assuming that it continued in the same growth path and retained the same morphology) was equal to half of the diameter of the hypha.

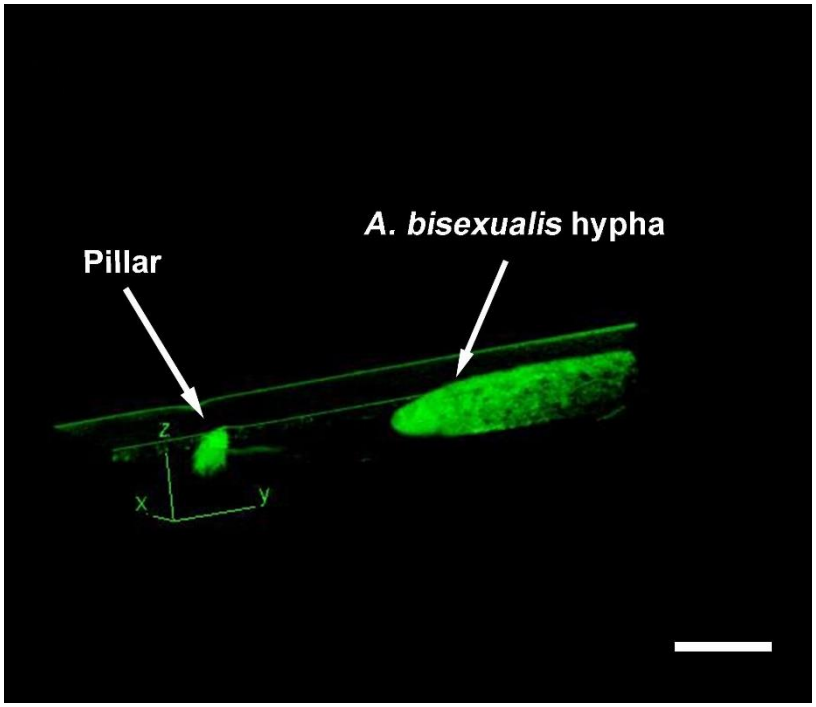

Figure 4.1. A reconstructed confocal image of a hypha, which has taken up the yellow food dye, Tetrazine, approaching a pillar on a Version 5 *A. bisexualis* chip. The hypha has a cylindrical shape with a tapered tip and is on track to hit the pillar at half of its body height (i.e. half of the hyphal diameter). The x-, y- and z-coordinates are shown and represent the channel width, channel length and channel depth respectively. Scale bar = 20 μm.

To compensate for variations in hyphal size towards the very tip due to differences in the taper, the width of each hypha was measured 10 μm behind the tip using ImageJ. Half of this value was then used as the contact height *l* in equation 4.1. This was further confirmed by measuring the vertical distance between the top of the pillar and the hyphal tip at the moment of contact using the micrometer scale on the microscope focus dial. The precision of this approach is estimated to be ±1 μm, which equates to a force error of ± 6.7%.

4.5 Pillar deflection tracking

To track pillar deflection with sub-pixel accuracy, optical microscopy was used combined with the ImageJ particle tracking plugin TrackMate (Tinevez 2017). Hyphae were first visually tracked using optical microscopy at low magnification while they grew into the measurement channels. Figure 4.2a shows an example of *A. bisexualis* hyphae growing into the tapering channels leading off from the central seeding area on a Version 3 chip. Once hyphal tips approached within 50–100 µm of the measurement pillar, further extension was recorded using a 20x objective. Recorded image sequences were imported into ImageJ and the graphical user interface of TrackMate was used to define tracking parameters. First, a Laplacian of Gaussian (LoG) filter was applied with an estimated pillar diameter that was specified in pixels. Using the plugin interface, sub-pixel localization was implemented by activating a quadratic fitting scheme and a threshold parameter was used to further reduce the number of circles identified for tracking. The resulting circular features were overlaid onto the image sequence using the ImageJ hyperstack viewer, after applying a suitable filter to limit tracking to only the pillar of interest. Figure 4.2b shows this step for the hypha, which was depicted in the top channel of Figure 4.2a, once it had reached the pillar. The in-built simple linear assignment problem (LAP) tracker was used and was very robust, even in instances when there was debris from the fabrication of the chips close to the pillar, as evident in Figure 4.2b. This tracker allowed specification of the maximum linking and gap-closing distances, which can be used to bridge discontinuities in the tracking, due to any misidentification. As a final step, tracking data was exported in 2D coordinate/time (X, Y, t) format to an eXtensible markup language (XML) file. A custom algorithm previously developed for the tracking of pillars actuated by *C. elegans*, was also

trialled, which was based on least-squares circle detection (Ghanbari et al., 2010, 2012). However, this algorithm did not yield as satisfactory results as TrackMate, possibly due to the smaller size and larger pillar deflections observed with the oomycete and fungal chips. Both these methods are ultimately limited by the ability to determine the position of the pillar top circle. With very large extreme deflections, for example when large diameter hyphae grew into smaller diameter pillars, the tracking, and thus force measurement was only successful for a short period of time after contact. In fact, several larger diameter hyphae fully flattened smaller pillars after short periods of time. While a force measurement is still possible under these conditions, a larger pillar diameter (larger stiffness) was needed if a longer measurement time was desired. Typically, the best results were obtained for *A. bisexualis* with the 7 μm wide pillars and, unless stated otherwise, these were used in the experiments described below and in Chapter 5. In addition, there were a number of experiments where the tops of pillars could not be tracked and in later experiments, which are described in Chapter 5, this reduced the sample size in a number of experiments. Approaches to resolve this issue are considered in Chapter 6.

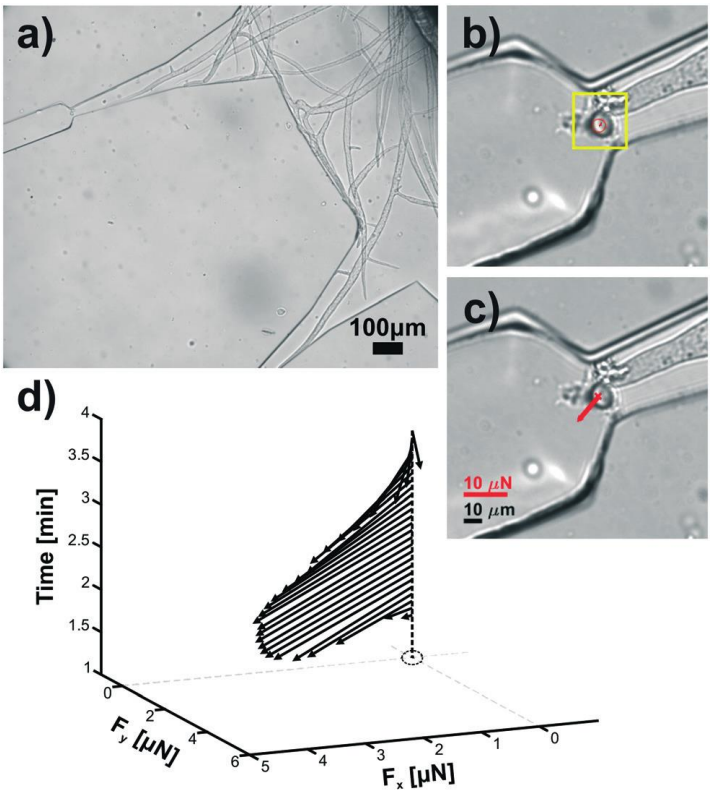

Figure 4.2: Force sensing of individual *A. bisexualis* hyphal tips on a Version 3 chip. a) An optical micrograph showing hyphae growing out from a mycelial plug placed in the central seeding area. Hyphae grew radially outwards into the tapering channels. Individual 10 µm diameter pillars were located at constrictions 400 µm down the second taper of each channel. b) A close-up of a pillar, 30 s after initial contact, showing the circle tracking data generated by TrackMate as a red line. The box corresponds to an area-crop defined in ImageJ to reduce the number of features tracked. c) A force direction and magnitude overlay at the same time-point as in (b) generated using custom code in Matlab. d) A plot of the force vector of the hyphal tip–pillar interaction as a function of time. Both force magnitude and direction are recorded and can be related to contact phases. F_y represents protrusive force parallel to the axis of growth and F_x represents a squeezing force perpendicular to the axis of growth. Figure reproduced from Tayagui et al. (2017) with permission.

4.6 Force data processing

Force vector data was generated from the TrackMate output via custom code (written by Dr Volker Nock) that was implemented as a MATLAB script. While it was possible to implement some of this functionality via the ImageJ scripting language, this would ultimately not have been as powerful as the use of a dedicated data analysis tool such as Matlab. The script itself contained the force model described in equation 4.1 and allowed the input of mechanical and geometrical properties, as well as the calibration of image dimensions. The tracking data was imported via the ImageJ–Matlab extensions and converted to force values for each image in the sequence. These values were used to generate directional force vectors and these were overlaid onto the image files together with scale bars, as shown in Figure 4.2c. In the image sequences hyphae are typically depicted growing up or down (i.e. vertically in the image), which means that the x-direction (and thus the force F_x) is perpendicular to the axis of growth and the y-direction (and thus the force F_y) is parallel to the axis of growth. The overall output of the script included individual frames, an animated movie of the sequence and force data as a text file and 2D and 3D force versus time plots. Figure 4.2d shows an example of a force vector plot generated by the hypha shown in Figure 4.2c. Both magnitude and direction of the protrusive force exerted on the pillar could be recorded. In the example shown, pillar contact and protrusive force generation were initiated 1.5 min after the recording started. Over a period of 30 s, F_x and F_y force components applied by the hypha could be seen to increase rapidly from 0 to 4.5 and 5.2 μN, respectively. After this, a gradual decrease in force components and a change of direction in the vector was observed, indicating that the hypha deflected to the right of the pillar.

In general, smaller hyphae of *A. bisexualis* that were less than 18 μm diameter tended to deflect off the stiffer, 10 μm wide pillars after applying an initial protrusive force. Larger hyphae that were more than 25 μm diameter) would, however, grow straight through the softer 5 μm wide pillars, bending these entirely flat in the process. For this reason, the majority of the later experiments with the Version 4 and 5 chips were done with 7 μm wide pillars.

The force resolution was estimated using the product of the pillar stiffness, pixel size *u* in either direction, and the visual tracking resolution σ. The pixel size was calibrated to be 0.47 × 0.47 μm and σ estimated to be 0.5 pixel (Ghanbari et al., 2012). From this it follows that, for a pillar diameter of 10 μm and a hypha width of 20.4 μm, the force resolution was 0.11 μN (Table 4.1). It should be noted that this model does not take into account substrate warping, which has been found to systematically overestimate forces at low aspect ratios and low Poisson ratio (Schoen et al, 2010). Given that the pillars were attached at one end (bottom of the channel) and free at the other end, a protrusive force in the z-direction may also be generated. However, all observations indicated that this protrusive force in the z-direction, if it indeed existed, was very small compared to forces in the x- and y-directions, as vertical deflections were not evident in confocal images when the hyphae interacted with the pillars.

Chip Version	Pillar height (μm)	Pillar widths (μm)	Pillar stiffness (μN/μm)	Force resolution (μN)
Achlya bisexualis				
Version 2	30	10	0.42	0.1
Version 3	30	10	0.41	0.097
Version 4	25	5	0.035	0.008
Version 4	25	7	0.13	0.03
Version 4	25	10	0.46	0.11
Version 5	25	5	0.033	0.008
Version 5	25	7	0.12	0.028
Version 5	25	10	0.43	0.1
Neurospora crassa				
Version 1	13	5	0.055	0.013
		7	1.59	0.38
Version 2	11.4	5	0.049	0.012
		7	1.42	0.34

Table 4.1 Calculated pillar stiffness and force resolution for the different chips. For the calculations, the average hyphal diameters on each of the chips, as detailed in chapter 3 were used (i.e. 20 μm, 20 μm, 20.4 μm, 21 μm and 21.8 μm for Version 2, 3, 4 and 5 *A. bisexualis* chips and 6 μm and 6.9 μm for Version 1 and 2 *N. crassa* chips respectively).

4.7 Force patterns in hypha–pillar interactions

To demonstrate the capability of the chips for investigations of the relationship between hyphal growth, morphology and force generation, examples using the Version 2 *A. bisexualis* chips are shown. The spacing of the pillars on these chips allowed for a hypha to contact individual pillars, apply force and subsequently move around them. A representative hyphal tip–pillar interaction is shown in Figure 4.3 and the plots of force in the x- and y-directions, hyphal width, hyphal growth rate and total force are shown in Figure 4.4.

In Figure 4.3, multiple hyphae can be seen growing from the seeding area into a tapered channel towards the tapered array of pillars. In the time series of images, one of these hyphae grew towards a single pillar and made contact around the 70 s mark. Firstly, within a few seconds after contact, the pillar deflects and thus force is measurable (as depicted by the red arrow from 85 s onwards). The length of the force vector increased steadily and remained in the same direction. A plot of the extracted F_x- and F_y-components of this force are shown in Figure 4.3a, which shows a steady increase of both components initially while the hypha increased force generation. These were matched by changes in the rate of hyphal extension (Figure 4.4b). From the onset of force generation at 70 s, the hypha slowed down from a relatively constant rate of 4 µm/min to less than 1 µm/min as it contacted the pillar.

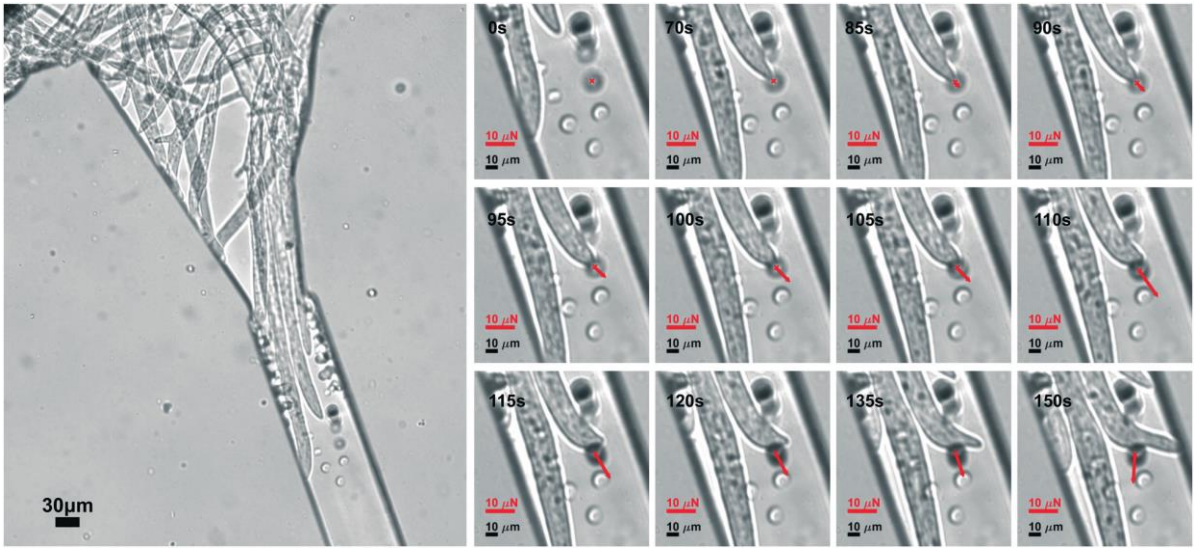

Figure 4.3. Example of a hyphal tip–pillar interaction on an *A. bisexualis* Version 2 chip. On the left, hyphae grow out from the seeding area into a tapered channel towards a tapered array of pillars. The time series of images on the right show an individual hypha interacting with one of the measurement pillars. The pillar tracking data output from Matlab was overlaid onto the images depicting the pillar centre-point tracking (red cross) and force direction and magnitude (red vector). One hyphal tip can be observed extending towards the pillar, making contact and then displacing the pillar. After the 105 s mark the hypha deflects off the pillar and the contact changes from the tip of the hypha to the side of the hypha, leading to a transition from protrusive to a squeezing force. Figure reproduced from Tayagui et al. (2017) with permission.

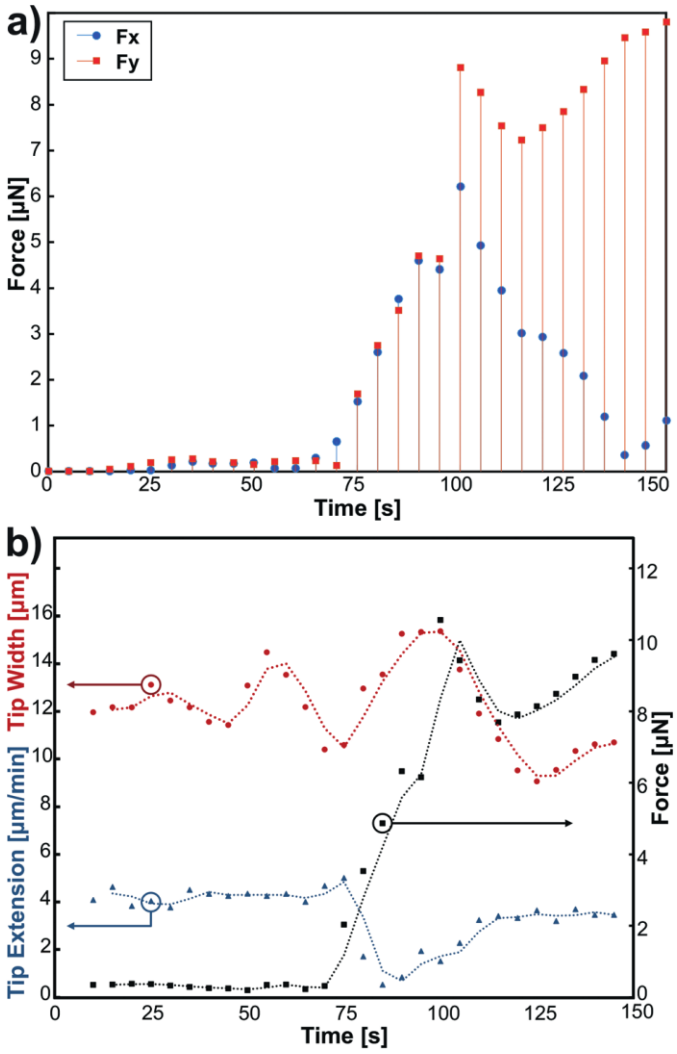

Figure 4.4. The x- and y-directions of the force, total force, extension rate and diameter of a hypha growing on a Version 3 *A. bisexualis* chip, as it hits and deflects a pillar. a) A plot of measured force components F_x and F_y as a function of time. Directional changes can be observed as the tip goes through different stages of interaction with the pillar. b) A comparison of the total force, hyphal diameter and extension rate, as a function of time. Tip extension was measured by the change of tip position along the current orientation of the tip between frames (as depicted in Figure 4.3). Figure reproduced from Tayagui et al. (2017) with permission.

The diameter of the hypha, as measured 10 µm behind the tip, varied as the hypha grew towards the pillar, increasing and decreasing in a sinusoidal manner. Upon pillar contact, the diameter of the hypha increased from 12 µm to 15 µm. This

appeared to match the decrease in tip extension rate (Figure 4.4b). After approximately 100 s, the tip of the hyphae changed direction and, through images 105 s to 135 s, extended past the pillar during which tip extension returned to close to its initial rate.

4.8 Concurrent measurement of force in several hyphae

While the Version 2 and 3 *A. bisexualis* chips enabled the development of the force sensing principles, the radial arrangement of the channels meant that it was difficult to obtain measurements of more than one or two hyphae per chip. For this reason, the Version 4 and 5 *A. bisexualis* chips, and later the Version 1 and 2 *N. crassa* chips, were designed with a linear arrangement. Ten parallel channels in the Version 4 and 5 *A. bisexualis* chips, and 24 and 12 parallel channels in the Version 1 and 2 of *N. crassa*, respectively, emanated out from the seeding area.

Figure 4.5a shows a Version 4 *A. bisexualis* chip with hyphae extending towards the ten measurement channels. To reliably track the pillar tops for force sensing, the higher magnification objective lens had to be used, which meant that only three parallel channels could be imaged concurrently (Figure 4.5b). However, this did not significantly reduce the number of hyphae that force measurements could be obtained from, as hyphae typically reached the central channels first, possibly due to their closer proximity to the inoculation plug. Once measurements had been made on hyphae growing in these channels, other channels could be moved into the field of view, and measurements could then be made on hyphae growing in the outer channels.

To demonstrate the potential of this layout for measurements in multiple hyphae, Figure 4.5c shows an example of total force measurements for ten hyphae that were growing on the same chip. In the example shown, these measurements were made irrespective of whether the tip or the side of the hypha hit the pillar, as the purpose was to illustrate the suitability of the arrangement of the channels and pillars for multiple measurements. It should be noted that the part of the hypha that initially hits the pillar is a crucial consideration with respect to protrusive force, and this is considered in more detail below.

Force curves were similar for the ten hyphae – for a period of around 20 s upon hypha–pillar contact force values rapidly increased, which was associated with force generation. After this period, the forces increased more gradually. Smaller diameter hyphae (i.e. hyphae 1, 2, 3 and 4, which had diameters of 9.3, 8.9, 9.1 and 10.2 μm, respectively) appeared to generate smaller force values than medium sized (i.e. hyphae 5, 6, and 7 which had diameters of 16.4, 15.6 and 15.0 μm, respectively) and larger hyphae (i.e. hyphae 8, 9 and 10 which had diameters of 29.7, 27.7 and 28.6 μm, respectively) (Figure 4.5c, d), although as detailed further below with the Version 4 and 5 chips, these differences were not statistically significant. During the initial phase of contact and pillar displacement there was an increase in both hyphal diameter (as measured 10 μm behind the tip) and force over time (Figure 4.5d) but again these were not statistically significant. Because they enabled the measurement of force of multiple hyphae on the same chip the linear arrangement of channels, rather than the radial arrangements, were used in subsequent experiments both on *A. bisexualis* and *N. crassa*.

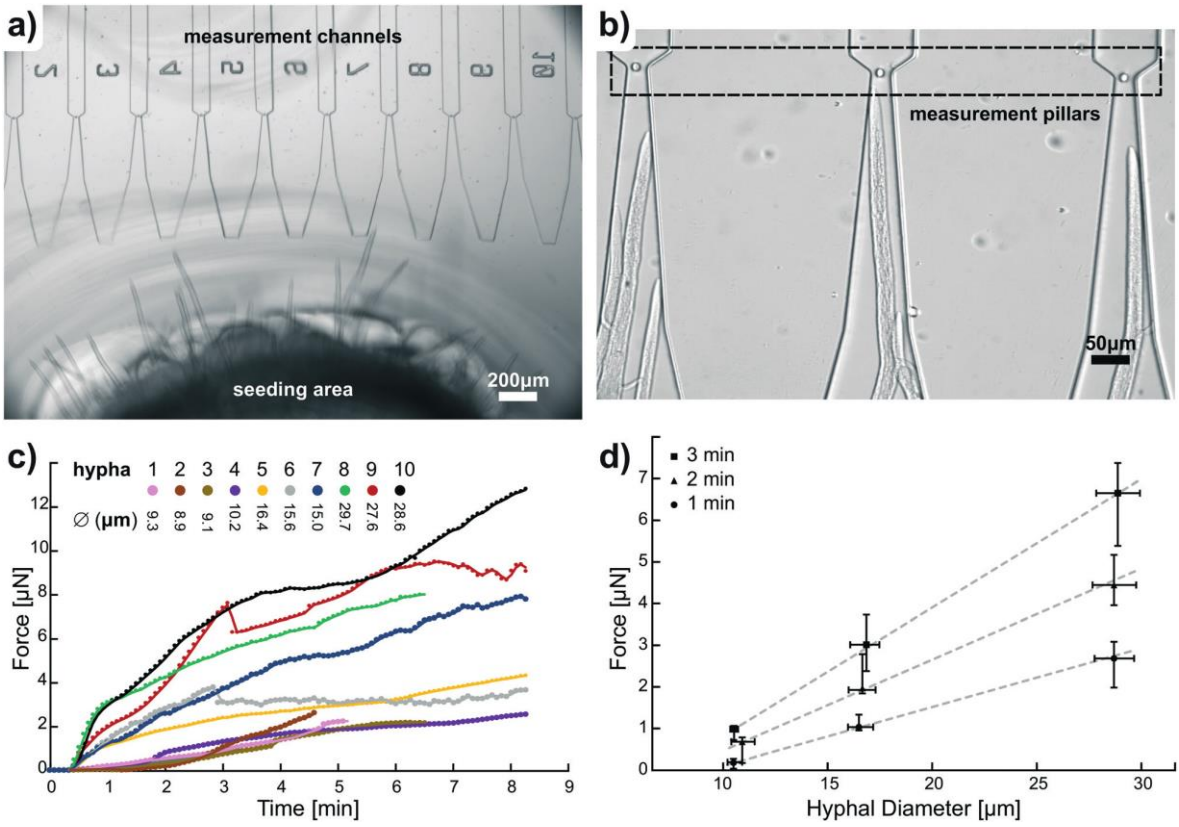

Figure 4.5. The measurement of force and diameter in multiple hyphae on a single Version 4 *A. bisexualis* chip. a) Ten parallel channels emanated out from the seeding area and each channel contained a single pillar. Hyphae extended out of the inoculation plug and grew into the channels. b) At the magnification required to reliably track the movement of the pillars, three channels could be observed in the field of view. The highlighted area indicates a top-view of the pillars at the channel constrictions. Hyphae are growing down each of the channels towards the pillars. Given the width of the channels at the start of the taper, in some instances several hyphae grew down the same channel. c) A plot of the total force exerted, as a function of time, by ten hyphae growing individually in separate measurement channels on the same chip. Individual hyphal diameters ranged from 8.9 µm to 29.7 µm, measured 10 µm behind the tip prior to the hyphae hitting the pillars. d) A plot of the force of the same ten hyphae as a function of hyphal diameter which increased with time, measured at 1, 2 and 3 min after pillar contact. For simplicity, hyphae were placed into three groups: small (hyphae 1 – 4, plotted as the data points on the left), medium (hyphae 5 – 7, plotted as the middle data points) and large (hyphae 8 – 10, plotted as the data points on the right). Figure reproduced from Tayagui et al. (2017) with permission.

4.9 Tip deflections versus side deflections

4.9.1 *Achlya bisexualis* hyphae

In studying protrusive force and invasive growth, it is the force at the very tips of hyphae that are most relevant. On the *A. bisexualis* chips described in this chapter, hyphae made initial contact with the pillars, either with their tips (Figure 4.6, 4.7) if they were growing down the centre of the channel, or with their sides, if they were growing more towards the edges of the channels. In some instances, contact with the tip was brief (1 - 2 min) as the tip either redirected or slipped off the pillar and the hypha squeezed by and then displaced the pillar with its side (Figure 4.8, 4.9). This had a significant impact on the forces that were measured.

In Figure 4.6, a hyphal tip is shown growing down the centre of a channel towards a pillar on a Version 4 chip. In the time series on the right, initial contact is made by the tip of the hypha with the pillar. Tracking of the pillar movement is shown by the red arrow which indicates the magnitude and direction of force. The deflection of the pillar up to around 10 min was parallel to the axis of growth, i.e. the red arrow is pointing upwards. This is corroborated by the fact that a large proportion of total force, up until around 10 minutes was due to the F_y-component (Figure 4.7b), because of the initial contact, and then the continued contact between the very tip of the hypha (which maintains a straight course of growth) and the pillar. In this instance, it is highly likely that it is protrusive force at the tip of the hypha that was being measured.

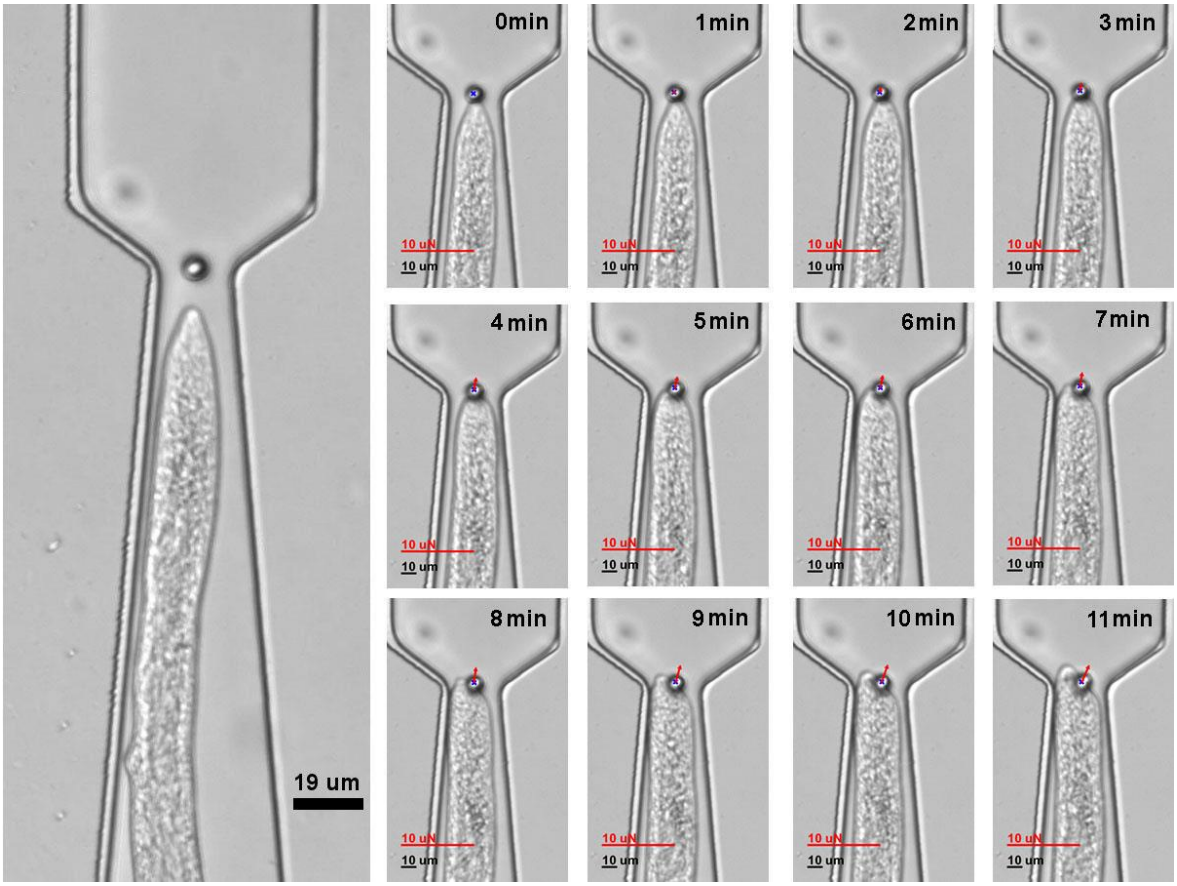

Figure 4.6. Measurement of protrusive force (F_y) of *A. bisexualis* on a Version 4 chip. The hyphal tip grew down the channel and the initial contact was made between the pillar and the very tip (0 min). The initial deflection of the pillar was parallel to the axis of growth (indicated by the upward pointing red arrow). This is also evident in that a large proportion of total force is due to the F_y component in Figure 4.7b.

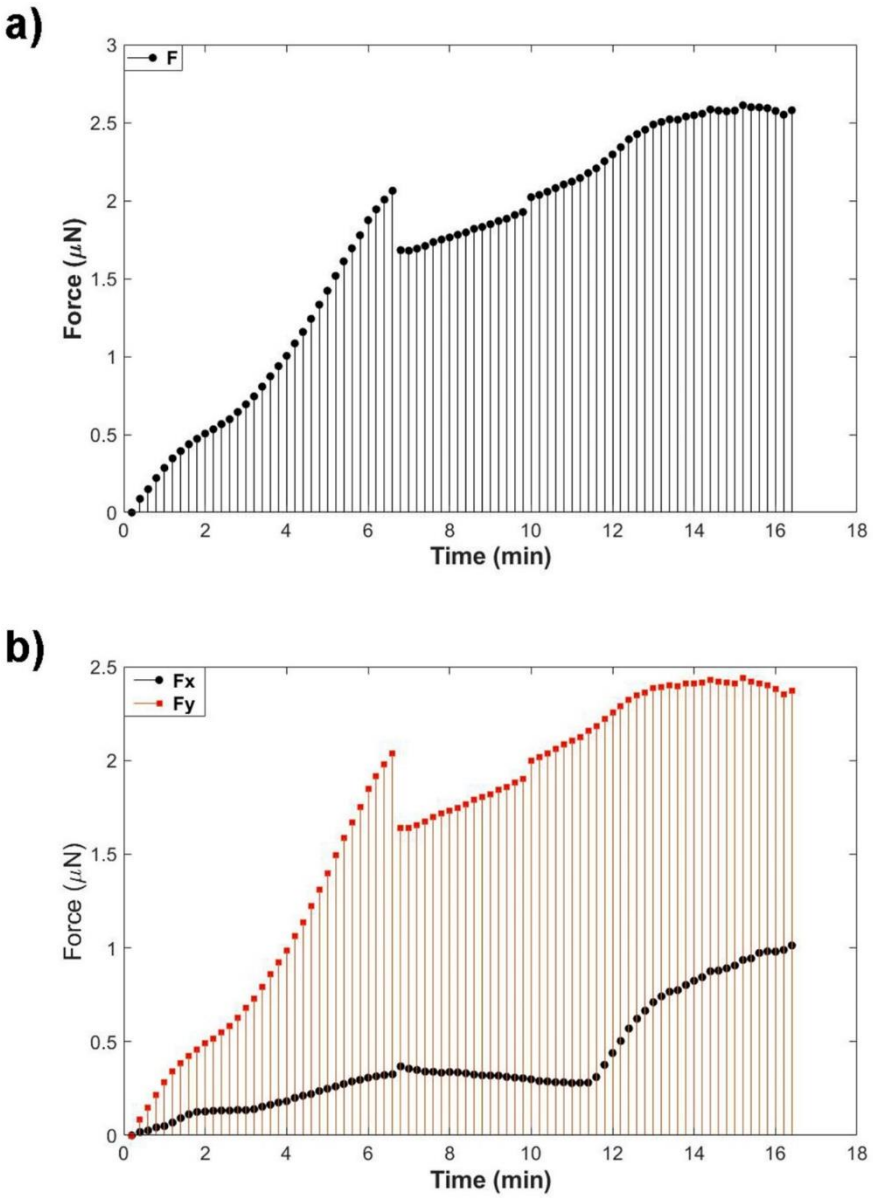

Figure 4.7. Force plots for the hypha shown in Figure 4.6. After initial contact was made (at time 0 min) the total force was seen to increase (a). The increase was largely due to the F_y component (b), parallel to the axis of growth, due to the initial and continued contact between the very tip of the hypha (which maintained a straight course of growth) and the pillar. The drop that occured around 10 mins appeared to be due to the tip of the hypha slipping off the pillar, but there was a slight recovery from 7 – 10 min before the F_x component increased as the side of the hypha pushed against the pillar (b).

In Figure 4.8, a hyphal tip is shown growing down the centre of a channel on a Version 5 chip. In the time series of images on the right side of the figure, the initial contact with the pillar can be seen to occur at the very tip at 2 min. However, by 3 - 4 min contact with the pillar was at the side of the hypha, subapical to the tip. This meant that the force plots for this series of images, shown in Figure 4.9a and b, are different from those in Figure 4.7. In this instance, there is a short initial protrusive force from the tip (F_y in Figure 4.9b), which gives way at 4 min to an increase in F_x (i.e. force exerted by the side of the hypha).

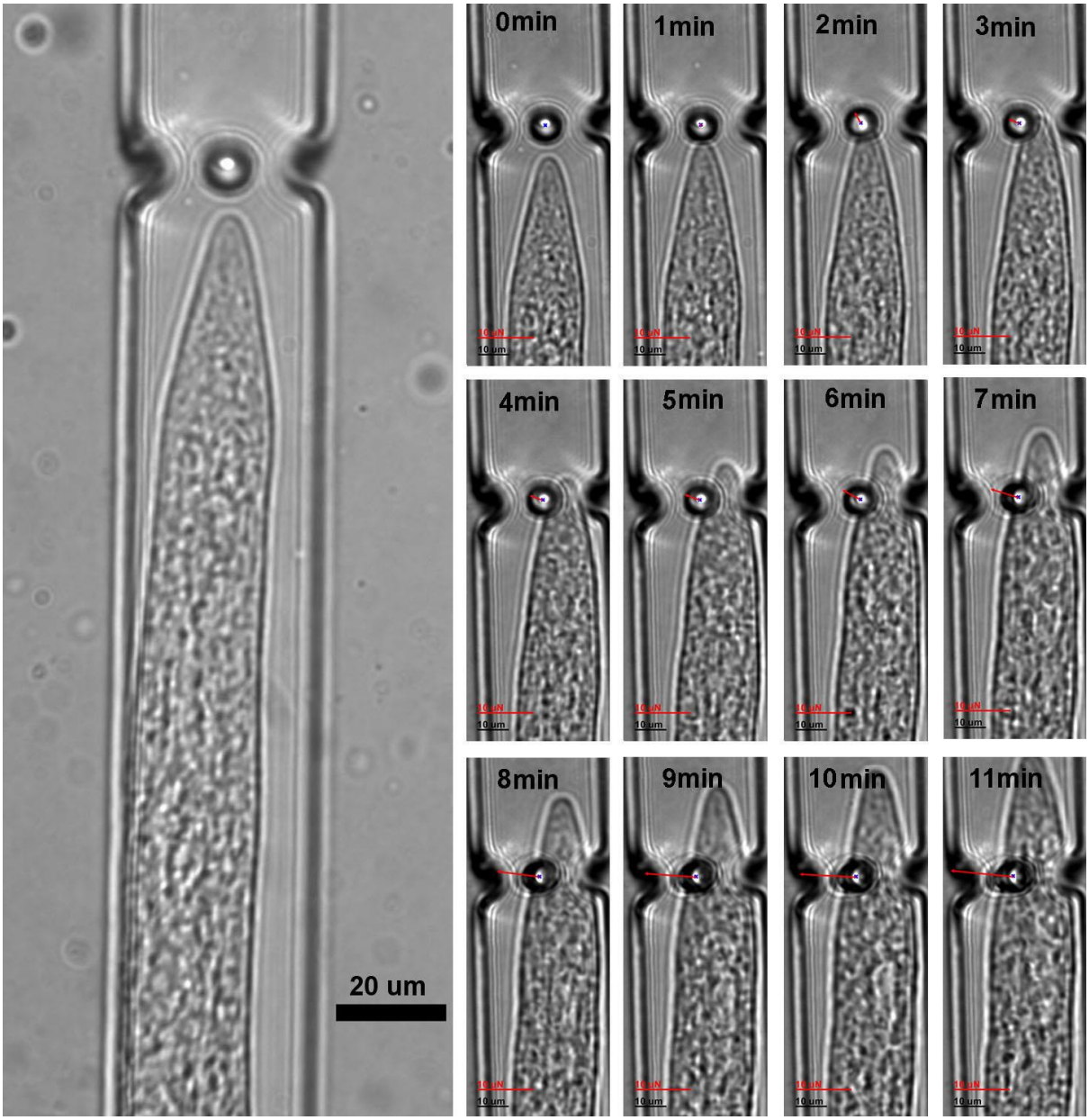

Figure 4.8. Growth of an *A. bisexualis* hypha on a Version 5 chip. The hyphal tip grew down the centre of the channel and the initial contact (shown in the time series at 1 min) was made between the pillar and the very tip. However, by 3 - 4 min it was the side of the hypha that exerted force on the pillar. This can be seen in the force plots in Figure 4.9, with a short initial period where most of the force was in the y-direction, which changed to the x-direction around 3 – 4 min.

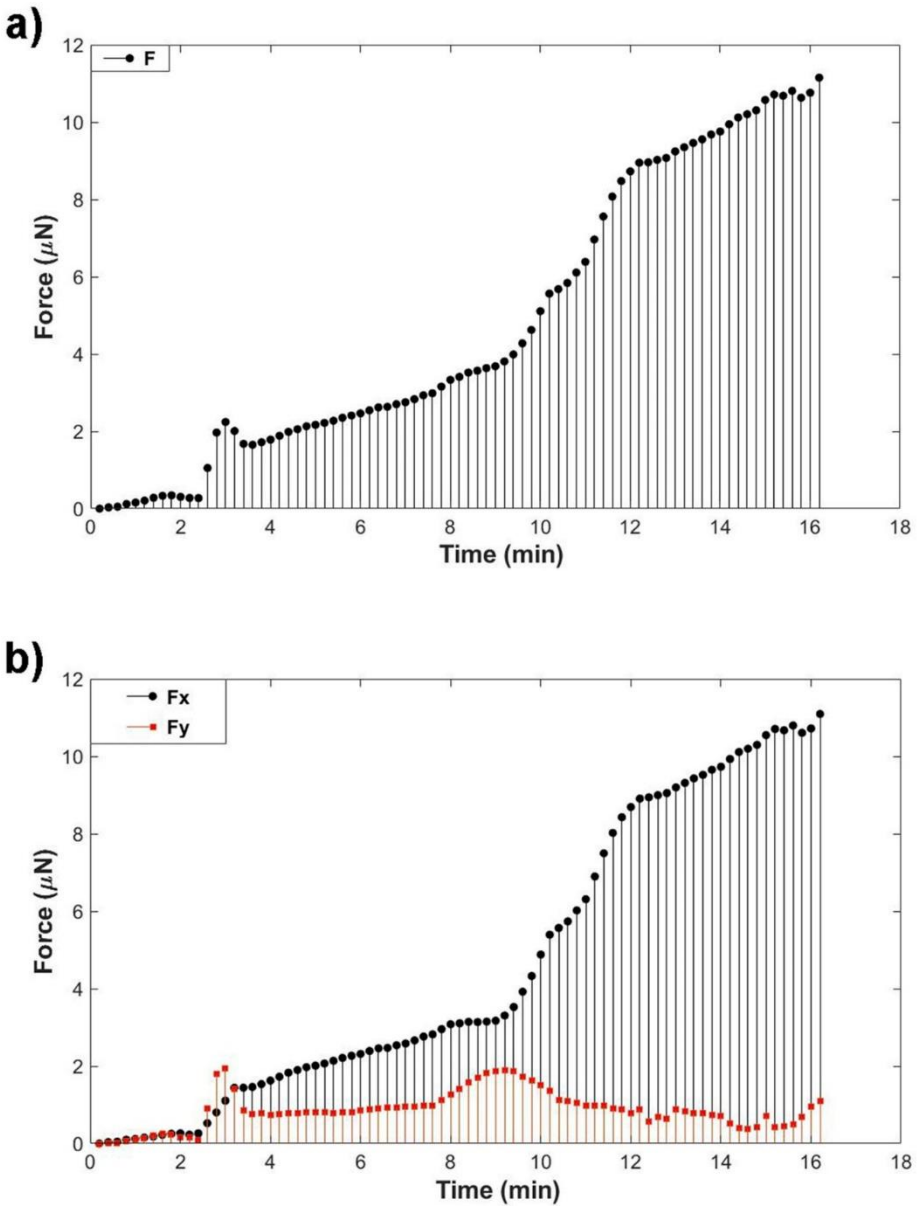

Figure 4.9. Force plots for the hypha shown in Figure 4.8. Initial contact is made around 2 min and the total force was seen to increase (a). This was largely due to the initial contact at the very tip of the hypha (Figure 4.8 at 0 - 2 min) and the generation of protrusive force (F_y in (b)). As the tip moved past the tip, it was then the side of the hypha that was exerting the force (Figure 4.8 at 3 - 4 min) and this was evident by the increase in F_x.

The proportions of hyphae that made initial contact the pillars via their tips versus those who contacted with their sides is summarised in Table 4.2. Of the 37 hyphae that were tested on Version 4 chips, only 8 of these were observed to contact the pillars with the very tip, with the remaining 33 (80%) contacting the pillar with their sides. Similarly, with the Version 5 chips 11 out of 43 (26%) contacted with their tips, compared to 56 (84%) with their sides. As indicated later in the thesis, (Table 6.1) the number of independent experiments carried out was 10 for Version 4 chips, and 24 for Version 5 chips. In the 10 experiments with Version 4 chips hyphae hit 48 pillars of which 41 were able to be tracked and a force measurement was obtained (an average of just over four measurements per experiment). In the 24 experiments with Version 5 chips, hyphae hit 89 pillars, of which 67 were able to be tracked and a force measurement was obtained (an average of just under three pillars per experiment).

	A. bisexualis chip	
Initial contact point	Version 4	Version 5
Tip	8 (20%)	11 (16%)
Side	33 (80%)	56 (84%)

Table 4.2. The initial contact points between *A. bisexualis* hyphae and pillars on Version 4 and 5 chips. In the majority of experiments, the contact between the pillar and a hypha occurred initially at the side of the hypha. 41 hyphae were observed on a Version 4 chip and 67 hyphae on a Version 5 chip. The numbers represent the number of hyphae that initially contacted the pillars, with their tip or their side, with the percentages of the total observations shown in brackets. It should be noted that this data set includes experiments where inhibitors were added just prior to the hyphae hitting the pillar (described more in Chapter 5). In these instances, the inhibitors did not impact on whether it was the tip or the side that then subsequently hit the pillar. The sample sizes in this table may thus not match those in subsequent tables or figures in this chapter as the inhibitor treated hyphae are excluded.

A summary of the average total force, F_x, F_y, growth rate and hyphal diameter, for

hyphae growing on Version 4 and 5 chips at the initial point of contact (0 min) and 2 and 5 min after contact are shown in Tables 4.3 and 4.4. Table 4.3 shows the data from those hyphae that hit the pillars with their tips first, and Table 4.4 for those hyphae that hit with their sides first. Consistent with the Version 3 chip data (Figure 4.4) there was a statistically significant decrease in the growth rate from 6.3 to 2.3 μm/min on the Version 4 chips and from 5.7 to 3.3 μm/min on the Version 5 chips as the tips hit the pillar ($P<0.05$, students t-test). and the hyphal diameter increases. The forces measured on the two chips were not significantly different, apart from the F_x value 5 min after contact (1.7 μN on the Version 4 chips compared to 0.5 μN on the Version 5 chips ($P < 0.05$, student t-test)). As would be expected, for those hyphae that hit with the tip first, a greater proportion of the total force is due to F_y (Table 4.3) and for those that hit with the sides a greater proportion of the total force is due to F_x (Table 4.4).

Time (min)	Total Force (μN)	F_x (μN)	F_y (μN)	Growth rate (μm/min)	Diameter (μm)
Version 4					
0	-	-	-	6.3 ± 0.7	19.2 ± 3.1
(range)	-	-	-	(5.5 – 7.3)	(14.3 – 22.9)
2	2.5 ± 1.7	0.5 ± 0.4	2.5 ± 1.7	3.9 ± 1.5	20.1 ± 3.0
(range)	(0.9 – 9.2)	(0.1 – 5.3)	(0.8 – 7.5)	(2.5 – 6.1)	(16.1 – 24.4)
5	5.6 ± 4.1	1.7 ± 1.2	5.2 ± 4.0	2.6 ± 1.4	21.6 ± 3.5
(range)	(1.9 – 13.6)	(0.4 – 3.5)	(1.8 – 13.3)	(1.4 – 5.1)	(16.4 – 25.3)
Version 5					
0	-	-	-	5.7 ± 0.5	20.9 ± 3.2
(range)	-	-	-	(4.8 - 6.5)	(15.0 – 24.6)
2	1.9 ± 2.6	0.3 ± 0.4	1.6 ± 1.9	4.4 ± 1.3	22.6 ± 3.2
(range)	(0.4 – 9.5)	(0.01 – 0.1)	(0.4 – 7.1)	(1.9 – 5.8)	(16.1 – 25.6)
5	4.3 ± 2.9	0.5 ± 0.4	4.1 ± 2.9	3.3 ± 0.6	21.2 ± 4.3
(range)	(1.8 – 8.7)	(0.1 – 1)	(1.6 – 8.7)	(2.6 – 3.9)	(15.9 – 25.7)

Table 4.3. Total force, F_x and F_y for *A. bisexualis* hyphae growing on Version 4 and Version 5 chips which made initial contact with the pillars with their tips. Values shown are mean ± SD. Sample sizes for Version 4 chips were n = 8 (t = 0 and t = 2 min) and n = 7 (t = 5 min) and for Version 5 were n = 11 (t = 0 and t = 2 min) and n = 7 (t = 5 min).

It is possible to convert the protrusive force values into the pressure applied to the pillar, if the area of contact between the hypha and the pillar is known. This was estimated by measuring the width of the hypha in direct contact with the pillar. Assuming the area was a circle (and hence equal to πr^2), for Version 4 and Version 5 chips 2 mins after initial contact, the mean areas were 27.1 and 26.1 μm^2 respectively. Given the F_y values of 1.6 and 2.5 μN (Table 4.3) for the Version 4 and

5 chips these would give pressure values of 0.06 and 0.096 $\mu N/\mu m^{2.}$

For those hyphae which hit the pillars with their tips, the relationship between F_y at 2 min after initial contact and hyphal growth rate and diameter prior to contact for the Version 4 and Version 5 chips are presented in Figures 4.10 – 4.13. Regression analyses indicated no significant relationship between F_y (at either 2 or 5 min) and growth rate or hyphal diameter on either of the chips.

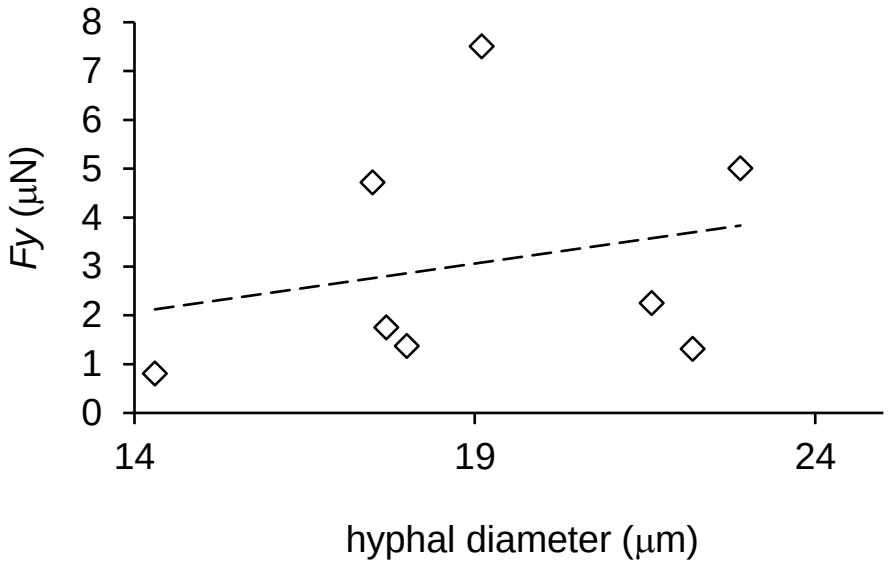

Figure 4.10. A scatter plot of hyphal diameter prior to contact and F_y 2 min after contact with the pillar on a Version 4 chip. A multilinear regression analysis revealed no relationship between diameter and force either at 2 min (P = 0.56) or at 5 min (P = 0.23) (data not shown for clarity). Data are fitted with a linear trend line (R^2 = 0.06).

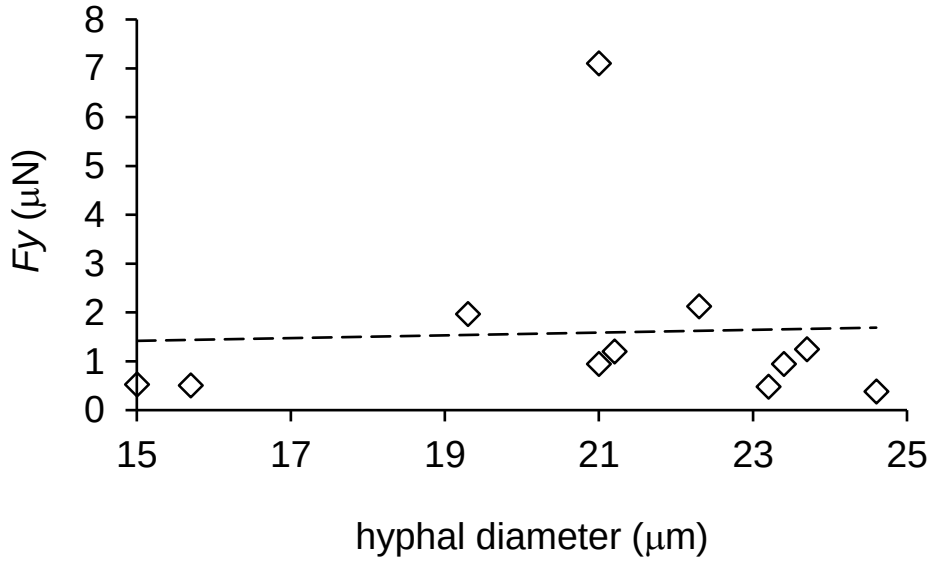

Figure 4.11. A scatter plot of hyphal diameter prior to contact and F_y 2 min after contact with the pillar on a Version 5 chip. A multilinear regression analysis revealed no relationship between diameter and force either at 2 min (P = 0.89) or at 5 min (P = 0.92) (data not shown for clarity). Data are fitted with a linear trend line (R^2 = 0.002).

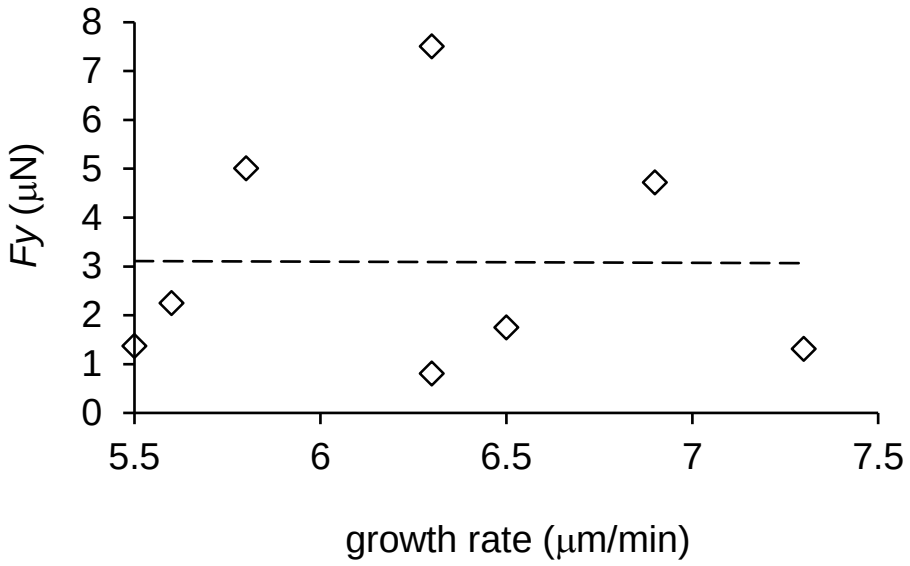

Figure 4.12. A scatter plot of hyphal growth rate prior to contact and F_y 2 min after contact with the pillar on a Version 4 chip. A multilinear regression analysis revealed no relationship between growth rate and force either at 2 min (P = 0.98) or at 5 min (P = 0.6) (data not shown for clarity). Data are fitted with a linear trend line (R^2 = 0.00004).

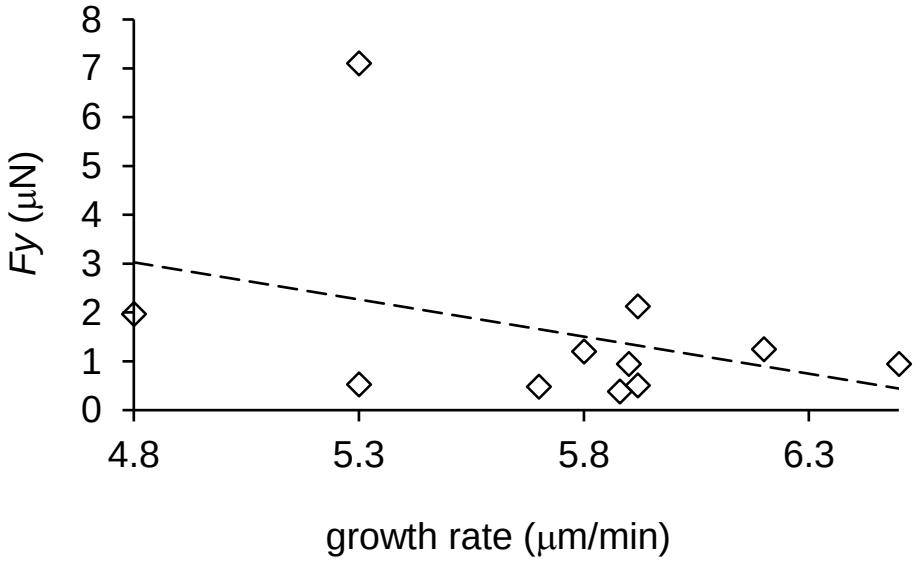

Figure 4.13. A scatter plot of hyphal growth rate prior to contact and F_y 2 min after contact with the pillar on a Version 5 chip. A multilinear regression analysis revealed no relationship between growth rate and force either at 2 min (P = 0.26) or at 5 min (P = 0.22) (data not shown for clarity). Data are fitted with a linear trend line (R^2 = - 0.14).

Time (min)	Total Force (μN)	F_x (μN)	F_y (μN)	Growth rate (μm/min)	Diameter (μm)
Version 4					
0	-	-	-	5.6 ± 1.2	19.7 ± 3.8
(range)	-	-	-	(4.3 – 6.8)	(17.5 – 22.3)
2	1.4 ± 1.7	1.2 ± 1.3	0.2 ± 0.3	5.0 ± 1.2	20.4 ± 4.0
(range)	(0.02 – 7.3)	(0.02 – 5.17)	(0 – 1.2)	(3.7 – 6.2)	(18.3 – 22.9)
5	3.7 ± 4.0	3.2 ± 3.4	0.4 ± 0.4	4.4 ± 1.1	21.2 ± 4.2
(range)	(0.4 – 17.2)	(0.4 – 13.9)	(0.01 – 1.5)	(3.1 – 5.8)	(19.1 – 23.4)
Version 5					
0	-	-	-	5.2 ± 0.8	20.0 ± 1.6
(range)	-	-	-	(3.9 – 6.5)	(16.5 – 22.5)
2	3.9 ± 3.4	3.6 ± 3.2	0.5 ± 0.4	4.5 ± 0.9	20.8 ± 1.6
(range)	(0.2 – 14.3)	(0.2 – 13.0)	(0.02 – 1.3)	(3.1 – 5.9)	(17.6 – 23.1)
5	5.7 ± 6.7	4.9 ± 5.3	0.7 ± 0.6	3.9 ± 0.9	21.8 ± 1.7
(range)	(1.5 – 17.3)	(1.4 – 14.1)	(0.2 – 1.8)	(3.6 – 5.2)	(19.0 – 23.4)

Table 4.4. Total force, F_x and F_y for *A. bisexualis* growing on Version 4 and Version 5 chips which made initial contact with the pillars with the sides of hyphae. Values shown are mean ± SD. Sample sizes for the Version 4 chips were n = 29 (t = 0 and t = 2 min) and n = 27 (t = 5 min) and for the Version 5 chips were n = 23 (t = 0 and t = 2 min) and n = 5 (t = 5 min).

While a detailed analysis of the forces imparted by the sides of hyphae (i.e. F_x) is beyond the scope of this thesis it is interesting to note that there were significant differences between the Version 4 and Version 5 chips for the total force, F_x and F_y (all of which were greater on the Version 5 chips, 2 min after initial contact with the pillar ($P < 0.05$, students t-test)). Furthermore on the Version 4 chips total force, F_x , F_y and hyphal diameter significantly increased between 2 and 5 min while growth rate significantly decreased (all $P < 0.05$, students t-test). For the Version 5 chips significant decreases in growth rate were observed at 2 and 5 min after contact,

relative to the initial growth rate ($P < 0.05$, students t-test).

4.9.2 *Neurospora crassa* hyphae

The same force sensing techniques were used for experiments with *N. crassa*, although the smaller size of the fungal hyphae meant modifications to the chip design. As described in Chapter 3, the Version 1 and 2 *N. crassa* chips were based on the Version 4 and 5 *A. bisexualis* chips, with parallel channels emanating out from a seeding area. Each of these channels contained a single pillar towards the end of a narrow taper. Given the smaller hyphae, the channel and pillar dimensions were modified, channels were either 10 or 17 μm wide and the pillars had a diameter of 5 μm. This meant a smaller gap between the edge of the pillar and the side of the channel, and compared to *A. bisexualis*, this resulted in more hyphal tip-pillar interactions than sides of the hyphae – pillar interactions (Table 4.5). As indicated later in the thesis (Table 6.1), 21 independent experiments were carried out with the *N. crassa* Version 2 chips. In these experiments, hyphae hit 78 pillars of which 51 were able to be tracked and a force measurement was obtained (an average of just under four measurements per experiment).

	N. crassa chip	
Initial contact point	P5C17	P5C10
Tip	17 (42%)	10 (100%)
Side	24 (58%)	-

Table 4.5. The initial contact points between *N. crassa* hyphae and pillars on two different Version 2 chips. The chips contained pillars with the same width (5 μm (P5) but differed in the width of the channels (either 10 μm (C10) or 17 μm (C17)). In the majority of experiments the contact between the pillar and hypha occurred initially at the tip. In total 41 hyphae were observed on the P5C17 chip and 10 hyphae on the P5C10 chip. The numbers represent the number of hyphae that initially contacted the pillars with their tip or their side with the percentages of the total observations shown in brackets. As for the *A. bisexualis* data in Table 4.2 it should be noted that this data set includes experiments where inhibitors were added just prior to the hyphae hitting the pillar (described more in Chapter 5). In these instances, the inhibitors did not impact on whether it was the tip or the side that then subsequently hit the pillar. The sample sizes in this table may thus not match those in subsequent tables or Figures in this chapter as the inhibitor-treated hyphae are excluded.

A hypha is shown growing down the final taper of a channel on a Version 2 chip (P5C17) in Figure 4.14. The hyphal tip can be seen contacting the pillar in the initial time series image. Force tracking as shown by the blue arrow indicates the force parallel to the axis of growth (F_y) (Figure 4.15). As for the *A. bisexualis* hypha in Figures 4.6 and 4.7, the directionality of this would suggest that it is likely to be a protrusive force. The F_x component then increases as the side of the contacts the pillar as it squeezes into the gap between the pillar and the channel wall (Figure 4.14, 4.15).

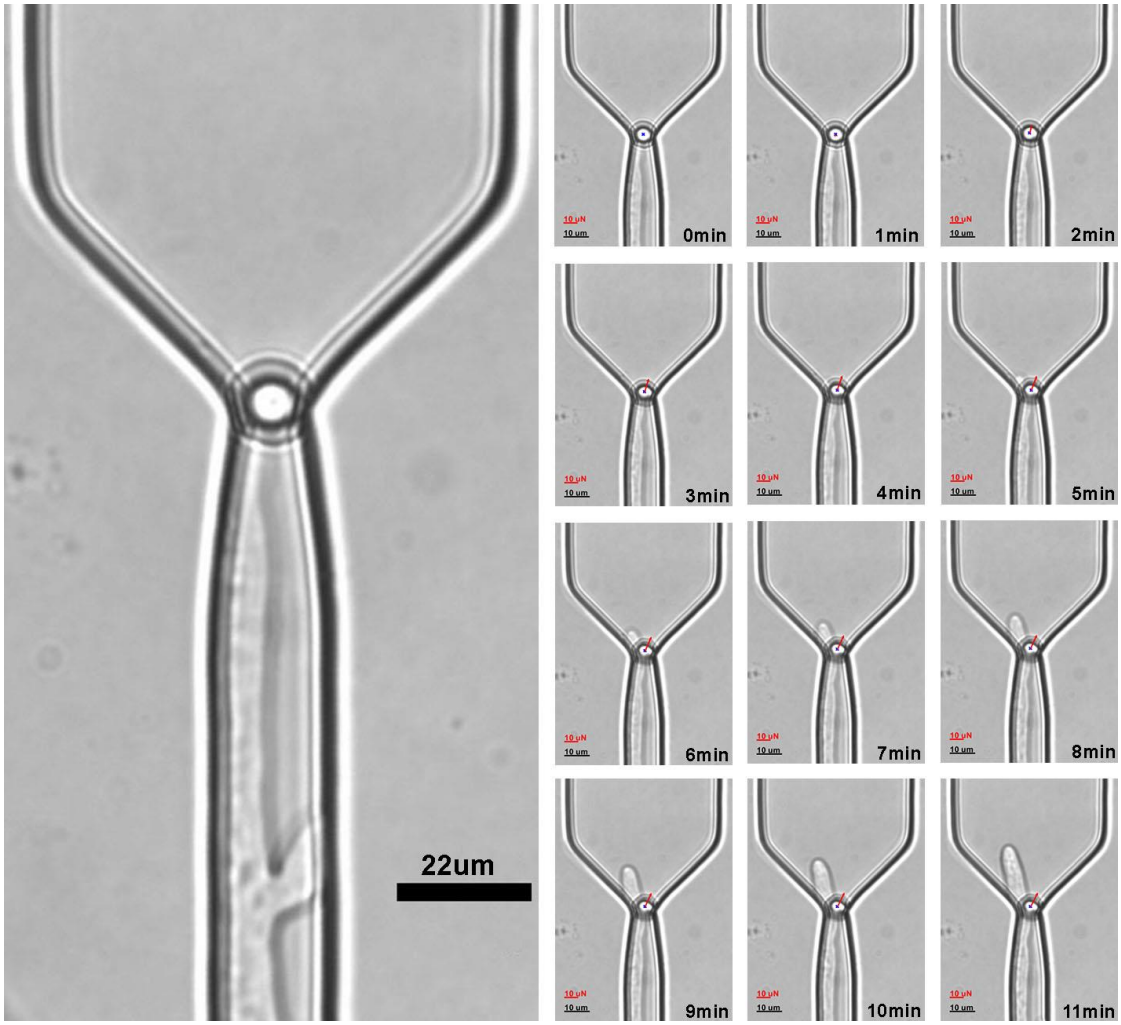

Figure 4.14. Growth of a *N. crassa* hypha on a Version 2 (P5C17) chip. The hyphal tip grew down the left edge of the channel, possibly due to the force applied as a branch formed and grew into the channel wall, but because of the taper the initial contact (shown in the time series at 0 min) was made between the pillar and the tip. Because of the contact by the tip, the force generation was primarily in the y-direction as indicated by the upward pointing red arrow. The force was likely a protrusive force at the tip. As the hypha began to squeeze between the pillar and the channel wall there was increasing force applied in the x-direction by the side of the hypha.

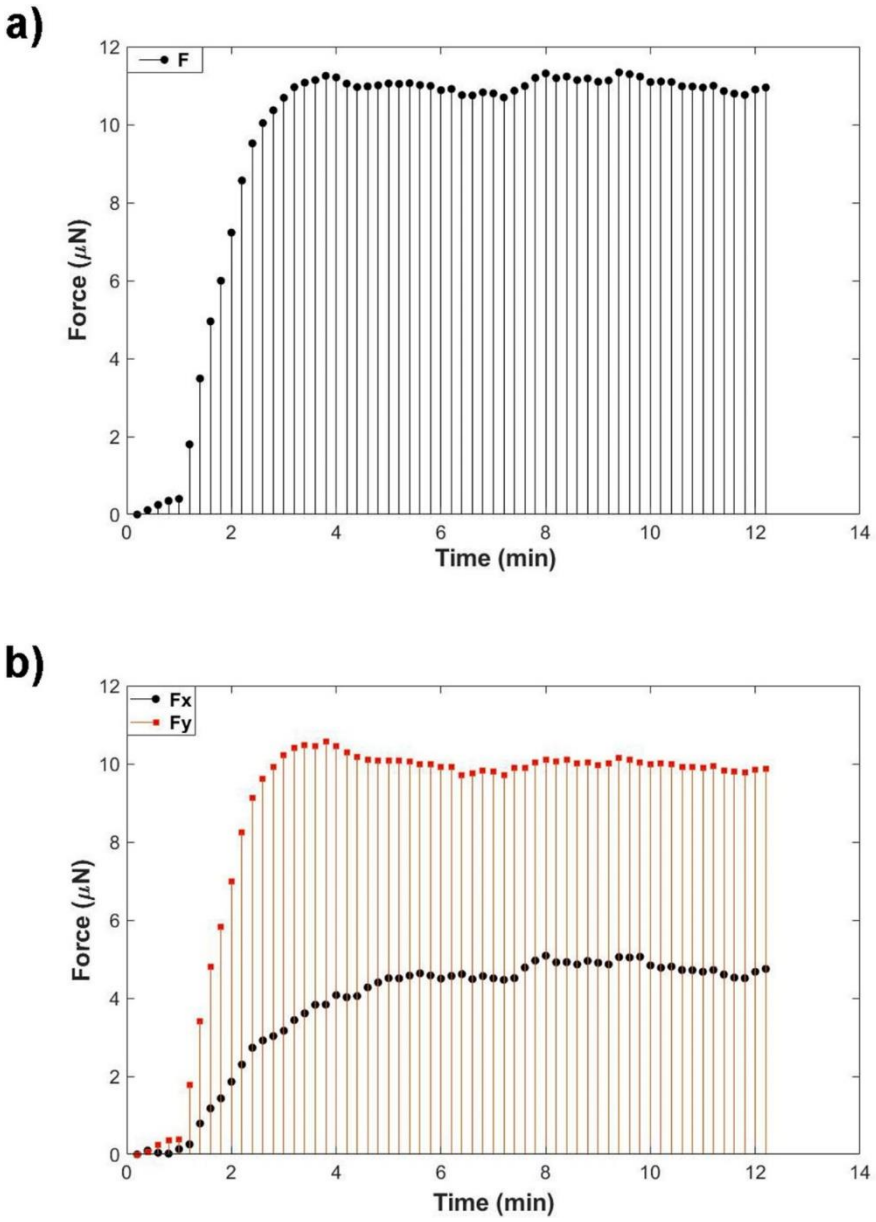

Figure 4.15. Force plots for the *N. crassa* hypha shown in Figure 4.14. Initial contact was made at 0 min and the total force was seen to increase slowly prior to a more rapid increase (a). The initial and subsequent force was primarily in the y-direction (F_y), parallel to the axis of growth, due to the contact between the very tip of the hypha, which maintained a relatively straight course of growth, and the pillar. As the side of the hypha pushed against the pillar there was a resultant increase in F_x.

A summary of the average total force, F_x, F_y, hyphal growth rate, hyphal diameter, contact area and pressure for hyphae growing on the two different chips immediately prior (0 min) to contact, and 2 and 5 min after contact is shown in Table 4.6. As for *A. bisexualis*, there were significant decreases in growth rate as the hyphae hit the pillars on both versions of the chip ($P < 0.05$, students t-test), and an increase in hyphal diameter as the hypha imparted force onto the pillar. No significant differences were observed in the forces measured on the two versions of the chip nor in the diameters of the hyphae. Due to the relatively small diameter of *N. crassa* hyphae measurements of contact area could not be reliably made and so it was not possible to estimate the pressures applied by the hyphae on the pillars.

Time (min)	Total Force (μN)	F_x (μN)	F_y (μN)	Growth rate (μm/min)	Diameter (μm)
P5C17					
0	-	-	-	3.2 ± 1.0	4.9 ± 0.9
(range)	-	-	-	(2.1 – 5.2)	(4 – 7.4)
2	3.4 ± 3.1	1.4 ± 1.8	3.0 ± 2.7	2.5 ± 0.9	5.3 ± 0.8
(range)	(0.6 – 11.8)	(0.05 – 6.0)	(0.5 – 10.2)	(1.3 – 4.7)	(4.2 – 7.4)
5	6.3 ± 4.5	2.8 ± 2.4	5.5 ± 4.1	1.6 ± 0.6	5.3 ± 0.6
(range)	(1.5 – 13.8)	(0.6 – 7.9)	(1.1 – 12.1)	(1.1 – 2.6)	(5.3 – 6.8)
P5C10					
0	-	-	-	2.6 ± 0.3	5.7 ± 1.1
(range)	-	-	-	(2.1 – 3.1)	(4.3 – 7.5)
2	2.3 ± 1.9	0.9 ± 1.1	2.1 ± 1.7	2.1 ± 0.5	6.0 ± 0.8
(range)	(0.5 – 5.6)	(0 – 3.3)	(0.5 – 5.4)	(1.2 – 2.7)	(4.7 – 7.4)
5	5.3 ± 3.6	2.2 ± 1.5	4.7 ± 3.6	1.6 ± 0.5	5.8 ± 0.7
(range)	(1.5 – 12.1)	(0.9 – 4.6)	(1.1 – 12.1)	(0.5 – 2.1)	(5.0 – 7.1)

Table 4.6. Total force, F_x and F_y for *N. crassa* growing on Version 2 P5W17 and P5W10 chips which made initial contact with the pillars with the tips of the hypha. Values shown are mean ± SD. Sample sizes for the P5C17 chips were n = 19 (t = 0 and t = 2 min) and n = 11 (t = 5 min) and for the Version P5C10 chips were n = 9 (t = 0 and t = 2 min) and n = 8 (t = 5 min).

For those hyphae which hit the pillars with their tips, the relationship between F_y at 2 min after initial contact and hyphal growth rate and diameter prior to contact for the P5C17 and the P5C10 chips are presented in Figures 4.16 – 4.19. As for the *A. bisexualis* data, regression analyses indicated no significant relationship between F_y (at either 2 or 5 min) and growth rate or hyphal diameter on either of the chips.

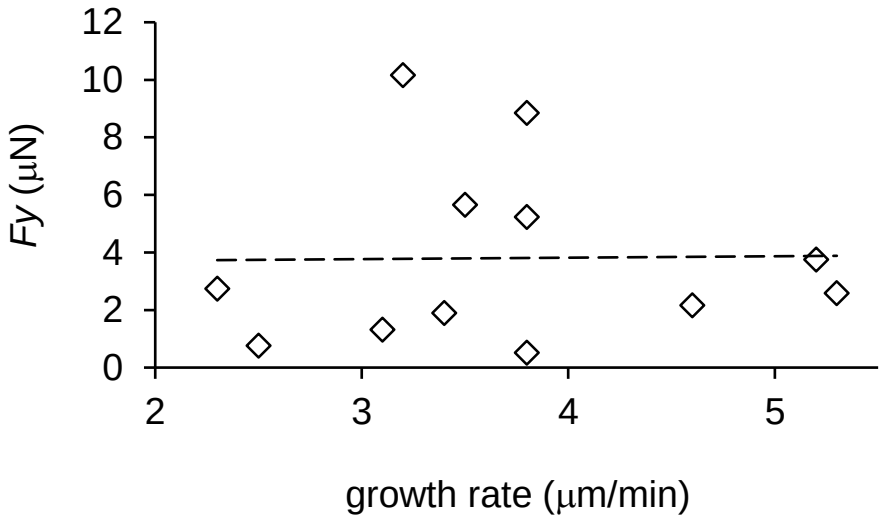

Figure 4.16. A scatter plot of *N. crassa* hyphal growth rate prior to, and F_y 2 min after, contact with the pillar on a P5C17 chip. A multilinear regression analysis revealed no relationship between growth rate and force either at 2 min (P = 0.96) or at 5 min (P = 0.33) (data not shown for clarity). Data are fitted with a linear trend line (R^2 = 0.0002).

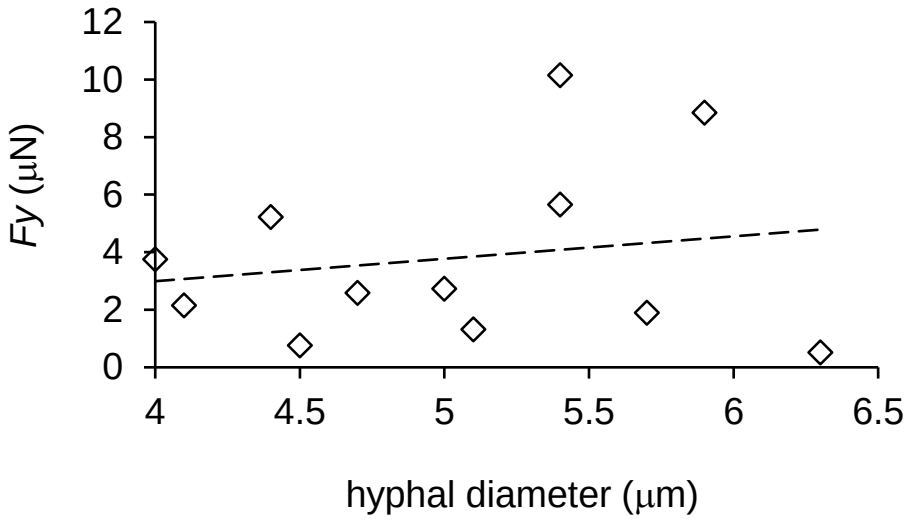

Figure 4.17. A scatter plot of *N. crassa* hyphal diameter prior to, and $F_{y,}$ 2 min after, contact with the pillar on a P5C17 chip. A multilinear regression analysis revealed no relationship between growth rate and force either at 2 min (P = 0.57) or at 5 min (P = 0.064) (data not shown for clarity). Data are fitted with a linear trend line (R^2 = 0.03).

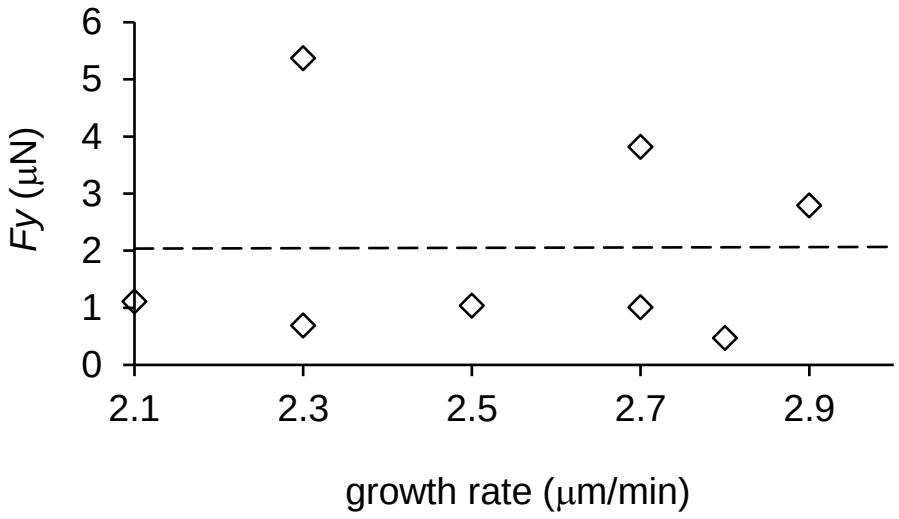

Figure 4.18. A scatter plot of *N. crassa* hyphal growth rate prior to, and F_y, 2 min after, contact with the pillar on a P5C10 chip. A multilinear regression analysis revealed no relationship between growth rate and force either at 2 min (P = 0.98) or at 5 min (P = 0.8) (data not shown for clarity). Data are fitted with a linear trend line (R^2 = 0.01).

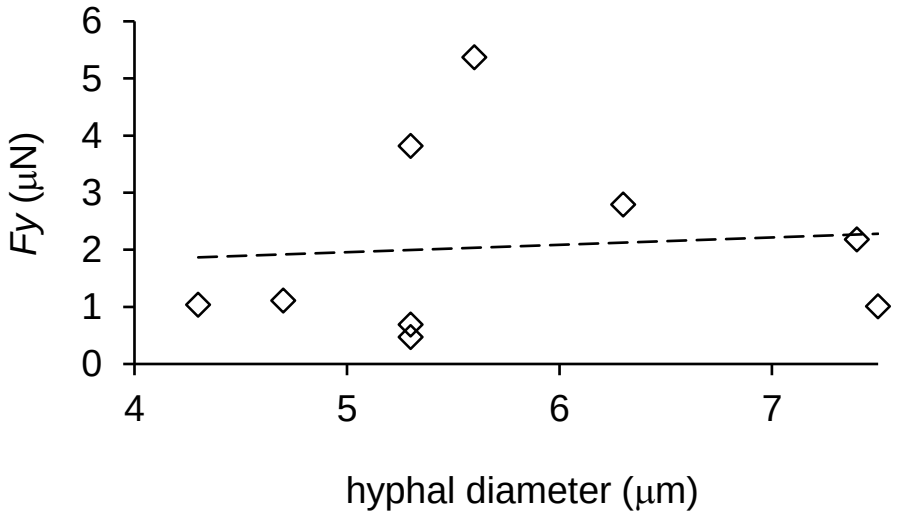

Figure 4.19. A scatter plot of *N. crassa* hyphal growth rate prior to, and F_y, 2 min after, contact with the pillar on a P5C10 chip. A multilinear regression analysis revealed no relationship between growth rate and force either at 2 min (P = 0.49) or at 5 min (P = 0.6) (data not shown for clarity). Data are fitted with a linear trend line (R^2 = 0.083).

A detailed analysis of the forces imparted by the sides of *N. crassa* hyphae (i.e. F_x) is beyond the scope of this thesis. A smaller proportion of hyphae hit the pillars with their sides relative to *A. bisexualis*, which meant a lower sample size and also, they only did so on the P5C17 chips. Total force, Fx, Fy 2 and 5 mins after initial contact as well as growth rate and hyphal diameters are presented in Table 4.7. Significant differences were seen only in the growth rates which decreased from 0 min to 2 and 5 min ($P< 0.05$, students t-test).

Time (min)	Total Force (μN)	F_x (μN)	F_y (μN)	Growth rate (μm/min)	Diameter (μm)
P5C17					
0	-	-	-	2.8 ± 0.3	5.8 ± 0.8
(range)	-	-	-	(2.1 – 3.2)	(4.1 – 6.7)
2	6.5 ± 4.2	5.6 ± 3.6	0.8 ± 0.5	2.1 ± 0.4	5.2 ± 0.7
(range)	(0.7 – 13.0)	(0.7 – 10.7)	(0.2 – 1.4)	(1.6– 2.7)	(3.8 – 6.1)
5	9.2 ± 9.6	8.8 ± 9.2	2.3 ± 3.2	1.4 ± 0.5	4.1 ± 1.4
(range)	(1.6 – 20.0)	(1.4 – 19.1)	(0.2– 5.9)	(0.9 – 1.9)	(3.0 – 5.7)

Table 4.7. Total force, F_x and F_y for *N. crassa* growing on Version 2 P5W17 chips which made initial contact with the pillars with the sides of the hypha. Values shown are mean ± SD. Sample sizes were n = 9 (t = 0 and t = 2 min) and n = 3 (t = 5 min).

4.10 Discussion

This chapter describes the first use of elastomeric pillars for the measurement of protrusive forces in fungal and oomycete hyphae. Devices were designed with tapered or straight narrow channels that directed hyphae toward flexible pillars that were displaced when hyphae grew into them. These displacements enabled the measurement of forces in the micro-Newton range, and at the same time, measurements of growth rate and hyphal diameter.

The Version 2 and 3 chips were useful in the development of the force-sensing principle. However, their use was discontinued due to the radial arrangements of channels, which made imaging of several hyphae on the same chip difficult. Given that all channels and pillars were equidistant from one side of the inoculation plug, hyphae tended to hit the pillars around approximately the same time and so typically only one or two hyphae could be imaged hitting the pillars for each chip. Also, as the inoculation plug was taken from the growing edge of a colony, hyphae tended to grow out more quickly from one side of the plug compared to the other. This meant that channels on the other side (not facing the growing edge of the inoculation plug) were either redundant or there was a very long-time gap between the hyphae growing down channels on one side of the chip compared to the others. In the Version 4 and 5 *A. bisexualis* and Version 2 *N. crassa* chips, multiple linear channels meant that measurements could be made on multiple hyphae on the same chip. The observation that several hyphae could concurrently grow down the tapered channels of the Version 4 *A. bisexualis* chips (see for example the left most channel in Figure 4.5b) meant that any force measurements may have been compromised by the proximity of other hyphae. In view of this, for most of the subsequent experiments on

the cytoskeleton described in Chapter 5, the Version 5 chips were used.

Various techniques, including optical wave-guides (Bechinger et al., 1999), micro-strain gauges (Money et al., 2004) and optical tweezers (Wright et al., 2005) have previously been used to measure forces at the tips of hyphae or in infection structures, and these also all point to forces in the micro-Newton range. These equate to pressures ranging from 0.2 MPa in hyphae to >5 MPa in appressoria (Money et al., 2004). LOC devices have thus far only been used to measure forces in one fungal species, the fission yeast *S. pombe* (Minc et al., 2009). These devices contained small chambers that buckled as the cells grew and enabled measurement of the elastic modulus of the cell wall of 20.2 N/m, and estimations of turgor pressure of 0.85 MPa. In tip growing pollen tubes LOC devices have been used to measure penetrative pressures of 0.15 MPa (Nezhad et al., 2013).

With the pillars, an important attribute is the ability not just to measure total force, but also to differentiate this into the F_x and F_y components. This means that protrusive forces, which are generated by the tips of the hyphae growing against the pillars, can be differentiated from the squeezing or pushing forces, generated by the sides of hyphae as they grow between the pillars and the channel walls. While it is possible to observe which part of the hypha is in contact with the pillar through the microscope (which would be prone to subjectivity), the different force components provide an additional means to determine this. Furthermore, with small hyphae it can be difficult to be certain which part is in contact, and so in these instances the different force components are invaluable. The hyphae depicted in Figure 4.6 (*A. bisexualis*) and Figure 4.14 (*N. crassa*), made initial pillar contact with their tips and the force vector plots (Figures 4.7 and 4.15) showed significant contributions of F_y to

the total force. Thus, in these hyphae it is likely that it was the protrusive force that was being measured. Conversely, the *A. bisexualis* hypha depicted in Figure 4.8, despite initial contact with the tip, imparted a squeezing force 2 – 3 min after contact, rather than a protrusive force. This can be seen in the shift in the contributions of the F_y and the F_x components to the total force (Figure 4.9). Thus, if this hypha were to be used to study protrusive force only the first 1 – 2 min would be relevant. With the other methodologies that have previously been used to study force in fungal hyphae observations of the contact through the microscope would be the only way to differentiate protrusive from squeezing forces. Thus, the use of pillars and force vectors with the LOC-based approach removes any potential subjectivity associated with microscopic observations alone.

Given that force measurements were reliant upon the tips of hyphae growing into the pillars, the channels were designed with tapers that directed the growth of the hyphae towards either an array of pillars or a single pillar. While this was on the whole successful, the hyphae were still quite adept at avoiding tip contact with the pillars. With the Version 4 and 5 *A. bisexualis* chips, many of the hyphae grew into the gaps beside the channels or made initial contact with the tips, but then reoriented their growth or slid off the pillar (as in Figure 4.8) – in all of these instances a squeezing force (F_x) was imparted on the chip. This meant that many recordings were not usable and led to the lower sample sizes for tip deflections.

The *N. crassa* chips were more successful at recording protrusive forces, with a higher proportion of tips contacting the pillars rather than the sides of the hyphae. It is unlikely that this difference is due to the relative widths of the channels and hyphae of *N. crassa* and *A. bisexualis*. The channel widths on the *N. crassa* P5C10

chips were 10 μm and the average hyphal diameter was around 6.0 μm, this compares to a channel width of 35 μm on the *A. bisexualis* chips and average hyphal diameters around 20.0 μm for the Version 4 and 5 chips. Thus, the ratio of hyphal diameter/channel width is approximately the same in the two species - 0.6 (P5C10 *N. crassa*) and 0.57 (Version 4 *A. bisexualis*). The ratio for the P5C17 chips is 0.35 but on these a lower proportion of hyphae contacted pillars with their tips first compared to the P5C10 chips. While the *N. crassa* hyphae appeared healthy, they grew slowly on the chips. It is not clear whether this was due to the PDMS or to the dimensions of the channel. Previous workers have reported *N. crassa* growth rates to be affected by the length of channels on LOC devices (Geng et al., 2015). With a slower rate of growth, it is possible that there is a corresponding slower process of reorienting growth, meaning the hyphae are not able to avoid the pillars. Thigmotropic response has been reported for *Candida albicans* hyphae growing against PDMS obstacles (Thomson et al., 2015, 2016). For *C. albicans*, it was concluded that hyphal reorientation occurs at tip pressures higher than those required for plasma membrane penetration.

While there were no statistically significant differences in hyphal diameters as they hit the pillars, it was possible to observe a trend of hyphae widening as they hit the pillar. The lack of statistical significance may reflect the relatively low sample size. Any increase in the diameter of the hyphae as they contact the pillar would be consistent with observations made using strain gauges to measure force (Money et al., 2004). Published micrographs of hyphae growing into micro-strain gauges suggest that *A. bisexualis* hyphae widen subapically as they make contact with the gauge (Money et al., 2004). It is not clear if this response is analogous to the crumpling of a car hitting a wall or may in fact reflect the hyphae temporarily stopping

growth and then building up sufficient turgor and/or modulating the plasticity of the wall to generate the protrusive force required to displace the pillar and continue growing beyond it. While in the present study the hyphal diameter was measured 10 μm behind the tip, it is likely that this widening of the hyphae may also impact on the surface area of the hypha that is in contact with the pillar, which in turn will affect the pressure that is applied - the greater the surface area the lower the pressure.

The pressure applied to the pillars by *A. bisexualis* hyphae has been calculated to be 0.06 and 0.096 $\mu N/\mu m^2$ for Version 4 and 5 chips respectively. As described above, to obtain these pressures, it was assumed that the contact area was a circle, the diameter of which was the length of visible contact between the tip and the pillar in images. The resolution of the images at the actual contact point meant that these measurements were at best an estimate and, in the case of *N. crassa,* these could not be reliably obtained.

This pressure can be used as an indication of the compliance of the cell wall at the tip. Turgor values of 0.65 MPa have been measured using a single cell pressure probe on *A. bisexualis* hyphae (Lew et al., 2004, Walker et al., 2006). As a consequence, this suggests that between 9 (Version 5 chip data) and 15 (Version 4 chip data) percent of the turgor pressure is generating protrusive force and the rest must presumably be overcoming wall/cytoskeletal resistance, indicating low compliance of the cell wall. This is consistent with the findings of others who have measured protrusive force in hyphae using a micro-strain gauge. For *A. bisexualis*, pressures of 0.11 MPa were exerted by hyphae with measured turgor pressures of 0.69 MPa (Money et al., 2004), thus only 16 percent of turgor was generating protrusive force at the tip. For other oomycete species values ranged from 2 percent

to 54 percent, with the higher value only observed with certain media, and for fungi values ranged from 9 percent to 32 percent (Money et al., 2004). These values contrast with those from tip growing pollen tubes, where the maximum pressure exerted on the sides of a micro-gap in channels was 0.15 MPa. In pollen tubes typical turgor pressures of between 0.2 MPa up to 0.35 MPa have been reported, suggesting a much more compliant cell wall, i.e. a much higher proportion of turgor is generating protrusive force rather than overcoming wall/cytoskeletal resistance (Nezhad et al., 2013).

The lack of a relationship between F_y and the diameter of hyphae or the growth rate in the present thesis is difficult to explain. Certainly, an increase in F_y with larger and/or faster growing hyphae would have been expected (Money et al., 2004). Using the micro-strain gauge, Money et al. (2004) accounted for any differences in force measurement that may have been due to the variability in hyphal size by converting force measurements into pressure. While estimates have been made of pressure, as described above, this was difficult due to poor resolution at the point of contact. The lack of a relationship may be due to the resolution of the imaging system and poor tracking of pillar movements, due to optical noise. It would certainly suggest that, while micro-Newton forces are measurable, the LOC systems at present may need significant refinement for more detailed study of the mechanisms of protrusive force generation at the cellular level. This is considered in more depth in the conclusions in Chapter 7.

While they were not the focus of this thesis, the squeezing forces (and thus recordings where the major component of the total force was the F_x component) are of interest with respect to cell wall properties. With the appropriate chip design,

hyphae may be directed down channels towards pillars, in such a way that different parts of a hypha will contact the pillar first. The measurement of the forces, coupled with microscopic observations of the wall may present a means to map the viscoelastic properties of the cell wall along a hypha. This is a somewhat similar approach to micro-indentation techniques, which have been used to indicate the importance of the extensibility of the cell wall as a key determinant of extension rates (Zerzour et al., 2009) and also the constriction channels that have been used to measure protrusive force in pollen tubes (Nezhad et al., 2013). As detailed in Chapter 1, models of tip growth espouse a plastic cell wall at the tip, which will yield to turgor pressure, and a non-yielding elastic cell wall further back (Riquelme, 2013).

Given that some of the measurements of force on the chips were made using the confocal microscope, this means that measurements of protrusive force and observations of the dynamics of the cytoskeleton are possible with the use of appropriately transformed or stained strains of oomycete or fungi (Delgado-Alvarez et al., 2010). Thus, direct investigations of the potential role of the cytoskeleton in modulating protrusive forces are possible. The media supply centers, at the ends of the channels also enable solution changes, which means that inhibitor studies are possible. These approaches form the basis of Chapter 5 of this thesis.

CHAPTER 5

AN INVESTIGATION OF THE ROLE OF THE CYTOSKELETON IN PROTRUSIVE FORCE GENERATION AND INVASIVE GROWTH IN HYPHAE

Portions of the work in this chapter have been published in the following conference proceedings:

- **Tayagui A**., Garrill A., Collings DA. and Nock VM. (2016) On-chip measurement of protrusive force exerted by individual hyphal tips during hyphal growth. *Proceedings of the 20th MicroTas Conference*, Dublin Ireland, pp 150-151.

5.1 Introduction

In Chapters 3 and 4, the design and fabrication of LOC devices, which were used to measure micro-Newton range forces in oomycete and fungal hyphae were described. These devices enabled the x- and y-components of the total force to be differentiated, and thus enabled protrusive forces at the tips of hyphae (the F_y component) to be measured. Protrusive forces are thought to enable hyphae to act like pressurized drill bits, growing through material in a constant search for nutrients. These are then broken down, via the secretion of hydrolytic enzymes and absorbed (Money, 2004). This is a crucial process in most ecosystems on the planet, as it facilitates nutrient recycling. Invasive growth can also have important consequences to the health and well-being of other organisms, as it enables the hyphae and infection structures of parasitic and pathogenic fungi and oomycetes to penetrate cells and tissues. The ability to measure protrusive force in hyphae is an important step towards understanding the process of invasive growth. The next stage in the process is to study the cellular mechanisms that underlie force generation and regulation. One of the key players in this process is thought to be the cytoskeleton (Walker et al., 2006).

As detailed in Chapter 1, both microfilaments and microtubules play very important roles in the tip growth process. Both provide tracks along which their respective motor proteins, members of the myosin family for microfilaments, and members of the kinesin and dynein families for microtubules, transport organelles. In fungi, an example of this are the vesicles containing cell wall-synthesizing enzymes that move along microfilaments from the Spk to the tip of the cell. Exocytosis of these vesicles enables the continued synthesis of the cell wall as well as the deposition of new membrane (Riquelme, 2013). Movement of vesicles along microtubules enables the

delivery of material to the Spk as well as the movement of endosomes, which are important components involved in the recycling of membrane material and removal from the apical region the determinants of polarity (Steinberg et al., 2017). The endocytotic process is also likely to involve the generation of force by microfilaments. This is thought to occur subapically at sites where plaques of actin associated with the membrane have been imaged (Steinberg et al., 2017). Microtubules are also likely to play a key role in the delivery of cell end markers that determine the polarity of the cell and hence the axis of growth (Fischer et al., 2008). While the oomycetes do not contain a distinct Spk, it is likely that tip growth occurs by a similar mechanism with cell wall-synthesizing vesicles accumulating at the tips of hyphae. An apical cap of actin microfilaments has historically been thought of as a polarity determinant in oomycete hyphae (Heath, 1987).

In addition to these roles, the actin cytoskeleton may also play a role in the regulation of tip yielding and, in the case of invasive growth, increasing the protrusive force at the hyphal tip. This was an idea that was first postulated in a classic review of tip growth by Picton and Steer (1982), who suggested that a population of microfilaments at the tips of hyphae and pollen tubes formed a tension-bearing structure that yielded to turgor pressure. A gradient in yielding along the hypha or pollen tube was postulated to generate the cylindrical cell shape. Heath (1987) first reported a cap of microfilaments (termed the F-actin cap) in the oomycete *Saprolegnia ferax*, which was consistent with the ideas of Picton and Steer (1982). Subsequent evidence suggested that this cap was a tension-bearing structure, as the hyphal tips swelled if the microfilaments were disrupted (Allen et al, 1980; Grove and Sweigard, 1980; Jackson and Heath, 1990; Ketelaaret al., 2012; Meijer et al., 2014; Tucker et al., 1986). A potential role of this actin cap in regulating growth is

supported by reports of transient increases in growth rate in response to cytochalasin and latrunculin B (Jackson and Heath, 1990; Gupta and Heath, 1997), both of which cause the disassembly of microfilaments.

If microfilaments at the tips of hyphae do regulate tip yielding by resisting turgor, it might be expected that, in instances where a greater protrusive force is required for growth, there might be rearrangement of the microfilaments. The earlier study of Heath (1987) used chemical fixation and staining with rhodamine-phalloidin to visualize the F-actin cap. Subsequent work with live *S. ferax* hyphae, which had been microinjected with rhodamine-phalloidin (Jackson and Heath, 1993), or *A. bisexualis* hyphae, which had been fixed with an improved combination fixative (Yu et al., 2004), indicated the presence of an F-actin depleted zone in the cap. This was a dynamic structure that predicted the direction of growth (Jackson and Heath, 1993), and was more prevalent if hyphae were growing invasively, and thus required a greater protrusive force (Walker et al., 2006). This F-actin depleted zone was also found to be present in invasive hyphae of another oomycete, *Phytophthora cinnamomi* (Walker et al., 2006). Subsequently, a similar F-actin depleted zone was reported in the tips of invasive hyphae of the fungus *N. crassa* and the size of this increased with increasing stiffness of the growth media (Suei & Garrill, 2008). The depleted zone in *N. crassa* was also a site where the actin-severing protein cofilin was located (Suei & Garrill, 2008). Pollen tubes similarly have an area at the tip that is depleted in microfilaments (termed the clear zone) (Rounds et al., 2014).

While the F-actin depleted zone may regulate tip yielding, there is still obviously a need for some microfilaments at the tip to facilitate the delivery of vesicles from to Spk to the membrane at the tip. This may come about through different populations of microfilaments at the tip, each fulfilling a different role (Walker et al., 2006). One

such population could be the tension-bearing microfilaments. These might be anchored to the membrane sub-apically where they would bear the load of turgor. There have been several reports of attachment points between F-actin and the plasmamembrane/cell wall (Chitcholtan and Garrill, 2005; Kaminskyj and Heath, 1995; Bachewich and Heath, 1997; Chitcholtan et al., 2012). It is the rearrangement of these that might play a role in force generation. Another population would be the vesicle delivering microfilaments that would run from the Spk toward the tip. These would not be subject to the same remodeling as the tension bearing population when greater protrusive force is needed, because there would still be a need for vesicle delivery. Consistent with the idea of different populations of F-actin, Suei and Garrill (2009) reported a very faint staining region of F-actin between the Spk and the tip of invasive hyphae of *N. crassa*, which otherwise had a very prominent F-actin depleted zone. The dynamics of these populations of microfilaments would presumably be regulated by different actin-binding proteins.

It has also been suggested that microfilaments may provide a protrusive force at the tips when the turgor is low. Thus, the tip would extend forward due to the polymerization of microfilaments, which would push on the membrane, similar to the protrusive structures at the leading edge of migrating animal cells (Heath and Steinberg, 1999). These ideas originated from the observations of Reinhardt (1892), who considered fungi to resemble tube dwelling amoebae, and were supported by observations that oomycetes could grow even in the absence of measurable turgor (Money and Harold, 1993). This may also be the case in the fungi, as wall-less mutants of *N. crassa*, which, in the absence of a wall cannot generate turgor, form pseudopodial-like extensions (Steinberg and Schliwa, 1993).

It has also been suggested that microtubules could play a role in the positioning of proteins and organelles via a pushing force on the cytoplasmic matrix (Fischer et al., 2008). At the tips of hyphae, most microtubules extend towards the cortex and as such could generate retrograde flow of the cytoplasm (Mouriño-Pérez et al., 2006; Sampson and Heath, 2005). In animal cells, microtubules are known to migrate into growth cones of neurons, which extend in a polarized manner similar to hyphae. This process, termed engorgement, occurs after the initial protrusion of the membrane driven by microfilament polymerization and may give structural support rather than provide any force for extension (Dent and Gertler, 2003). At the back end of migrating cells however, microtubules, along with microfilaments, are likely to provide contractile forces that retract the rear of the cell such that its movement is coordinated with that of the advancing leading edge (Sheetz et al., 1998)

The goal of the work in the chapter was to understand the role of the cytoskeleton in the generation and regulation of protrusive force. This involved a series of experiments in which microfilaments and microtubules were inhibited and/or imaged in *A. bisexualis* and *N. crassa*. Latrunculin B and carbendazim (MBC) were used to disrupt microfilaments and microtubules and their effect on total force, F_x, F_y, growth rate and hyphal diameter were investigated using chips. Total force, F_x, F_y, growth rate and hyphal diameter were also measured in hyphae that were growing invasively (i.e. through agar) on the chips.

5.2 Materials and Methods

The materials and methods were as described in Chapter 2.

5.3 Results

To investigate the role of the cytoskeleton in generation of protrusive force, experiments were carried out in which drugs that affected microfilaments and microtubules were applied to the channels on a chip as a hypha approached a pillar. The forces that were generated as the hypha hit the pillar were measured, as described in Chapter 4. The effect that those drugs had on the cytoskeleton itself were investigated by staining the cytoskeleton or by using transformed strains. To image the microtubules and microfilaments in *N. crassa*, transformed strains were used that expressed β-tubulin-GFP and LifeAct-RFP, respectively. The β-tubulin-GFP expressing strain enabled imaging of the dynamics of the microtubules at the tips of hyphae, but unfortunately, attempts to image microfilaments at the tips using the LifeAct-RFP expressing strain were largely unsuccessful. With this strain, microfilaments were only very rarely seen at the tip and with a very faint signal (Figure 5.1a, b). Fluorescence was more prominent at septa (Figure 5.1c, d), which may reflect a greater role for LifeAct in modulating microfilaments that are involved in septa formation rather than those at the tip.

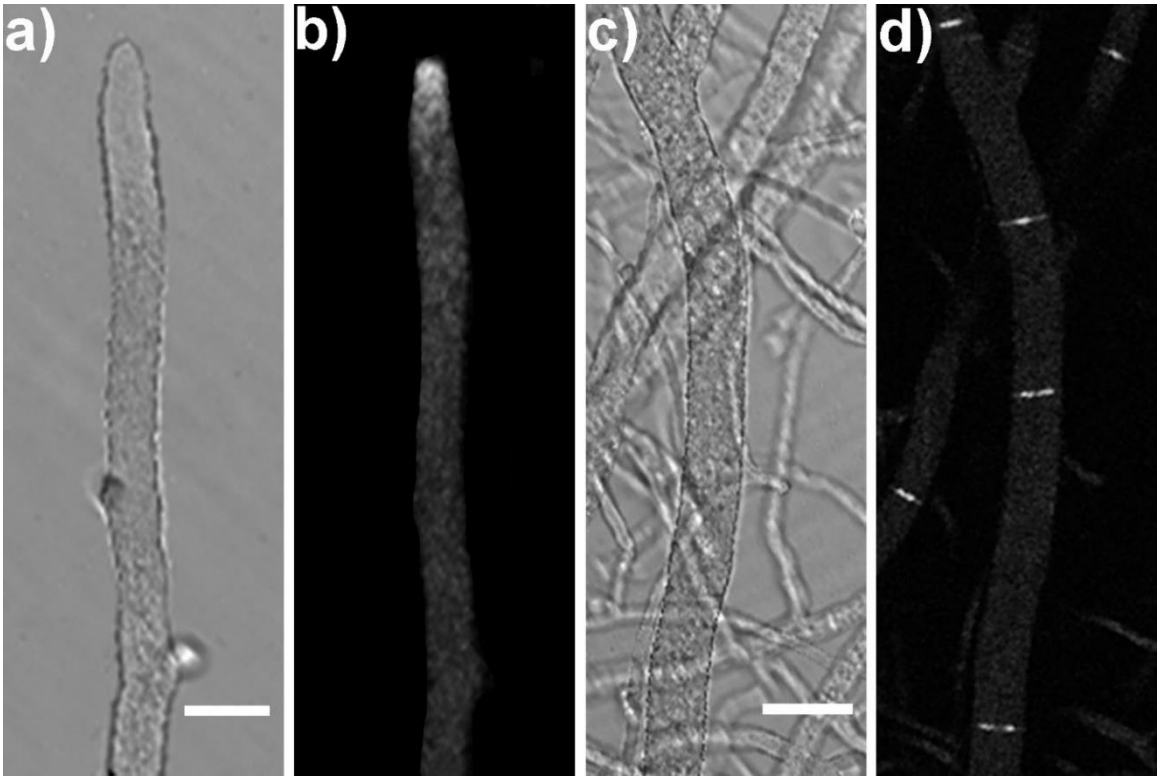

Figure 5.1. LifeAct-RFP expressing cells of *N. crassa* showed faint fluorescence at the tips of hyphae, but this was only seen in rarely (a, b). In contrast, prominent and bright fluorescence was seen around the septa in many hyphae (c, d). Images a and c are taken with bright field and b and d under fluorescence. Scale bars = 23 μm.

The use of the LifeAct-RFP expressing strain was therefore discontinued and, due to time contraints with respect to finishing the thesis, the use of immunochemical staining was not possible on the chips. With *A. bisexualis*, in the absence of any transformed strains, microfilaments were imaged after staining with Alexa 488-phalloidin. Again, this meant that the dynamics of the cytoskeleton were not observed and that images were obtained from chemically-fixed hyphae.

Latrunculin B is a drug that will bind to G-actin and thus prevent its polymerization into microfilaments (Spector et al., 1989). This has the effect of changing the equilibrium between G-actin and F-actin, and thus will lead to the depolymerization

of microfilaments. Experiments investigating the effects of latrunculin B were carried out with both *A. bisexualis* and *N. crassa*, although time constraints limited the imaging of microfilaments to the oomycete. Carbendazim (MBC) is an inhibitor that binds to tubulin heterodimers and affects the equilibrium between tubulin and microtubules, again causing their depolymerization (Davidse and Flach, 1977). The effect of this on force generation and the organization of microtubules was only investigated in *N. crassa,* as the MBC proved largely ineffective against the growth of *A. bisexualis*. Due to time constraints, experiments on the effect of invasive growth conditions on force generation and the organization of the microtubules were only carried out on *N. crassa*.

5.3.1 The effect of actin inhibition on growth and protrusive force – *Achlya bisexualis*

To determine the appropriate concentration of the actin inhibitor latrunculin B to use on the chips, the inhibitor was first included in PYG agar and its effect on radial extension of mycelial colonies in Petri dishes was measured. Radial extension was then converted into a growth rate (Section 2.2.5.1), and growth was seen to decrease with increasing concentrations of the latrunculin B, and at concentrations of 1 μM, growth was completed inhibited (Figure 5.2). Growth was significantly slower at all concentrations tested relative to the DMSO control ($P < 0.05$, student's t-test). A concentration of 0.05 μM (which caused approximately 50% growth inhibition) was chosen for subsequent work with the chips to determine the effect of actin inhibition on protrusive force generation.

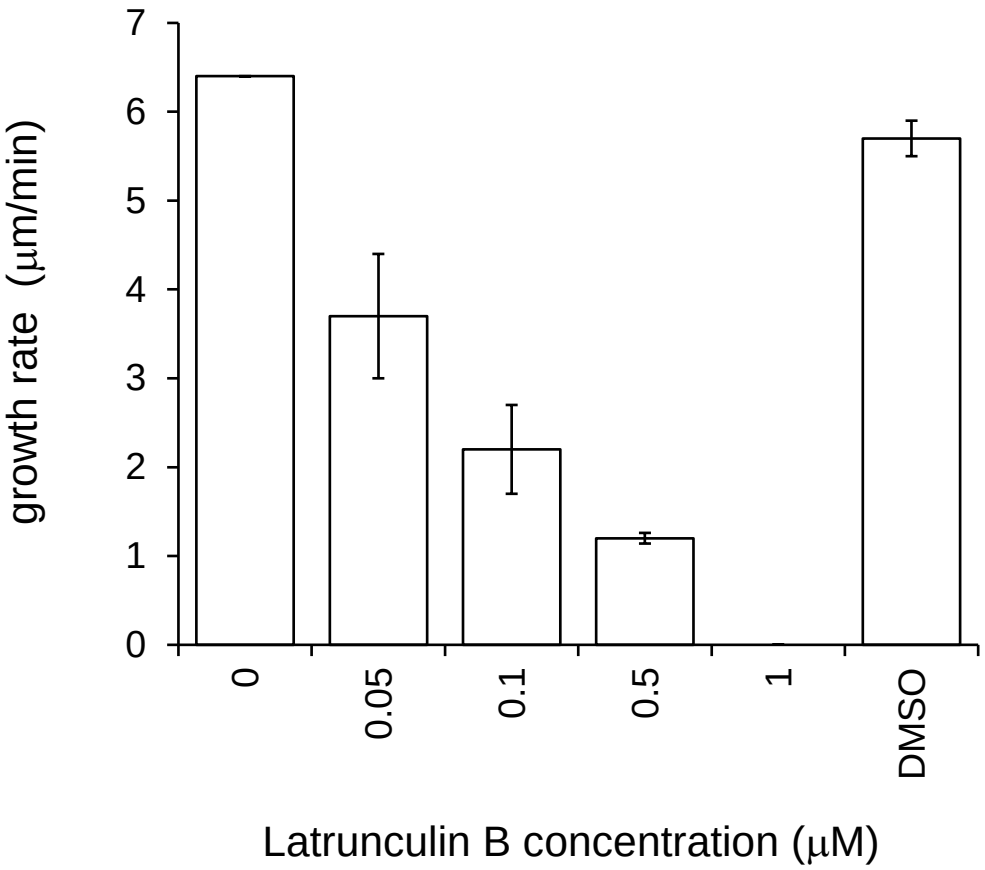

Figure 5.2. The effect of various concentrations of latrunculin B on growth rates of *A. bisexualis* colonies in Petri dishes. Rates were calculated by measuring radial extension of the mycelia and then converting this to a growth rate. Extension was inhibited in a dose dependent manner. Data are shown as mean growth rates ± SD (n = 6 Petri dishes). DMSO at the same concentration that the latrunculin-treated hyphae were exposed to was used as a control.

The effect of latrunculin B was then investigated on the rate of growth in a channel on a chip (Figure 5.3). Growth rates were determined prior to the hyphae moving close to the pillar. Growth rates were measured over 30s periods and are presented with 0 s representing the time of the addition of latrunculin B, thus -30 to 0 s represents the growth rate in the 30 s period prior its addition, 0 to 30 s the 30 s

period after addition, 30 to 60 s the following 30 s and so on. The growth rate of hyphae increased significantly ($P<0.05$, students t-test) in the 30 s after the addition of the inhibitor, but then decreased to rates that were significantly slower than DMSO controls. At all time points, apart from -30 to 0 s, the growth rates of the latrunculin-treated hyphae were significantly different from the relevant DMSO control hyphae (all $P < 0.05$, student's t-test). Hyphae stopped growing after approximately 7 min.

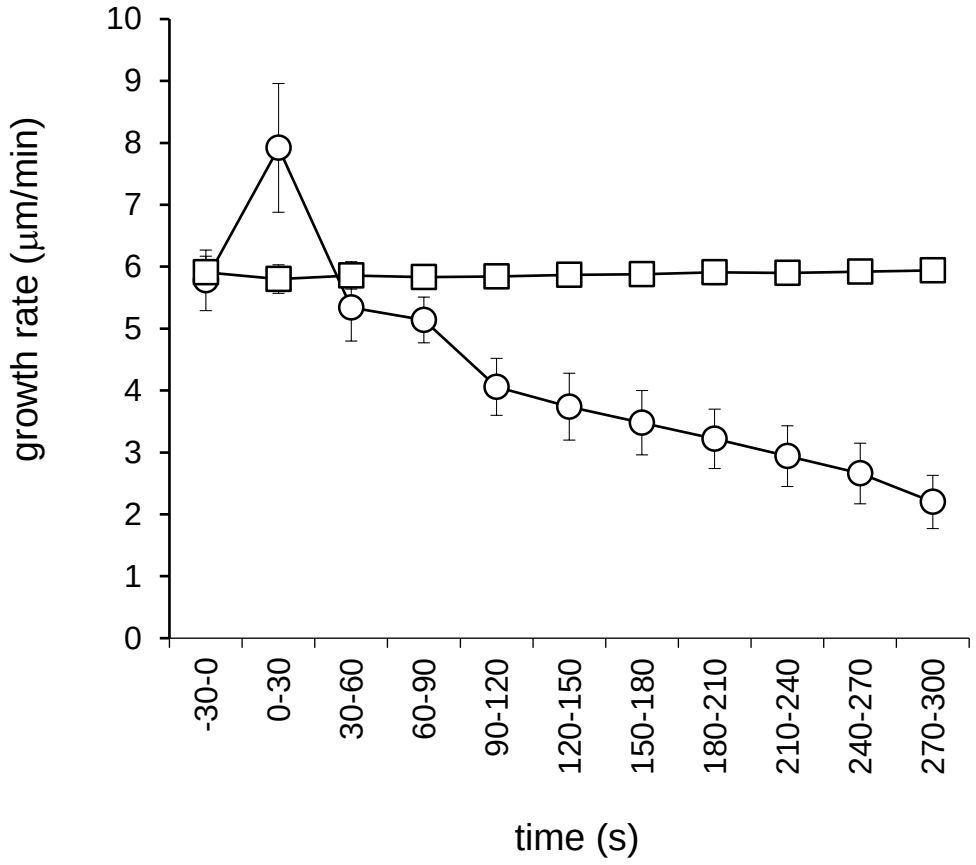

Figure 5.3. The effect of 0.05 μM latrunculin B (○) on the growth rate of *A. bisexualis* hyphae on a Version 5 chip. 0.05 μM latrunculin B was added at 0 s, so that data for - 30 – 0 s represents the growth rate in the 30 s period prior to addition, 0 – 30 s the 30 s period after addition, and so on in 30 s increments until 5 min after addition. Data are shown as mean growth rates ± SD (n = 13 hyphae). DMSO at a concentration of 0.025% (v/v) was used as a control (□).

The effects of latrunculin B were next tested on total force, F_x, F_y, growth rate and diameters of *A. bisexualis* hyphae growing on chips. The latrunculin B was added from a 2 mM stock solution, via the media supply inlet, to give the required final concentration. As detailed in Chapter 2 the latrunculin was added with a pipette and was expelled with force from the tip, such the inhibitor reached the hypha mostly by convectional flow rather than simple diffusion.

The measurement of protrusive force is reliant upon the tip of a hypha hitting the pillar initially and an ability to differentiate the F_x and F_y components of the total force. In this series of experiments, only one hypha exposed to latrunculin B initially hit the pillar of a Version 4 chip with the tip (Figures 5.4 and 5.5), while seven hyphae initially hit the pillar with their sides (Figures 5.6 and 5.7). This precludes any meaningful conclusions with respect to the effect of latrunculin B on protrusive force. Compounding this problem was that all of the DMSO control hyphae first hit the pillar with the sides of their hyphae (Figures 5.8 and 5.9). Due to the confines of time, further attempts to get measurements of hyphae growing into pillars were not possible. Thus, in the data that are presented in Table 5.1 the force measurements are considered together, irrespective of whether the tip or the side of the hyphae hit the pillar first.

The single hypha which hit with the tip first generated a force in the y-direction of 5.4 μN and a total force of 9.19 μN, 2 min after its initial contact with the pillar (Figures 5.4 and 5.5). While obviously no conclusion can be drawn from this, if forces of that magnitude were to be seen with other hyphae, then this would be of significant interest. This compares to the average total force of 1.7 μN in the presence of latrunculin B and 1.9 μN in the presence of DMSO for the hyphae that hit the pillar

with their sides (Table 5.1, Figures 5.6, 5.7, 5.8 and 5.9). In addition, the values are much higher than the F_y values of 2.5 μN (Version 4 chips) and 1.6 μN (Version 5 chips) for the hyphae that hit the pillars with their tips first that were reported in Table 4.3. Clearly, this is an area where further experiments are warranted.

The data presented in Table 5.1 are consistent with latrunculin B affecting the hyphal growth rate. There was a significant increase in growth rate, 2 min after initial contact with the pillar, when 0.05 μM latrunculin B was added relative to both the initial growth rate and also the DMSO control (both $P < 0.05$, student's t-test). Despite the greater growth rate, there was no increase in total force or F_x, which is consistent with the data presented in Chapter 4, suggesting no relationship between growth rate and force. However, this is not really relevant with respect to F_y, given that the hyphae were hitting the pillars with their sides.

Time (min)	Total Force (μN)	F_x (μN)	F_y (μN)	Growth rate (μm/min)	Diameter (μm)
latrunculin					
0	-	-	-	5.7 ± 0.3	21.0 ± 0.8
(range)	-	-	-	(5.1 – 6.0)	(19.7 – 22.1)
2	1.7 ± 1.1	1.5 ± 1.1	0.3 ± 0.3	7.0 ± 0.4	20.3 ± 1.1
(range)	(0.1 – 2.9)	(0.1 – 2.7)	(0 – 0.8)	(6.5 – 7.5)	(19.0 – 21.5)
5	2.9 ± 2.0	2.9 ± 2.0	0.5 ± 0.3	5.8 ± 0.4	20.8 ± 1.6
(range)	(1.3 – 5.2)	(1.1 – 5.2)	(0.2 – 0.8)	(5.2 – 6.1)	(19.0 – 22.1)
DMSO					
0	-	-	-	5.6 ± 0.2	20.6 ± 0.1
(range)	-	-	-	(5.4 – 5.8)	(20.5 – 20.7)
2	1.9 ± 0.8	1.6 ± 0.7	0.3 ± 0.5	5.2 ± 0.3	20.2 ± 0.7
(range)	(0.9 – 2.5)	(0.9 – 2.1)	(0 – 0.9)	(5.0 – 5.5)	(19.7 – 21.0)

Table 5.1. The effect of 0.05 μM latrunculin B on total force, F_x, F_y, growth rate and hyphal diameter for *A. bisexualis* hyphae that hit the pillar of a Version 5 chip with the sides of the hyphae. Force values are given at the time of contact with the pillar, and 2 and 5 min after contact. Where no 5 min value is given, the hypha had slipped off the pillar and the recording had been stopped. Experiments were done with DMSO as a control. Sample sizes were n = 7 for the latrunculin B treatment and n = 3 for DMSO controls. The growth rate at 2 min in latrunculin B was significantly faster than the rate at 0 min and the DMSO control at 2 min.

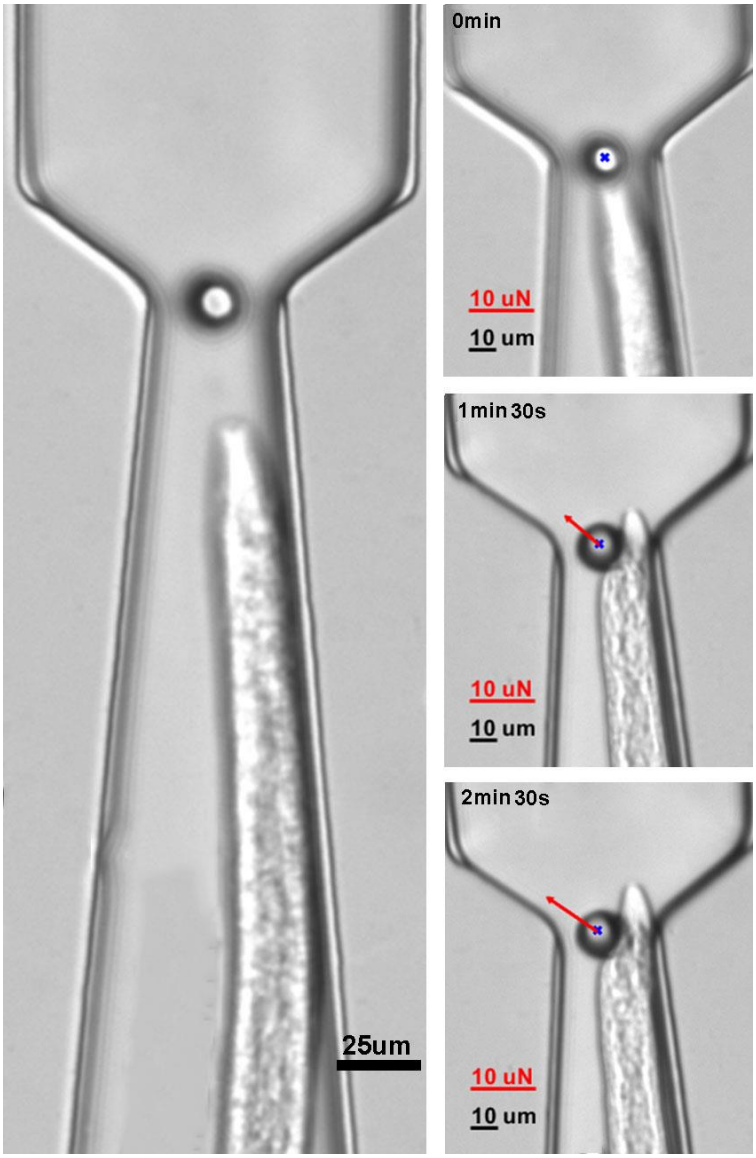

Figure 5.4. An *A. bisexualis* hypha growing on a Version 4 chip in the presence of 0.05 μM latrunculin B. The latrunculin B was added when the hypha was around 25 μm from the pillar. The hypha extended toward the pillar and hit with the tip first (0 min). By 1 min 30 s, the tip had moved into the gap between the pillar and the channel wall and the side of the hypha was in contact with the pillar.

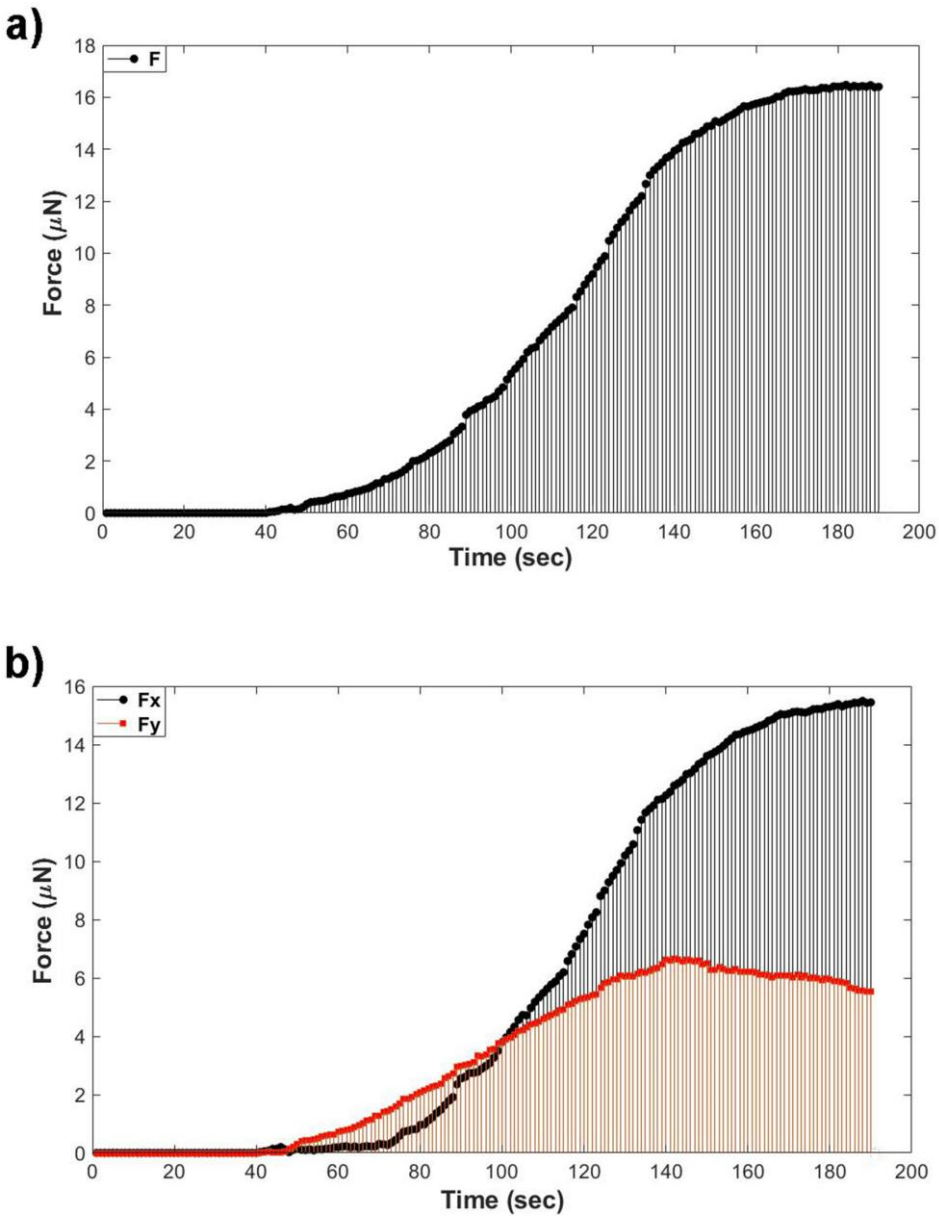

Figure 5.5. Plots of total force (a) and the F_x and F_y (b) components of force for the hypha depicted in Figure 5.4 that was growing on a Version 4 chip in the presence of 0.05 μM latrunculin B. The initial force was due to the F_y component indicating that the tip of the hypha was in contact with the pillar and was thus a protrusive force. At around 70 s, there was an increasing F_x component as the tip of the hypha grew into the gap between the pillar and the channel wall and the contact between the side of the hypha and the pillar generated a squeezing force. From 100 s onwards, this was responsible for the majority of the force.

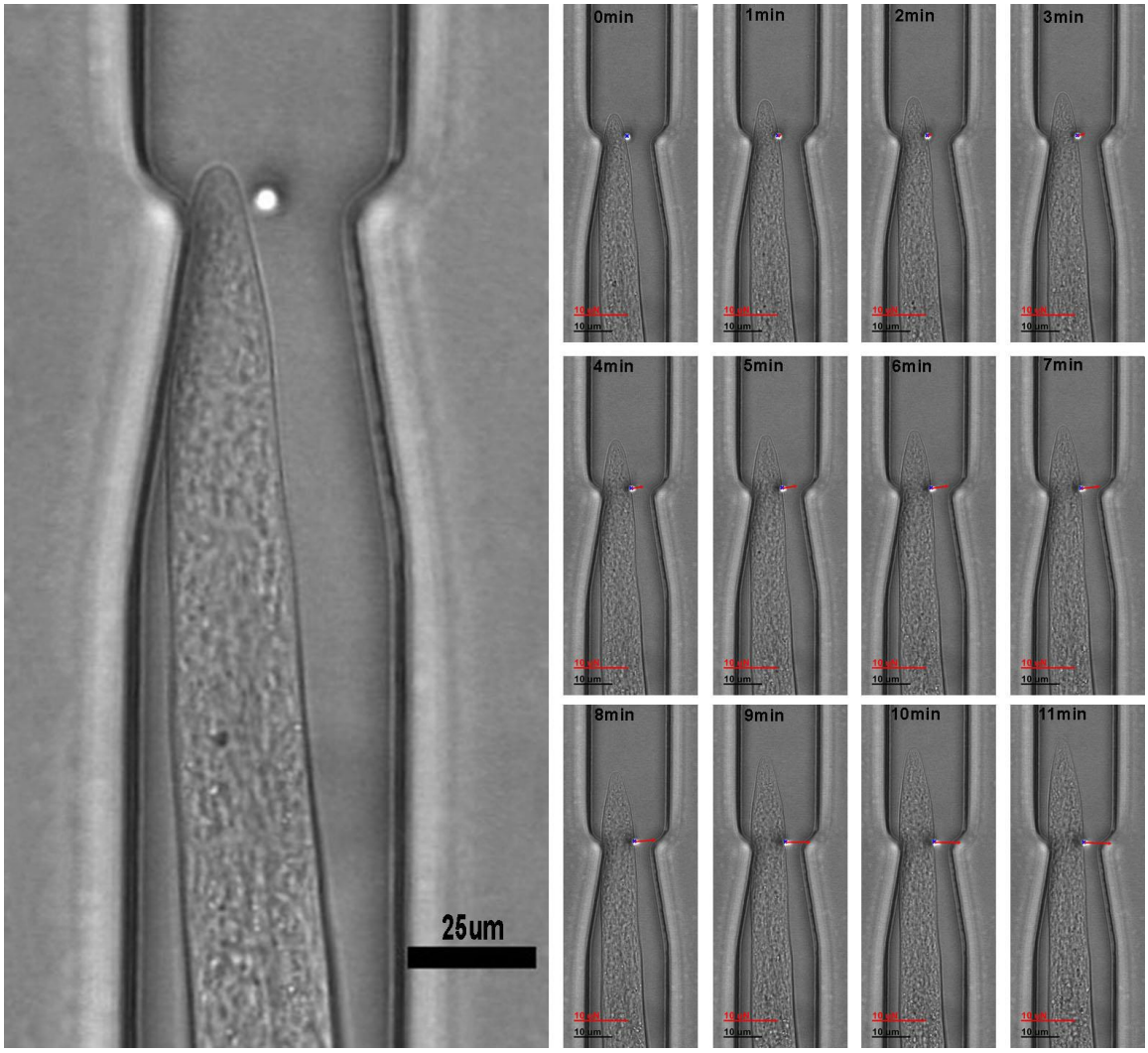

Figure 5.6. An *A. bisexualis* hypha growing on a Version 5 chip in the presence of 0.05 μM latrunculin B. The experiment shown is a representative example of a hypha exerting a squeezing force on a pillar. The latrunculin B was added when the hypha was 10 μm from the pillar. As the hypha extended down the channel and approached the pillar, the tip passed between the pillar and the channel wall (image on the left and in the time series at 0 min). The side of the hypha made contact with the pillar (0 – 1 min) and began to generate force in the x-direction (F_x) as indicated by the red arrow.

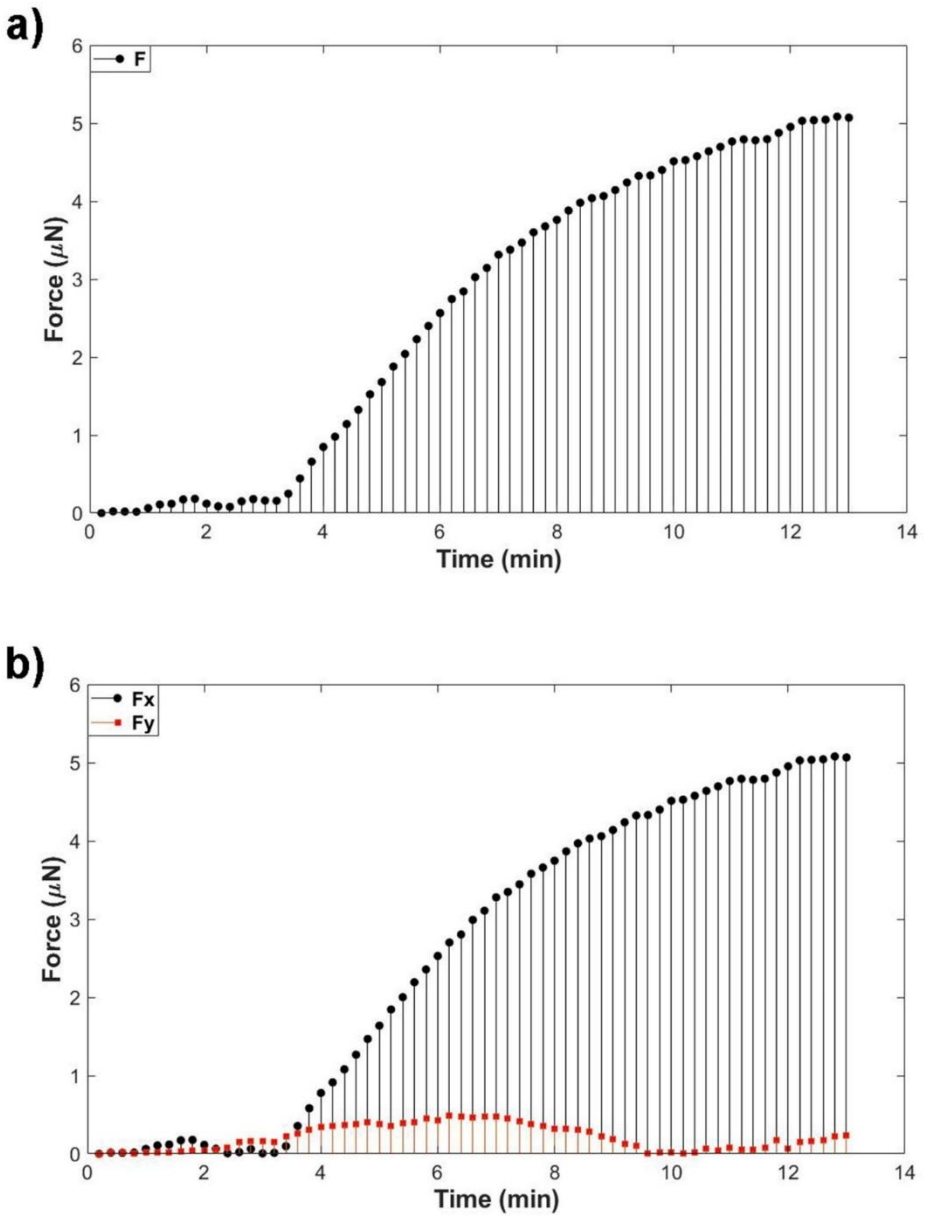

Figure 5.7. Plots of total force (a) and the F_x and F_y (b) components of force for the hypha depicted in Figure 5.6 that was growing on a Version 5 chip in the presence of 0.05 μM latrunculin B. The F_x component was responsible for the majority of the total force and began to increase at 3 min. This was indicative of the side of the hypha making contact with the pillar rather than the tip. Only very small amounts of force were generated in the y-direction.

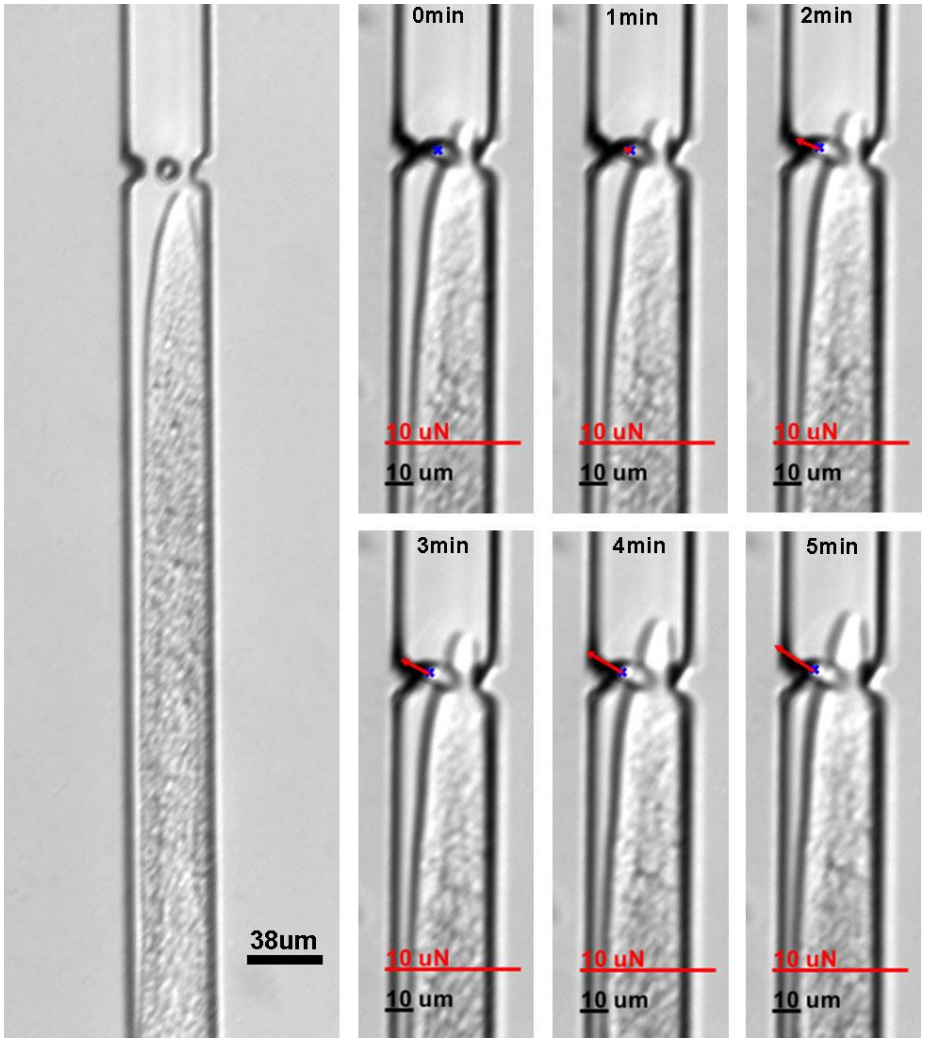

Figure 5.8. An *A. bisexualis* hypha growing on a Version 5 chip in the presence of 0.025% (v/v) DMSO. This was a control experiment for the latrunculin B experiments in Figures 5.4 and 5.6. Hyphae were exposed to the highest concentration of DMSO that they were exposed to with the addition of latrunculin B. The DMSO was added as the hypha approached the pillar. As the hypha extended down the channel and approached the pillar the tip passed between the pillar and the channel wall (image on the left and in the time series at 0 min). The side of the hypha exerted a force on the pillar (1 min) that was predominantly in the x-direction (F_x) as indicated by the red arrow.

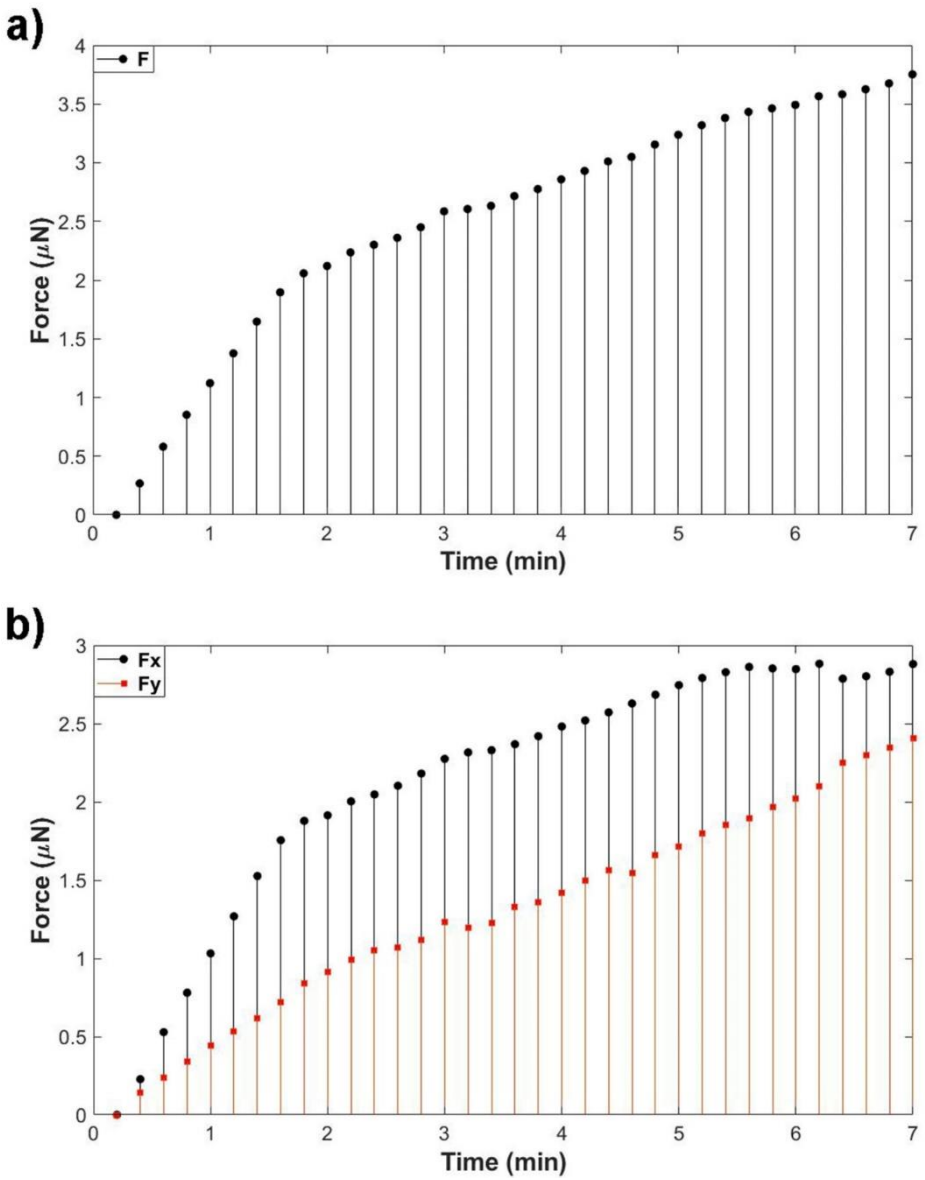

Figure 5.9. Plots of total force (a) and the F_x and F_y (b) components of force for the hypha depicted in Figure 5.8 that was growing on a Version 5 chip in the presence of 0.025% (v/v) DMSO. The greater force was imparted as an F_x component, reflecting the fact that the side of the hypha hit the pillar first.

The effect of latrunculin B was next tested on the arrangements of microfilaments in fixed and stained hyphae of *A. bisexualis*. Previous studies in the laboratory have utilized a combination fixative to preserve the hyphae, followed by staining with Alexa-488 phalloidin (Yu et al., 2003; Walker et al., 2006). On the chips, the fixation and staining proved more difficult than in previous work. Various modifications to the protocol were attempted: in one of these growths of the hyphae in Vogel's medium rather than PYG broth provided better fixation and staining. In *A. bisexualis* hyphae growing non-invasively, hyphae stain with a prominent F-actin cap (n = 50 hyphae in 10 independent experiments). When hyphae were exposed to latrunculin B for 15 s prior to fixation, the cap was still present, but was less prominent at the very tip of the hyphae (Figure 5.10a, b). Subapically, more diffuse filaments and plaques were observed (Figure 5.10a, b). If the hyphae were exposed to latrunculin B for 30 s prior to fixation, the tip were swollen and staining at the tip was lost. Further back from the tip, faint plaques were present (Figure 5.10c, d) (n = 30 hyphae in 10 independent experiments) There was no autofluorescence from the hyphae (Figure 10e, f).

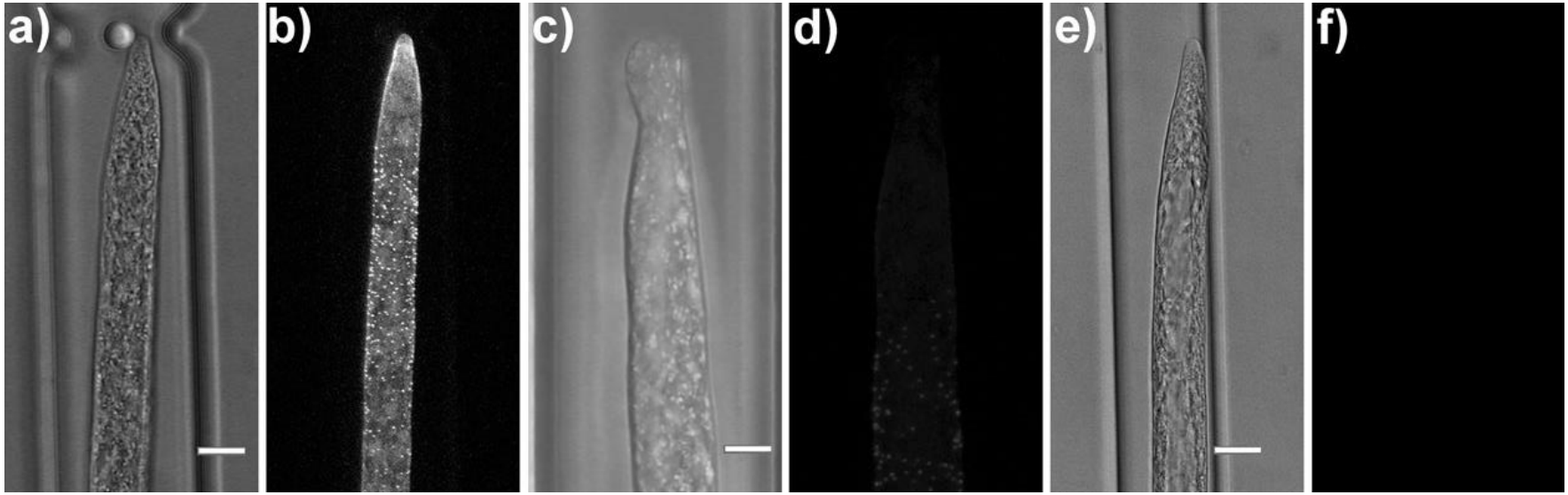

Figure 5.10. Bright field and fluorescent images of *Achlya bisexualis* hyphae on Version 5 chips that had been exposed to 0.05 µM latrunculin B for 15 sec (a, b) or 30 sec (c, d) prior to fixation and staining with Alexa phalloidin. While a prominent F-actin cap is present at the tip of the hypha in (b) the area at the very tip has less staining. Subapically the cap gives way to more diffuse filaments and distinct plaques. With the longer exposure to latrunculin B the tip is swollen and there is no distinct F-actin at the tip just diffuse background staining and sub apically there are faint plaques (d). In (e) and (f), an unstained hypha is shown, which indicates that there is little to no autofluorescence. Scale bars = 17 µm.

5.3.2 The effect of actin inhibition on growth and protrusive force – *Neurospora crassa*

Initial experiments were carried out to determine the appropriate concentration of latrunculin B to use on the chips with *N. crassa*. The inhibitor was included in Vogel's medium and its effect on radial extension of mycelial colonies in Petri dishes was measured and this was converted to a growth rate (Section 2.2.5.1) (Figure 5.11). *N. crassa* colony growth rate decreased with increasing concentrations of the latrunculin B, but *N. crassa* was much less sensitive compared to *A. bisexualis* as higher concentrations were required to inhibit growth by 50%. Even with this, however, growth was significantly slower at all concentrations tested relative to the DMSO control ($P < 0.05$, student's t-test). A concentration of 1 μM was chosen for subsequent work with hyphae on the chips.

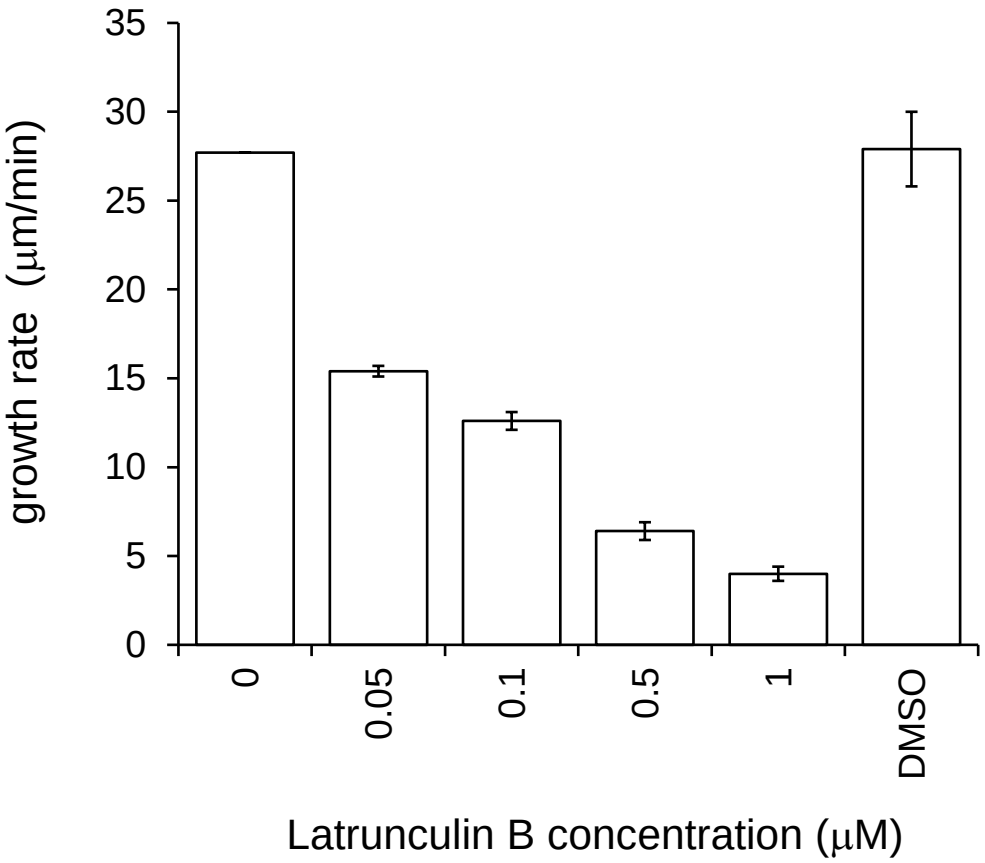

Figure 5.11. The effect of various concentrations of latrunculin B on growth rates of *N. crassa* mycelial colonies in Petri dishes. Rates were calculated by measuring radial extension of the mycelia and then converting this to a growth rate. Extension was inhibited in a dose dependent manner. Data are shown as mean growth rates ± SD (n = 6 Petri dishes). DMSO at the same concentration that the latrunculin treated hyphae were exposed to was used as a control (0.025% v/v).

The effects of latrunculin B were next tested on total force, F_x, F_y, growth rate and diameters of hyphae growing on P5C17 chips (Table 5.2). Due to time constraints, data from only 3 hyphae were obtained, each on a different P5C17 chip. These hyphae all initially hit the pillars with their tips and representative images and force plots for one of these hyphae are shown in Figures 5.12 and Figure 5.13. Data from only three hyphae were obtained in the DMSO control experiments, and of these, two hit the pillars initially with their sides. The other hypha, while appearing to hit with its side (Figure 5.14), actually generated more force in the y-direction than the x-direction, as indicated by the force arrow in Figure 5.14, and the force plots in Figure 5.15. Two minutes after initial contact, this hypha generated a force in the y-direction of 1.5 μN, which compares to an average force in the y-direction of 5.9 μN with the latrunculin- treated hyphae. Again, this is an area where further experiments are warranted. In contrast to *A. bisexualis*, there were no significant differences in the growth rates in the latrunculin B-treated hyphae compared to the control, nor was there any significant difference in the growth rate prior to contact and 2 min after contact in the latrunculin B-treated hyphae. However, it should again be noted that in comparing the latrunculin B-treated hyphae with the DMSO treated hyphae they hit the pillars with different parts of the hyphae.

Time (min)	Total Force (μN)	F_x (μN)	F_y (μN)	Growth rate (μm/min)	Diameter (μm)
latrunculin					
0	-	-	-	3.0 ± 0.3	4.4 ± 0.7
(range)	-	-	-	(2.7 – 3.2)	(4.0 – 5.2)
2	6.4 ± 5.0	2.5 ± 2.4	5.9 ± 4.4	2.4 ± 0.5	5.0 ± 0.7
(range)	(3.4 – 12.2)	(1.0 – 5.3)	(3.3 – 11.0)	(1.8 – 2.8)	(4.5 – 5.8)
DMSO					
0	-	-	-	2.9 ± 0.2	4.5 ± 0.4
(range)	-	-	-	(2.7 – 3.0)	(4.1 – 4.8)
2	2.7 ± 0.5	2.0 ± 1.6	0.7 ± 0.7	2.5 ± 0.0	5.1 ± 0.3
(range)	(2.1 – 3.1)	(0.1 – 3.0)	(0.1 – 1.5)	(2.5)	(4.7 – 5.3)

Table 5.2. The effect of 1 μM latrunculin B on total force, F_x, F_y, hyphal growth rate and hyphal diameter for *N. crassa* on a P5C17 chip that hit the pillar with the tip of the hyphae. Values are given at the time of contact with the pillar (0 min) and 2 min after contact. Experiments were done with DMSO as a control but in these experiments the hyphae hit the pillars with their sides. One of these (described further in the text) did however generate a significant force in the y-direction. Sample sizes were n = 3 for latrunculin and n = 3 for DMSO.

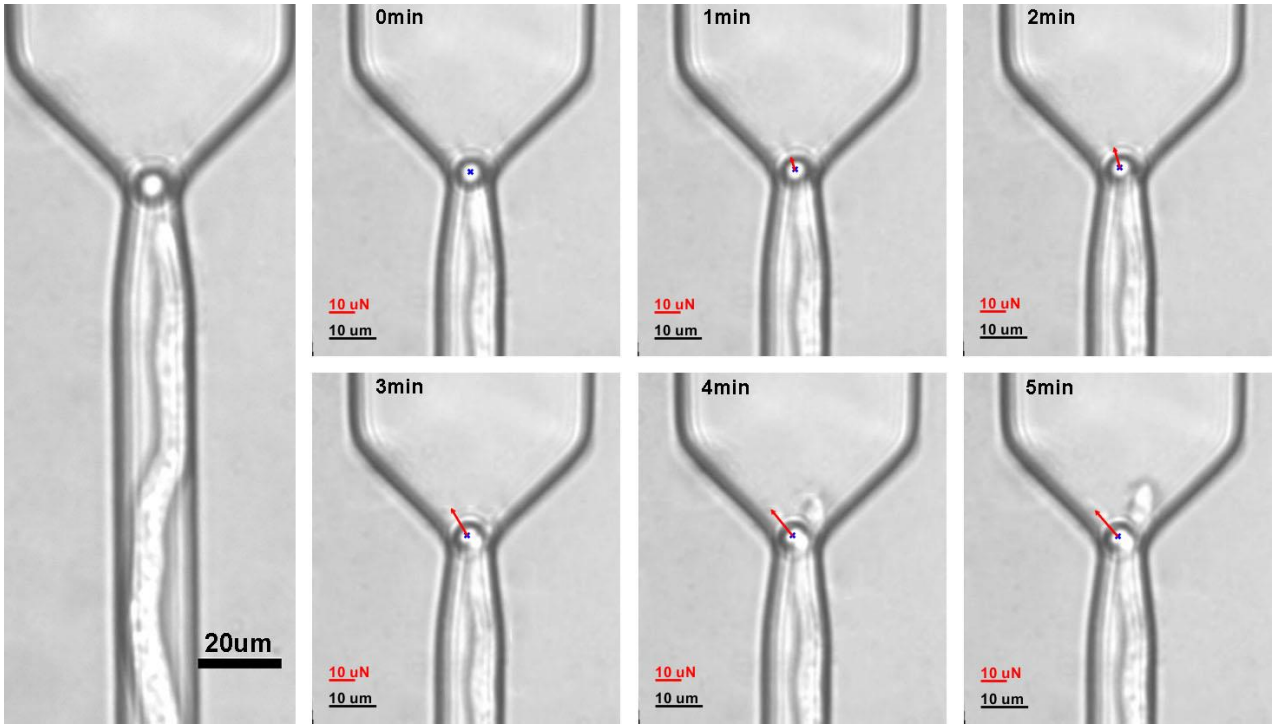

Figure 5.12. A *N. crassa* hypha growing on a P5C17 chip in the presence of 1 μM latrunculin B. The latrunculin B was added as the hypha approached the pillar. The hypha extended into the pillar and hit with the tip first (0 min). The initial force is predominantly in the y-direction as indicated by the upward pointing red arrow (at 1 - 2 min).

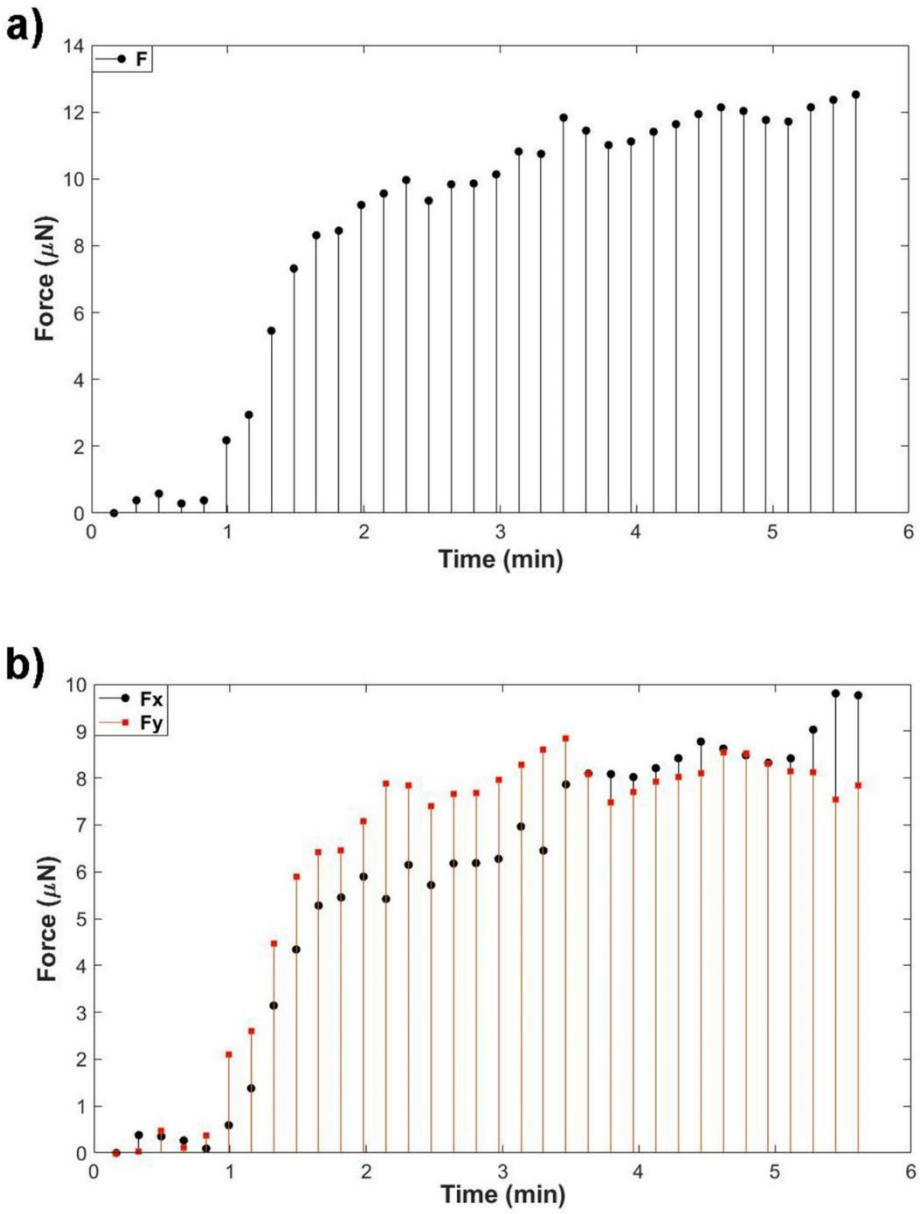

Figure 5.13. Plots of total force (a) and the F_x and F_y (b) components of force for the hypha depicted in Figure 5.12 that was growing on a P5C17 chip in the presence of 1 μM latrunculin B. The initial increase in force between 1 - 2 min was due to the F_y component indicating that the tip of the hypha was in contact with the pillar and thus exerted a protrusive force. At around 2 - 3 min there was an increasing F_x component as the tip of the hypha grew into the gap between the pillar and the channel wall. The contact between the side of the hypha and the pillar generated a squeezing force.

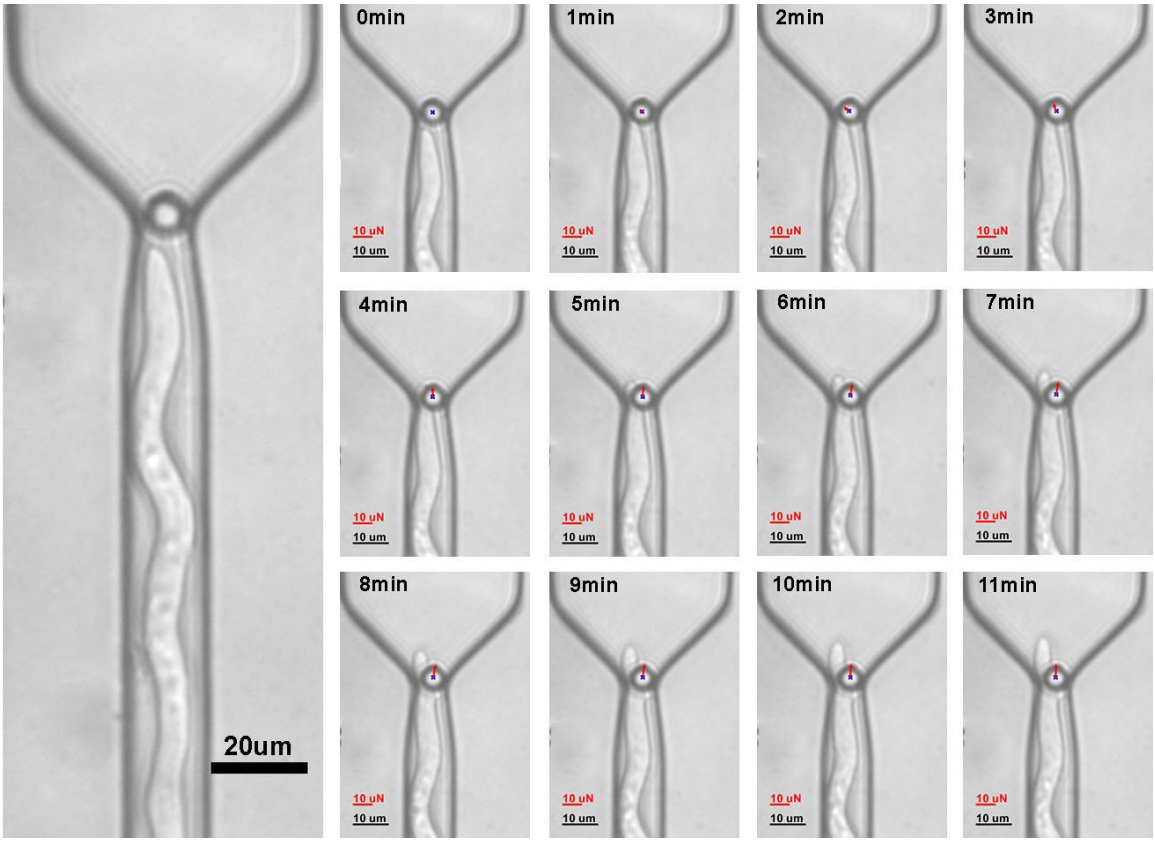

Figure 5.14. A *N. crassa* hypha growing on a P5C17 chip in the presence of 0.025% (v/v) DMSO, which was the highest concentration that they were exposed to in the latrunculin B experiments (0.025% v/v). The DMSO was added as the hypha approached the pillar. As the hypha extended down the channel and approached the pillar the tip appeared to initially hit the pillar with its side just behind the tip (image on the left and in the time series at 1 min). Despite this, the main component from around 3 min onwards was F_y, as indicated by the red arrow.

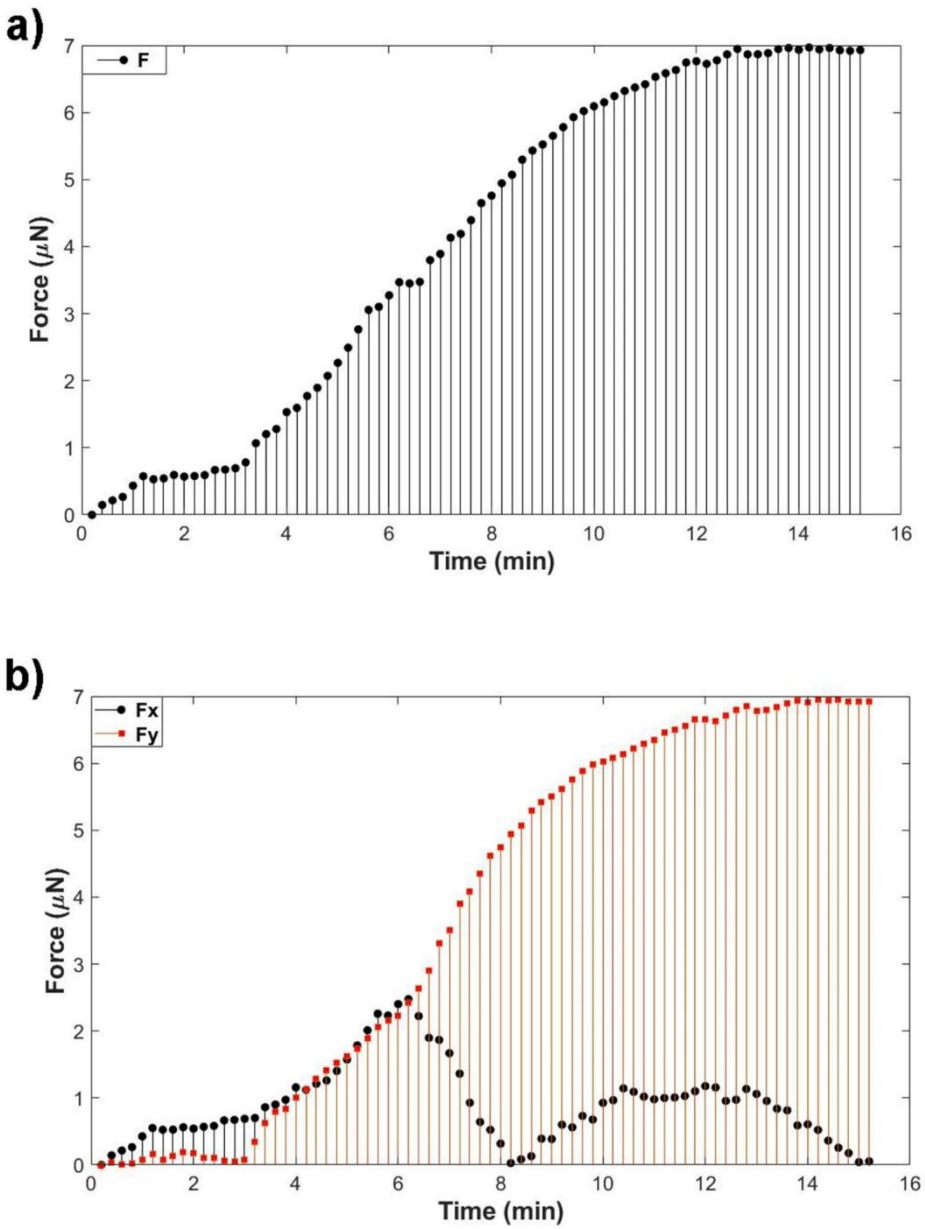

Figure 5.15. Plots of total force (a) and the F_x and F_y (b) components of force for the hypha depicted in Figure 5.14 that was growing on a P5C17 chip in the presence of 0.025% (v/v) DMSO. The initial increase in force at 0 min was due to the F_x component indicating that the side of the hypha was in contact with the pillar. However, at around 3 min there was an increasing F_y component, which would indicate a protrusive force.

5.6 The effect of microtubule inhibition on growth and protrusive force – *Neurospora crassa*

Initial experiments were carried out to determine the appropriate concentration of the microtubule-disrupting agent MBC to use on the chips by growing hyphae on Vogel's agar Petri dishes containing a range of concentrations of MBC. Radial extension was measured and converted to a growth rate (Section 2.2.5.1). This was seen to decrease with increasing concentrations of MBC (Figure 5.16). Hyphal growth rates at MBC concentrations of 0.05 and 0.07 μg/mL were significantly lower than with the DMSO controls ($P < 0.05$, t-test). A concentration of 0.05 μg/mL was chosen for subsequent work with hyphae on the chips.

The effects of MBC were next tested on total force, F_x, F_y, growth rate and diameters of hyphae growing on P5C17 chips (Table 5.3). In these experiments, the maximum concentration of DMSO that the hyphae were exposed was the same as for the latrunculin B experiments (0.025% v/v), and so the DMSO-treated hyphae from Table 5.2 were used as a control. On the chips, 3 hyphae hit pillars initially with their sides and 2 with the tip in the presence of 0.05 μg/mL MBC. Given this, averages are given for the hyphae that made contact with their sides and the actual values for the two hyphae that made contact with their tips (Table 5.3). Images and force plots from one of the hyphae that hit the pillar with its tip are shown in Figures 5.17 and 5.18. The hyphae that hit with their sides showed no significant statistical differences in total force, F_x, F_y or diameter relative to the control hyphae. The growth rate at 2 min after contact was significantly lower in the MBC-treated hyphae compared to the control and to the rate prior to contact ($P < 0.05$, student's t-test). In addition, in the MBC-treated hyphae there was a significant decrease in the growth rate and a

significant increase in hyphal diameter at 0 min compared to 2 min ($P < 0.05$, student's t-test). This was not the case with the DMSO controls (although for growth rate at 0 min compared to 2 min, a P value of 0.053 may indicate significance if a larger sample size were obtained, given the slowing of growth rate upon pillar contact reported in Chapter 4). The sample size of just two for MBC-treated hyphae that hit the pillars with their tips precluded any statistical analysis.

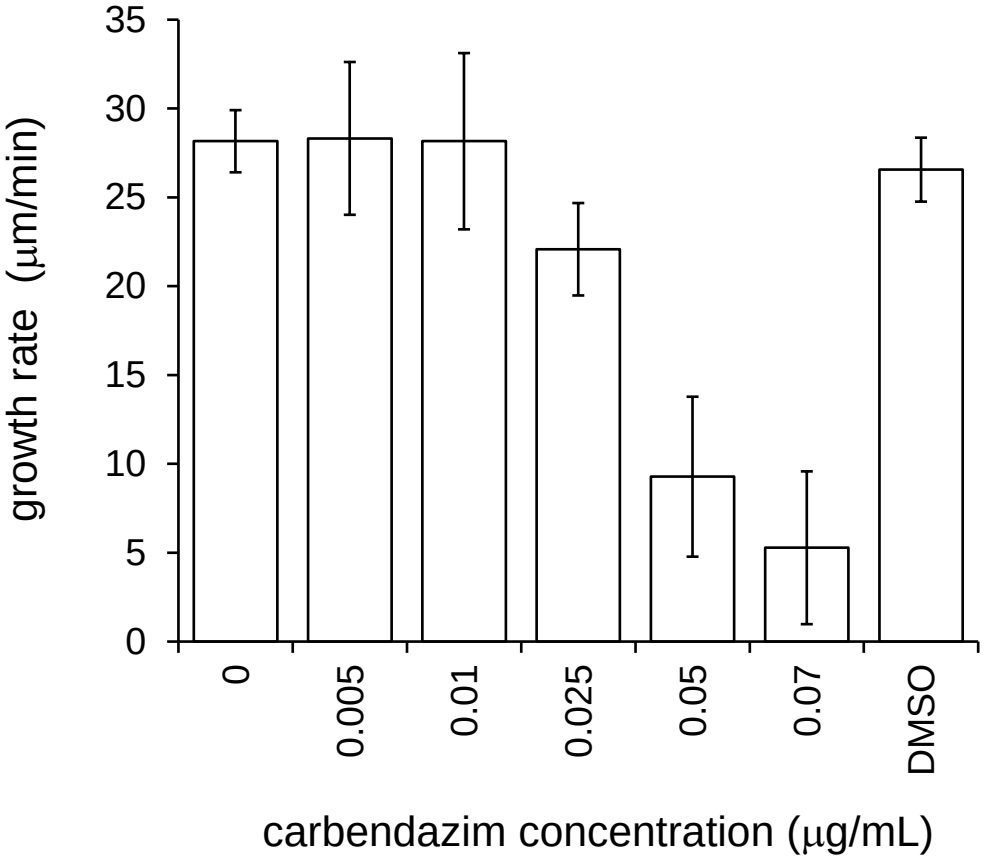

Figure 5.16. The effect of various concentrations of carbendazim on growth rates of *N. crassa* mycelial colonies in Petri dishes. Growth rates were calculated by measuring the radial extension of mycelia and then converting this to a growth rate. Extension was inhibited in a dose dependent manner at concentrations above 0.025 μg/mL. Data are shown as mean growth rates ± SD (n = 6 Petri dishes). DMSO at the same maximum concentration that the latrunculin treated hyphae were exposed to was used as a control.

Time (min)	Total Force (μN)	F_x (μN)	F_y (μN)	Growth rate (μm/min)	Diameter (μm)
MBC (side)					
0	-	-	-	2.5 ± 0.2	4.7 ± 0.3
(range)	-	-	-	(2.3 – 2.7)	(4.5 – 5.0)
2	3.1 ± 0.7	3.0 ± 0.8	0.9 ± 0.5	1.6 ± 0.2	5.7 ± 4.5
(range)	(2.4 – 3.7)	(2.1 – 3.7)	(0.3 – 1.2)	(1.5 – 1.8)	(5.3 – 5.8)
MBC (tip)					
0	-	-	-	2.1, 2.5	4.8, 4.3
2	1.9, 2.5	0.5, 1.5	1.8, 2.0	1.2, 1.5	5.7, 4.5
DMSO					
0	-	-	-	2.9 ± 0.2	4.5 ± 0.4
(range)	-	-	-	(2.7 – 3.0)	(4.1 – 4.8)
2	2.7 ± 0.5	2.0 ± 1.6	0.7 ± 0.7	2.5 ± 0.0	5.1 ± 0.3
(range)	(2.1 – 3.1)	(0.1 – 3.0)	(0.1 – 1.5)	(2.5)	(4.7 – 5.3)

Table 5.3. The effect of 0.05 μg/mL MBC on total force, F_x, F_y, growth rate and hyphal diameter for *N. crassa* on a P5C17 chip. Three hyphae hit the pillar with their sides and the values for these are given as an average ± SD. Only two hyphae hit with their tips and so for these hyphae the raw values are given for each. Data are given at the time of contact with the pillar and 2 min after contact. Experiments were done with DMSO as a control – these were the same experiments as for the latrunculin experiments and are reproduced from Table 5.2. The DMSO-treated hyphae hit the pillars with their sides. Sample sizes were n = 3 for MBC (side hyphae), n = 2 for MBC (tip hyphae) and n = 3 for DMSO.

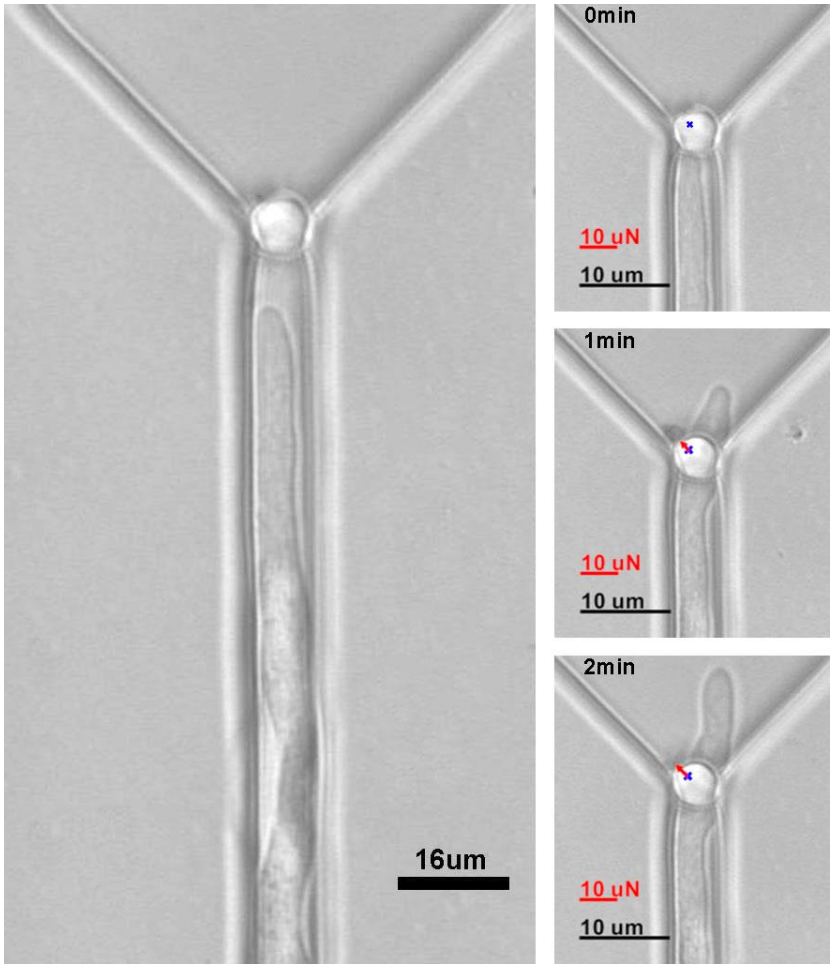

Figure 5.17. A *N. crassa* hypha growing on a P5C17 chip in the presence of 0.05 μg/mL MBC. The MBC was added as the hypha approached the pillar. The hypha extended into the pillar and hit with the tip first (0 min). At 1 min the tip could be seen redirecting to grow into the gap to the right of the pillar. This gave a force vector arrow (red) that had both F_x and F_y components.

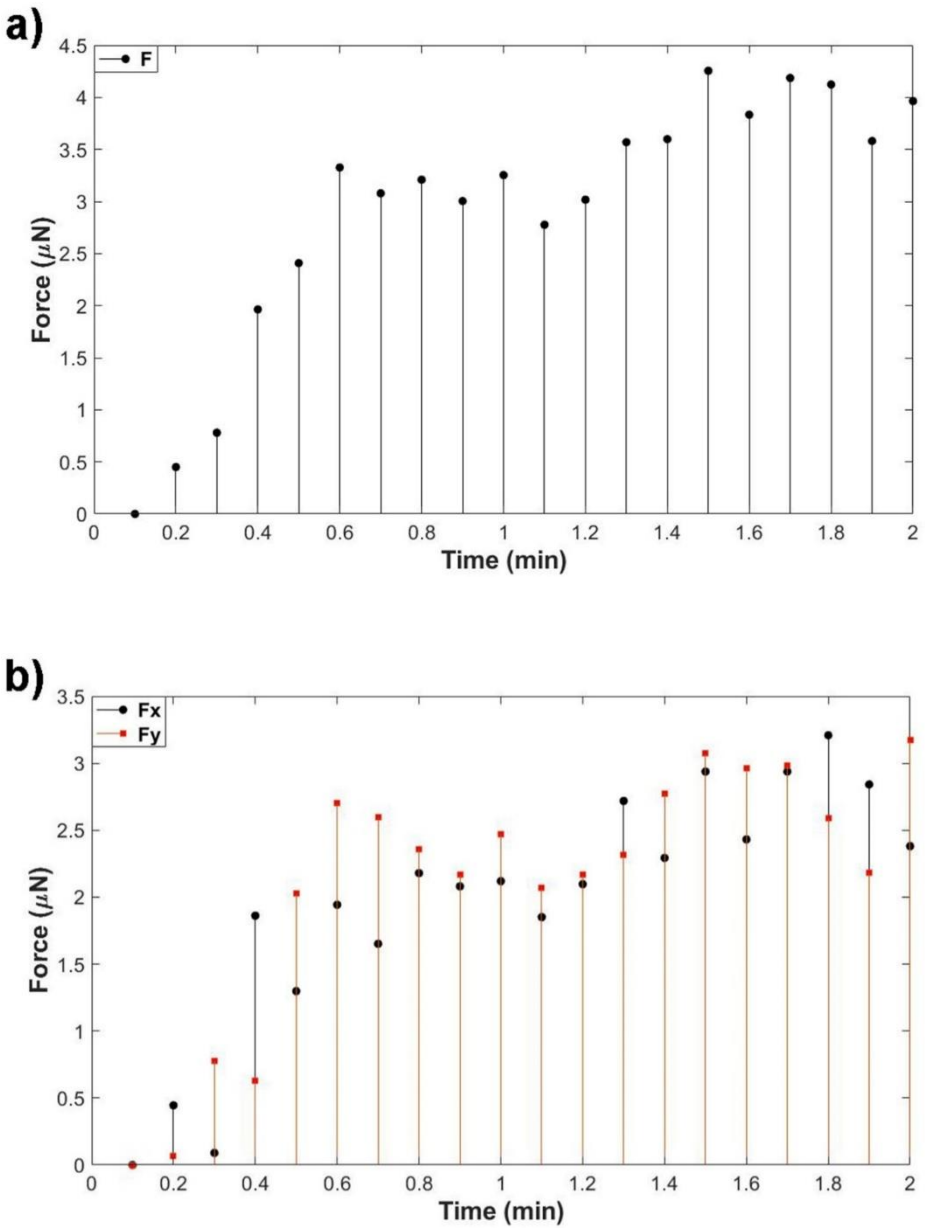

Figure 5.18. Plots of total force (a) and the F_x and F_y (b) components of force for the hypha depicted in Figure 5.17 that was growing on a P5C17 chip in the presence of 0.05 μg/mL MBC. The hypha hit the pillar with the tip but then redirected its growth towards the gap between the pillar and the channel side. Both F_x and F_y made approximately equal contributions to the total force.

To investigate the effect of the MBC on the microtubules and also how microtubule dynamics might change as hyphae hit the pillar, the β-tubulin-GFP expressing *N. crassa* strain 9519 was used. Firstly, an experiment carried out without MBC is shown in Figure 5.19 and shows microtubules extending to the tip as the hypha approaches, hits, and then grows past the pillar. In the presence of MBC, the microtubules appeared fainter with more diffuse staining (Figure 5.20) and were less visible at the tip. In both of the examples shown in Figures 5.19 and 5.20, attempts to track the movement of the pillar and present force vectors were unsuccessful as the software was unable to track the movement due to optical noise. As detailed in Chapter 4, this proved to be a problem with a significant number of the experiments, which was a contributing factor to the low sample sizes in this present Chapter. This is considered further, and the relative numbers of experiments and sample sizes are given in Chapter 6.

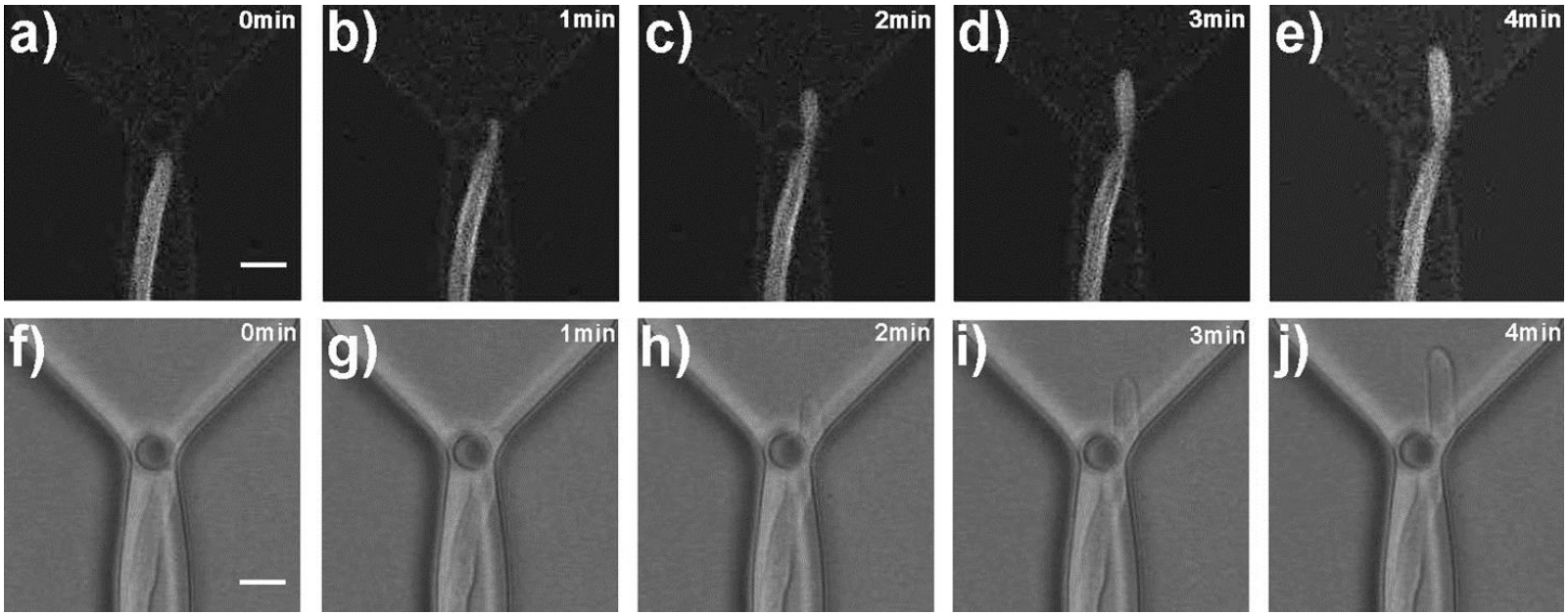

Figure 5.19. Microtubule dynamics as a hypha approaches (a, f), hits (b, g) and then extends beyond a pillar (c, d, e, h, I, j) on a P5C17 chip. Fluorescent images are shown in (a – e) with the respective bright field images in (f – g). The time series represents the time after the initial image was obtained. Microtubules can be seen extending toward the tip in the fluorescent images. Scale bar = 7 µm

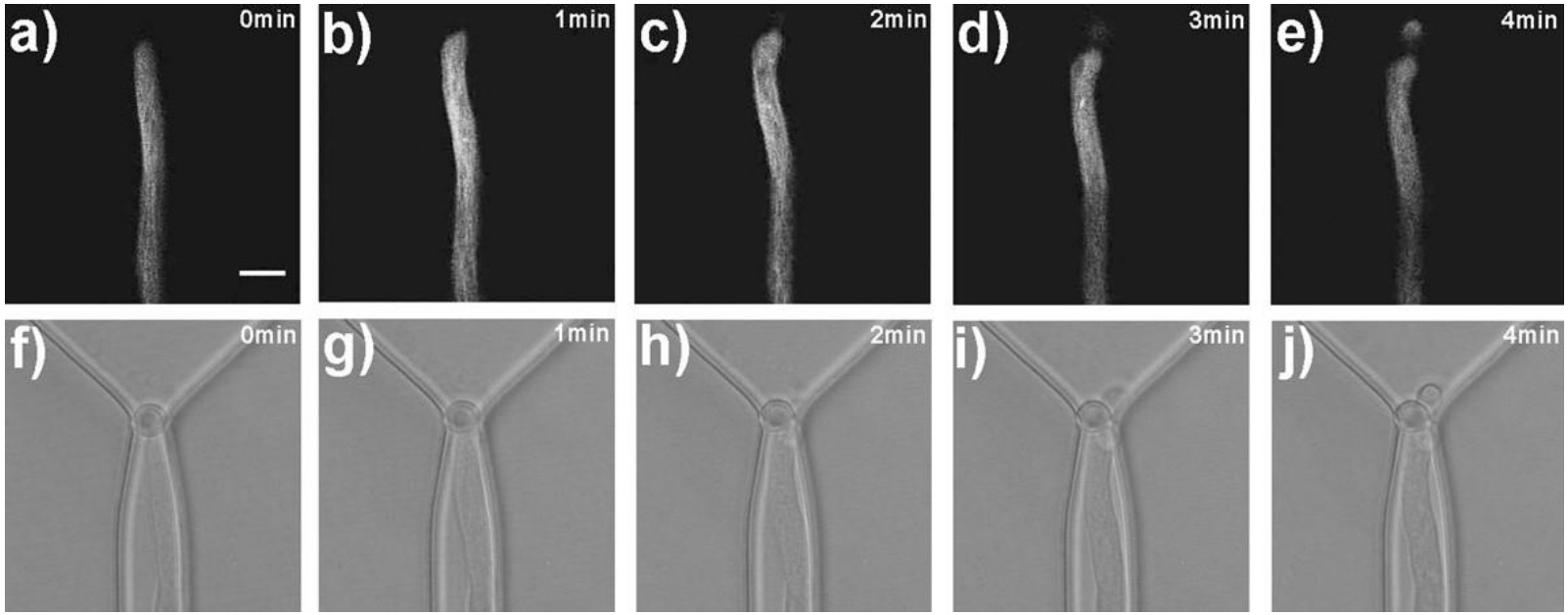

Figure 5.20. Microtubule dynamics as a hypha, which has been exposed to 0.05 µg/mL MBC approaches (a, f), hits (b, g) and then extends beyond a pillar (c, d, e, h, I, j) on a P5C17 chip. Fluorescent images are shown in (a – e) with the respective bright field images in (f – g). The time series represents the time after the initial image was obtained. Staining is more diffuse than in Figure 5.16 and microtubules were less visible at the tip in the fluorescent images. Scale bar = 7 µm

5.7 Invasive growth – force measurement in *Neurospora crassa*

In an attempt to generate invasive growth conditions chips were filled with 1 and 2% agar prior to inoculation. Chips were placed in a 60ºC oven, prior to being filled with agar, to ensure that the liquid agar flowed through and filled the channels completely before it set. All chips were examined prior to inoculation to ensure that their interior was a continuum of solidified agar media and that no air pockets were present. There were no apparent differences in the growth rates of hyphae or in their morphologies as they grew down agar-filled channels compared to non-invasive broth filled channels.

The effects of invasive growth conditions were next tested on total force, F_x, F_y, growth rate and diameters of hyphae growing on P5C17 chips (Table 5.4). In total, five hyphae hit the pillars, three in 2% agar which made initial contact with their sides, one in 2% agar that made initial contact with the tip and one in 1% agar that made initial contact with its side. Thus, in Table 5.4 average values are given for the three in 2% agar that hit with their sides, whereas for the others the actual values are given. Example images and force plots are presented for one of the hyphae that hit the pillar with its side (Figures 5.21 and Figure 5.22). For the hyphae that were grown in 2% agar that hit the pillars with their sides there was no significant difference between the growth rates and diameters of hyphae between 0 and 2 min.

While force values are presented, it should be noted that with agar in the channels, the pillar deflection will be different, compared to when there is no agar. The effect of the resistance of the agar to the pillar has yet to be calibrated. Computer simulations have been made and these indicate that the pillars will move in 2% agar but that this movement is affected by the agar (Volker Nock, personal communication). It is likely

that the forces measured here will be underestimates of the actual forces generated by the hyphae.

Time (min)	Total Force (μN)	F_x (μN)	F_y (μN)	Growth rate (μm/min)	Diameter (μm)
2% agar (side)					
0	-	-	-	2.9 ± 0.2	5.4 ± 0.7
(range)	-	-	-	(2.7 – 3.1)	(4.7 – 6.0)
2	4.7 ± 1.5	3.8 ± 0.4	0.8 ± 0.2	3.0 ± 0.1	5.3 ± 0.5
(range)	(3.7 – 6.5)	(3.4 – 4.3)	(0.5 – 1.0)	(2.9 – 3.1)	(5.0 – 5.9)
2% agar (tip)					
0	-	-	-	2.4	3.9
2	1.4	0.05	1.4	1.7	4.2
1% agar (side)					
0	-	-	-	2.9	4.7
2	2.2	2.1	0.6	2.8	5.1

Table 5.4. The effect of invasive growth conditions on total force, F_x, F_y, growth rate and hyphal diameter, for *N. crassa* on a P5C17 chip. Three hyphae hit the pillar with their sides and the values for these are given as an average ± SD. Only one hyphae hit with its tip in 2% agar and one hit with its tip in 1% agar – the individual actual values for these hyphae are presented. Data are given at the time of contact with the pillar and 2 min after contact.

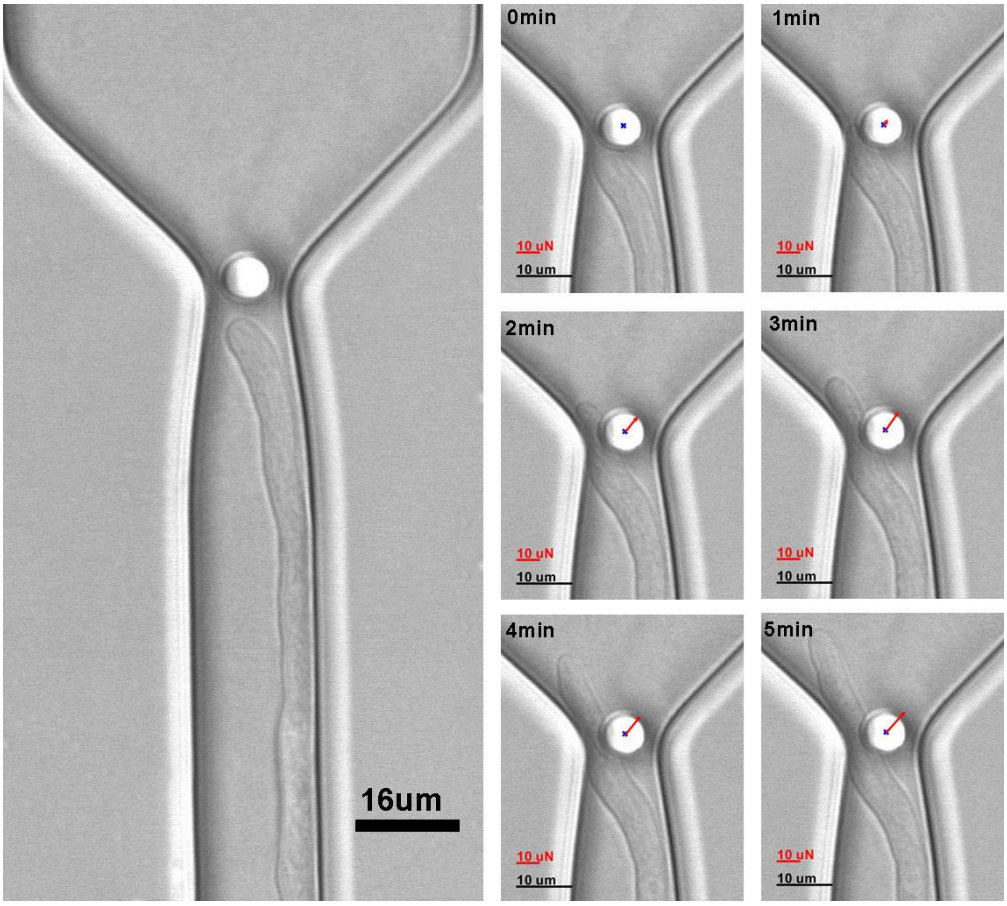

Figure 5.21. A *N. crassa* hypha growing invasively through 2% agar on a P5C17 chip. The hypha extended along the side of a channel, changing direction just before the pillar (image on the left). It appeared to hit the pillar with its side just behind the tip. The time series shows a force plot (red arrow) that is approximately 45^{o} to the perpendicular, indicative of force in both the x- and y-direction.

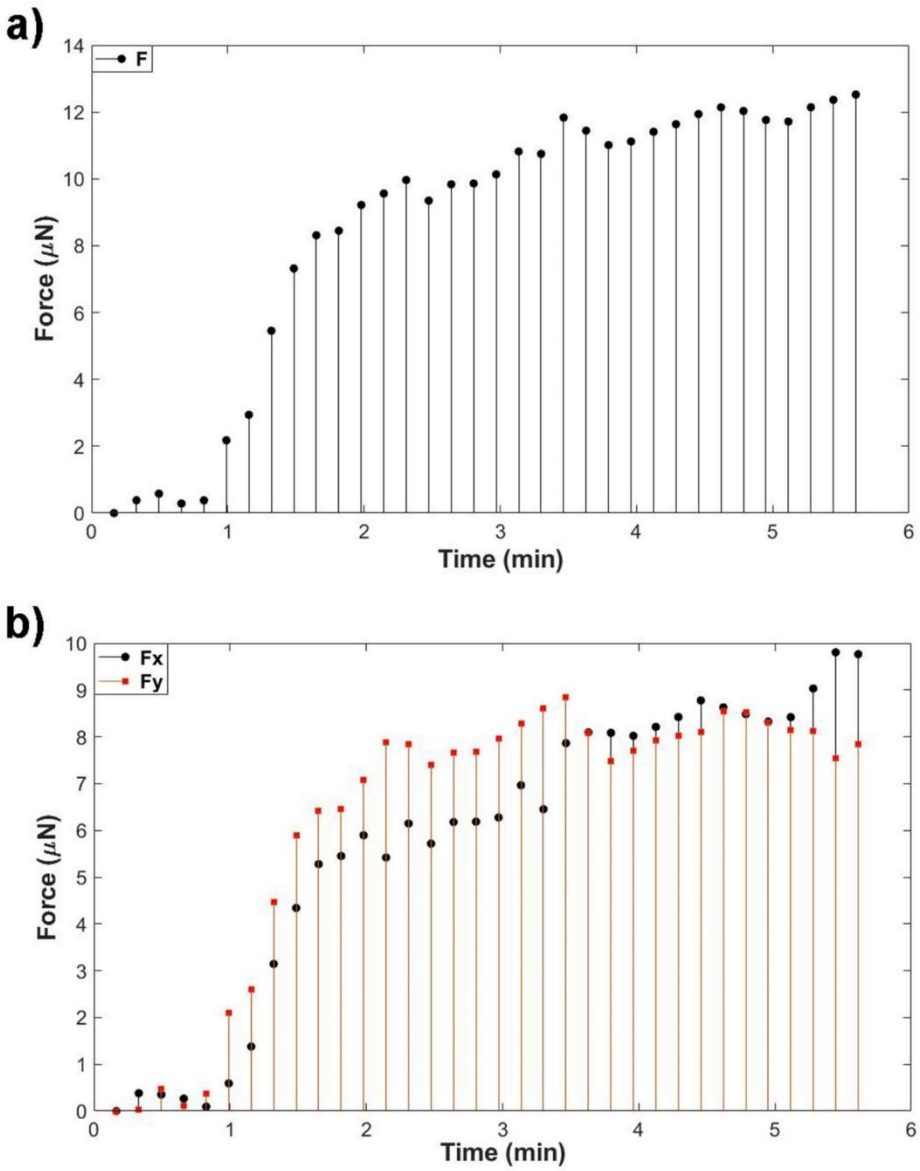

Figure 5.22. Plots of total force (a) and the F_x and F_y (b) components of force for the hypha depicted in Figure 5.21 that was growing invasively on a P5C17 chip in 2% agar. The hypha hit the pillar with its side, just behind the tip. Both F_x and F_x made approximately equal contributions to the total force as indicated by the force vector arrow in Figure 5.21 that was approximately at 45^o to the perpendicular.

5.8 Invasive growth – microtubule dynamics in *Neurospora crassa*

As discussed earlier, there have been reports of changes to the F-actin cytoskeleton in response to invasive growth conditions (Walker et al., 2006; Suei and Garrill, 2008), but as far as I am aware there have been no corresponding studies on microtubules. To address this, and to see if imaging is possible on the chips, a series of experiments were carried out with the β-tubulin-GFP expressing *N. crassa* hyphae. Firstly, hyphae were imaged on well-plates after they had been overlayed with low melting point (LMP) agar and had resumed growth. Four concentrations of agar were used, 1%, 2%, 3% and 4% which were intended to present conditions where increasing protrusive forces were needed for growth (Figure 5.23). In each of these concentrations, microtubules were observed to move to the tips of the cells.

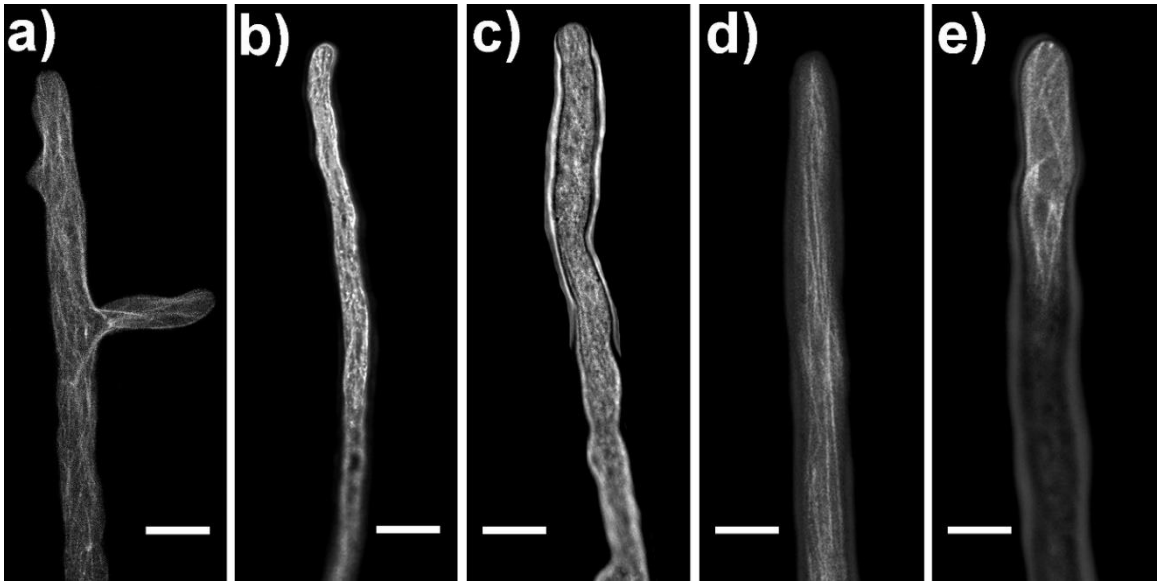

Figure 5.23. Fluorescent images of β-tubulin-GFP expressing *N. crassa* hyphae growing non-invasively (a) and invasively (b = 1% agar, c = 2% agar, d = 3% agar and e = 4% agar) on well-plates. Many of the microtubules were not linear and had distinct bends and twists. Irrespective of the agar concentration, microtubules were dynamic and extended parallel to the axis of growth. In (a) where a branch has formed the microtubules extend transversely from the axis of the main hypha into the branch. Images are representative of 10 hyphae that were observed at each agar concentration. Scale bars = 23 µm

In a second series series of experiments, hyphae were grown invasively on P5C17 chips and the microtubules were imaged. Agar was poured onto the chips as described in the previous section and these were inoculated with the β-tubulin-GFP expressing *N. crassa* 9519 strain. Microtubules were dynamic and extended to the tips as the hyphae grew down the channels towards the pillars (Figure 5.24).

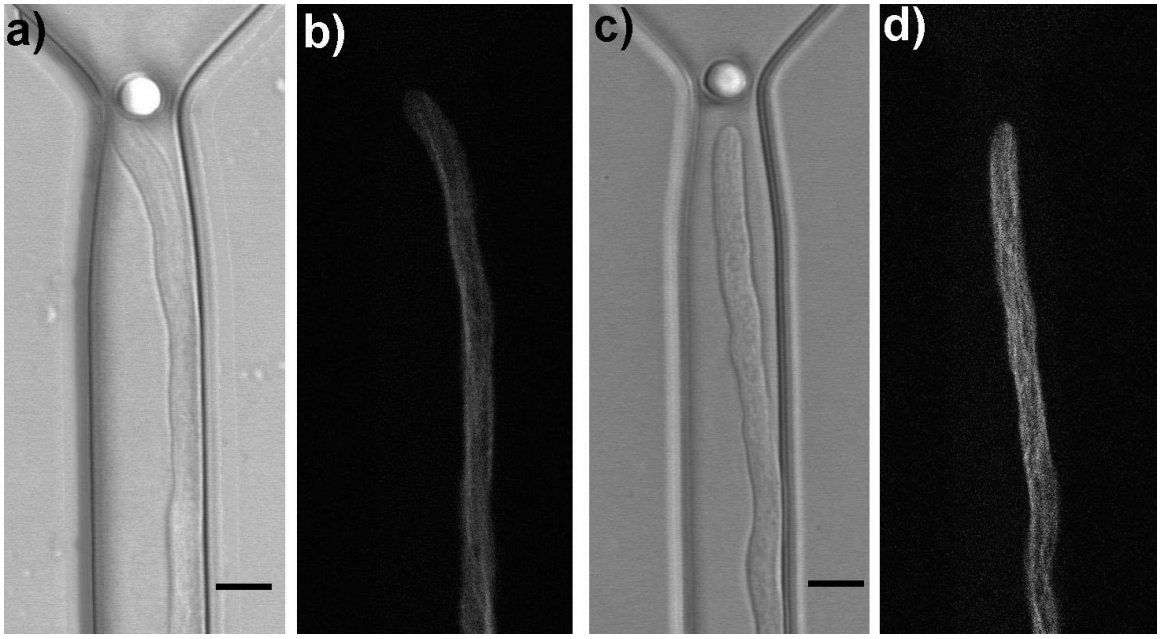

Figure 5.24. Bright field and fluorescent images of β-tubulin-GFP expressing *N. crassa* hyphae growing invasively on a P5C17 chip. In (a) and (b) a hypha was growing in 1% agar and in (c) and (d) it was growing through 2% agar. In both instances microtubules extended to the tip of the hyphae ((b) and (d)). Scale bars = 10 µm.

5.9 Discussion

Elements of the cytoskeleton have long been thought of as crucial and multi-functional players in the process of tip growth. The polymerization and growth of microtubules parallel to the axis of growth and towards the tip is required for the delivery of cell end markers that define polarity, a crucial step in anisotropic growth (Fischer et al., 2008). These markers are likely to include the actin-nucleating protein formin which, once activated, will nucleate and elongate microfilaments at the tip. These microfilaments may then provide a means of delivering vesicles that contain new cell wall synthesizing machinery to the tip (Riquelme, 2013). Further back from the tip, microfilaments may provide the force that enables endocytosis and the recycling of membrane material and polarity determinants (Steinberg et al., 2017). There have also been suggestions that the microfilaments may, in concert with wall loosening enzymes, play a role in the regulation of protrusive force (Walker et al., 2006; Suei and Garrill, 2008), and in the case of oomycetes growing in low turgor conditions, that their polymerization may itself provide the force that is required for growth (Heath and Steinberg, 1999).

Chapters 3 and 4 detailed the design, fabrication and use of chips to measure forces generated by hyphae as they grew. A key facet of these chips was the ability to not just measure total force, but also F_x and F_y, the forces exerted perpendicular and parallel to the axis of growth. With respect to invasive growth, it is F_y that is most of interest as this is the protrusive force that is generated at the very tip of the hypha and is the one that presumably facilitates growth through material. The design of the chips included a media supply centre that enabled solution change. This makes it possible to add cytoskeletal inhibitors as hyphae approach the pillars and the effect

of cytoskeletal disruption on total force, F_x, F_y, as well and growth rate and hyphal diameter is possible. Furthermore, the chips can be imaged on a confocal microscope, meaning that it is possible to image the cytoskeleton in fixed and stained and/or genetically transformed hyphae expressing fluorescently-labelled cytoskeletal elements.

The results described in this chapter detail a series of experiments in which microfilaments and microtubules were inhibited and/or imaged in *A. bisexualis* and *N. crassa* hyphae growing on the chips. Latrunculin B was used to disrupt microfilaments in both species, and the effect of this on total force, F_x, F_y, growth rate and hyphal diameter was investigated. Carbendazim (MBC) was used to disrupt microtubules; the effect of this was investigated in *N. crassa* only, as the inhibitor proved largely ineffective with *A. bisexualis* hyphae that were growing invasively (i.e. through agar) on the chips.

Initial experiments to determine the best concentration of latrunculin B for use on the chips revealed differing sensitivities of the two species to latrunculin B. Growth could be inhibited in *A. bisexualis* at lower concentrations than in *N. crassa*. A concentration of 0.05 μM was chosen for subsequent work on the chips with *A. bisexualis* and 1 μM with *N. crassa*, both of which slowed the growth rate on Petri dishes by around 50%. These concentrations are comparable to those that have been used in other studies on the oomycetes *S. ferax* and *P. infestans*, and the fungus *N. crassa* (Gupta & B, 1997; Ketelaar et al., 2012; Ramos-García, et al., 2009; Roca et al., 2010)

The transient increase in the growth rate of *A. bisexualis* hyphae in the presence of latrunculin B is similar to what has been reported for the oomycete *S. ferax* with

latrunculin B (Gupta and Heath, 1997). In that study, growth increased around 10 s after the application of the inhibitor and then slowed down and stopped after 60 s. Concurrent with the slowing and cessation of growth was a swelling of the tip and disruption of the F-actin cap (Gupta and Heath, 1997). In earlier studies using another actin inhibitor, cytochalasin, similar effects were also reported (Allen et al., 1980; Grove and Sweigard, 1980; Tucker et al., 1986; Jackson and Heath, 1990), although the high concentration needed for an effect raises question as to the effect of the DMSO that is needed for solubility (up to 4% in the study of Jackson and Heath, 1990).

In *A. bisexualis* in the presence of latrunculin B there was a significant increase in growth rate of hyphae growing on chips, 2 min after initial contact with the pillar, relative to both the initial growth rate and the DMSO control. This contrasts with the data presented in Chapter 4, where growth rates slowed down 2 min after initial contact with the pillar irrespective of whether contact was with the tip or the side of the hypha (e.g. Table 4.4). It is also interesting that the hyphal growth rate increased 2 min after pillar contact. The inhibitor was added as the hypha approached close to the pillar (around 1 min prior to contact), thus given the data presented in Figure 5.2 and the images presented in Figure 5.9, if the hypha had been exposed to the inhibitor for 3 min then growth should be slowing down. It is unclear why there is this discrepancy, but it may be that the proximity of the pillar is exerting some effect.

Increases in growth rate and tip swelling are consistent with a role for the microfilaments in restraining the tip. Thus, as the actin is disrupted the tip will initially yield more to turgor pressure and the tip surges forward. The tip would have a bulbous appearance without the obvious taper as seen in the bright field image of Figure 5.10c. It is predicted that this would lead to an increase in the protrusive

force, but as described in the results section, only one hypha that was exposed to latrunculin B initially hit the pillar with the tip, therefore this is at present speculation. It was interesting to note the large forces (total force of 9.19 μN and F_y of 5.4 μN) generated by this hypha, but obviously this is an area where further measurements are required.

In the images of the microfilaments in latrunculin-treated *A. bisexualis* hyphae on the chips, it appears that those at the tip are more susceptible to disruption than the subapical plaques. While in the present study only one concentration was tested, these observations are consistent with reports on the effects of different concentrations of latrunculin B on microfilaments in *P. infestans* (Ketelaar et al., 2013; Meijer et al., 2016). In those studies, the microfilaments were imaged in fixed hyphae that were stained with phalloidin (Ketelaar et al., 2013) or in transformed strains expressing LifeAct-RFP (Meijer et al., 2016). The microfilaments were organized into cables that were located toward the tip and into plaques that were located subapically. When hyphae were exposed to what were described as low latrunculin B concentrations (200 nM) the cables depolymerized while the plaques remained intact. At higher concentrations (750 nM) both cables and plaques depolymerized. Furthermore, with the higher levels of latrunculin B the more robust plaques were able to recover after depolymerisation whereas the more labile cables were not. The behavior and dynamics of the plaques led Meijer et al. (2016) to question a role for plaques in endocytosis in oomycetes. In contrast, they are known to play a role in endocytosis in fungi.

Latrunculin and cytochalasin have also been used to disrupt microfilaments in several species of fungi and the effects of this have led to suggested roles for actin in growth, hyphal morphology and polarized enzyme secretion (Harris, et al., 1999;

McDaniel, and Roberson, 2000; McGoldrick et al, 1995; Taheri-Talesh et al., 2008; Torralba et al, 1998). As in this study, the concentrations required to elicit an effect in *N. crassa* were typically greater than those needed for the oomycetes. Due to time constraints, I was unable to study the effects of microfilament disruption in *N. crassa* in as much detail as for *A. bisexualis*. Only three hyphae hit pillars with their tips and in the presence of latrunculin B these generated an average protrusive force (F_y) of 5.9 μN. This is comparable to the protrusive force value for the single *A. bisexualis* hypha that hit the pillar with its tip of 5.4 μN. The F_y value for *N. crassa* in latrunculin B cannot however be compared to the DMSO control values, as all of these hyphae hit the pillars with their sides first. While this and the data from the *A. bisexualis* hypha are consistent with greater protrusive force generation after microfilament disruption, it is obvious that more work is needed before anything can be concluded. In contrast, the growth rates in the latrunculin B-treated hyphae did not increase after contact with the pillars. It is unclear why there might be a difference between the two species here, but clearly this is an area where further research is warranted.

Carbendazim (MBC) was used to disrupt the microtubules of *N. crass*a in order to see if they played a role in protrusive force generation. Again, it is not possible to conclude too much, given that only two hyphae hit the pillars with their tips. These generated forces in the y-direction of 1.8 and 2.0 μN respectively, which is lower than the value for the single hyphae that hit with its tip in the presence of latrunculin. It is not possible to compare the two hyphae with the DMSO control hyphae, as these all hit the pillars with their sides. With respect to growth rate, the MBC-treated hyphae grew significantly more slowly at 2 min after contacting the pillar and their diameter increased. While MBC has previously been reported to slow growth in *N. crassa* (Heath et al., 2000) and in other filamentous ascomycete fungi (Sampson et

al., 2005), the rates reported here at 0 min were not different from those in the absence of MBC.

Microtubules were less abundant at the tip with more diffuse faint staining in the presence of MBC. Other studies report that MBC causes a complete loss of microtubules with only dispersed fine granular structures throughout the cytoplasm (Heath et al., 2000). Given that they were still able to grow, this observation calls into question the role of the microtubules in tip growth. In many other fungal species, microtubule depolymerisation does not lead to a cessation of growth, but to a loss of growth directionality (Howard and Aist, 1980; Raudaskoski et al., 1994; Temperli et al., 1991; Torralba et al., 1998). This has led to the suggestion that microtubules may not be essential for the transport of material needed for growth to the hyphal tips, but that they are necessary for stabilization of the Spk and play a role in the maintainance of hyphal morphogenesis (Riquelme et al., 2011).

The microtubules of *N. crassa* have been reported to be more complex than those of other filamentous fungi (Riquelme et al., 2011). In those other species, microtubules are nucleated subapically and the plus end will extend toward the hyphal tip (Zhang et al., 2003; Konzack et al., 2005). This also occurs in *N. crassa*, but there is evidence to suggest that nucleation can also occur at the tip and the microtubules can polymerise in a retrograde direction (Mouriño-Pérez et al., 2006). In the present study, when microtubules were imaged in hyphae on the chips they appeared as dynamic, long structures that were longitudinally arranged along the hypha parallel to the axis of growth. Many of the microtubules appeared to have a distinct curvature, which is similar to those reported in other studies (Mouriño-Pérez et al., 2006).

Where hyphal branches formed, the microtubules were arranged perpendicular to the axis of the main hypha and extended into the branch. Microtubules were also observed to extend into the apical dome and others have reported that they can traverse the Spk towards the tip while others extend just to the periphery of the Spk (Mouriño-Pérez et al., 2006). In the present study it would have been of interest to also image the Spk at the same time as the microtubules in hyphae on the chips using the membrane stain FM4-64, but time constraints precluded this. Previously, Suei and Garrill (2008) successfully imaged the Spk in invasively growing hyphae and found that it had a similar morphology and dynamics to the Spk in non-invasive growing hyphae.

The possible use of the chips to study invasive growth was investigated by filling the chips with 1% or 2% agar. It was found that by preheating the chips in an oven the chips and channels were sufficiently warm that agar could be pipetted onto the chips via the media supply centre and would completely fill the channels. Subsequent observation of the channels after the agar had set revealed no air pockets. Hyphae grew on these chips and down the channels and showed characteristics of invasive growth that have previously been reported. Diffraction patterns were present along the flanks of the hyphae as they grew through the agar (see for example Figure 5.21a and Figure 5.21c) and also, if the side of the microscope was tapped lightly, the tips did not move (with non-invasive conditions the tips will typically jiggle when this is done). Again, a low sample size and the fact that some hyphae hit the pillars with their sides meant that no meaningful conclusion could be drawn regarding protrusive forces. The fact that pillars deflected in the agar filled channels when hyphae grew into them means that this is an area where future work is warranted and would be of great interest. Microtubules extended to the tips irrespective of the

agar concentration and so they may differ from the microfilaments. In an earlier study, Suei and Garrill (2008) reported changes to F-actin at the tip, with an F-actin depleted zone in invasive hyphae, the size of which increased with increasing agar concentration in the growth media. Furthermore, immunochemical staining and western blots suggested that cofilin was located at the tip in the invasive hyphae and may have played a role in the actin remodeling. This was proposed to enable the generation of a greater protrusive force through modulation of tip yielding. As mentioned above, the measurement of protrusive force in invasive conditions is an area of interest, given that the chips appear to provide a means to measure this. Previous studies using microstrain gauges (Money et al., 2004) required hyphae to grow out of agar prior to hitting the cantilever and so it is questionable whether these were truly invasive conditions (Walker et al., 2006). Computer simulations of pillar mechanics suggest that the pillars bend when they are in agar concentrations of 2% or lower. However, the bending is influenced by the agar and there is a need for calibration of this in agar.

In conclusion, the chips have enabled measurement of total force, F_x, F_y, growth rates and hyphal morphology in hyphae that have been exposed to cytoskeletal inhibitors. They have also enabled the imaging of both microfilaments (in *A. bisexualis*) and microtubules (in *N. crassa*) and their responses to the inhibitors and growth into pillars. Unfortunately, low sample sizes, which were partly due to the technically difficult experiments that were being carried out, meant that no detailed conclusions can be drawn regarding the role of the cytoskeleton in protrusive force generation, but this work sets the platform for future studies in this area.

CHAPTER 6

CONCLUSIONS AND FUTURE DIRECTIONS

This thesis describes an investigation of the use of LOC devices to measure protrusive forces at the tips of hyphae of an oomycete (*A. bisexualis*) and a fungus (*N. crassa*) and are summarized below. The hypotheses that were tested in the work were detailed in Chapter 1. In concluding this thesis, each of these hypotheses will be considered in turn and suggestions for future work will also be covered.

6.1 Protrusive force in hyphae of fungi and oomycetes can be measured using pillars on LOC devices.

Protrusive forces in the micro-Newton range were measured with the pillars for both *A. bisexualis* and *N. crassa*. These could be identified as protrusive forces as, firstly, the very tip of the hypha could be observed hitting the pillar. Secondly, and less subjectively, the total force could be differentiated into its x- and y-components (F_x and F_y). F_y, which was parallel to the axis of growth, represented the protrusive force. In contrast, F_x, which was perpendicular to the axis of growth, represented a squeezing force as the side of the hypha contacted the pillar.

One of the main problems with the pillars was to get the hyphae to grow into them. Efforts were made to direct the growth through the use of tapered and/or narrow channels, and while through the course of this thesis improvements were made, a significant proportion of hyphae would still hit pillars with their sides first, rather than with their tips. This is clearly an area where further work is required. Narrower channels are likely to help, although this can make fabrication difficult and also may affect the behavior of the hyphae. Another possibility is to have some chemo-attractant that will induce the growth of the hyphal tip into the pillar. One possibility

might be a mixture of phenylalanine and lanthanum. In a study of hyphal branching, in *A. bisexualis*, Morris et al. (2011) used a micropipette to apply phenylalanine close to the sides of hyphae to induce the formation of branches. If lanthanum, which is an inhibitor of mechanosensitive ion channels, were included with the phenylalanine, Morris and colleague observed that the hypha changed its direction of growth and tried to extend up the micropipette toward the source of the phenylalanine and lanthanum. If such a combination were to be applied to the pillars, then this could induce a similar chemotropic response in a hypha in the channel and ensure that the tip made contact with the pillar first. Obviously, in changing the growth pattern of the hypha it is possible that this could have some impact on protrusive force that was generated.

While protrusive forces can be measured in both fungi and oomycetes using the chips, it should be noted that this conclusion is based on experiments on only two species. Further work is, therefore, needed on additional species. For the oomycetes, work has already started with *Phytophthora* species. As these have a comparable hyphal diameter to *N. crassa*, chips have been designed using the Version 2 P5C17 chips as a blueprint. *Phytophthora. nicotianae* has been shown to grow on the chips and exert micro-Newton forces on the pillars (Heather Shearer, Yiling Sun, Ayelen Tayagui, Volker Nock and Ashley Garrill, unpublished data). This work could be further extended to transformed strains of *P. infestans*, which express LifeAct-GFP (Kots et al., 2016) and, in a New Zealand context, to *P. agathidicida*, the species that is responsible for Kauri dieback disease. Additional fungal species could include species of *Aspergillus* or *Puccinia*. In the case of *Puccinia* species, this would have special relevance for New Zealand, given the spread of myrtle rust disease in the iconic pōhutukawa and rata plants.

6.2 The LOC devices will enable concurrent measurement of protrusive force and cytoskeletal imaging.

The use of a β-tubulin-GFP expressing strain of *N. crassa* enabled the imaging of microtubules in hyphae that were growing in channels and the dynamics of the microtubules to be observed as the hyphae hit the pillars. Unfortunately, in these experiments, optical problems meant that the top of the pillar could not be adequately tracked. One possible reason for this may have been inconsistencies in the thickness of the PDMS, which impacted on the illumination of the pillar. While every effort was made to ensure consistency in chip manufacture this cannot be guaranteed. Thus, at this stage concurrent measurements of force and cytoskeletal dynamics have not been possible. Further work to increase the sample size would likely give rise to some experiments where concurrent measurements are possible. Pillar tracking proved a problem throughout the work, not just with the experiments on the cytoskeleton. Only 69% of pillars were able to be tracked when they were displaced by *N. crassa* hyphae, compared to 75% (Version 5 chips) and 85% (Version 4 chips) for *A. bisexualis* (Table 6.1).

	Total Experiments	Total pillars	Number of pillars tracked	%
A. bisexualis				
Chip V4	10	48	41	85
Chip V5	24	89	67	75
N. crassa				
V2	21	78	51	69

Table 6.1. Total number of pillars that were able to be tracked for the *A. bisexualis* Version 4 and 5 chips and the *N. crassa* Version 2 chips. The percentage that these represent of total pillars which hyphae hit is also given.

One solution to this problem may be to label the pillars to enhance their tracking. To this end, preliminary experiments have been carried out using the cell labeling solution, Vybrant-DiD (Kajzar et al., 2008) and this has been shown to fluorescently stain the pillars (Figure 6.1). Work is currently underway using these pillars with transformed hyphae and it is hoped that these will enable concurrent measurements and observations to be made.

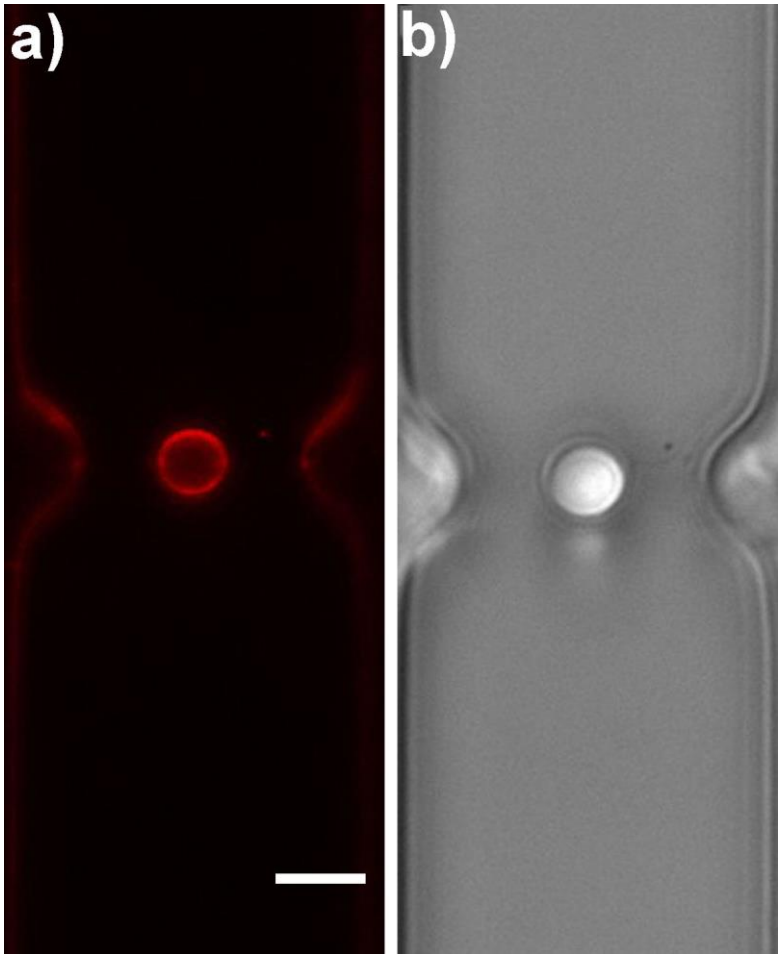

Figure 6.1. An *A. bisexualis* Version 5 chip, showing a pillar that had been labeled with Vybrant DiD. (a) A fluorescent image of the pillar and (b) a bright field image. Scale bar = 20 μm.

While experiments were successful in imaging the dynamics of microtubules in *N. crassa*, attempts to follow the dynamics of microfilaments were less so. The LifeAct-RFP gave abundant and bright staining in septa, but staining was rarely observed at the tips of hyphae. This may be in part due to the fact that the microfilaments at the tip are highly dynamic and possibly labile. It may also be due to LifeAct, which is an actin-binding protein, being more commonly associated with actin populations at septa. It is possible that the transformed strains of *P. infestans* may provide a better

system to study the dynamics of microfilaments on the chips, as these seem to have more reliable staining of actin at the tips (Kots et al., 2017).

6.3 LOC devices will enable the measurement of protrusive force in invasive hyphae.

Invasive growth conditions could be invoked by pouring Vogel's media, made up with 1 or 2% LMP agar into the channels. By preheating the chips in a 60^{o}C oven, the agar did not set until it had completely filled the channels. *N. crassa* hyphae were inoculated onto the chips and grew invasively toward the pillars. Invasive growth was confirmed with a distinct diffraction pattern of a distinct "furrow" that was formed by the hypha as it grew through the agar. Also, hyphae that are growing invasively do not jiggle if the microscope is gently tapped while they are being observed as has been previously reported (Walker et al., 2006). Pillars were displaced as the hyphae grew into them, although only one hypha hit the pillar with the tip and thus generated an invasive protrusive force. However, as discussed in Chapter 5, the invasive forces presented in this thesis are likely to be lower than the actual forces as with agar in the channels, the pillar deflection will be different (i.e. smaller) than without, due to the resistance of the agar. Pillar mechanics in agar have not yet been calibrated, although their potential responses have been simulated (Volker Nock, personal communication). These simulations suggest that at agar concentrations of 2% or lower the pillars will still deflect, but in a different way to those that are not in agar. This is clearly an area where further work is needed, it will require the development of a setup capable of applying force to pillars embedded in agar (i.e. micromanipulator with force sensor). At the present time, it can be concluded that

invasive conditions can be created on the chips and hyphae will grow invasively on these and hit the pillars. What remains uncertain at this stage is how pillar movements can reliably be converted into force measurements.

6.4 Microfilaments restrain the tips in hyphae and an F-actin depleted zone at the tip is responsible for the provision of protrusive force.

Due to the low sample sizes in the experiments with latrunculin B, described in Chapter 5, no conclusions with respect to this are possible. Only one *A. bisexualis* hypha hit the pillar with its tip first in the presence of latrunculin B, although this did generate a large protrusive force. If additional replicates showed the same response, then this would be of significant interest. The suggestions above for increasing the numbers of hyphae hitting the pillars with their tips first and the better tracking of pillar tops should help increase the success of these experiments and thus increase the sample size. Also, as suggested above, the use of transformed *Phytophthora* strains may be applicable in addressing this question.

6.5 Microtubules extend to the tips of invasive hyphae.

Microtubules were observed extending to the tips of invasive hyphae of *N. crassa*. This occurred irrespective of the concentration of agar that the hyphae were growing through. At higher agar concentrations it is likely that a greater protrusive force is required for growth and this has been proposed to be, in part, due to an F-actin depleted zone. The size of this F-actin depleted zone has been shown to increase with increasing agar concentration in the media (Suei and Garrill 2008). If the microtubules extend to the tip and deliver cell end markers and components necessary for F-actin nucleation, then the observation that they do this irrespective of agar concentration may mean that microfilaments are still nucleated at the tips of invasive hyphae. The F-actin depleted zone may thus come about due to the action of cofilin and possibly capping proteins, rather than a decrease in microfilament formation. This is consistent with the observations of Suei and Garrill (2008), who reported cofilin at the tips of invasive hyphae but not non-invasive hyphae.

In summary, this thesis reports work that suggests that protrusive force measurement is possible at the tips of fungi and oomycetes, and that, with further work, the dynamics of the cytoskeleton and its role in the generation and regulation of these forces will be possible. This work will be challenging, as the experiments described here were technically demanding, but the potential of any findings and their relevance with respect to understanding the mechanisms of growth in these two groups of vitally important microorganism is extremely exciting.

REFERENCES

Agudelo, C. G., Nezhad, A. S., Ghanbari, M., Naghavi, M., Packirisamy, M., & Geitmann, A. (2013). TipChip: a modular, MEMS-based platform for experimentation and phenotyping of tip-growing cells. *Plant Journal*, *73*(6), 1057–1068. https://doi.org/10.1111/tpj.12093

Alberts, B., Johnson, A., Lewis, J., Raff, M., Roberts, K., & Walter, P. (2008). *Molecular Biology of the Cell* (5th ed.). Garland.

Alexopoulus, C. J., Mims, C. W., & Blackwell, M. (1996). Kingdom Fungi. In *Introductory Mycology* (4th ed., pp. 1–25). New York, USA: John Wiley & Sons.

Allen, E. D., Aiuto, R., and Sussman, A. S. (1980). Effects of cytochalasins on *Neurospora crassa. Protoplasma*, *102*(1–2), 63–75.

Amir, R., Steudle, E., Levanon, D., Hadar, Y., & Chet, I. (1995). Turgor changes in *Morchella esculenta* during translocation and sclerotial formation. *Experimental Mycology*, *19*(2), 129–136.

Bartnicki-Garcia, S. (1973). Fungal cell wall composition. *CRC Handb Microbiol [Chem Rubber Co]*.

Bartnicki-Garcia, S. (2002). Hyphal tip growth: outstanding questions. *Molecular Biology of Fungal Development*, 29–58. https://doi.org/10.1201/9780203910719.ch2

Bartnicki-Garcia, S., Hergert, F., & Gierz, G. (1989). Computer simulation of fungal morphogenesis and the mathematical basis for hyphal (tip) growth. *Protoplasma*, *153*(1–2), 46–57. https://doi.org/https://doi.org/10.1007/BF01322464

Bartnicki-Garcia, S., & Lippman, E. (1969). Fungal Morphogenesis : Cell wall construction in *Mucor rouxii*. *Science*, *165*(3890), 302–304.

Bebber, D. P., Ramotowski, M. A. T., & Gurr, S. J. (2013). Crop pests and pathogens move polewards in a warming world. *Nature Climate Change*, *3*(11), 985–988. https://doi.org/10.1038/nclimate1990

Bechinger, C., Giebel, K. F., Schnell, M., Leiderer, P., Deising, H. B., & Bastmeyer, M. (1999). Optical measurements of invasive forces exerted by appressoria of a plant pathogenic fungus. *Science*, *285*(5435), 1896–1899. https://doi.org/10.1126

Beever, R. E., Waipara, N. W., Ramsfield, T. D., Dick, M. A., & Horner, I. J. (2007). Kauri (*Agathis australis*) Under threat from *Phytophthora*? In *Phytophthoras in forests and natural ecossystems* (pp. 74–85).

Bellgard, S. E., Pennycook, S. R., Weir, B. S., Ho, W., & Waipara, N. W. (2016). *Phytophthora agathidicida*. *Forest Phytophthoras*, *6*(1), 1–8. https://doi.org/10.5399/osu/fp.5.1.3748

Benkert, R., Obermeyer, G., & Bentrup, F.-W. (1997). The turgor pressure of growing lily pollen tubes. *Protoplasma*, *198*(1–2), 1–8. https://doi.org/10.1007/BF01282125

Berepiki, A., Lichius, A., & Read, N. D. (2011). Actin organization and dynamics in filamentous fungi. *Nature Reviews. Microbiology*, *9*(12), 876–87. https://doi.org/10.1038/nrmicro2666

Berepiki, A., Lichius, A., Shoji, J.-Y., Tilsner, J., & Read, N. D. (2010a). F-actin dynamics in *Neurospora crassa*. *Eukaryotic Cell*, *9*(4), 547–557. https://doi.org/10.1128/EC.00253-09

Berepiki, A., Lichius, A., Shoji, J., Tilsner, J., & Read, N. D. (2010b). F-actin dynamics in *Neurospora crassa* □ †, *9*(4), 547–557. https://doi.org/10.1128/EC.00253-09

Berlin, A., Samils, B., & Andersson, B. (2017). Multiple genotypes within aecial clusters in *Puccinia graminis* and *Puccinia coronata*: improved understanding of the biology of cereal rust fungi. *Fungal Biology and Biotechnology*, *4*(1), 3. https://doi.org/10.1186/s40694-017-0032-3

Borkovich, K. A., Alex, L. A., Yarden, O., Freitag, M., Turner, G. E., Read, N. D., Seiler, S., Bell-pedersen, D., Paietta, J., Plesofsky, N., Plamann, M., Goodrich-tanrikulu, M., Schulte, U., Mannhaupt, G., Nargang, F. E., Radford, A., Selitrennikoff, C., Galagan, J. E., Dunlap, J. C., Loros, J. J., Catcheside, D., Inoue, H., Aramayo, R., Polymenis, M., Selker, E. U., Sachs, M. S., Marzluf, Paulsen ,I., Davis, R., Ebbole, D.J., Zelter, A., Kalkman, E. R., Rourke, R. O., & Bowring, F. (2004). Lessons from the genome sequence of *Neurospora crassa* : Tracing the path from genomic blueprint to multicellular organism. *Microbiology and Molecular Biology Reviews*, *68*(1), 1–108. https://doi.org/10.1128/MMBR.68.1.1

Brundrett, M. C. (2002). Coevolution of root and mycorrhizas of land plants. *New Phytologist*, *154*(2), 275–304.

Brunswick, D. (1924). The effect of emotional stimuli on the gastro-intestinal tone. *Journal of Comparative Psychology*, *4*(1), 19.

Carefoot, G. L., & Sprott, E. R. (1967). Famine on the Wind.

Carlile, M. J. (1995). The success of the hypha and mycelium. In G. M. Neil, A R & Gadd (Ed.), *The Growing Fungus* (pp. 3–19). London: Chapman & Hall.

Chang, F., & Peter, M. (2003). Yeasts make their mark. *Nature Cell Biology*, *5*(4), 294–299. https://doi.org/10.1038/ncb0403-294

Charras, G. T., Lehenkari, P. P., & Horton, M. A. (2001). Atomic force microscopy can be used to mechanically stimulate osteoblasts and evaluate cellular strain distributions. *Ultramicroscopy*, *86*(1–2), 85–95. https://doi.org/10.1016/S0304-3991(00)00076-0

Chitcholtan, K., and Garrill, A. (2005). A β4 integrin-like protein co-localises with a phosphotyrosine containing protein in the oomycete *Achlya bisexualis*: inhibition of tyrosine phosphorylation slows tip growth. *Fungal Genetics and Biology*, *42*(6), 534-545. https://doi.org/https://doi.org/10.1016/j.fgb.2005.03.010

Christensen, M. J., Bennett, R. J., Ansari, H. A., Koga, H., Johnson, R. D., Bryan, G. T., … Voisey, C. R. (2008). *Epichloë endophytes* grow by intercalary hyphal extension in elongating grass leaves. *Fungal Genetics and Biology : FG & B*, *45*(2), 84–93. https://doi.org/10.1016/j.fgb.2007.07.013

Coker, W. C. (1927). Other water molds from the soil. *Journal of the Elisha Mitchell Scientific Society*, *42*(3–4), 207–226.

Conia, J., Edwards, B. S. &, & Voelkel, S. (1997). The micro-robotic laboratory: Optical trapping and scissing for the biologist. *Journal of Clinical Laboratory Analysis*, *11*(1), 28–38. https://doi.org/10.1002/(SICI)1098-2825

Crampin, H. (2005). *Candida albicans* hyphae have a Spitzenkörper that is distinct from the polarisome found in yeast and pseudohyphae. *Journal of Cell Science*, *118*(13), 2935–2947. https://doi.org/10.1242/jcs.02414

Davidse, L. C., & Flach, W. (1977). Differential binding of methyl benzimidazol-2-yl carbamate to fungal tubulin as a mechanism of resistance to this antimitotic agent in mutant strains of *Aspergillus nidulans*. *The Journal of Cell Biology*, *72*(1), 174–193.

Delgado-Alvarez, D. L., Callejas-Negrete, O. a, Gómez, N., Freitag, M., Roberson, R. W., Smith, L. G., & Mouriño-Pérez, R. R. (2010). Visualization of F-actin localization and dynamics with live cell markers in *Neurospora crassa*. *Fungal Genetics and Biology FG B*, *47*(7), 573–586. https://doi.org/10.1016/j.fgb.2010.03.004

Dent, E. W., and Gertler, F. B. (2003). Cytoskeletal dynamics and transport in growth cone motility and axon guidance. *Neuron*, *40*(2), 209–227. https://doi.org/https://doi.org/10.1016/S0896-6273(03)00633-0

Desai, A., & Mitchison, T. J. (1997). Microtubule polymerization dynamics. *Annual Review of Cell and Developmental Biology*, *13*(1), 83–117. https://doi.org/10.1146/annurev.cellbio.13.1.83

Du, P., Lin, I., Lu, H., & Zhang, X. (2010). Extension of the beam theory for polymer bio-transducers with low aspect ratios and viscoelastic characteristics, *20*. https://doi.org/10.1088/0960-1317/20/9/095016

Du Roure, O., Saez, A., Buguin, A., Austin, R. H., Chavrier, P., Silberzan, P., & Ladoux, B. (2005). Force mapping in epithelial cell migration. *Proceedings of the National Academy of Sciences*, *102*(7), 2390–2395. https://doi.org/10.1073/pnas.0408482102

Earle, G., & Hintz, W. (2014). New approaches for controlling saprolegnia parasitica, the causal agent of a devastating fish disease. *Tropical Life Sciences Research*, *25*(2), 101–109.

Eisenstein, M. (2017). A measure of molecular muscle. *Nature*, *544*, 255–257.

Evangelista, M., Pruyne, D., Amberg, D. C., Boone, C., & Bretscher, A. (2002). Formins direct Arp2/3-independent actin filament assembly to polarize cell growth in yeast. *Nature Cell Biology*, *4*(3), 260–269. https://doi.org/10.1038/ncb718

Faix, J., & Grosse, R. (2006). Staying in Shape with Formins. *Developmental Cell*, *10*(6), 693–706. https://doi.org/10.1016/j.devcel.2006.05.001

Fass, J. N., & Odde, D. J. (2003). Tensile force-dependent neurite elicitation via Anti-β1 integrin antibody-coated magnetic beads. *Biophysical Journal*, *85*(1), 623–636. https://doi.org/10.1016/S0006-3495(03)74506-8

Feierbach, B., Verde, F., & Chang, F. (2004). Regulation of a formin complex by the microtubule plus end protein tea1p. *Journal of Cell Biology*, *165*(5), 697–707. https://doi.org/10.1083/jcb.200403090

Felekis, D., Vogler, H., Mecja, G., Muntwyler, S., Nestorova, A., Huang, T., … Nelson, B. J. (2015). Real-time automated characterization of 3D morphology and mechanics of developing plant cells. *International Journal of Robotics Research*, *34*(8), 1136–1146. https://doi.org/10.1177/0278364914564231

Fischer, R., Zekert, N., & Takeshita, N. (2008). Polarized growth in fungi - Interplay between the cytoskeleton, positional markers and membrane domains. *Molecular Microbiology*, *68*(4), 813–826. https://doi.org/10.1111/j.1365-2958.2008.06193.x

Fisher, M. C., Gow, N. A. R., & Gurr, S. J. (2016). Tackling emerging fungal threats to animal health, food security and ecosystem resilience. *Philosophical Transactions of the Royal Society B: Biological Sciences*, *371*(1709), 20160332. https://doi.org/10.1098/rstb.2016.0332

Fisher, M. C., Henk, D. A., Briggs, C. J., Brownstein, J. S., Madoff, L. C., Mccraw, S. L., & Gurr, S. J. (2012). Emerging fungal threats to animal , plant and ecosystem health. *Nature*, *484*(7393), 186–194. https://doi.org/10.1038/nature10947

Galagan, J., Calvo, S., Borkovich, K., Selker, E., Read, N., Jaffe, D., … Birren, B. (2003). The genome sequence of the filamentous fungus *Neurospora crassa*. *Nature*, *422*(6934), 859–868. https://doi.org/doi: 10.1038/nature01554

Garrill, A., Clipson, N. J. W. & Jennings, D. H. (1992). Preliminary observations on the monovalent cation relations of *Thraustochytrium aureum*: a fungus requiring sodium for growth. *Mycological Research* 96 (4), 295 - 304.

Geitmann, A. (1999). The Rheological Properties of the Pollen Tube Cell Wall. In M. A. Cresti M., Cai G. (Ed.), *Fertilization in Higher Plants* (pp. 283–302). Berlin: Springer, Berlin, Heidelberg. https://doi.org/https://doi.org/10.1007/978-3-642-59969-9_20

Geitmann, A., & Emons, A. M. C. (2000). The cytoskeleton in plant and fungal cell tip growth, *198*(January), 218–245.

Geng, T., Bredeweg, E. L., Szymanski, C. J., Liu, B., Baker, S. E., Orr, G., Evans, J. E. & Kelly, R. T. (2015). Compartmentalized microchannel array for high-throughput analysis of single cell polarized growth and dynamics. *Scientific Reports*, *5*, 16111. https://doi.org/10.1038/srep16111

Girbardt, M. (1956). A method for comparison of living and fixed structures in fungi. *Zeitschrift Fur Wissenschaftliche Mikroskopie Und Mikroskopische Technik*, *63*(1), 16–21.

Gladfelter, A. S. (2006). Control of filamentous fungal cell shape by septins and formins. *Nature Reviews. Microbiology*, *4*(3), 223–229. https://doi.org/10.1038/nrmicro1345

Gooday, G. W. (1978). Enzymology of hyphal growth. *Filamentous Fungi*.

Greer, C. A., & Webster, R. K. (2001). Occurrence, distribution, epidemiology, cultivar reaction, and management of rice blast disease in California. *Plant Disease*, *85*(10), 1096–1102. https://doi.org/10.1094/PDIS.2001.85.10.1096

Griffin, D. H. (1994). *Fungal Physiology* (2nd ed.). New York: Wiley-Liss.

Grove, S. N., and Sweigard, J. A. (1980). Cytochalasin A inhibits spore germination and hyphal tip growth in *Gilbertella persicaria. Experimental Mycology*, *4*(3), 239–250. https://doi.org/https://doi.org/10.1016/0147-5975(80)90028-6

Grove, S. N., Bracker, C. E., & Morre, D. J. (1970). An ultrastructural basis for hyphal tip growth in *Pythium ultimum*. *American Journal of Botany*, 245–266.

Gupta, M., Kocgozlu, L., Sarangi, B. R., Margadant, F., Ashraf, M., & Ladoux, B. (2015). Micropillar substrates: a tool for studying cell mechanobiology. *Methods in Cell Biology*, *125*, 289–308. https://doi.org/https://doi.org/10.1016/bs.mcb.2014.10.009

Gupta, G. D., & B, H. I. (1997). Actin disruption by latrunculin B causes turgor-related changes in tip growth of *Saprolegnia ferax* hyphae. *Fungal Genetics and Biology*, *21*(1), 64–75. https://doi.org/https://doi.org/10.1006/fgbi.1997.0957

Hanson, K. L., Nicolau, D. V., Filipponi, L., Wang, L., Lee, A. P., & Nicolau, D. V. (2006). Fungi use efficient algorithms for the exploration of microfluidic networks. *Small*, *2*(10), 1212–1220. https://doi.org/10.1002/smll.200600105

Hardham, A. R., & Blackman, L. M. (2017). *Phytophthora cinnamomi*. *Molecular Plant Pathology*, *19*(2), 260–285. https://doi.org/10.1111/mpp.12568

Harold, R. L., Money, N. P., & Harold, F. M. (1996). Growth and morphogenesis in *Saprolegnia ferax*: Is turgor required? *Protoplasma*, *191*(1–2), 105–114. https://doi.org/https://doi.org/10.1007/BF01280830

Harris, J. P., Capadona, J. R., Miller, R. H., Healy, B. C., Shanmuganathan, K., Rowan, S. J., Weder C., & Tyler, D. J. (2011). Mechanically adaptive intracortical implants improve the proximity of neuronal cell bodies. *Journal of Neural Engineering*, *8*(6), 66011.

Harris, S. D., Hofmann, A. F., Tedford, H. W., & Lee, M. P. (1999). Identification and characterization of genes required for hyphal morphogenesis in the filamentous fungus *Aspergillus nidulans*. *Genetics*, *151*(3), 1015–1025.

Harris, A. K., Wild, P., & Stopak, D. (1980). Silicone rubber substrata: a new wrinkle in the study of cell locomotion Author(s): Albert K. Harris, Patricia Wild and David Stopak Source: *Science*, *208*(4440), 177–179.

Harris, S. D., Read, N. D., Roberson, R. W., Shaw, B., Seiler, S., Plamann, M., & Momany, M. (2005). MINIREVIEWS Polarisome meets Spitzenkörper: Microscopy , Genetics , and Genomics Converge. *Society*, *4*(2), 225–229. https://doi.org/10.1128/EC.04.2.225

Heath, I B, Gupta, G, & Bai, S. (2000). Plasma membrane-adjacent actin filaments, but not microtubules, are essential for both polarization and hyphal tip morphogenesis in *Saprolegnia ferax* and *Neurospora crassa*. *Fungal Genetics and Biology*, *30*(1), 45–62.

Heath, I. B. (1980). Variant mitoses in lower eukaryotes: indicators of the evolution of mitosis? *International Review of Cytology*, *64*(1), 1–80.

Heath, I. B. (1987). Preservation of a labile cortical array of actin filaments in growing hyphal tips of the fungus *Saprolegnia ferax*. *European Journal of Cell biologyCell Biology*, *44*, 10–16.

Heath, I. B., & Steinberg, G. (1999). Mechanisms of hyphal tip growth: tube dwelling amebae Revisited. *Fungal Genetics and Biology*, *28*(2), 79–93. https://doi.org/https://doi.org/10.1006/fgbi.1999.1168

Hoch, H. C., & Mitchell, J. E. (1973). The effects of osmotic water potentials on *Aphanomyces euteiches* during zoosporogenesis. *Canadian Journal of Botany*, *51*(2), 413–420. https://doi.org/https://doi.org/10.1139/b73-048

Holdaway-Clarke, T. L., & Hepler, P. K. (2003). Control of pollen tube growth: Role of ion gradients and fluxes. *New Phytologist*, *159*(3), 539–563. https://doi.org/10.1046/j.1469-8137.2003.00847.x

Howard, R., & Aist, J. R. (1980). Cytoplasmic microtubules and fungal morphogenesis : ultrastructural effects of methyl benzimidazole-2-ylcarbamate determined by freeze-substitution of hyphal tip cells, (9), 55–64.

Howard, R. J., Ferrari, M. A., Roach, D. H., & Money, N. P. (1991). Penetration of hard substrates by a fungus employing enormous turgor pressures. *Proceedings of the National Academy of Sciences*, *88*(24), 11281–11284. https://doi.org/10.1073/pnas.88.24.11281

Hu, C., Munglani, G., Vogler, H., Ndinyanka Fabrice, T., Shamsudhin, N., Wittel, F. K., … Nelson, B. J. (2017). Characterization of size-dependent mechanical properties of tip-growing cells using a lab-on-chip device. *Lab on a Chip*, *17*(1), 82–90. https://doi.org/10.1039/C6LC01145D

Hunsley, D., & Burnett, J. H. (1970). The ultrastructural architecture of the walls of some hyphal fungi. *Journal of General Microbiology*, *62*(2), 203–218. https://doi.org/10.1099/00221287-62-2-203

Iskratsch, T., Wolfenson, H., & Sheetz, M. P. (2014). Appreciating force and shape—the rise of mechanotransduction in cell biology. *Nature Reviews Molecular Cell Biology*, *15*(12), 825. https://doi.org/10.1038/nrm3903

Iskratsch, T., Yu, C. H., Mathur, A., Liu, S., Stévenin, V., Dwyer, J., Hone, J., Ehler, E., & Sheetz, M. (2013). FHOD1 is needed for directed forces and adhesion maturation during cell spreading and migration. *Developmental Cell*, *27*(5), 545–559. https://doi.org/10.1016/j.devcel.2013.11.003

Jackson, S. L., and Heath, I. B. (1990). Evidence that actin reinforces the extensible hyphal apex of the oomycete *Saprolegnia ferax*. *Protoplasma*, *157*(1–3), 144–153.

Jackson, S. L., and Heath, I. B. (1993). Roles of calcium ions in hyphal tip growth. *Microbiological Reviews*, *57*(2), 367–382.

Jackson, S. L., & Heath, I. B. (1990). Evidence that actin reinforces the extensible hyphal apex of the oomycete *Saprolegnia ferax*. *Protoplasma*, *157*(1–3), 144–153. https://doi.org/https://doi.org/10.1007/BF01322647

Johari, S., Nock, V., Alkaisi, M. M., & Wang, W. (2013). On-chip analysis of C. elegans muscular forces and locomotion patterns in microstructured environments. *Lab on a Chip*, *13*(9), 1699. https://doi.org/10.1039/c3lc41403e

Kajzar, A., Cesa, C. M., Kirchgeßner, N., Hoffmann, B., & Merkel, R. (2008). Toward physiological conditions for cell analyses: Forces of heart muscle cells suspended between elastic micropillars. *Biophysical Journal*, *94*(5), 1854–1866. https://doi.org/10.1529/biophysj.107.115766

Kaksonen, M., Sun, Y., & Drubin, D. G. (2003). A pathway for association of receptors, adaptors, and actin during endocytic internalization. *Cell*, *115*(4), 475–487. https://doi.org/10.1016/S0092-8674(03)00883-3

Kaksonen, M., Toret, C. P., & Drubin, D. G. (2005). A modular design for the clathrin- and actin-mediated endocytosis machinery. *Cell*, *123*(2), 305–320. https://doi.org/10.1016/j.cell.2005.09.024

Kaminskyj, S. G., & Heath, I. B. (1995). Integrin and spectrin homologues, and cytoplasm-wall adhesion in tip growth. *Journal of Cell Science*, *108*, 849–56. Retrieved from http://www.ncbi.nlm.nih.gov/pubmed/7769021

Kaminskyj, S. G. W., Garrill, A., & Heath, I. B. (1992). The relation between turgor and tip growth in *Saprolegnia ferax*: Turgor is necessary, but not sufficient to explain apical extension rates. *Experimental Biology*, *16*(1), 64–75. https://doi.org/https://doi.org/10.1016/0147-5975(92)90042-P

Kamoun, S. (2009). Plant Pathogens : Oomycetes (water mold), 689–695.

Kamoun, S., Furzer, O., Jones, J. D. G., Judelson, H. S., Ali, G. S., Dalio, R. J. D., … Govers, F. (2015). The Top 10 oomycete pathogens in molecular plant pathology. *Molecular Plant Pathology*, *16*(4), 413–434. https://doi.org/10.1111/mpp.12190

Kelly, D. J. A., & Budd, K. (1990). Osmotic adjustment in the mycelial ascomycete *Neocosmospora vasinfecta* (E. F. Smith). *Experimental Mycology*, *14*(2), 136–144. https://doi.org/https://doi.org/10.1016/0147-5975(90)90072-2

Ketelaar, T., Meijer, H. J. G., Spiekerman, M., Weide, R., & Govers, F. (2012). Effects of latrunculin B on the actin cytoskeleton and hyphal growth in *Phytophthora infestans*. *Fungal Genetics and Biology*, *49*(12), 1014–1022. https://doi.org/10.1016/j.fgb.2012.09.008

Konzack, S, Rischitor, PE, Enke, C, Fischer, R. (2005). The role of the kinesin motor KipA in microtubule organization and polarized growth of *Aspergillus nidulans*. *Molecular Biology of the Cell*, *16*, 497–506.

Kortekamp, A. (2005). Growth, occurrence and development of septa in *Plasmopara viticola* and other members of the *Peronosporaceae* using light-and epifluorescence-microscopy. *Mycological Research*, *109*(5), 640–648. https://doi.org/https://doi.org/10.1017/S0953756205002418

Kots, K., Meijer, H. J. G., Bouwmeester, K., Govers, F., & Ketelaar, T. (2017). Filamentous actin accumulates during plant cell penetration and cell wall plug formation in *Phytophthora infestans*. *Cellular and Molecular Life Sciences*, *74*(5), 909–920. https://doi.org/10.1007/s00018-016-2383-y

Krajaejun, T., Lerksuthirat, T., Garg, G., Lowhnoo, T., Yingyong, W., Khositnithikul, R., … Sullivan, T. D. (2014). Transcriptome analysis reveals pathogenicity and evolutionary history of the pathogenic oomycete *Pythium insidiosum*. *Fungal Biology*, *118*(7), 640–653. https://doi.org/10.1016/j.funbio.2014.01.009

Krings, M., Taylor, T. N., & Dotzler, N. (2011). The fossil record of the *Peronosporomycetes* (Oomycota). *Mycologia*, *103*(3), 445–457. https://doi.org/10.3852/10-278

Latijnhouwers, M., De Wit, P. J. G. M., & Govers, F. (2003). Oomycetes and fungi: Similar weaponry to attack plants. *Trends in Microbiology*, *11*(10), 462–469. https://doi.org/10.1016/j.tim.2003.08.002

Lee, K. K., Labiscsak, L., Ahn, C. H., & Hong, C. I. (2016). Spiral-based microfluidic device for long-term time course imaging of *Neurospora crassa* with single nucleus resolution. *Fungal Genetics and Biology*, *94*, 11–14. https://doi.org/https://doi.org/10.1016/j.fgb.2016.06.004

Lee, S. H. (2009). Microtechnology to Fabricate Lab-on-a-Chip for Biology Applications. *Lab-on-a-Chip Technology for Biomedical and Biological Applications*, *1*, 125–138.

Levina, N. N., Lew, R. R., & Heath, I. B. (1994). Cytoskeletal regulation of ion channel distribution in the tip-growing organism *Saprolegnia ferax*. *Journal of Cell Science*, *107*(36051), 127–134.

Lew, D. J. (2002). Formin' actin filament bundles. *Nature Cell Biology*, *4*(2), 29–31. https://doi.org/10.1038/ncb0202-e29

Lew, R. R. (2011). How does a hypha grow? The biophysics of pressurized growth in fungi. *Nature Reviews Microbiology*, *9*(7), 509–518. https://doi.org/10.1038/nrmicro2591

Lew, R. R., Levina, N. N., Walker, S. K., & Garrill, A. (2004). Turgor regulation in hyphal organisms q, *41*, 1007–1015. https://doi.org/10.1016/j.fgb.2004.07.007

Lichius, A., Berepiki, A., & Read, N. D. (2011). Form follows function -- the versatile fungal cytoskeleton. *Fungal Biology*, *115*(6), 518–540. https://doi.org/10.1016/j.funbio.2011.02.014

Lorch, J. M., Lankton, J., Werner, K., Falendysz, E. A., McCurley, K., & Blehert, D. S. (2015). Experimental infection of snakes with ophidiomyces ophiodiicola causes pathological changes that typify snake fungal disease. *mBio*, *6*(6), 1–9. https://doi.org/10.1128/mBio.01534-15

Luard, E. J. (1982). Effect of osmotic shock on some intracellular solutes in two filamentous fungi. *Microbiology*, *128*(11), 2575–2581. https://doi.org/10.1099/00221287-128-11-2575

Ludwig, N., Löhrer, M., Hempel, M., Mathea, S., Schliebner, I., Menzel, M., … Horbach, R. (2014). Melanin is not required for turgor generation but enhances cell-wall rigidity in appressoria of the corn pathogen *Colletotrichum graminicola*. *Molecular Plant-Microbe Interactions*, *27*(4), 315.

MacDonald, E., Millward, L., Ravishankar, J. P., & Money, N. P. (2002). Biomechanical interaction between hyphae of two *Pythium* species (Oomycota) and host tissues. *Fungal Genetics and Biology*, *37*(3), 245–249. https://doi.org/10.1016/S1087-1845(02)00514-5

Madania, A., Dumoulin, P., Grava, S., Kitamoto, H., Schärer-Brodbeck, C., Soulard, A., Moreau, V. & Winsor, B. (1999). The *Saccharomyces cerevisiae* homologue of human Wiskott–Aldrich syndrome protein Las17p interacts with the Arp2/3 complex. *Molecular Biology of the Cell*, *10*(10), 3521–3538.

Madden, L. V., Ellis, M. A., Lalancette, N., Hughes, G., & Wilson, L. L. (2000). Evaluation of a Disease Warning System for Downy Mildew of Grapes. *Plant Disease*, *84*(5), 549–554. https://doi.org/10.1094/PDIS.2000.84.5.549

Mark, J. E. (2009). *Polymer Data Handbook*. Oxford University Press.

McDaniel, D P, and Roberson, R. W. (2000). Microtubules are required for motility and positioning of vesicles and mitochondria in hyphal tip cells of *Allomyces macrogynus. Fungal Genetics and Biology*, *31*(3), 233–244. https://doi.org/https://doi.org/10.1006/fgbi.2000.1249

Mcdonald, J. C., Duffy, D. C., Anderson, J. R., Chiu, D. T., Wu, H., Schueller, O. J. A., & Whitesides, G. M. (2000). Fabrication of microfluidic systems in poly(dimethylsiloxane). *Electrophoresis*, *21*, 27–40.

McGoldrick, C A, Gruver, C, and May, G. S. (1995). myoA of *Aspergillus nidulans* encodes an essential myosin I required for secretion and polarized growth. *Tha Journal of Cell Biology*, *128*(4), 577–587.

McKerracher, L. J., & Heath, I. B. (1987). Cytoplasmic migration and intracellular organelle movements during tip growth of fungal hyphae. *Experimental Mycology*, *11*(2), 79–100. https://doi.org/https://doi.org/10.1016/0147-5975(87)90041-7

Meijer, H. J. G., Hua, C., Kots, K., Ketelaar, T., & Govers, F. (2014). Actin dynamics in *Phytophthora infestans*; rapidly reorganizing cables and immobile, long-lived plaques. *Cellular Microbiology*, *16*(6), 948–961. https://doi.org/10.1111/cmi.12254

Minc, N., Boudaoud, A., & Chang, F. (2009). Mechanical forces of fission yeast growth. *Current Biology*, *19*(13), 1096–1101. https://doi.org/10.1016/j.cub.2009.05.031

Minc, N., Boudaoud, A., & Chang, F. (2009). Report mechanical forces of fission yeast growth. *Current Biology*, *19*(13), 1096–1101. https://doi.org/10.1016/j.cub.2009.05.031

Money, N. (1994). Osmotic adjustment and the role of turgor in mycelial fungi. In M. F. Wessels J.G.H. (Ed.), *The Mycota (A Comprehensive Treatise on Fungi as Experimental Systems for Basic and Applied Research)* (1st ed., pp. 67–88). Springer, Berlin, Heidelberg. https://doi.org/https://doi.org/10.1007/978-3-662-11908-2_4

Money, N. (2007). *Biomechanics of invasive hyphal growth*. (N. A. R. G. R.J. Howard, Ed.), *The Mycota. Vol. VIII. Biology of the Fungal Cell* (Second edi). New York: Springer Verlag.

Money, N. P., Davis, C. M., & Ravishankar, J. P. (2004). Biomechanical evidence for convergent evolution of the invasive growth process among fungi and oomycete water molds. *Fungal Genetics and Biology*, *41*(9), 872–876. https://doi.org/10.1016/j.fgb.2004.06.001

Money, N. P., & Harold, F. M. (1993). Two water molds can grow without measurable turgor pressure. *Planta*, *190*, 426–430.

Money, N. P., & Hill, T. W. (1997). Correlation between endoglucanase secretion and cell wall strength in oomycete hyphae : Implications for Growth and Morphogenesis. *Mycologia*, *89*(5), 777–785. Retrieved from http://www.jstor.org/stable/3761134

Morris, E. J. S., Jackson, S. L., & Garrill, A. (2011). An investigation of the effects of Ca2+channel inhibitors on branching and chemotropism in the oomycete *Achlya bisexualis:* Support for a role for Ca2+in apical dominance. *Fungal Genetics and Biology*, *48*(5), 512–518. https://doi.org/10.1016/j.fgb.2010.10.008

Mouriño-Pérez, R. R., Roberson, R. W., and Bartnicki-García, S. (2006). Microtubule dynamics and organization during hyphal growth and branching in *Neurospora crassa*. *Fungal and Genetics Biology*, *43*, 389–400. https://doi.org/10.1016/j.fgb.2005.10.007

Mullins, R. D., & Pollard, T. D. (1999). Structure and function of the Arp2 / 3 complex. *Current Opinion in Structural Biology*, *9*, 244–249.

Muralidhar, A., Novis, P. M., Broady, P. A., Collings, D. A., & Garrill, A. (2013). An estuarine species of the alga *Vaucheria (Xanthophyceae)* displays an increased capacity for turgor regulation when compared to a freshwater species. *Journal of Phycology*, *49*(5), 967–978. https://doi.org/https://doi.org/10.1111/jpy.12106

Muralidhar, A., Swadel, E., Spiekerman, M., Suei, S., Fraser, M., Ingerfeld, M., Tayagui, A. B.*,* Garrill, A. (2016). A pressure gradient facilitates mass flow in the oomycete *Achlya bisexualis. Microbiology*, *162*, 206–213. https://doi.org/10.1099/mic.0.000216

Nelson, W. J. (2003). Adaptation of core mechanisms to generate cell polarity. *Nature*, *422*(6933), 766–774. https://doi.org/10.1038/nature01602

Nezhad, A. S., & Geitmann, A. (2013). The cellular mechanics of an invasive lifestyle. *Journal of Experimental Botany*, *64*(15), 4709–4728. https://doi.org/10.1093/jxb/ert254

Nezhad, A. S., Naghavi, M., Packirisamy, M., Bhat, R., & Geitmann, A. (2013). Quantification of the Young's modulus of the primary plant cell wall using Bending-Lab-On-Chip (BLOC). *Lab on a Chip*, *13*, 2599–2608. https://doi.org/10.1039/c3lc00012e

Petre, B., & Kamoun, S. (2014). How do filamentous pathogens deliver effector proteins into plant cells? *PLoS Biology*, *12*(2). https://doi.org/10.1371/journal.pbio.1001801

Picton, J. M., and Steer, M., & W. (1982). A model for the mechanism of tip extension in pollen tubes. *Journal of Theoretical Biology*, *98*(1), 15–20. https://doi.org/https://doi.org/10.1016/0022-5193(82)90054-6

Pollard, T. D. (2007). Regulation of actin filament assembly by Arp2/3 complex and formins. *Annual Review of Biophysics and Biomolecular Structure*, *36*, 451–77. https://doi.org/10.1146/annurev.biophys.35.040405.101936

Pollard, T. D., & Beltzner, C. C. (2002). Structure and function of the Arp2/3 complex. *Current Opinion in Structural Biology*, *12*(6), 768–774. https://doi.org/https://doi.org/10.1016/S0959-440X(02)00396-2

Pring, M., Evangelista, M., Boone, C., Yang, C., & Zigmond, S. H. (2003). Mechanism Formin-induced nucleation of actin filaments. *Current Opinion in Cell Biology*, *42*(2), 486–496. https://doi.org/10.1016/j.ceb.2003.10.019

Pruyne, D., Evangelista, M., Yang, C., Bi, E., Zigmond, S., Bretscher, A., & Boone, C. (2002). Role of formins in actin assembly : Nucleation and barbed-end association. *Science*, *297*(5581), 612–615. Retrieved from http://www.jstor.org/stable/3832167

R. Fischer. (2007). The cytoskeleton and polarized growth of filamentous fungi. In R. J. H. and N. A. R. Gow (Ed.), *Biology of the Fungal Cell* (2nd ed., pp. 121–134). Springer-Verlag Berlin Heidelberg.

Ramos-García, S. L., Roberson, R. W., Freitag, M., Bartnicki-García, S., & Mouriño-Pérez, R. R. (2009). Cytoplasmic bulk flow propels nuclei in mature hyphae of *Neurospora crassa*. *Eukaryotic Cell*, *8*(12), 1880–1890. https://doi.org/10.1128/EC.00062-09

Raudaskoski, M, Mao, W Z, and Y.-M. (1994). Microtubule cytoskeleton in hyphal growth. Response to nocodazole in a sensitive and a tolerant strain of the homobasidiomycete *Schizophyllum commune*. *European Journal of Cell Biology*, *64*(1), 131–141.

Reinhardt, M. O. (1892). Das Wachsthum der Pilzhyphen: ein Beitrag zur Kenntniss des Flachenwachsthums vegetablischer Zellmembranen. *Bot*, *23*, 479–566.

Riquelme, M. (1998). What determines growth direction in fungal hyphae? *Fungal Genetics and Biology*, *24*(12), 101–109. https://doi.org/https://doi.org/10.1006/fgbi.1998.1074

Riquelme, M. (2013). Tip growth in filamentous fungi: a road trip to the apex. *Annual Review of Microbiology*, *67*(1), 587–609. https://doi.org/10.1146/annurev-micro-092412-155652

Riquelme, M., Bartnicki-García, S., González-Prieto, J. M., Sánchez-León, E., Verdín-Ramos, J. A., Beltrán-Aguilar, A., & Freitag, M. (2007). Spitzenkörper localization and intracellular traffic of green fluorescent protein-labeled CHS-3 and CHS-6 chitin synthases in living hyphae of *Neurospora crassa*. *Eukaryotic Cell*, *6*(10), 1853–1864. https://doi.org/10.1128/EC.00088-07

Riquelme, M., Oded, Y., Bartnicki-Garcia, S., Bowman, B., Castro-Longoria, E., Free, S. J., … Watters, M. K. (2011). Architecture and development of the *Neurospora crassa* hypha – a model cell for polarized growth. *Fungal Biology*, *115*(6), 446–474. https://doi.org/https://doi.org/10.1016/j.funbio.2011.02.008

Riquelme, M., & Sánchez-León, E. (2014). The Spitzenkörper: a choreographer of fungal growth and morphogenesis. *Current Opinion in Microbiology*, *20*, 27–33. https://doi.org/10.1016/j.mib.2014.04.003

Robertson, A. S., Smythe, E., & Ayscough, K. R. (2009). Functions of actin in endocytosis. *Cellular and Molecular Life Sciences*, *66*(13), 2049–2065. https://doi.org/https://doi.org/10.1007/s00018-009-0001-y

Robertson, N. F., & Rizvi, S. R. H. (1968). Some Observations on the Water-Relations of the Hyphae of *Neurospora crassa*. *Annals of Botany*, *32*(2), 279–291. https://doi.org/https://doi.org/10.1093/oxfordjournals.aob.a084208

Roca, M. G., Kuo, H.-C., Lichius, A., Freitag, M., & Read, N. D. (2010). Nuclear dynamics, mitosis, and the cytoskeleton during the early stages of colony initiation in *Neurospora crassa*. *Eukaryotic Cell*, *9*(8), 1171–1183. https://doi.org/10.1128/EC.00329-09

Rossi, V., & Caffi, T. (2012). The role of rain in dispersal of the primary inoculum of *Plasmopara viticola*. *Phytopathology*, *102*(2), 158–165. https://doi.org/10.1094/PHYTO-08-11-0223

Rounds, C. M., Hepler, P. K., & Winship, L. J. (2014). The apical actin fringe contributes to localized cell wall deposition and polarized growth in the lily pollen tube. *Plant Physiology*, *166*(1), 139–151. https://doi.org/10.1104/pp.114.242974

Roy, S. J., Holdaway-Clarke, T. L., Hackett, G. R., Kunkel, J. G., Lord, E. M., & Hepler, P. K. (1999). Uncoupling secretion and tip growth in lily pollen tubes: Evidence for the role of calcium in exocytosis. *Plant Journal*, *19*(4), 379–386. https://doi.org/10.1046/j.1365-313X.1999.00515.x

Ryder, L. S., & Talbot, N. J. (2015). Regulation of appressorium development in pathogenic fungi. *Current Opinion in Plant Biology*, *26*, 8–13. https://doi.org/10.1016/j.pbi.2015.05.013

Sagot, I., Rodal, A. A., Moseley, J., Goode, B. L., & Pellman, D. (2002). An actin nucleation mechanism mediated by Bni1 and profilin. *Nature Cell Biology*, *4*(8), 626–631. https://doi.org/10.1038/ncb834

Sampson, K., & Heath, I. B. (2005). The dynamic behaviour of microtubules and their contributions to hyphal tip growth in *Aspergillus nidulans*. *Microbiology*, *151*(5), 1543–1555. https://doi.org/10.1099/mic.0.27750-0

Sampson, K., Heath, I. B., & Sampson, K. (2005). The dynamic behaviour of microtubules and their contributions to hyphal tip growth in *Aspergillus nidulans* Printed in Great Britain, 1543–1555. https://doi.org/10.1099/mic.0.27750-0

Saral, R. (1191). *Candida* and *Aspergillus* infections in immunocompromised patients: An Overview. *Reviews of Infectious Diseases*, *13*(3), 487–492. https://doi.org/10.1093/clinids/13.3.487

Schmitz, H. P., Kaufmann, A., Ko¨ hli, M., Laissue, P. P., & Philippsen, P. (2006). From function to shape: a novel role of a formin in morphogenesis of the fungus *Ashbya gossypii*. *Molecular Biology of the Cell*, *17*, 130–145.

Schoen, I., Hu, W., Klotzsch, E., & Vogel, V. (2010). Probing cellular traction forces by micropillar arrays: contribution of substrate warping to pillar deflection. *Nano Letters*, *10*(5), 1823–1830. https://doi.org/10.1021/nl100533c

Shamsudhin, N., Laeubli, N., Atakan, H. B., Vogler, H., Hu, C., Haeberle, W., … Nelson, B. J. (2016). Massively parallelized pollen tube guidance and mechanical measurements on a lab-ona-chip platform. *PLoS ONE*, *11*(12), 1–16. https://doi.org/10.1371/journal.pone.0168138

Sharpless, K. E., & Harris, E. D. (2002). Functional characterization and localization of the *Aspergillus nidulans* formin SEPA. *Molecular Biology of the Cell*, *13*, 469–479.

Shear, C. L., & Dodge, B. O. (1927). Life histories and heterothallism of the red bread-mold fungi of the *Monilia sitophila* group. *Journal of Agricultural Research*, *34*(11), 1019–1042.

Sheetz, M. P., Felsenfeld, D. P., and Galbraith, C. G. (1998). Cell migration: regulation of force on extracellular-matrix-integrin complexes. *Trends in Cell Biology*, *8*(2), 51–54.

Si, H., Justa-Schuch, D., Seiler, S., & Harris, S. D. (2010). Regulation of septum formation by the Bud3-Rho4 GTPase module in *Aspergillus nidulans. Genetics*, *185*(1), 165–176. https://doi.org/10.1534/genetics.110.114165

Spector, I., Shochet, N. R., Blasberger, D., & Kashman, Y. (1989). Latrunculins—novel marine macrolides that disrupt microfilament organization and affect cell growth: I. Comparison with cytochalasin D. *Cytoskeleton*, *13*(3), 127–144.

Stanley, C. E., & Der, M. G. A. Van. (2017). Microbiome-on-a- Chip : New frontiers in plant – microbiota research microbiome-on-a-Chip. *Trends in Microbiology*, *25*(8), 610–613. https://doi.org/10.1016/j.tim.2017.05.001

Stechmann, A., & Cavalier-smith, T. (2002). Rooting the eukaryote tree by using a derived gene fusion. *Science*, *297*(5578), 89–91. Retrieved from http://www.jstor.org.ezproxy.canterbury.ac.nz/stable/3077224

Steinberg, G. (2007). Hyphal growth: a tale of motors, lipids, and the Spitzenkörper. *Eukaryotic Cell*, *6*(3), 351–360. https://doi.org/10.1128/EC.00381-06

Steinberg, G., Peñalva, M. A., Riquelme, M., Wösten, H. A. N. A., & Harris, S. D. (2017). Cell Biology of hyphal growth. *Microbioly Spectrum*, *5*(2), 1–34. https://doi.org/10.1128/microbiolspec

Steinberg, G., & Schliwa, M. (1993). Organelle movements in the wild type and wall-less fz;sg;os-1 mutants of *Neurospora crassa* are mediated by cytoplasmic microtubules. *Journal of Cell Science*, *106 (Pt 2*, 555–564.

Suei, S., & Garrill, A. (2008). An F-actin-depleted zone is present at the hyphal tip of invasive hyphae of *Neurospora crassa*. *Protoplasma*, *232*(3–4), 165–172. https://doi.org/10.1007/s00709-008-0289-8

Sun, Y., Martin, A. C., & Drubin, D. G. (2006). Endocytic internalization in budding yeast requires coordinated actin nucleation and myosin motor activity. *Developmental Cell*, *11*(1), 33–46. https://doi.org/https://doi.org/10.1016/j.devcel.2006.05.008

Taheri-Talesh, N, Horio, T, Araujo-Bazán, L, Dou, X, Espeso, E A, Peñalva, M A and Oakley, B. R. (2008). The tip growth apparatus of *Aspergillus nidulans*. *Molecular Biology of the Cell*, *19*(4), 1439–1449.

Takeshita, N., Manck, R., Grün, N., de Vega, S. H., & Fischer, R. (2014). Interdependence of the actin and the microtubule cytoskeleton during fungal growth. *Current Opinion in Microbiology*, *20*, 34–41. https://doi.org/https://doi.org/10.1016/j.mib.2014.04.005

Takeshita, N., Mania, D., Herrero, S., Ishitsuka, Y., Nienhaus, G.U., Podolski, M., Howard, J. & Fischer, R. (2013). The cell-end marker TeaA and the microtubule polymerase AlpA contribute to microtubule guidance at the hyphal tip cortex of *Aspergillus nidulans* to provide polarity maintenance. *Journal of Cell Science*, *126*(23), 5400–5411. https://doi.org/10.1242/jcs.129841

Takeshita, N., & Fischer, R. (2011). On the role of microtubules, cell end markers, and septal microtubule organizing centres on site selection for polar growth in *Aspergillus nidulans. Fungal Biology*, *115*(6), 506–517. https://doi.org/10.1016/j.funbio.2011.02.009

Takeshita, N., Higashitsuji, Y., Konzack, S., & Fischer, R. (2008). Apical sterol-rich membranes are essential for localizing cell end markers that determine growth directionality in the filamentous fungus *Aspergillus nidulans*. *Molecular Biology of the Cell*, *19*, 339–351.

Tan, W., & Desai, T. A. (2003). Therapeutic micro and nanotechnology : microfluidic patterning of cellular biopolymer matrices for biomimetic 3-D structures. *Biomedical Microdevices*, *5*(3), 235–244. https://doi.org/https://doi.org/10.1023/A:1025764310391

Tatum, E. L., & Beadle, G. W. (1945). Biochemical genetics of *Neurospora*. *Annals of the Missouri Botanical Garden*, *32*(2), 125–129. https://doi.org/10.2307/2394252

Temperli, E, Roos, U P, and Hohl, H. R. (1991). Germ tube growth and the microtubule cytoskeleton in *Phytophthora infestans*: Effects of antagonists of hyphal growth, microtubule inhibitors, and ionophores. *Mycology*, *95*, 611–617.

Thomson, D. D., Berman, J., & Brand, A. C. (2016). High frame-rate resolution of cell division during *Candida albicans* filamentation. *Fungal Genetics and Biology*, *88*, 54–58. https://doi.org/10.1016/j.fgb.2016.02.001

Thomson, D. D., Wehmeier, S., Byfield, F. J., Janmey, P. A., Caballero-Lima, D., Crossley, A., & Brand, A. C. (2015). Contact-induced apical asymmetry drives the thigmotropic responses of *Candida albicans* hyphae. *Cellular Microbiology*, *17*(3), 342–354. https://doi.org/10.1111/cmi.12369

Torralba, S, Raudaskoski, M, and Pedregosa, A. (1998). Effects of methyl benzimidazole-2-yl carbamate on microtubule and actin cytoskeleton in *Aspergillus nidulans*. *Protoplasma*, *202*, 54–64.

Tripathy, S., Pandey, V. N., Fang, B., Salas, F., & Tyler, B. M. (2006). VMD: a community annotation database for oomycetes and microbial genomes. *Nucleic Acids Research*, *34*(February), D379–D381. https://doi.org/10.1093/nar/gkj042

Tucker, B. E., Hoch, H. C., and Staples, R. C. (1986). The involvement of F-actin in *Uromyces* cell differentiation: The effects of cytochalasin E and phalloidin. *Protoplasma*, *135*(2–3), 88–101.

Tyler, B. M. (2001). Genetics and genomics of the oomycete-host interface. *Trends in Genetics : TIG*, *17*(11), 611–4. Retrieved from http://www.ncbi.nlm.nih.gov/pubmed/11672843

Uchida, M., Mouriño-Pérez, R. R., & Roberson, R. W. (2010). Live-cell imaging of microtubule dynamics in hyphae of *Neurospora crassa*. *Methods in Molecular Biology*, *638*, 259.

Valiron, O., Caudron, N., & Job, D. (2001). Cellular and Molecular Life Sciences Microtubule dynamics. *Cellular and Molecular Life Sciences*, *58*, 2069–2084.

Virag, A., & Harris, S. D. (2006). The Spitzenkörper: a molecular perspective. *Mycological Research*, *110*(1), 4–13. https://doi.org/10.1016/j.mycres.2005.09.005

Voisey, C. R. (2010). Intercalary growth in hyphae of filamentous fungi. *Fungal Biology Reviews*, *24*(3–4), 123–131. https://doi.org/10.1016/j.fbr.2010.12.001

Volkmann, N., Amann, K. J., Stoilova-mcphie, S., Egile, C., Winter, D. C., Hazelwood, L., Heuser, J. E., Li, R., Li, T. D., Hanein, D. & von Zastrow, M. (2001). Structure of Arp2 / 3 complex in its activated state and in actin filament branch junctions. *Science*, *293*(5539), 2456–2459.

Walker, S. K., Chitcholtan, K., Yu, Y., Christenhusz, G. M., & Garrill, A. (2006). Invasive hyphal growth : An F-actin depleted zone is associated with invasive hyphae of the oomycetes *Achlya bisexualis* and *Phytophthora cinnamomi. Fungal Genetics and Biology*, *43*, 357–365. https://doi.org/10.1016/j.fgb.2006.01.004

Walker, S. K. & Garrill, A. (2006). Actin microfilaments in fungi. *Mycologist* 20 (1), 26-31.

Wallar, B. J., & Alberts, A. S. (2003). The formins: Active scaffolds that remodel the cytoskeleton. *Trends in Cell Biology*, *13*(8), 435–446. https://doi.org/10.1016/S0962-8924(03)00153-3

Weaver, A. M., Young, M. E., Lee, W.-L., & Cooper, J. a. (2003). Integration of signals to the Arp2/3 complex. *Current Opinion in Cell Biology*, *15*(1), 23–30. https://doi.org/10.1016/S0955-0674(02)00015-7

Weir, B. S., Paderes, E. P., Anand, N., Uchida, J. Y., Pennycook, S. R., Bellgard, S. E., & Beever, R. E. (2015). A taxonomic revision of *Phytophthora* clade 5 including two new species, *Phytophthora agathidicida* and *P. Cocois*. *Phytotaxa*, *205*(1), 21–38. https://doi.org/10.11646/phytotaxa.205.1.2

Welch, M. (1997). The human Arp2/3 complex is composed of evolutionarily conserved subunits and is localized to cellular regions of dynamic actin filament assembly. *The Journal of Cell Biology*, *138*(2), 375–384.

Welch, M. D., & Mullins, R. D. (2002). Cellular control of actin nucleation. *Annual Review of Cell and Developmental Biology*, *18*(1), 247–288. https://doi.org/10.1146/annurev.cellbio.18.040202.112133

Wessels, D., Soll, D. R., & Knecht, D. (1988). Cell motility and chemotaxis in *Dictyostelium amebae* lacking myosin heavy chain. *Developmental Biology*, *128*(1), 164.

Woods, D. M., & Duniway, J. M. (1986). Some effects of water potential on growth, turgor, and respiration of *Phytophthora cryptogea* and *Fusarium moniliforme*. *Phytopathology*. https://doi.org/10.1094/Phyto-76-1248

Wright, G. D., Arlt, J., Poon, W. C. K., & Read, N. D. (2007). Optical tweezer micromanipulation of W lamentous fungi, *44*, 1–13. https://doi.org/10.1016/j.fgb.2006.07.002

Yarm, F., Sagot, I., & Pellman, D. (2001). The social life of actin and microtubules: interaction versus cooperation. *Current Opinion in Microbiology*, *4*(6), 696–702. Retrieved from http://www.ncbi.nlm.nih.gov/pubmed/11731322

Yu, Y. P., Jackson, S. L., & Garrill, A. (2004). Two distinct distributions of F-actin are present in the hyphal apex of the oomycete *Achlya bisexualis*. *Plant & Cell Physiology*, *45*(3), 275–280. Retrieved from http://www.ncbi.nlm.nih.gov/pubmed/15047875

Zerzour, R., Kroeger, J., & Geitmann, A. (2009). Polar growth in pollen tubes is associated with spatially confined dynamic changes in cell mechanical properties. *Developmental Biology*, *334*(2), 437–446. https://doi.org/10.1016/j.ydbio.2009.07.044

Zhang J, Li S, Fischer R, X. X. (2003). Accumulation of cytoplasmic dynein and dynactin at microtubule plus ends in Aspergillus nidulans is kinesin dependent. *Molecular Biology of the Cell*, *14*, 1479–1488.

Zhao, Y., & Zhang, X. (2006). Cellular mechanics study in cardiac myocytes using PDMS pillars array. *Sensors and Actuators, A: Physical*, *125*(2), 398–404. https://doi.org/10.1016/j.sna.2005.08.032